



Kowalczyk, Dominika (2019) *Structural and biochemical characterisation of p14ARF – E3 ubiquitin ligase complexes*. PhD thesis.

<https://theses.gla.ac.uk/41040/>

Copyright and moral rights for this work are retained by the author

A copy can be downloaded for personal non-commercial research or study, without prior permission or charge

This work cannot be reproduced or quoted extensively from without first obtaining permission from the author

The content must not be changed in any way or sold commercially in any format or medium without the formal permission of the author

When referring to this work, full bibliographic details including the author, title, awarding institution and date of the thesis must be given

Enlighten: Theses

<https://theses.gla.ac.uk/>
research-enlighten@glasgow.ac.uk

Structural and biochemical characterisation of p14ARF - E3 ubiquitin ligase complexes

Dominika Kowalczyk (MSc)

Submitted in fulfilment of the requirements for the Degree of Doctor
of Philosophy

CRUK Beatson Institute
School of Medicine
College of Medical, Veterinary and Life Sciences
University of Glasgow

September 2018

Abstract

Post-translational modifications are a common mechanism in defining proteins role, fate and engagement in different intracellular processes. One of such modifications is ubiquitination - attachment of a small ubiquitin polypeptide to the target's lysine residue. This process involves a complex enzymatic cascade, consisting of three enzymes - E1, E2 and E3. As a result, ubiquitin is activated, conjugated and ligated to the target in a well-controlled but poorly understood manner. Ubiquitination can designate proteins for proteasomal degradation, endocytosis or alter their interaction with other partners. Any disorganisation and misregulation of that process can lead to severe disruption of cellular processes, resulting in the development of serious diseases, such as cancer or neurodegenerative disorders.

MDM2 is a RING-E3 ubiquitin ligase, mainly known for its ability to ubiquitinate tumour suppressor p53 and is overexpressed in different types of cancer. MDM2 can act either as a homodimer or a heterodimer, when it's bound with its homolog - MDM4. Interestingly, despite the high sequence homology, the two proteins behave differently, depending on the dimerisation state. HUWE1 is a HECT-E3 ubiquitin ligase, which has been shown to influence the activity of a range of pro- and anti-apoptotic proteins, such as p53, MCL1 and c-MYC. Both MDM2 and HUWE1 have been reported to be inhibited by p14ARF protein, which has a prominent effect on cell survival and homeostasis.

This thesis presents my work on deciphering how p14ARF influences the activity of MDM2 and HUWE1. I have focused my work on recombinant proteins grown in bacterial expression system, which were further analysed with an implementation of a range of biochemical and structural techniques. Defining an exact mechanism of p14ARF-driven inhibition of MDM2 and HUWE1 could provide long awaited knowledge, relevant for the design of new anti-cancer therapeutics.

Table of Contents

| | |
|---|-----------|
| <i>Abstract</i> | 2 |
| <i>List of Tables</i> | 5 |
| <i>List of Figures</i> | 6 |
| <i>List of Equations</i> | 8 |
| <i>Acknowledgements</i> | 9 |
| <i>Author's Declaration</i> | 10 |
| <i>Abbreviations</i> | 11 |
| 1 INTRODUCTION | 14 |
| 1.1 Ubiquitin and the importance of protein ubiquitination | 14 |
| 1.2 Ubiquitin conjugation pathway | 17 |
| 1.3 E3 ligase families | 20 |
| 1.3.1 RING E3 Ligases | 21 |
| 1.3.2 HECT E3 Ligases | 27 |
| 1.4 ARF protein | 32 |
| 1.4.1 Gene structure | 32 |
| 1.4.2 Protein structure | 32 |
| 1.4.3 ARF and Nucleophosmin | 35 |
| 1.4.4 p53-independent functions of ARF | 35 |
| 1.4.5 Regulation of ARF | 37 |
| 1.5 p53 protein | 40 |
| 1.6 Mouse Double Minute Homologue 2 (MDM2) | 43 |
| 1.6.1 Gene structure | 43 |
| 1.6.2 Protein architecture and structure | 44 |
| 1.6.3 MDM4 | 45 |
| 1.6.4 MDM2/MDM4 RING structure | 46 |
| 1.6.5 Regulation of MDM2 upon DNA damage | 50 |
| 1.7 MDM2-ARF-p53 axis | 52 |
| 1.7.1 MDM2-p53 interaction | 52 |
| 1.7.2 MDM2-ARF interaction | 53 |
| 1.7.3 ARF-induced stabilisation of p53 | 54 |
| 1.7.4 Targeting MDM2-p53 interaction | 58 |
| 1.8 HUWE1 | 59 |
| 1.8.1 Protein architecture | 59 |
| 1.8.2 HUWE1 HECT structure | 60 |
| 1.8.3 HUWE1 role in cell | 62 |
| 1.8.4 Targeting HUWE1 activity | 63 |
| 1.9 Objectives of the thesis | 65 |
| 2 MATERIALS AND METHODS | 66 |
| 2.1 Materials | 66 |
| 2.2 Methods | 68 |
| 2.2.1 Preparation of competent E. coli cells | 68 |
| 2.2.2 Subcloning into expression vectors and SDM | 69 |
| 2.2.3 Protein expression | 73 |
| 2.2.4 Protein purification | 73 |

| | | |
|------------|---|------------|
| 2.2.5 | Analytical gel filtration and HPLC | 76 |
| 2.2.6 | Denaturing and native gel analysis | 77 |
| 2.2.7 | Single-turnover lysine discharge assays | 78 |
| 2.2.8 | Auto-ubiquitination assay | 79 |
| 2.2.9 | Surface plasmon resonance assay (SPR) | 83 |
| 2.2.10 | Fluorescence polarisation assay (FP) | 83 |
| 2.2.11 | Small angle X-ray scattering (SAXS) | 87 |
| 2.2.12 | X-ray crystallography | 88 |
| 3 | RESULTS | 94 |
| 3.1 | Purification of MDM2 constructs | 94 |
| 3.1.1 | MDM2 acidic domain is required for p14ARF binding | 94 |
| 3.1.2 | MDM2 240-C forms higher-order oligomers | 98 |
| 3.1.3 | Examining MDM2 oligomerisation under different expression and buffer conditions | 101 |
| 3.1.4 | Dimeric MDM2 240-C can be isolated using anion exchange chromatography | 105 |
| 3.1.5 | MDM2 oligomerisation is reversed in the presence of denaturing agents | 110 |
| 3.1.6 | Discussion | 120 |
| 3.2 | Biochemical characterisation of MDM2-p14ARF complexes | 123 |
| 3.2.1 | p14ARF constructs design | 124 |
| 3.2.2 | p14ARF constructs bind MDM2 230-C | 126 |
| 3.2.3 | p14ARF affects MDM2 catalytic activity in vitro | 126 |
| 3.2.4 | MDM2/p14ARF complex purification is hindered by its extensive oligomerisation | 132 |
| 3.2.5 | p14ARF alone does not express in a soluble form | 136 |
| 3.2.6 | N37p14ARF peptide inhibits MDM2 ligase activity | 138 |
| 3.2.7 | N37p14ARF peptide induces MDM2 oligomerisation | 141 |
| 3.2.8 | Fusion construct facilitates purification of ARF-MDM2 complex | 146 |
| 3.2.9 | p14ARF-MDM2 RING fusion constructs confirms ARF-driven inhibition of MDM2 ligase activity | 151 |
| 3.2.10 | Discussion | 157 |
| 3.3 | Structural and biochemical characterisation of HUWE1-p14ARF complexes | 162 |
| 3.3.1 | Purification of HUWE1 constructs | 162 |
| 3.3.2 | HUWE1 constructs show high in vitro activity | 166 |
| 3.3.3 | HUWE1 pulls down N56p14ARF | 168 |
| 3.3.4 | N37p14ARF peptide induces oligomerisation of HUWE1 constructs | 170 |
| 3.3.5 | HUWE1 3796-C binds N37p14ARF with low micro-molar affinity | 174 |
| 3.3.6 | N37p14ARF does not influence HUWE1 activity | 176 |
| 3.3.7 | Structural analysis of the HUWE1 – N37p14ARF complexes | 178 |
| 3.3.8 | HUWE1 3900-C dimerises in solution | 196 |
| 3.3.9 | p14ARF does not influence HUWE1 catalytic activity | 201 |
| 3.3.10 | Discussion | 208 |
| 4 | CONCLUDING REMARKS | 213 |
| | <i>List of References</i> | 216 |

List of Tables

| | |
|---|-----|
| TABLE 1 PFUULTRA II HS DNA POLYMERASE 50 μ L-REACTION MIX | 71 |
| TABLE 2 LIST OF CONSTRUCTS DESCRIBED IN THIS THESIS | 72 |
| TABLE 3 REACTION MIX FOR THE PREPARATION OF 4.5% NATIVE POLYACRYLAMIDE GELS | 78 |
| TABLE 4 COMPONENTS OF THE LYSINE DISCHARGE PULSE REACTION | 80 |
| TABLE 5 COMPONENTS OF THE LYSINE DISCHARGE STOP SOLUTION | 80 |
| TABLE 6 COMPONENTS OF THE LYSINE DISCHARGE CHASE SOLUTION | 80 |
| TABLE 7 AN EXAMPLE OF THE TIME POINTS IMPLEMENTED TO COMPARE THREE INDEPENDENT LYSINE DISCHARGE REACTIONS | 81 |
| TABLE 8 AN EXAMPLE OF A SINGLE-TURNOVER AUTO-UBIQUITINATION ASSAY MIX | 81 |
| TABLE 9 INCREASE IN DIMERIC SPECIES OF MDM2 DURING REFOLDING EXPERIMENT | 115 |
| TABLE 10 K_D FOR INTERACTIONS BETWEEN GST-MDM2 230-C / HIS-MBP-P14ARF VARIANTS AND UBCH5B S22R C85K-UB | 129 |
| TABLE 11 EFFECTS OF N32P14ARF ON THE K_D FOR INTERACTIONS BETWEEN UBCH5B S22R C85K-UB AND MDM2 HOMODIMER OR MDM2/MDM4 HETERODIMER | 152 |
| TABLE 12 R_G AND D_{MAX} VALUES OBTAINED FROM SAXS ANALYSIS OF HUWE1 / N37P14ARF COMPLEXES | 180 |
| TABLE 13 X-RAY CRYSTALLOGRAPHIC DATA COLLECTION AND REFINEMENT STATISTICS. VALUES IN THE BRACKETS CORRESPOND TO THE HIGHEST RESOLUTION SHELL. | 191 |

List of Figures

| | |
|--|-----|
| FIGURE 1.1-1 STRUCTURE OF UBIQUITIN | 16 |
| FIGURE 1.2-1 UBIQUITIN CONJUGATION PATHWAY | 19 |
| FIGURE 1.3-1 MECHANISM OF E2~UB DISCHARGE BY RING AND HECT E3 LIGASES | 25 |
| FIGURE 1.3-2 STRUCTURE OF THE BIRC7 RING DOMAIN | 25 |
| FIGURE 1.3-3 STRUCTURE OF THE BIRC7 RING DIMER BOUND TO E2-UB | 26 |
| FIGURE 1.3-4 COMPARISON OF HECT DOMAINS FROM E6AP AND WWP1 | 30 |
| FIGURE 1.3-5 NEDD4L HECT – E2-UB INTERACTIONS | 31 |
| FIGURE 1.4-1 INK4B/ARF/INK4A LOCUS STRUCTURE | 34 |
| FIGURE 1.4-2 SEQUENCE COMPARISON BETWEEN P14ARF AND P19ARF | 34 |
| FIGURE 1.4-3 NMR STRUCTURE OF N37P19ARF | 34 |
| FIGURE 1.4-4 MECHANISM OF ARF REGULATION UPON GENOTOXIC AND ONCOGENIC STRESS SIGNALS | 39 |
| FIGURE 1.5-1 DOMAIN ARCHITECTURE OF P53 PROTEIN | 42 |
| FIGURE 1.6-1 DOMAIN ARCHITECTURE OF MDM2 AND MDM4 PROTEINS | 47 |
| FIGURE 1.6-2 SEQUENCE COMPARISON BETWEEN MDM2 AND MDM4 FROM DIFFERENT SPECIES | 48 |
| FIGURE 1.6-3 X-RAY STRUCTURE OF MDM2/MDM4 RING HETERO-DIMER | 49 |
| FIGURE 1.7-1 STRUCTURE OF THE MDM2 P53-BINDING DOMAIN BOUND TO P53 PEPTIDE | 57 |
| FIGURE 1.7-2 SCHEMATIC REPRESENTATION OF THE INTERPLAY BETWEEN P53, MDM2 AND ARF | 57 |
| FIGURE 1.8-1 DOMAIN ARCHITECTURE OF HUWE1 PROTEIN | 61 |
| FIGURE 1.8-2 STRUCTURE OF HUWE1 HECT DOMAIN | 61 |
| FIGURE 2.2-1 <i>E. COLI</i> EXPRESSION VECTORS USED IN MDM2 AND HUWE1 STUDY | 71 |
| FIGURE 2.2-2 COMPARISON OF LYSINE-DISCHARGE AND AUTO-UBIQUITINATION REACTIONS | 82 |
| FIGURE 2.2-3 PRINCIPLE OF THE SPR EXPERIMENT | 85 |
| FIGURE 2.2-4 PRINCIPLE OF THE FP EXPERIMENT | 86 |
| FIGURE 2.2-5 SCHEMATIC REPRESENTATION OF A SAXS EXPERIMENT | 92 |
| FIGURE 2.2-6 AN EXAMPLE OF DATA OBTAINED FROM A SAXS EXPERIMENT | 92 |
| FIGURE 2.2-7 BRAGG DIFFRACTION | 93 |
| FIGURE 3.1-1 MDM2 DOMAIN ARCHITECTURE AND CONSTRUCT DESIGN | 96 |
| FIGURE 3.1-2 THE AD OF MDM2 IS REQUIRED TO PULL DOWN N56P14ARF | 97 |
| FIGURE 3.1-3 OLIGOMERISATION OF MDM2 240-C CONSTRUCT | 100 |
| FIGURE 3.1-4 MDM2 OLIGOMERISATION UNDER A VARIETY OF EXPRESSION AND BUFFER CONDITIONS | 104 |
| FIGURE 3.1-5 PURIFICATION OF MDM2 240-C CONSTRUCT WITH SOURCEQ ANION EXCHANGE CHROMATOGRAPHY | 107 |
| FIGURE 3.1-6 PURIFICATION OF MDM2 240-C CONSTRUCT WITH MONOQ ANION EXCHANGE CHROMATOGRAPHY | 108 |
| FIGURE 3.1-7 ACTIVITY OF MDM2 240-C AT DIFFERENT STAGES OF THE PURIFICATION PROTOCOL | 109 |
| FIGURE 3.1-8 PURIFICATION OF THE OLIGOMERIC FRACTION OF MDM2 230-C | 114 |
| FIGURE 3.1-9 THE EFFECT OF DIFFERENT UREA CONCENTRATIONS ON MDM2 230-C REFOLDING | 115 |
| FIGURE 3.1-10 COMPARISON OF UREA AND GDNHCL IN THE REFOLDING EXPERIMENT | 116 |
| FIGURE 3.1-11 PURITY OF MDM2 230-C SAMPLES USED IN LYSINE DISCHARGE ASSAYS | 117 |
| FIGURE 3.1-12 ACTIVITY OF REFOLDED MDM2 230-C | 117 |
| FIGURE 3.1-13 LARGE-SCALE REFOLDING OF MDM2 230-C | 119 |
| FIGURE 3.2-1 P14ARF PREDICTED DOMAIN ARCHITECTURE AND CONSTRUCT DESIGN | 125 |
| FIGURE 3.2-2 DOUBLE PULL-DOWN OF MDM2 230-C AND P14ARF VARIANTS | 127 |
| FIGURE 3.2-3 INFLUENCE OF P14ARF CONSTRUCTS ON MDM2 CATALYTIC ACTIVITY | 128 |
| FIGURE 3.2-4 SPR ANALYSIS OF THE BINDING AFFINITY BETWEEN GST-MDM2 230-C/HIS-MBP-P14ARF VARIANTS AND UBCH5B-UB COMPLEX | 131 |
| FIGURE 3.2-5 PURIFICATION OF MDM2 230-C/HIS-MBP*-N56P14ARF COMPLEX WITH SOURCEQ CHROMATOGRAPHY | 134 |
| FIGURE 3.2-6 PURIFICATION OF MDM2 230-C/HIS-MBP*-N56P14ARF COMPLEX BY SIZE EXCLUSION CHROMATOGRAPHY | 135 |
| FIGURE 3.2-7 TEST EXPRESSION OF N56P14ARF CONSTRUCT | 137 |
| FIGURE 3.2-8 N37P14ARF PEPTIDE INFLUENCES THE ACTIVITY OF MDM2 HOMODIMER BUT NOT MDM2/MDM4 HETERODIMER | 140 |
| FIGURE 3.2-9 N37P14ARF PEPTIDE INDUCES MDM2 OLIGOMERISATION | 143 |
| FIGURE 3.2-10 OLIGOMERISATION OF MDM2/P14ARF COMPLEX IS NOT REVERSIBLE FOLLOWING DENATURATION IN GDNHCL AND REFOLDING | 144 |
| FIGURE 3.2-11 SDS-PAGE SHOWING THE ACTIVITY OF REFOLDED MDM2 230-C/N37P14ARF COMPLEX | 145 |

| | |
|---|-----|
| FIGURE 3.2-12 ARCHITECTURE OF THE N56P14ARF~MDM2 210-C CONSTRUCT | 148 |
| FIGURE 3.2-13 SDS-PAGE SHOWING GST-N56P14ARF~MDM2 210-C AND CLEAVAGE BY TEV AND THROMBIN PROTEASES | 148 |
| FIGURE 3.2-14 SIZE EXCLUSION ELUTION PROFILE OF GST-N56P14ARF~MDM2 210-C FOLLOWING TREATMENT WITH THROMBIN | 149 |
| FIGURE 3.2-15 SIZE EXCLUSION ELUTION PROFILE OF N56P14ARF~MDM2 210-C | 150 |
| FIGURE 3.2-16 SCHEMATIC DIAGRAM OF THE P14ARF-MDM2 350-C CONSTRUCTS | 153 |
| FIGURE 3.2-17 DETERMINATION OF GST-P14ARF-MDM2 350-C CONSTRUCT CONCENTRATION | 153 |
| FIGURE 3.2-18 SDS-PAGE SHOWING THE EFFECT OF N32P14ARF FUSION ON THE ACTIVITY OF MDM2 HOMODIMER AND MDM2/MDM4 HETERODIMER | 154 |
| FIGURE 3.2-19 SPR ANALYSIS OF THE EFFECT OF N32P14ARF FUSION ON THE BINDING AFFINITY BETWEEN GST MDM2 350-C AND UBCH5B-UB | 155 |
| FIGURE 3.2-20 SDS-PAGE SHOWING THE EFFECT OF P14ARF FUSION VARIANTS ON THE ACTIVITY OF GST-MDM2 350-C | 156 |
| FIGURE 3.2-21 POSSIBLE MODEL OF MDM2 INHIBITION DRIVEN BY P14ARF | 161 |
| FIGURE 3.3-1 PURIFICATION OF PGEX-4T-1-EXPRESSED HUWE1 3753-C | 164 |
| FIGURE 3.3-2 PURIFICATION OF HIS-TAGGED HUWE1 3753-C EXPRESSED IN PRSFDUET-1 | 165 |
| FIGURE 3.3-3 ACTIVITY OF HUWE1 CONSTRUCTS | 167 |
| FIGURE 3.3-4 HIS-MBP-N56P14ARF CAN PULL DOWN GST-HUWE1 | 169 |
| FIGURE 3.3-5 N37P14ARF INDUCES OLIGOMERISATION OF SELECTED HUWE1 CONSTRUCTS | 172 |
| FIGURE 3.3-6 HUWE1 IS FOUND IN THE INSOLUBLE FRACTION OF THE HUWE1/N37P14ARF COMPLEX | 173 |
| FIGURE 3.3-7 HPLC ELUTION PROFILE OF HUWE1 3796-C MIXED WITH LOWER MOLAR RATIOS OF N37P14ARF | 173 |
| FIGURE 3.3-8 BINDING AFFINITY BETWEEN HUWE1 3796-C AND FAM-N37P14ARF | 175 |
| FIGURE 3.3-9 EFFECT OF N37P14ARF ON HUWE1-CATALYSED UB TRANSFER | 177 |
| FIGURE 3.3-10 SIGNAL PLOTS FOR HUWE1 3796-C AND HUWE1 3796-C / N37P14ARF OBTAINED AFTER SEC SAXS | 182 |
| FIGURE 3.3-11 SIGNAL PLOTS FOR HUWE1 3900-C AND HUWE1 3900-C/N37P14ARF OBTAINED AFTER SEC SAXS | 183 |
| FIGURE 3.3-12 GUINIER ANALYSIS FOR HUWE1 3796-C | 184 |
| FIGURE 3.3-13 GUINIER ANALYSIS FOR HUWE1 3900-C | 185 |
| FIGURE 3.3-14 ANALYSIS OF THE SEC SAXS DATA OBTAINED FOR HUWE1 3796-C +/- N37P14ARF PEPTIDE | 186 |
| FIGURE 3.3-15 ANALYSIS OF THE SEC SAXS DATA OBTAINED FOR HUWE1 3900-C +/- N37P14ARF PEPTIDE | 187 |
| FIGURE 3.3-16 CRYSTAL STRUCTURE OF HUWE1 3900-C | 192 |
| FIGURE 3.3-17 HYDROPHOBIC CONTACTS STABILISE THE HUWE1 DIMER | 193 |
| FIGURE 3.3-18 SUPERIMPOSITION OF HUWE1 3900-C AND HUWE1 3993-C | 194 |
| FIGURE 3.3-19 SUPERIMPOSITION OF HUWE1 3900-C AND HUWE1 3951-C | 195 |
| FIGURE 3.3-20 HUWE1 3900-C DIMERISES IN SOLUTION | 198 |
| FIGURE 3.3-21 HUWE1 3900-C DIMERISATION CAN BE REVERSED BY DISRUPTING THE HYDROPHOBIC DIMER INTERFACE | 199 |
| FIGURE 3.3-22 THE DIMERISATION STATE OF HUWE1 3900-C DOES NOT INFLUENCE ITS CATALYTIC ACTIVITY | 199 |
| FIGURE 3.3-23 ACTIVATION SEGMENT DOES NOT INFLUENCE THE ACTIVITY OF HUWE1 3796-C | 200 |
| FIGURE 3.3-24 HUWE1 3753-3843 AND HUWE1 3843-3902 BIND SEVERAL FRAGMENTS OF P14ARF | 203 |
| FIGURE 3.3-25 P14ARF VARIANTS DO NOT INFLUENCE HUWE1 CATALYTIC ACTIVITY | 204 |
| FIGURE 3.3-26 P14ARF VARIANTS INDUCE OLIGOMERISATION OF HUWE1 3796-C | 205 |
| FIGURE 3.3-27 HPLC ELUTION PROFILES OF HUWE1 3796-C AND BSA INCUBATED WITH A 1:1 MOLAR RATIO OF N76P14ARF | 206 |
| FIGURE 3.3-28 N76P14ARF COELUTES WITH HUWE1 3796-C IN THE HIGH-MW PEAK | 207 |
| FIGURE 3.3-29 FIGURE FROM SANDER <i>ET AL.</i> (2017), SHOWING 45-75P14ARF-DRIVEN INHIBITION OF VARIOUS HUWE1 CONSTRUCTS | 212 |

List of Equations

| | |
|--|----|
| EQUATION 1 THE BEER-LAMBERT LAW STATES THAT THE ABSORBANCE VALUE AT 280 NM WAVELENGTH (A_{280}) IS PROPORTIONAL TO THE PROTEIN CONCENTRATION (CONC), WHERE ϵ - MOLAR EXTINCTION COEFFICIENT, L- LIGHT PATH LENGTH (SWINEHART, 1962) | 74 |
| EQUATION 2 FLUORESCENCE POLARISATION IS DEFINED AS A DIFFERENCE BETWEEN FLUORESCENCE INTENSITIES PARALLEL () AND PERPENDICULAR (\perp) TO THE EXCITATION PLANE, NORMALISED BY THE TOTAL EMISSION INTENSITY | 84 |
| EQUATION 3 SCATTERING INTENSITY (Q) IS A FUNCTION OF THE MOMENTUM TRANSFER, WHERE λ IS THE WAVELENGTH AND θ REPRESENTS HALF OF THE SCATTERING ANGLE | 87 |
| EQUATION 4 THE GUINIER APPROXIMATION PROVIDES INFORMATION ON THE RADIUS OF GYRATION AND INTENSITY VALUE AT $Q=0$ OF A PARTICLE IN SOLUTION | 87 |
| EQUATION 5 THE P(R) FUNCTION DESCRIBES THE DISTANCES BETWEEN ELECTRONS IN THE ANALYSED MOLECULE | 88 |
| EQUATION 6 ELECTRON DENSITY AS A FOURIER SUM | 90 |

Acknowledgements

First of all, I would like to thank my parents for their tremendous support and encouragement.

I would like to express my gratitude to Dr. Danny Huang for giving me the opportunity to work in his group and for the guidance throughout my PhD research. I am very grateful to Lori Buetow for her help throughout my project, as well as during the thesis writing. I would also like to thank Mads Gabrielsen and Gary Sibbet for all their advice and help with my work.

Special thanks go to my advisor, Shehab Ismail, for all his advice and support. I would also like to acknowledge Shehab's group, especially Tamas Yelland, for being great co-workers and for all the suggestions and help with my project.

I would also like to thank all my friends from Glasgow, especially Christin Bauer, for the great time and fun we had together during those 4 years.

A great deal of appreciation goes to Beatson Central Services and Molecular technology service for facilitating our work.

Last but not least, I am thankful to Cancer Research UK for funding the research.

Author's Declaration

I declare that this dissertation is the result of my own work, except where acknowledge to others. This thesis does not include work that has been submitted for consideration for another degree at the University of Glasgow or any other institution.

Abbreviations

| | |
|------------|--|
| °C | Degrees Celsius |
| Å | Ångström |
| aa | Amino acid |
| AD | Acidic domain |
| ARF | Alternate reading frame |
| BME | 2-Mercaptoethanol |
| BSA | Bovine serum albumin |
| CBP | Calmodulin binding protein |
| CD | Circular dichroism |
| D_{\max} | Maximum dimension |
| DMSO | Dimethyl sulfoxide |
| DTT | Dithiothreitol |
| E1 | Ubiquitin-activating enzyme |
| E2 | Ubiquitin-conjugating enzyme |
| E3 | Ubiquitin ligase |
| FP | Fluorescence polarisation |
| GdnHCl | Guanidinium chloride |
| GSH | Glutathione |
| GST | Glutathione S-transferase |
| HECT | Homologous to the E6-AP carboxyl terminus |
| His | 6x histidine tag |
| HPLC | High pressure liquid chromatography |
| I | Scattering intensity |
| IPTG | Isopropyl β -D-1-thiogalactopyranoside |
| K_d | Dissociation constant |
| kDa | Kilodaltons |
| L | Litre |
| M | Molar |
| LB | Lysogeny broth medium |
| mAU | Absorbance value |

| | |
|-------------------|--------------------------------------|
| MBP | Maltose binding protein |
| MDM2 | Mouse double minute 2 |
| MDM4 | Mouse double minute 4 |
| mg/ml | Milligram per millilitre |
| min | Minutes |
| ml | Millilitre |
| mM | Millimolar |
| NES | Nuclear export signal |
| NLS | Nuclear localisation signal |
| NoLS | Nucleolar localisation signal |
| nm | Nanometre |
| NMR | Nuclear magnetic resonance |
| NPM | Nucleophosmin |
| OD ₆₀₀ | Optical density at 600 nm wavelength |
| P(r) | Pair-distance distribution function |
| p53 | Tumour protein p53 |
| PAGE | Polyacrylamide gel electrophoresis |
| PDB | Protein database |
| pI | Isoelectric point |
| PMSF | Phenylmethylsulfonyl fluoride |
| PTM | Post-translational modification |
| q | Scattering vector |
| R _g | Radius of gyration |
| RING | Really interesting new gene |
| RMSD | Root mean square deviation |
| RT | Room temperature |
| s | Seconds |
| SAXS | Small angle X-ray scattering |
| SDS | Sodium dodecyl sulfate |
| SEC | Size exclusion chromatography |
| SPR | Surface plasmon resonance |
| TCEP | Tris(2-carboxyethyl) phosphine |

| | |
|------------------|----------------------------------|
| TEV | Tobacco etch virus protease |
| Tris | Tris(hydroxymethyl) aminomethane |
| Ub | Ubiquitin |
| $\mu\text{g/ml}$ | Microgram per millilitre |
| μl | Microliter |
| μM | Micromolar |
| WT | Wild type |

1 INTRODUCTION

1.1 Ubiquitin and the importance of protein ubiquitination

Post-translational modification of proteins (PTM) controls a plethora of cellular processes. The most common PTM include the attachment of phospho-, acetyl- or methyl- groups to different amino acids, which influences protein function and affects a wide range of cellular processes, such as gene expression, metabolism and cell cycle regulation (Cohen, 2002; Verdin and Ott, 2015). Small proteins can also be used to transiently modify protein substrates. The first such modifier to be discovered was ubiquitin (Ciechanover, Elias and Heller, 1980; Hershko *et al.*, 1982, 1983).

Ubiquitin (Ub) is a small (8.5 kDa) protein that is covalently attached to a target protein's lysine residue via an enzymatic cascade. Modification of a target protein with Ub alters its function and fate. Ub structure comprises a compact globular body with a β -grasp fold and a flexible C-terminal tail (Figure 1.1-1) (Vijay-kumar, Bugg and Cook, 1987). The C-terminal tail ends with a di-glycine motif that is required for Ub activation and formation of an isopeptide bond with a lysine ϵ -amino group on a target protein, whereas the globular core contains various surfaces that are important in eliciting protein-protein interactions (Vijay-kumar, Bugg and Cook, 1987; Komander, 2009; Komander and Rape, 2012). Ub can be attached to a substrate as a single species (mono-ubiquitination) or a polymeric chain, in which the Ub C-terminus is covalently linked to one of its seven lysine residues or to the amino group on its first methionine residue, thereby forming a poly-Ub chain (Dye and Schulman, 2007; Komander, 2009; Komander and Rape, 2012; Yau and Rape, 2016). The type of Ub modification impacts the fate of the substrate. Met-1 and Lys-63 chains play a role in the regulation of the NF- κ B pathway, thereby influencing cell survival mechanisms (Tokunaga *et al.*, 2009; Emmerich *et al.*, 2013). Lys-6 and Lys-27 chains have been linked to cellular response to DNA damage (Elia *et al.*, 2015; Gatti *et al.*, 2015). Lys-11 and Lys-48 chains are known primarily as degradation signals and function by marking substrates for proteasomal degradation (Rubin *et al.*, 1998; Kirkpatrick *et al.*, 2006; Grice *et al.*, 2015). Lys-33 has been found to play a role in protein trafficking (Yuan *et al.*, 2014).

Ub and Ub-like proteins are ligated to the target molecule via the sequential actions of three enzymes: Ub-activating enzyme (E1), Ub-conjugating enzyme (E2) and Ub-ligase (E3) (Dye and Schulman, 2007; Hochstrasser, 2009; Zheng and Shabek, 2017). There are two steps in the catalysis of poly-Ub chains: chain initiation (attachment of the first Ub) and chain elongation (formation of the poly-Ub chain on the previously attached mono-Ub). It has been shown that for RING E3s, these are distinct events and differ in reaction rate. The first event is usually the limiting factor in substrate ubiquitination, as it is much slower than chain elongation (Petroski and Deshaies, 2005). During Ub-chain elongation, the target Ub on the substrate is referred to as the “acceptor”, whereas E2-conjugated Ub which will be transferred to that available Ub is called the “donor” Ub (Wickliffe *et al.*, 2011).

The ubiquitination process is balanced by the presence of deubiquitinating enzymes (DUBs), which are responsible for the removal of the attached Ub molecules to replenish the free Ub pool in the cell. DUBs can function in a variety of ways, recognising and targeting certain sets of substrates, specific types of Ub linkages or specific Ub chains based on their length or flexibility (Komander and Rape, 2012).

Being a key-regulator of such a vast number of cellular processes, Ub plays an indispensable role in maintaining tissue homeostasis. Pitfalls during any stage of the ubiquitination process can lead to severe consequences that give rise to many human diseases. Some of the most well-known examples include vascular disorders, inflammatory and neurodegenerative diseases, muscle wasting disorders, and different types of cancers (Schwartz and Ciechanover, 2009). The importance and complexity of the ubiquitination system makes it very challenging yet interesting machinery to study.

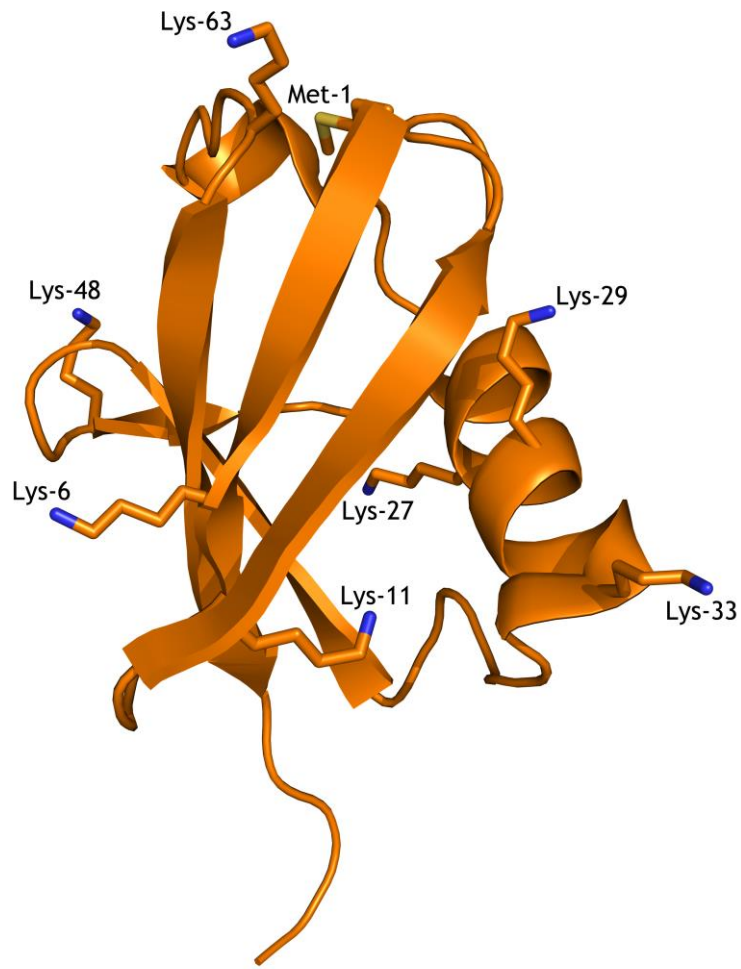


Figure 1.1-1 Structure of ubiquitin

Structure of ubiquitin (PDB code 1UBQ) comprises a globular body with a flexible C-terminal tail. All seven lysine residues of ubiquitin, together with its N-terminal methionine residue are shown in stick representation. Adapted from Vijay-kumar, Bugg and Cook (1987).

1.2 Ubiquitin conjugation pathway

Ub conjugation is dependent on the successive functions of three enzymes: E1 Ub-activating enzyme, E2 Ub-conjugating enzyme and E3 Ub ligase (Dye and Schulman, 2007). In the human genome there are 2 Ub-activating enzymes, almost 40 Ub-conjugating enzymes and more than 1000 Ub ligases (van Wijk and Timmers, 2010). This creates an immense cascade of enzymatic dependencies, tightly regulated to act as machinery for controlling protein function.

E1s have a modular architecture and comprise three flexibly connected domains: an adenylation domain, a domain containing a catalytic cysteine and an E2-binding domain (Dye and Schulman, 2007). In the first step, E1 binds Ub and Mg^{2+} -ATP via its adenylation domain and catalyses the formation of an acyl-phosphate linkage between the Ub C-terminal glycine and AMP (Lake *et al.*, 2001; Walden *et al.*, 2003; Lois and Lima, 2005; Olsen and Lima, 2013). Subsequently, the E1 catalytic cysteine attacks this acyl-phosphate linkage to form a thioester with the Ub C-terminal glycine. AMP acts as a leaving group, enabling the formation of the E1-Ub covalent intermediate (~ denotes a thioester bond) (Lois and Lima, 2005; Huang *et al.*, 2007; Olsen *et al.*, 2010). E1 repeats the adenylation process with another Ub molecule, resulting in an asymmetric complex of E1 bound to two molecules of Ub. Finally, the C-terminal region of E1, which contains a Ub-like fold, binds E2 and Ub is transferred from the E1 catalytic Cys to the catalytic Cys on E2 (Olsen *et al.*, 2010; Olsen and Lima, 2013; Schäfer, Kuhn and Schindelin, 2014). Transfer of Ub from the E1 to the E2 catalytic cysteine is a transthioesterification reaction. E3 is responsible for binding E2-Ub and a target protein to facilitate the transfer of Ub from E2 to the substrate lysine (Figure 1.2-1). E2 contains a conserved core-domain (UBC) and is divided into four classes, depending on the presence of additional N- and C-terminal extensions, which can further modulate its activity. Class I contains only the UBC domain; class II and III respectively have an additional C-terminal or N-terminal extension, and class IV contains extensions at both termini (Wenzel, Stoll and Klevit, 2011; Stewart *et al.*, 2016). Since E1-E2 and E2-E3 interactions are exclusive, in order to be re-charged with Ub, E2 needs to disassemble from the E3 (Eletr *et al.*, 2005). E3 can be divided into three main classes, depending on its E2-Ub interacting domain: HECT, RING and U-box. They

differ in terms of their structure and the mechanism that they employ to transfer Ub (Cappadocia and Lima, 2018).

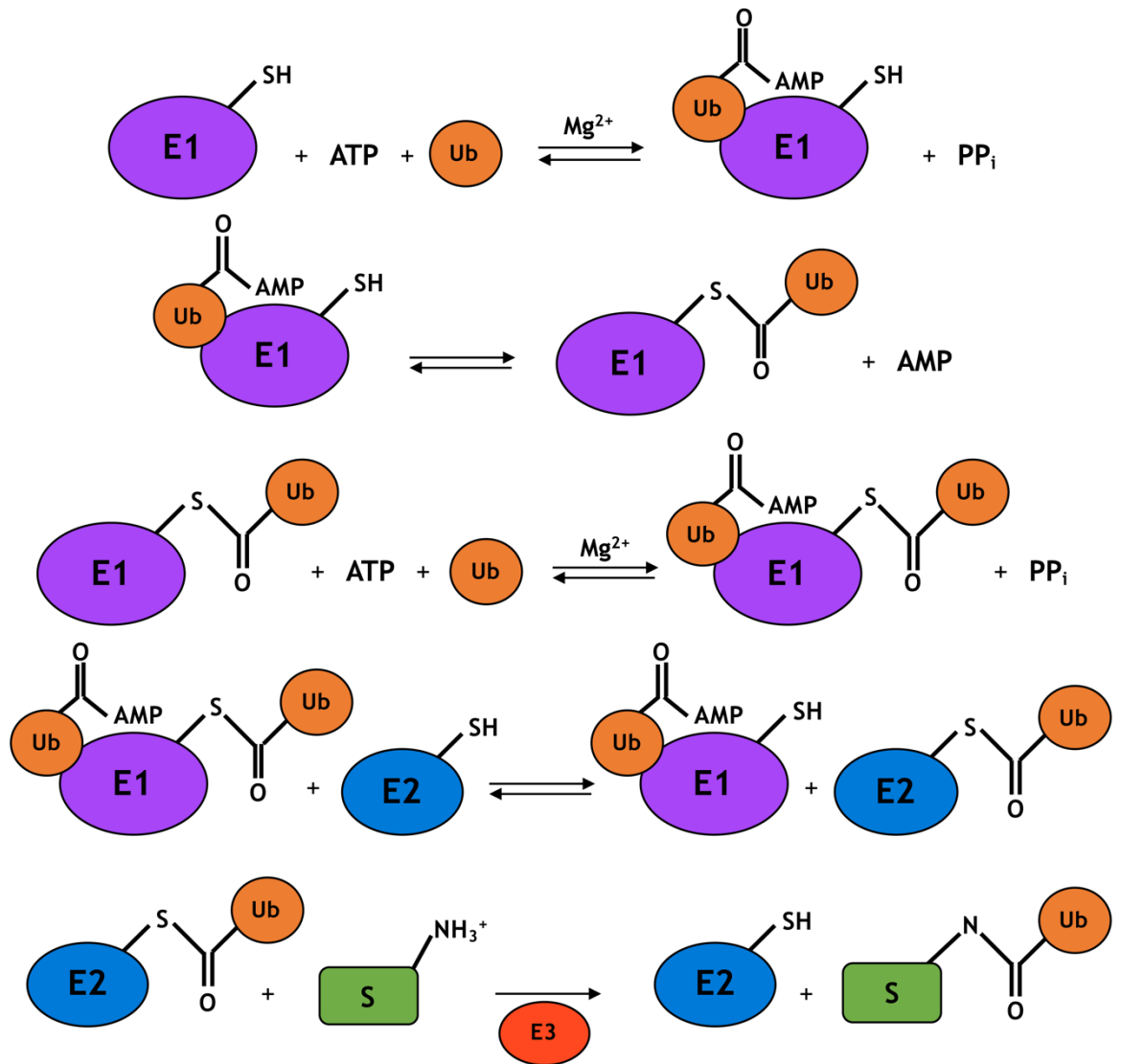


Figure 1.2-1 Ubiquitin conjugation pathway

The E1 enzyme uses ATP to form a Ub-adenylate intermediate (I a). Afterward, Ub is transferred to the E1 catalytic cysteine and the adenylation reaction is repeated with a second Ub molecule (I b and I c). The double loaded E1 is recognised by the E2 enzymes and Ub is transferred to E2 as a result of a transthiolation reaction (II). E3 binds E2-Ub and a substrate to facilitate the transfer of Ub to the target lysine residue (III). Figure adapted from Cappadocia and Lima (2018).

1.3 E3 ligase families

Classification of E3 ligases is based on the type of domain they use to recruit E2~Ub and their catalytic mechanism. RING (Really Interesting New Gene) and U-box E3s bind E2~Ub and transfer Ub directly to a substrate lysine residue (Figure 1.3-1). Structurally, RING E3s are characterised by the presence of two histidine and cysteine residues, which coordinate two Zn^{2+} ions that stabilise the fold of the RING domain (Buetow and Huang, 2016; Zheng and Shabek, 2017). U-box E3s are often classified as RINGs, as both share the same mechanism of Ub transfer; however, U-box E3s lack the Zn^{2+} ions (Buetow and Huang, 2016; Zheng and Shabek, 2017). The catalytic domain of HECT (Homologous to the E6-AP Carboxyl Terminus) E3s is characterised by the presence of two lobes: the N-lobe is responsible for the binding of E2~Ub, whereas the C-lobe contains the catalytic cysteine that accepts Ub from the E2. As a result, HECT E3s catalyse the transfer of Ub in a two-step reaction (Figure 1.3-1). A similar mechanism of Ub transfer is present in RBR E3s (Ring-between-Ring). They possess a RING1-IBR-RING2 motif in which RING1 binds E2~Ub and transfers Ub to the catalytic cysteine residue on RING2 before conjugating it to substrate (Buetow and Huang, 2016; Zheng and Shabek, 2017).

E3-substrate specificity is not uniformly categorised and can be driven by various mechanisms. Some E3s recognise and bind their targets directly via substrate-binding domains or indirectly by exploiting adaptor proteins, which serve as platforms for substrate recognition; some E3s use both types of mechanisms to bind a particular substrate as in the RING E3 ligase CBL, which can bind phosphorylated epidermal growth factor receptor (EGFR) directly via an N-terminal substrate-binding domain or indirectly via the adaptor Grb2 (Levkowitz *et al.*, 1999; Waterman, 2002; Buetow and Huang, 2016). Several Ub ligases utilise non-protein molecules to target substrates. For example, the cullin-RING ligase CRL^{FBS1} complex recognises N-linked glycosylated substrates via the N-linked glycans (Mizushima *et al.*, 2007; Buetow and Huang, 2016). Some E3s lack a defined substrate specificity, and instead contain a motif that directs them to particular cellular compartments where they ubiquitinate a variety of proteins. One such E3 is the CRL^{DDb} complex, which binds to pyrimidine dimer photolesions and ubiquitinates DNA-bound proteins in order to activate the repair

pathways upon UV light - induced DNA damage (Sugasawa *et al.*, 2005; Scrima *et al.*, 2008; Buetow and Huang, 2016).

The vast number of E3 ligases forms the basis for the complex interplay between ubiquitination machinery and target proteins. E3s play a role in practically every signalling pathway and regulate cell development and tissue homeostasis. This project focused on two E3 ligases - MDM2 and HUWE1, which respectively belong to the RING and HECT families of E3 ligases. Before introducing the biological role and significance of both proteins, a more general introduction on the RING and HECT ligases will be given.

1.3.1 RING E3 Ligases

This class of E3 enzymes uses a catalytic RING domain to recruit E2~Ub and promote Ub transfer directly from E2 to substrate. The canonical RING sequence Cys-X₂-Cys-X₍₉₋₃₉₎-Cys-X₍₁₋₃₎-His-X₍₂₋₃₎-Cys-X₂-Cys-X₍₄₋₄₈₎-Cys-X₂-Cys, where X denotes any amino acid, was first characterised by Freemont *et al.* in 1991 (Freemont, Hanson and Trowsdale, 1991; Deshaies and Joazeiro, 2009). These conserved cysteines and histidines coordinate two Zn²⁺ ions and form the foundation of the rigid, globular RING finger-fold (Barlow *et al.*, 1994; Borden *et al.*, 1995; Deshaies and Joazeiro, 2009). These residues and Zn²⁺ ions comprise two loops connected by an α -helix that together form the E2-binding cleft (Figure 1.3-2) (Zheng *et al.*, 2000). Some RING E3s function as monomers, as in RNF38, whereas others function only as dimers or higher-order oligomers. RING E3s can heterodimerise (e.g. MDM2/MDM4, RING1B/BMI1, BRCA1/BARD1), or homodimerise (e.g. MDM2, cIAP) (Hashizume *et al.*, 2001; Linares *et al.*, 2003; Wang *et al.*, 2004; Kozlov *et al.*, 2007; Mace *et al.*, 2008). For several of these E3s, oligomerisation influences catalytic activity (Kentsis, Gordon and Borden, 2002; Poyurovsky *et al.*, 2007).

In the absence of a RING domain, E2~Ub complexes are dynamic and Ub adopts multiple conformations in relation to the E2. When E2~Ub adopts a “closed” conformation in which the C-terminal tail of Ub is locked within the E2 active site, Ub is primed for transfer (Hamilton *et al.*, 2001; Pruneda *et al.*, 2011). The equilibrium between open conformations and this “closed”, primed conformation is enhanced by E2~Ub binding to the catalytic domain of a RING

E3. RING domains bind E2~Ub and facilitate a single step transfer of Ub from E2 to a substrate. Structural studies of two E3-E2~Ub complexes, RNF4 RING-Ubch5A-Ub and BIRC7 RING-Ubch5B-Ub, revealed how RING domains enhance stabilisation of the closed and primed E2-Ub conformation (Dou *et al.*, 2012; Plechanovov *et al.*, 2012; Zheng and Shabek, 2017). In both structures E2-Ub is in the “closed” conformation in which there are numerous interactions between the hydrophobic Ile-44 patch of Ub and the E2, and the C-terminal tail of Ub is stabilised by the interactions with E2. The primed Ub conformation is additionally stabilised by its interactions with residues on the surface of the RING. A highly conserved Arg on the RING domain of the E3 (called the “linchpin” Arg) interacts with Ub and the E2, which provides further, non-covalent stabilisation of the complex (Figure 1.3-3) (Dou *et al.*, 2012; Plechanovov *et al.*, 2012; Zheng and Shabek, 2017). Work done on the Ub-like proteins (such as SUMO) suggests that this E3-stabilised conformation leads to rearrangements in the E2 active site that place a conserved asparagine in close proximity to the catalytic cysteine. Non-covalent interactions provided by this Asn residue support the oxyanion intermediate and facilitate the transfer of Ub to a substrate lysine residue (Wu *et al.*, 2003; Reverter and Lima, 2005; Streich and Lima, 2016). To further improve the efficiency of Ub transfer, some E3s and E2s exploit additional mechanisms. The Ubch5 E2 family utilises a process called “Ub backside binding”. This family of E2s contains a secondary non-covalent Ub binding site, away from the catalytic Cys, that further amplifies the affinity of E2~Ub for the RING domain and, as a result, enhances Ub discharge (Brzovic *et al.*, 2006; Buetow *et al.*, 2015). Some RING E3s (i.e. Arkadia and ARK2C) utilise a second, non-covalent Ub-binding site on their catalytic domain to stabilise the E2-Ub complex and improve the efficiency of the enzyme (Wright, Mac and Day, 2016).

RING E3s represent the majority of all annotated human Ub ligases. Given that there are nearly 40 different E2s in the human genome, this gives rise to an enormous number of possible E3-E2 interacting pairs. As yet, little is known about the mechanisms behind E2~Ub selectivity by E3s. Often the high affinity of E3-E2 interactions does not correlate with catalytic activity. For example both Ubch5B and Ubch7 bind the RING E3 heterodimer BRCA1/BARD1, but this E3 is active only with Ubch5B (Brzovic *et al.*, 2003; Christensen, Brzovic and Klevit,

2007). In addition, the fundamentals of RING-mediated Ub transfer to a precise substrate lysine residue also remain elusive. RING E3s utilise various domains to bind their substrates. They are often spatially separated from the RING domain by unstructured, flexible regions. Available structural data suggest that major conformational changes need to occur in order for Ub to be transferred from E2 to the substrate (Hao *et al.*, 2007). The ubiquitination site selection on a substrate may be governed by the lysine side chain accessibility, the chemical environment in which the residue is found or the presence of additional “mediating” elements on the surface of the E3 (Scherer *et al.*, 1995; Highbarger, Gerlt and Kenyon, 1996; Jin *et al.*, 2008). More data are needed to fully understand the basis for selectivity in Ub transfer by RING E3 ligases.

Some RING E3s use multiple E2s for different stages of Ub-chain formation (Yu *et al.*, 1996; Christensen, Brzovic and Klevit, 2007). Interestingly, several E2s (for example UbcH5B) are able to form different poly-Ub topologies, depending on the type of E3 with which they interact (Nishikawa *et al.*, 2004; Kirisako *et al.*, 2006; Kirkpatrick *et al.*, 2006; Hyung *et al.*, 2007). Generally, in the case of RING E3-mediated substrate ubiquitination, the architecture of the poly-Ub chains is determined by the E2. It is worth mentioning that some E2s can discharge Ub *in vitro* without an E3 (i.e. Ube2G, Ube2K) (Haldeman *et al.*, 1997; Ryu *et al.*, 2008; Stewart *et al.*, 2016).

Regulation of RING E3 ligase activity is an indispensable aspect in maintaining proteome homeostasis. The demand for certain E3s in their active state varies and is context-dependent and includes factors such as cell compartment, developmental stage and tissue type. One of the most common mechanisms used to regulate ubiquitination is via phosphorylation of substrate, E2 or E3. For example, SCF^{Cdc4} ligase binds its substrate Sic1 only when phosphorylated, leading to its ubiquitination in conjunction with the E2 Cdc34 (Feldman *et al.*, 1997). Interestingly, Cdc34 itself undergoes phosphorylation, which influences its activity and cellular localisation (Cocchetti *et al.*, 2008). Another example is phosphorylation of the monomeric RING E3 ligase c-CBL on Tyr-371 - this abolishes autoinhibition and enhances catalytic activity towards E2-Ub discharge (Dou *et al.*, 2013). Another PTM often employed in the control of Ub ligases is ubiquitination itself. RING E3s can be downregulated by other E3 ligases but,

quite often, they utilise a self-control mechanism leading to their auto-ubiquitination and subsequent degradation (e.g. MDM2 and cIAPs). This event is an effective way of assuring an optimal pool of the active enzyme (Fang *et al.*, 2000; Yang *et al.*, 2000). In some cases, ubiquitination is also utilised to upregulate and activate E3 ligases (e.g. BARD1/BRCA1 and BMI1/RING1B) (Mallery, Vandenberg and Hiom, 2002; Ben-Saadon *et al.*, 2006). Some RING E3 ligases are controlled by binding to partner proteins (e.g. Cullin-RING E3s are regulated by Cand1 exchange factor) or to small molecules (e.g. enhanced activity of Ubr1 ligase is provided by its binding with dipeptides) (Turner, Du and Varshavsky, 2000; Bornstein, Ganoth and Hershko, 2006). Even though small binding partners and single molecules seem to play an important role in the control of RING E3 activity, we still often lack detailed information on the nature of their action. Broadening our understanding of the mechanism of E3s' regulation by their natural inhibitors may provide an essential prerequisite for future drug design and development.

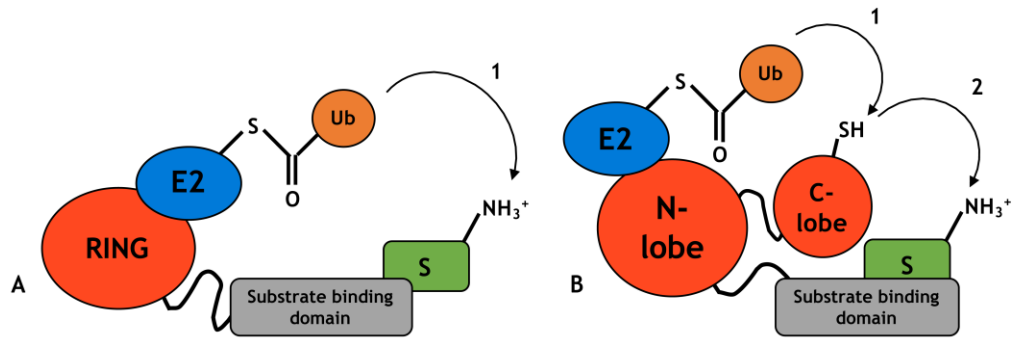


Figure 1.3-1 Mechanism of E2-Ub discharge by RING and HECT E3 ligases

A- RING E3s transfer Ub directly from E2 to the substrate lysine residue in a single step reaction.

B- In contrast, HECT E3s catalyse the substrate ubiquitination in two steps: after binding E2~Ub, Ub is first transferred to the catalytic cysteine located on the HECT C-lobe and subsequently transferred to the substrate lysine residue.

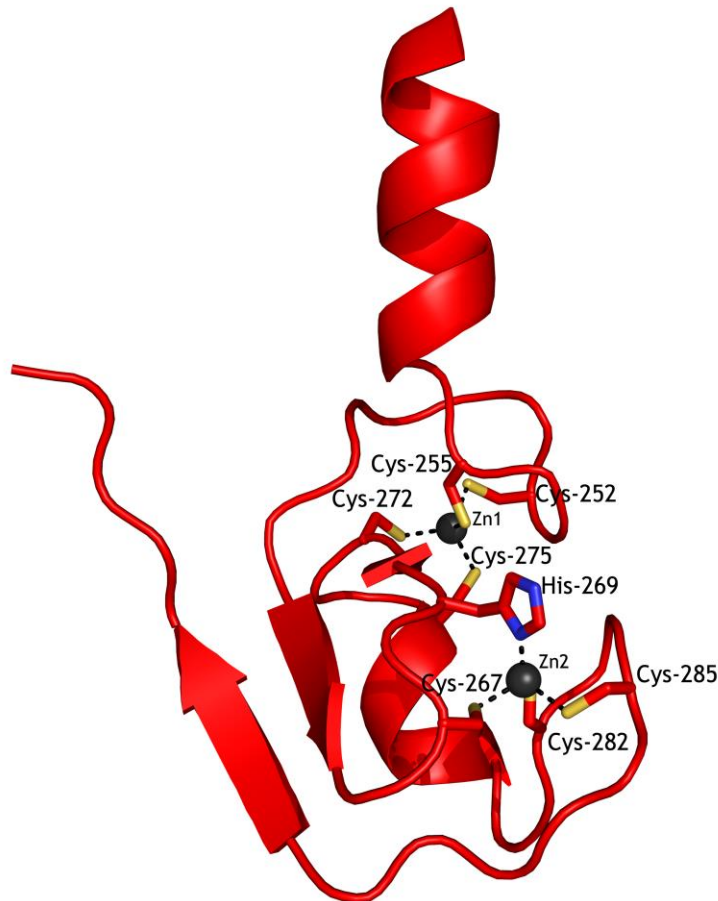


Figure 1.3-2 Structure of the BIRC7 RING domain

The example of the RING domain fold based on a BIRC7 RING structure (PDB code 4AUQ) – conserved cysteine and histidine residues coordinate two zinc ions, giving rise to a rigid and compact RING finger domain. Zinc coordination sites bring together two loops, connected via an α -helix, which give rise to the E2-binding site. Adapted from Dou *et al.* (2012).

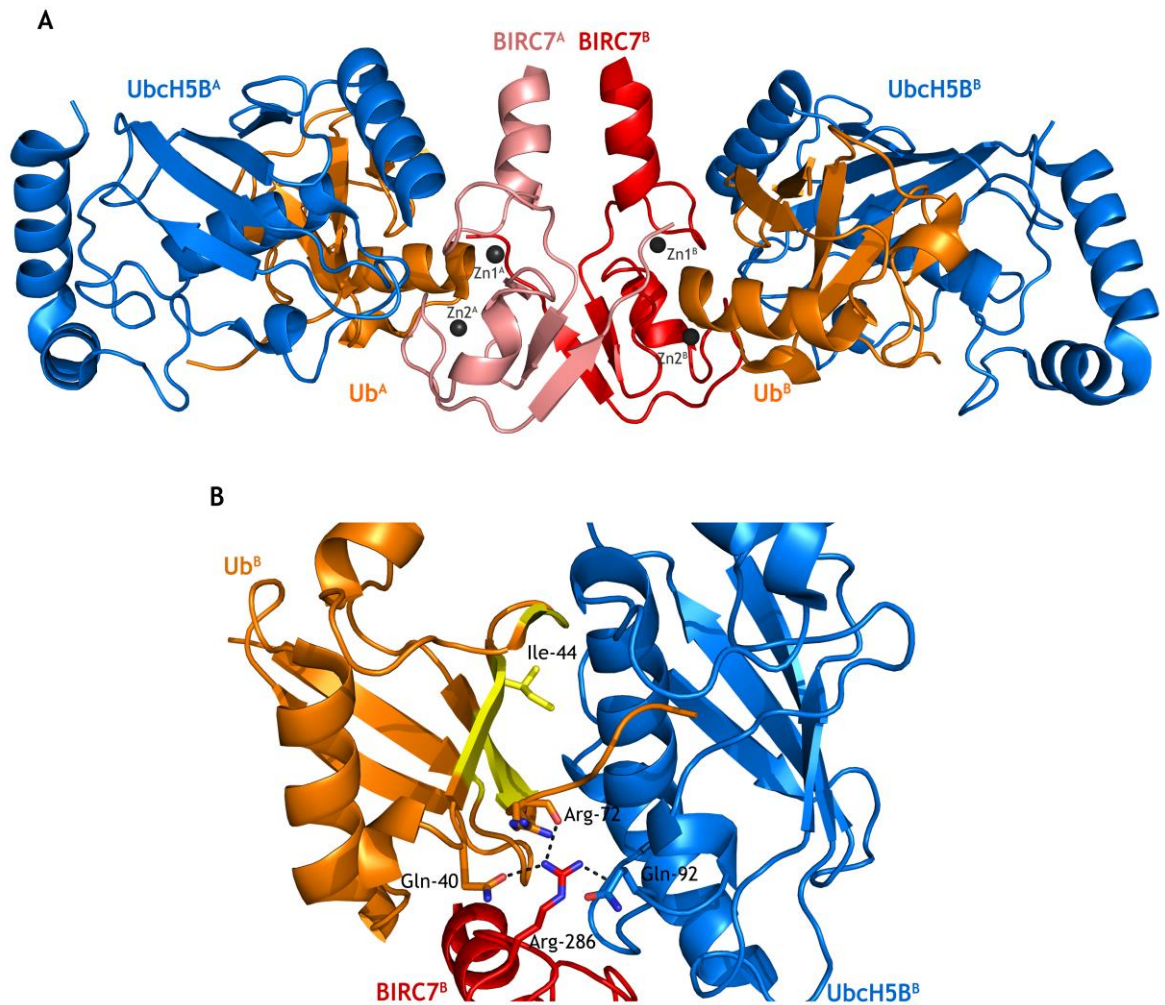


Figure 1.3-3 Structure of the BIRC7 RING dimer bound to E2-Ub

A - An example of a homo-dimeric RING E3 ligase. Two molecules of the BIRC7 RING (PDB code 4AUQ) give rise to a symmetrical RING homo-dimer. Each of the RING domains from the BIRC7 dimer can bind one E2 Ubch5B loaded with Ub.

B- Close up view of the linchpin arginine (Arg-286) of BIRC7 and its interactions with the carbonyl oxygen of Ubch5B Gln-92, as well as Ub Gln-40 and Arg-72, resulting in a stabilised, 'closed' conformation of Ubch5B-Ub. The main contacts between Ub and Ubch5B involve the hydrophobic interactions between the Ile-44 patch on Ub and Ubch5B α -helix2. Adapted from Dou *et al.* (2012).

1.3.2 HECT E3 Ligases

HECT E3 ligases have a specific, bimodal catalytic domain that is responsible for E2-Ub binding. This family of E3s was initially described in 1995 by Huibregtse *et al.* and the earliest structure of a HECT domain was determined in 1999 by Huang *et al.* (Huibregtse *et al.*, 1995; Huang *et al.*, 1999). The ~40 kDa HECT domain consists of two lobes referred to as the N-lobe and the C-lobe. The N-lobe is responsible for E2-Ub binding, whereas the C-lobe contains the catalytic cysteine (Huang *et al.*, 1999). In order to access Ub, the C-lobe needs to be in close proximity to the N-lobe's E2-binding site. The dynamic rearrangement of both lobes with respect to each other is provided by a flexible linker, which is essential for the catalytic activity of the HECT domain (Huang *et al.*, 1999; Verdecia *et al.*, 2003). E2-Ub binds to a hydrophobic groove on the surface of the N-lobe (Figure 1.3-4) (Huang *et al.*, 1999; Nuber and Scheffner, 1999; Kamadurai *et al.*, 2009). As in the case of RING E3s, how the binding affinities of different HECT-E2-Ub pairs relates to their interactions in cells remains unclear (Eletr and Kuhlman, 2007; Kamadurai *et al.*, 2009; Kar *et al.*, 2012).

HECT E3s comprise a much smaller group of Ub ligases compared with RING E3s, with only 28 members found in human genome (Buetow and Huang, 2016). HECTs are divided into three groups, depending on their N-terminal substrate binding domains. The NEDD4 family contains several WW domains, which interact with proteins containing PY (proline rich) motifs. The HERC family bind their substrates via RCC1 (Regulator of chromosome condensation 1) domains. Finally the third group consist of HECT E3 ligases with other protein binding domains (Rotin and Kumar, 2009). Similar to the RING E3 family, substrate-binding domains in HECT E3s are often connected to the HECT domain by intrinsically disordered regions. This allows for major conformational changes to take place during substrate binding and ubiquitination, but also makes structural studies of the full-length HECT ligases a daunting task.

HECT E3s conjugate Ub to substrate in a two-step reaction. In the first step, E2-Ub is recruited and a thioester bond between the C-terminus of Ub and the catalytic cysteine on the C-lobe of the HECT domain is formed. The surface of Ub comprising Ile-36, Leu-71 and Leu-73 forms hydrophobic interactions with a groove on the C-lobe of the HECT domain (Figure 1.3-5) (Kamadurai *et al.*, 2009,

2013; Maspero *et al.*, 2013). Subsequently, a nucleophilic attack on the E3-Ub thioester by a substrate lysine leads to the formation of an isopeptide linkage with Ub.

In HECT domains, the C-terminal tail of the C-lobe is believed to facilitate Ub transfer (Verdecia *et al.*, 2003; Kamadurai *et al.*, 2013). In all families of HECT E3s, a highly conserved phenylalanine residue (“-4 Phe”) near the end of the C-terminus of the HECT domain is suggested to assist in stabilising a geometry between the N- and C-lobes, as well as donor and acceptor Ub that is conducive to isopeptide bond formation (Salvat *et al.*, 2004; Kamadurai *et al.*, 2013). Furthermore, in the NEDD4 family of HECT E3s, the side chain of an aspartate on the C-terminal tail is postulated to stimulate deprotonation of the acceptor lysine residue (Maspero *et al.*, 2013). The C-lobe of the HECT domain also controls linkage specificity in poly-Ub chain formation. Although the HECT domain of HECT E3s governs the architecture of the poly-Ub chain (Wang and Pickart, 2005; Kim and Huibregtse, 2009; Sheng *et al.*, 2012), very little is known about how HECT E3s generate specific Ub-linkages. In part, this is due to a lack of understanding about how the acceptor lysine residue is positioned with respect to the donor Ub C-terminus.

Like RING E3s, the activity of HECT ligases is tightly regulated. Both of these families of E3s are susceptible to auto-ubiquitination and both employ small molecules and proteins to regulate or modulate their activity (Pandya *et al.*, 2010). For example, the NEDD4 family of HECT E3 ligases contains a conserved region on the N-lobe of that HECT domain called an “exosite” that binds the Ile-44 patch of Ub with low-affinity (French, Kretzmann and Hicke, 2009; Ogunjimi *et al.*, 2010; Kim *et al.*, 2011; Maspero *et al.*, 2011, 2013; Zhang *et al.*, 2016; French *et al.*, 2017). The exact role of this secondary Ub-binding site has not been fully determined but some reports suggest that the exosite stabilises the poly-Ub chain during chain elongation (Ogunjimi *et al.*, 2010; Kim *et al.*, 2011). Comparable to RING E3s, HECTs also employ small molecules or proteins to mediate a transition from an autoinhibited state to an active one. For example, in the NEDD4-family E3 SMURF2, the C2 domain folds back and binds to the HECT domain in close proximity to the catalytic cysteine, thereby interfering with access to the C-lobe active site (Wiesner *et al.*, 2007; Mari *et al.*, 2014); binding

of SMURF2 to Smad7 abolishes this autoinhibited conformation and enhances interactions between the HECT domain and E2. In another NEDD4-family, HECT E3s WWP2, ITCH and suppressor of Deltex, the linker between the two WW domains interferes with the flexibility between the N- and C-lobes, and also impairs the access to the exosite on the N-lobe (Riling *et al.*, 2015; Chen *et al.*, 2017; Zhu *et al.*, 2017; Yao *et al.*, 2018). Phosphorylation of a residue within this linker promotes flexibility and allows access to the N-lobe exosite, thereby activating the enzyme (Chen *et al.*, 2017). Another example involves the HECT E3 HUWE1 and the small tumour suppressor alternative reading frame product (ARF); ARF was reported to influence HUWE1 activity, maintaining the E3 in an inactive conformation. Interestingly, recent data suggest that p14ARF also regulates the activity of the RING E3 MDM2. How one small protein can control two mechanistically different enzymes is not well understood.

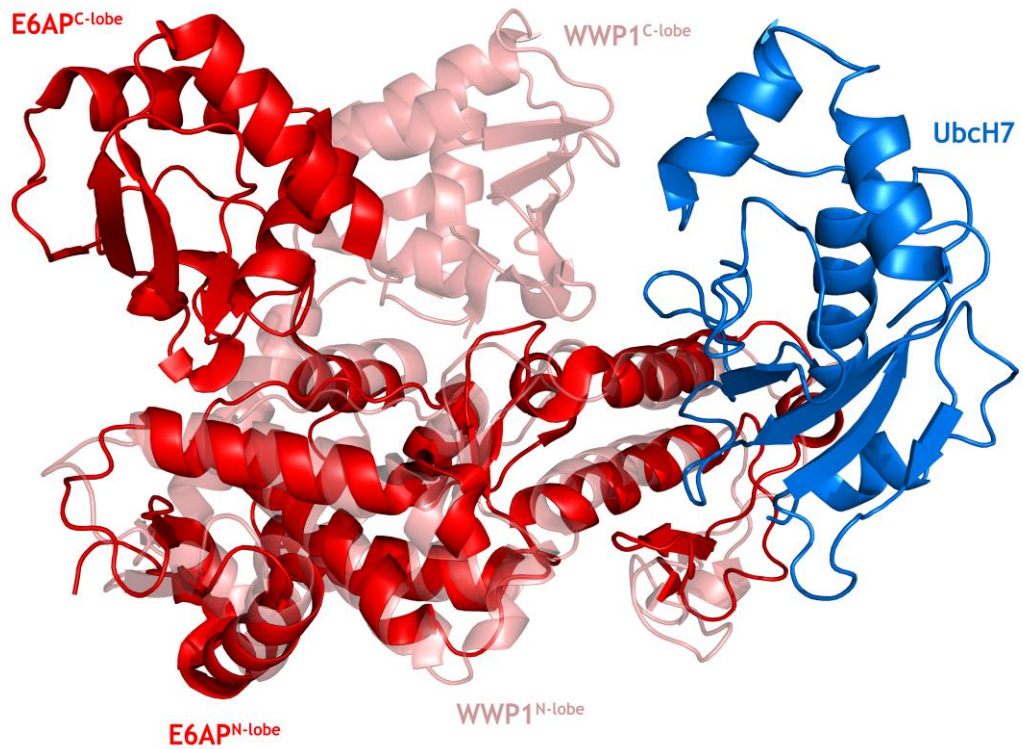


Figure 1.3-4 Comparison of HECT domains from E6AP and WWP1

HECT domains consist of two lobes – (N-lobe and C-lobe), which are connected via flexible linker. The C-lobe can rotate with respect to the N-lobe, giving rise to two distinct conformations: in the open, “L-shaped” conformation (i.e. E6AP, PDB code 1C4Z) the C-lobe is positioned away from the E2, whereas in the closed, “T-shaped” arrangement (i.e. WWP1, PDB code 1ND7), the C-lobe is positioned in proximity to the middle of the N-lobe, facing towards the E2. Adapted from Huang *et al.* (1999) and Verdecia *et al.* (2003).

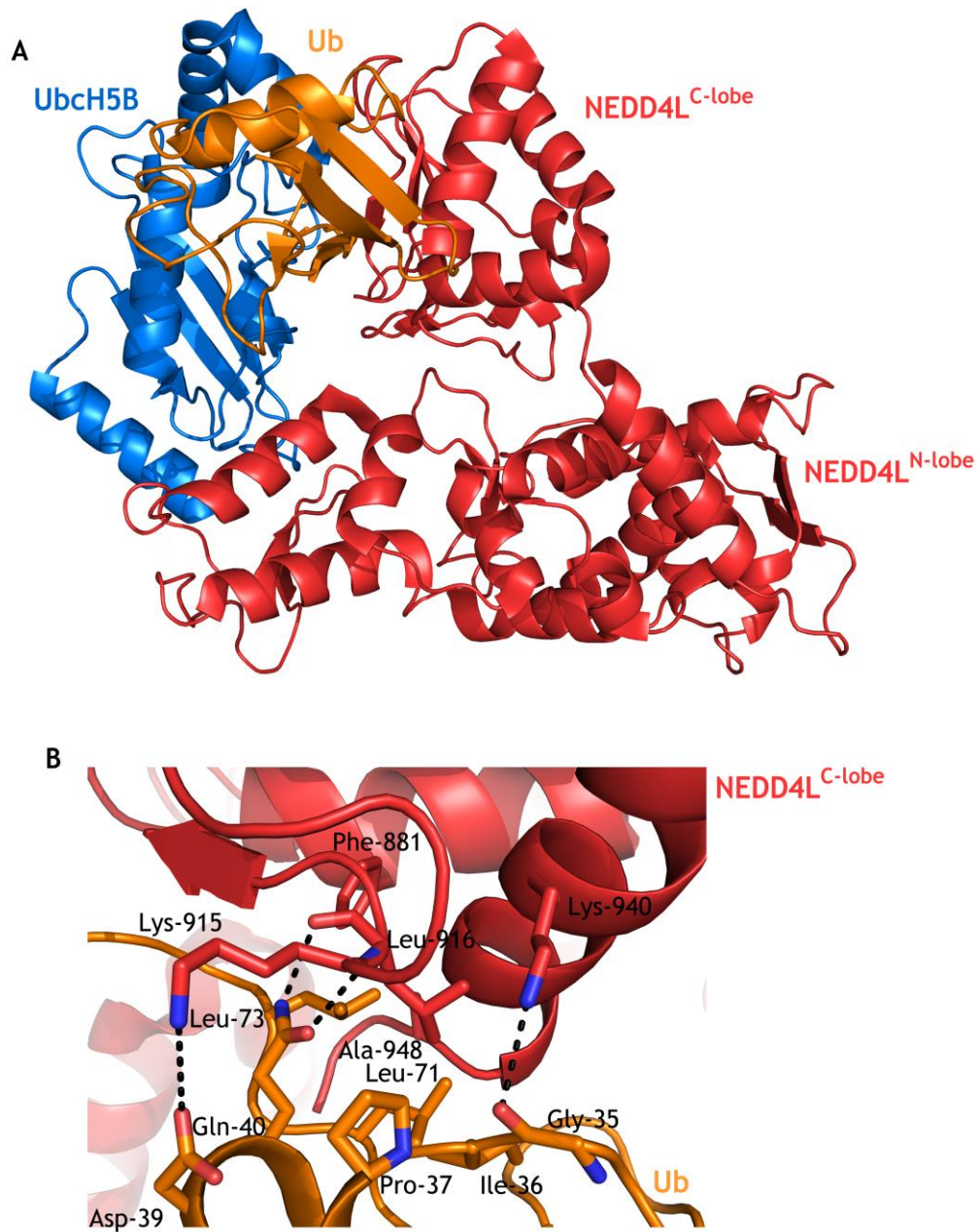


Figure 1.3-5 NEDD4L HECT – E2-Ub interactions

A- An example of HECT domain interactions with E2 and Ub. HECT E3 NEDD4L binds Ubch5B-Ub (PDB code 3JVZ). The N-lobe is responsible for the binding of Ubch5B, whereas the C-lobe directly contacts and stabilises Ub.

B- Close up view of the interactions between the NEDD4L C-lobe and Ub. The main contacts between Ub and HECT involve hydrophobic interactions between Ile-36, Leu-71 and Leu-73 of Ub and a groove on the C-lobe, comprising Leu-916, Ala-948 and Phe-881. Multiple hydrogen bonds further stabilise the NEDD4L-Ub interface. Adapted from Kamadurai *et al.* (2009).

1.4 ARF protein

1.4.1 Gene structure

ARF is expressed as an alternative transcript from the *INK4b/ARF/INK4a* locus on chromosome 9p21 (Ouelle *et al.*, 1995; Sherr, 2012). $p15^{INKb}$ is a product of exons 1 and 2 from the *INK4b* gene. Exons 2 and 3 from the *INK4a* gene are translated from alternative reading frames, producing either ARF protein (from exon 1 β), or $p16^{INK4a}$ (from exon 1 α) (Figure 1.4-1). $p15^{INK4b}$ and $p16^{INK4a}$ both support the growth-repressive functions of the retinoblastoma (RB) family of proteins by inhibiting two kinases - cyclin-dependent kinase 4 and 6 (CDK4 and CDK6) - that phosphorylate and inhibit RBs (Sherr, 2012). Since ARF and $p16^{INKa}$ are translated from different frames of exon 2, the two proteins are unrelated and have different functions in the cell (Ozenne *et al.*, 2010). In spite of the lack of the homology between them, both ARF and $p16^{INK4a}$ are tumour suppressors and their deletion leads to increased tumorigenesis in mouse models. *ARF*-only (disruption of exon 1 β) and *ARF/INK4a* (disruption of exons 2/3) deficient mice exhibit early development of tumours (within 8.5 months), including sarcomas, lymphomas and melanomas. Interestingly, *INK4a* null mice (disruption of exon 1 α) exhibit a similar profile of tumour susceptibility, but with a later onset (within 17 months) (Serrano *et al.*, 1996; Kamijo *et al.*, 1997, 1999; Krimpenfort *et al.*, 2001; Sharpless *et al.*, 2001). This suggests that ARF acts as a *bona fide* tumour suppressor. Nonetheless, both proteins regulate separate cellular events in inhibiting tumorigenesis.

Under normal conditions, ARF is expressed at low levels and has a very short half-life (Freeman-Anderson *et al.*, 2009; Iqbal *et al.*, 2014). ARF transcription is induced by overexpression of MYC, mutation of RAS, or expression of the transcription factor E2F1 and downregulated by expression of TWIST, BIM1 or RB-E2F complexes (Sherr, 2006).

1.4.2 Protein structure

Two well-known homologs of ARF are p14ARF (132 aa, found in humans) and p19ARF (169 aa, found in mice). Both are hydrophobic proteins and extremely basic (the predicted theoretical isoelectric point for p14ARF is 12.41) owing to a

high arginine content (19 % for p14ARF). Despite the similarity in physical and chemical properties, these two proteins share only 50 % overall sequence homology, which imposes some functional differences between them. Both p19 and p14ARF contain a nucleolar localisation signal (NoLS) in their exon 1 β , whereas p14ARF contains an additional NoLS in its exon 2 (Weber *et al.*, 1999; Rizos *et al.*, 2000; Xirodimas *et al.*, 2002). The p14ARF NoLS are important for the interaction of ARF with MDM2 in the MDM2-p53 pathway (Figure 1.4-2). Studies on p19ARF are more common as a result of accessibility to different genetic mouse models. Consequently, most of the available literature describes the role and function of the mouse ARF homologue.

In 2001, DiGiammarino *et al.* performed detailed structural studies of the first 37 residues of p19ARF, herein referred to as N37p19ARF. Circular dichroism (CD) studies on N37p19ARF suggested that the peptide is unfolded and lacks secondary structure in an aqueous environment and this observation was further supported by 2D ^1H - ^{15}N HSQC NMR data (DiGiammarino *et al.*, 2001). Upon incremental addition of 2,2,2 trifluoro ethanol (TFE), the N37p19ARF CD spectrum started to present features of a folded peptide. In addition, the NMR structure of the N-terminal region of p19ARF was solved in the presence of 30% TFE. The NMR data demonstrate that the ARF peptide adopts a bi-helical conformation in the presence of TFE. Helix1 (residues 4-14) and helix2 (residues 20-29) both contain a conserved motif (R*FLV**VR) and are connected via a flexible linker spanning residues 15-17. The NoLS signal (RRPR) is located in a flexible region, following α -helix 2 (Figure 1.4-3) (DiGiammarino *et al.*, 2001).

1.4.3 ARF and Nucleophosmin

ARF is stably expressed in the nucleolus, where it's bound in a complex with nucleophosmin (NPM) (Bertwistle, Sugimoto and Sherr, 2004). p14ARF forms higher-order oligomers in cells under normal growth conditions and oligomerisation is enhanced under the influence of an oxidative stress environment (Menéndez *et al.*, 2003). The role of NPM is to both sequester ARF in its inactive form in nucleoli and protect it from degradation signals (Korgaonkar *et al.*, 2005). When stabilised by NPM, the ARF half-life ranges from 6 to 8 hours but ARF is degraded within 90 minutes upon shuttling to the nucleoplasm (den Besten *et al.*, 2005; Colombo *et al.*, 2006; Sherr, 2006).

NPM is a highly conserved 37 kDa nuclear chaperone that is mostly found in the nucleoli; however, it contains a nuclear export signal (NES) and exhibits rapid shuttling to the cytoplasm (Borer *et al.*, 1989; Szebeni and Olson, 1999; Okuwaki *et al.*, 2001; Yun *et al.*, 2003). Cytoplasmic mutants of NPM in acute myeloid leukaemia demonstrate the importance of nuclear localisation of NPM and NPM-bound ARF (den Besten *et al.*, 2005; Colombo *et al.*, 2006). Other cellular processes NPM takes part in include ribosome biogenesis, response to UV radiation and regulation of DNA repair (Grisendi *et al.*, 2006). As a nuclear chaperone, NPM can bind nucleic acids, as well as associate with and prevent aggregation of different proteins (Wang *et al.*, 1994; Szebeni and Olson, 1999; Okuwaki, Tsujimoto and Nagata, 2002). p14ARF can bind the N-terminal domain of NPM (residues 16-123) via its N-terminal R-motif (residues 1-20), as well as the NoLS signal sequence (residues 84-103) (Mitrea *et al.*, 2016; Luchinat *et al.*, 2018). This interaction is believed to prevent ARF self-association and maintain it in its soluble form (Mitrea and Kriwacki, 2018).

1.4.4 p53-independent functions of ARF

Generally, the role of ARF is to counteract the effect of different types of cellular stresses, leading to p53 activation upon hyperproliferating signals and the inhibition of cell cycle progression or apoptosis (De Stanchina *et al.*, 1998; Palmero, Pantoja and Serrano, 1998; Radfar *et al.*, 1998; Zindy *et al.*, 1998). The mechanism via which ARF stabilises p53 will be described in the following section. Although ARF is primarily known as a negative regulator of MDM2, there

are a plethora of regulatory processes that involve ARF activity and are not related to the p53-MDM2 axis. Some of these processes are highlighted below:

- Control of cell growth:

In lung tumour cells, overexpression of human ARF can lead to cell cycle arrest or induce apoptosis independent of the presence of p53 (Hemmati *et al.*, 2002; Yarbrough *et al.*, 2002). Moreover, a comparison of ARF^{-/-} MDM2^{-/-} p53^{-/-} with MDM2^{-/-} p53^{-/-} mice as well as ARF^{-/-} versus p53^{-/-} shows that deletion of p19ARF increases the rate and spectrum of developed tumours (Eymin *et al.*, 2001, 2003; Beatrice Eymin *et al.*, 2006).

- DNA damage response:

ARF can play a role in the stability of the genome. One example is p14ARF-dependent activation of ATM-CHK2 and ATR-CHK1 signalling pathways in response to genotoxic stress, which leads to cell cycle arrest and apoptosis. The ATM/ATR/CHK cascade is activated by the acetyltransferase TIP60, which is stabilised by p14ARF (Sun *et al.*, 2005; Béatrice Eymin *et al.*, 2006).

- Induction of autophagy:

Both mouse and human ARF contain only one internal methionine residue. Alternative translation from that Met residue produces smARF (short mitochondrial ARF). In normal conditions smARF undergoes rapid degradation by the proteasome. Interestingly, proliferative signals lead to the accumulation of smARF in mitochondria, resulting in the induction of type II caspase-independent cell death (Reef *et al.*, 2006; Abida and Gu, 2008).

- SUMOylation:

ARF can promote attachment of the Ub-like protein SUMO to its binding partners (i.e. MDM2 or NPM). The mechanism or role of this ARF-driven modification is not yet understood, although ARF can directly interact with the SUMO E2 Ubc9. This interaction raises the possibility that ARF promotes transfer of SUMO from E2 to

substrate (Chen and Chen, 2003; Rizos, Woodruff and Kefford, 2005; Tago, Chiocca and Sherr, 2005).

1.4.5 Regulation of ARF

As explained earlier, in cells ARF is most stable in its NPM-bound form but undergoes a fast turnover when transferred to the nucleoplasm. ARF was reported to be very stable in cancer cells, indicating the existence of additional regulatory mechanisms that influence the levels of ARF protein upon proliferative signals (Tavana, Chen and Gu, 2014). One of the events influencing ARF stability is ubiquitination. Interestingly, p14ARF does not have any lysine residues in its sequence (p19ARF has only one), suggesting that ARF is degraded as a result of a non-canonical ubiquitination reaction (Kuo *et al.*, 2004). In 2010 Chen *et al.* identified a HECT E3 ligase that poly-ubiquitinates p14ARF on its N-terminus in a lysine-independent way (D. Chen *et al.*, 2010). Ubiquitin ligase for ARF (ULF) binds ARF both *in vitro* and *in vivo* and its deletion leads to ARF stabilisation. Furthermore, Chen *et al.* showed that oncogenic stress (induced by elevated level of c-MYC) leads to the inhibition of ULF, decreasing the proteasomal degradation of ARF (Chen, Yoon and Gu, 2010). Different groups have identified additional E3 ligases that influence the stability of ARF (i.e. SIVA1, MKRN1) but the exact mechanism of their action and their specificity towards p14 or p19 versions of ARF remains unknown.

ARF expression is influenced by oncogenic signals. In 2013 Chen *et al.* described the complex correlation between c-MYC expression and ARF stabilisation (Chen *et al.*, 2013). Normal human cells have low, basal levels of c-MYC expression that do not promote an increase in ARF protein levels. Overexpression of MYC deactivates ULF and stabilises the ARF/p53 pathway, resulting in inhibition of cell proliferation. Moreover, in healthy cells, DNA damage induces ULF-dependent degradation of ARF; this process can be reversed upon overexpression of MYC, leading to inhibition of ULF followed by activation of ARF and enhanced apoptosis (Figure 1.4-4) (Chen *et al.*, 2013).

DNA damage induced control of ARF protein levels is regulated by ataxia-telangiectasia mutated kinase (ATM). Kamijo *et al.* showed that ATM^{-/-} mouse embryonic fibroblasts (MEFs) exhibit elevated levels of p19ARF (Kamijo *et al.*,

1999). Velimezi et al. established that p14ARF protein levels are stabilised upon ATM depletion in human cancer cells but can be reversed by DNA-damage driven activation of ATM (Velimezi *et al.*, 2013). Further studies showed that ATM activity influences the phosphorylation state of NPM, which in turn affects its interaction with ARF. DNA damage leads to elevated expression of ATM, which activates PP1 phosphatase, leading to dephosphorylation and inactivation of NPM, as well as release of the ARF protein from the ARF-NPM complex and its degradation. A counter mechanism is provided by the kinase NEK2, which binds and phosphorylates NPM, leading to its activation and ARF stabilisation (Figure 1.4-4) (Velimezi *et al.*, 2013).

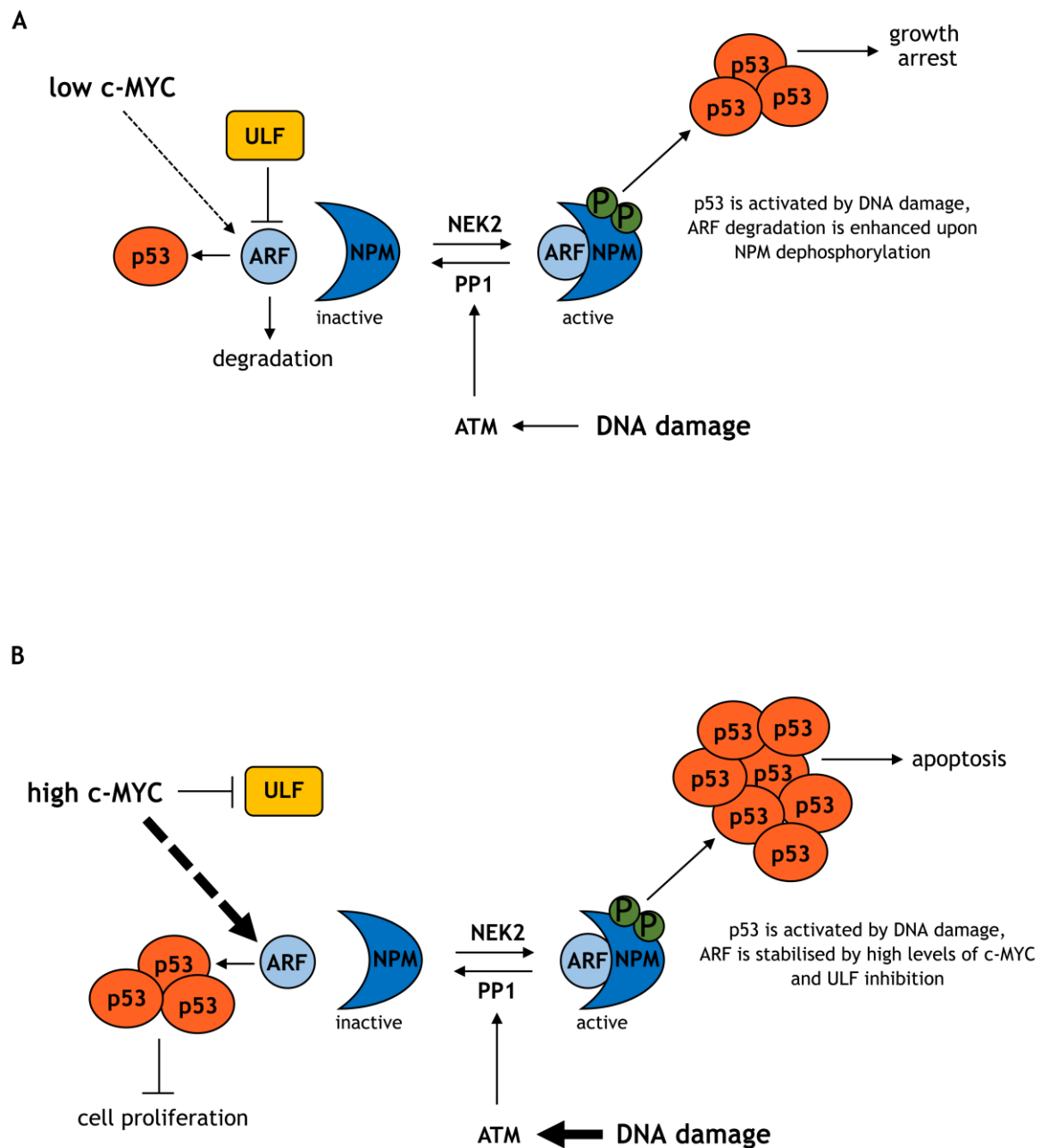


Figure 1.4-4 Mechanism of ARF regulation upon genotoxic and oncogenic stress signals

A- Low levels of oncogenic stress (low c-MYC) result in ARF degradation upon ULF-mediated ubiquitination. DNA damage leads to p53 activation, as well as PP1-driven dephosphorylation and inactivation of NPM, resulting in ARF destabilisation.

B-High levels of oncogenic stress (high c-MYC) lead to the inhibition of ULF and stabilisation of ARF. Together with DNA damage-induced activation of p53 this leads to the inhibition of cell proliferation and increased apoptosis. Adapted from Chen *et al.* (2013) and Tavana, Chen and Gu (2014).

1.5 p53 protein

p53 was first described almost 40 years ago (DeLeo *et al.*, 1979; Lane and Crawford, 1979; Linzer and Levine, 1979). p53 is a transcription factor involved in control of many essential genes in the human genome (i.e. *p21*, *BAX*, *PUMA*, *NOXA*, *TIGAR*) (Mirza *et al.*, 2003; Vousden and Prives, 2009; Meek, 2015). The main role of p53 is the coordination of cellular response to external stimuli, leading to activation of pro-survival or pro-apoptotic genes. Under homeostatic conditions, p53 is tightly controlled by a set of Ub ligases that promote its degradation, thereby maintaining a low basal level of p53 (Hu, Feng and Levine, 2012). This basal level of p53 is essential for the control of many processes, including fertility, metabolism and immunity (Vousden and Ryan, 2009; Feng and Levine, 2010; Levine *et al.*, 2011; Meek, 2015). Acute conditions, such as oncogene upregulation, DNA damage, ribosomal stress or viral infection lead to a reduction in p53 degradation and cause p53-dependent growth arrest or apoptosis (Goldberg *et al.*, 2002; Sherr, 2006; Ofir-Rosenfeld *et al.*, 2008; Cheng *et al.*, 2011). Since p53 is an essential gene regulator for controlling cell survival and death events, misregulation of p53 is often associated with a diversity of pathologies i.e. neurodegenerative diseases, myocardial infarction and a variety of cancers (Dagher, 2004; Bae *et al.*, 2005; Matsusaka *et al.*, 2006; Bretaud *et al.*, 2007; Illuzzi *et al.*, 2009; Gudkov and Komarova, 2010; Checler and Alves Da Costa, 2014; Checler and Da Costa, 2014). Because p53 controls such a range of essential genes, regulation of its pool is essential for cellular homeostasis.

p53 is a ~44 kDa protein consisting of a several domains with various functions. Starting from the N-terminus, there are two transactivation domains (TAD1, aa 1-40 and TAD2, aa 41-60), a proline rich region followed by a DNA-binding core domain (aa 102-292), an NLS signal (aa 305-322), a tetramerisation domain (TET, aa 320-356) and C-terminal regulatory domain encompassing the NES signal (aa 363-393) (Meek, 2015). Transactivation functions of p53 are provided by its core domain and regulation of p53 by PTMs takes place mostly in the C-terminal regulatory domain; the TET domain is responsible for the formation of homo- and hetero-tetramers with itself and p63 and p73 isoforms (Appella and Anderson, 2001; Dai and Gu, 2010; Marcel *et al.*, 2011; Bourdon, 2014).

The main negative regulator of p53 is the RING E3 ligase Mouse Double Minute Homologue 2 (MDM2). MDM2 can influence p53 activity in two ways - either by poly-ubiquitinating p53, thereby marking it for proteasomal degradation, or by inhibiting its transcriptional activity (Meek, 2015). There are many other E3 ligases described that can also target p53, influencing its stability, cellular localisation and oligomeric state (Love and Grossman, 2012). p53 activity and association with its binding partners is tightly controlled by a vast range of PTMs, including phosphorylation, acetylation, methylation and SUMOylation (Meek and Anderson, 2009; MacLaine and Hupp, 2011; Carr, Munro and Thangue, 2012; Jenkins *et al.*, 2012). Mass spectrometry analyses done by DeHart *et al.* suggest that there are more than 150 different PTMs that regulate p53 activity (DeHart *et al.*, 2014). One of the “canonical” PTMs that p53 undergoes upon DNA damage is ATM-driven phosphorylation of Ser-15 and subsequent phosphorylation of Thr-18 by CK1 (Craig *et al.*, 1999; Dumaz, Milne and Meek, 1999; Saito *et al.*, 2002). This event impairs p53-MDM2 binding, leading to p53 stabilisation, as well as preventing the nuclear export of p53 (Zhang and Xiong, 2001; Brown *et al.*, 2008). A similar effect occurs upon CHK2-dependent phosphorylation of Ser-20, which supports phospho-Ser-15 and phospho-Thr-18 in inhibiting MDM2-p53 complex formation (Dumaz *et al.*, 2001; Jabbur and Zhang, 2002).

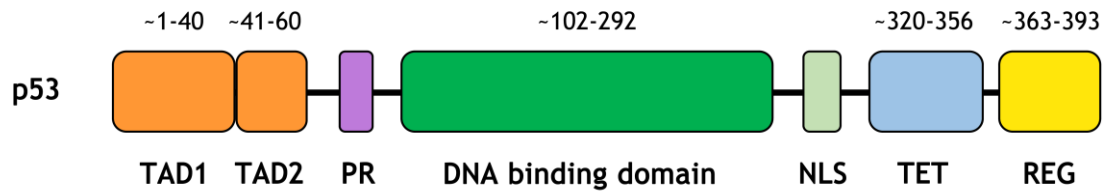


Figure 1.5-1 Domain architecture of p53 protein

Human p53 consists of 393 amino acids, arranged into several domains. Starting from the N-terminus, p53 contains two transactivation domains (TAD1 and TAD2) followed by a proline-rich region (PR). The central part of p53 acts as a DNA-binding domain and is followed by a nuclear localisation signal (NLS). At the C-terminus of p53 there is tetramerisation domain (TET) and regulatory domain (REG). Adapted from Meek (2015).

1.6 Mouse Double Minute Homologue 2 (MDM2)

The role of *MDM2* as an oncogene was described soon after its discovery almost 30 years ago (Momand *et al.*, 1992). In these early studies, *MDM2* was shown to bind p53 and inhibit its transactivation functions and *MDM2* gene amplification was observed in more than 30 % of wild type (WT) p53 human sarcomas (Oliner *et al.*, 1992). Later studies demonstrated that *MDM2* null mice die during the early stages of embryonic development and this phenotype can be rescued by concomitant deletion of p53 (Jones *et al.*, 1995; Luna, Wagner and Lozano, 1995). Soon after, studies started to emerge that described the role and mechanistic details of *MDM2* activity, defining the primary function of *MDM2* as a negative regulator of p53. Even though the name “*MDM2*” refers to the murine homolog of the protein and the human version is quite often annotated as *HDM2*, the two proteins show high sequence homology (over 80 % identical residues) and have indistinguishable functions. This project focuses on the human version of the protein wherein it is referred to as “*MDM2*”, otherwise pointing out the origin of the protein where necessary.

1.6.1 Gene structure

The *MDM2* gene is located at chromosome 12q13-14 and was one of the first genes shown to respond to DNA-damage in a p53-dependent way (Oliner *et al.*, 1992; Barak *et al.*, 1993; Perry *et al.*, 1993; Wu *et al.*, 1993). There are two independent ways in which the expression of *MDM2* mRNA can occur.

Transcription from the promoter 1 (P1) produces a transcript consisting of exons 1 and 3-12, whereas transcription initiated from a p53-dependent promoter 2 (P2) gives rise to a transcript containing exons 2-12 (Barak *et al.*, 1994; Zauberman *et al.*, 1995; Landers, Cassel and George, 1997). Since there are two ATG-initiation codons on *MDM2* mRNA (located on exon 3 and 4), both P1- and P2- driven transcripts can give rise to two versions of *MDM2* protein (Barak *et al.*, 1994). p90MDM2 is a full-length protein that is able to bind and inhibit p53, whereas p76MDM2 lacks the first N-terminal 49 amino acids and cannot target p53 for degradation (Perry *et al.*, 2000). Interestingly, the p53-dependent P2-transcript produces less of the p76MDM2 than the P1-transcript does (Barak *et al.*, 1994; Perry *et al.*, 2000). This creates a regulatory loop in which elevated p53 levels increase transcription of *MDM2* from P2, leading to increased

production of p90MDM2, which in turn targets p53 for degradation, thereby controlling its basal level in cells.

1.6.2 Protein architecture and structure

Consisting of 491 amino acids, full-length MDM2 is a ~55 kDa protein. It contains a set of domains and motifs connected by regions predicted to be unstructured and flexible. Starting from the N-terminus there is a hydrophobic pocket (aa 25-100), a nuclear localisation signal (NLS; aa 179-185), a nuclear export signal (NES; aa 190-202), an acidic domain (AD; aa 210-280), a zinc finger domain (Zn; aa 290-335) and at the C-terminus there is a RING domain that is responsible for MDM2 Ub ligase activity (aa 430-490) (Figure 1.6-1) (Fåhraeus and Olivares-Illana, 2014). MDM2 is an E3 that contains a rare C2H2C4 RING domain, which indicates a divergence from the canonical set of Zn²⁺-binding residues (Kostic *et al.*, 2006; Linke *et al.*, 2008). The “beads on a string” architecture, as well as the domain diversity, makes MDM2 a very promiscuous protein in terms of its binding partners. The BioGrid database describes more than 450 different interactors of MDM2 (Stark, 2006). MDM2 effectors influence transcription levels or impose PTMs. Amongst others, NF- κ B, SMAD3/4 and RAF activate *MDM2* mRNA expression, whereas PTEN, E2F1 and FLI-1 lead to transcriptional inhibition of *MDM2* (Ries *et al.*, 2000; Chang, Freeman and Wu, 2004; Truong *et al.*, 2005; Araki *et al.*, 2010; Busuttil *et al.*, 2010; Tian *et al.*, 2011). Kinases (i.e. ATM, AKT, c-ABL, CK1) bind and phosphorylate MDM2, affecting its stability, ligase activity and p53 inhibition potency (Maya *et al.*, 2001; Zhou *et al.*, 2001; Goldberg *et al.*, 2002; Inuzuka *et al.*, 2010). This process can be reversed by the actions of different phosphatases like WIP1 and CyclinG (Okamoto *et al.*, 2002; Lu *et al.*, 2007). Another set of proteins, called Ribosomal Proteins (i.e. RPL5, RPL11, RPL23) directly inhibit MDM2, leading to p53 activation (Marechal *et al.*, 1994; Lohrum *et al.*, 2003; Dai *et al.*, 2004). Besides p53, MDM2 also regulates other targets. Some of the downstream targets of MDM2 include p73, p63, RB, androgen receptor, RUNX3, RPL26 and CHK2 (Xiao *et al.*, 1995; Zeng *et al.*, 1999; Calabrò *et al.*, 2002; Lin *et al.*, 2002; Ofir-Rosenfeld *et al.*, 2008; Chi *et al.*, 2009; Kass *et al.*, 2009). This very complex network of interactions depends on aspects such as tissue type, cellular localisation and stress conditions.

1.6.3 MDM4

Human MDM4 was isolated in 1997 by Shvarts *et al.* and is a homologue of MDM2 (Shvarts *et al.*, 1997). There are three regions in which MDM4 shows very high sequence similarity to MDM2 - the N-terminal p53-binding, the zinc finger and the RING domains. Interestingly, although MDM4 also contains an acidic motif, the amino acid sequence is not homologous to the MDM2 sequence in this region (Marine and Jochemsen, 2005). MDM4 also lacks NLS and NES signals, which makes it predominantly a cytoplasmic protein that depends on binding partners like MDM2 for nuclear localisation (Figure 1.6-1 and Figure 1.6-2) (Migliorini *et al.*, 2002; Marine and Jochemsen, 2005). MDM4 binds p53 through its N-terminal domain to inhibit transcriptional activity, but does not exhibit ubiquitin ligase activity towards p53 despite having zinc finger and RING domains that are similar to MDM2 (Jackson and Berberich, 2000; Stad *et al.*, 2000, 2001; Migliorini *et al.*, 2002). Interestingly, *MDM4* transcription seems to be entirely p53-independent (Shvarts *et al.*, 1996).

MDM2 can either homo-dimerize or hetero-dimerize with MDM4, forming a more stable and more efficient complex in downregulating p53 than MDM2 homodimer (Badciong and Haas, 2002; Linke *et al.*, 2008). Little is known about the structural and mechanistic reasons for the hierarchy of MDM2 activity based on its oligomeric state: monomeric MDM2 is less active than MDM2 homodimer, which shows lower processivity than MDM2/MDM4 heterodimer (Badciong and Haas, 2002; Uldrijan, Pannekoek and Vousden, 2007; Linke *et al.*, 2008). Aromatic residues outside the RING domain in both MDM2 and MDM4 can form a scaffold for E2 recruitment when MDM2/MDM2 or MDM2/MDM4 oligomers are formed (Uldrijan, Pannekoek and Vousden, 2007; Linke *et al.*, 2008). It is noteworthy that phosphorylation of MDM2 blocks the formation of a stable homodimer and prevents degradation of p53 but does not disrupt MDM2/MDM4 oligomerisation (Cheng *et al.*, 2009). These results suggest that the profound difference in MDM2 and MDM4 E3 ligase activity is a result of minor, individual differences in their RING domains. Another possible reason for the differences in homodimer and heterodimer stability is that the MDM2 homodimer favours autoubiquitination whereas the MDM2/MDM4 heterodimer favours p53 ubiquitination (Badciong and Haas, 2002; Marine and Jochemsen, 2005).

1.6.4 MDM2/MDM4 RING structure

The first structure of the RING domains from the MDM2/MDM4 heterodimer was determined in 2008. The two RING domains bear a strong resemblance to one another - the two domains superpose with a root mean square deviation of 0.56 Å across C α atoms (Linke *et al.*, 2008). The structure is compact and the dimer interface is mainly composed of β 3 and the C-terminal tail from one subunit and β 2 from the other one. As a result, the core of the RING heterodimer is formed by a six-stranded β -barrel and filled with hydrophobic residues (Figure 1.6-3) (Linke *et al.*, 2008). Other interactions that contribute to the dimer interface include the following: hydrogen bonds involving five C-terminal residues and hydrophobic interactions involving six residues (Leu-483, Ile-485, Val-487, Phe-488, Ile-489, Ala-490) from the C-termini of both MDM RING domains, that are buried as a result of these interactions, as well as the N-terminal residues of MDM2 (Leu-430, Ala-434, Ile-435) that extend across the dimer interface as part of an irregular structure (Linke *et al.*, 2008). The fact that MDM2 homodimer and MDM2/MDM4 mediate ubiquitin transfer but not MDM4 alone indicates that there is a critical E2~Ub binding site present on the surface of MDM2 but absent from MDM4. Linke *et al.* predicted the E2 binding site by comparing the structure of the MDM2 RING domain with the RING domain of c-CBL in the UbcH7/c-CBL complex (Linke *et al.*, 2008). Overall, the defined surface is larger but stays in agreement with other RING domains. Furthermore, solvent-exposed C-terminal residues of both MDM RING domains seem to directly contribute to their ligase activity. These residues are positioned between the MDM2 putative E2-binding site and Lys-442 on MDM4, an established ubiquitination site (Linke *et al.*, 2008). These data indicate that there is a secondary surface extending across the dimer interface that is essential for E3 ligase activity. In summary, this model suggested that only MDM2 carries a primary E2 binding site, but the C-terminal residues of both MDM2 and MDM4 are contributing to the E3 ligase activity of the heterodimer (Linke *et al.*, 2008). Our group further confirmed this model and crystallised MDM2/MDM4 RING heterodimer bound with UbcH5B-Ub (Nomura *et al.*, 2017).

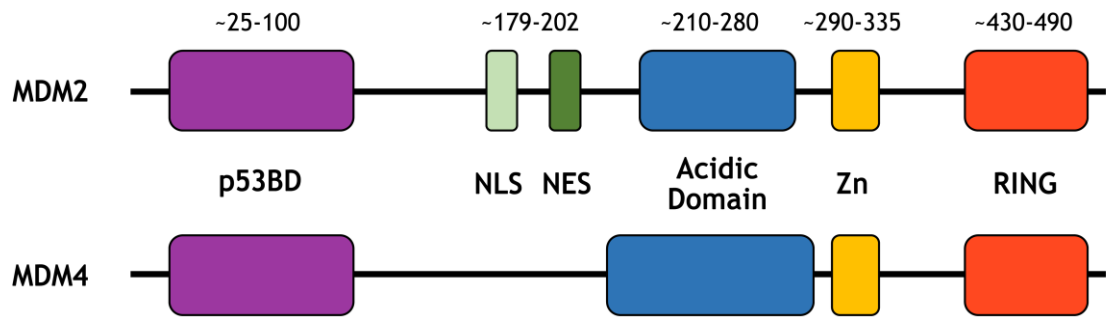


Figure 1.6-1 Domain architecture of MDM2 and MDM4 proteins

MDM2 and MDM4 show high similarity in the type and arrangement of their domains and both proteins share a “beads on a string” topology. Starting from the N-terminus, both MDMs contain a hydrophobic pocket responsible for p53 binding followed by the NLS and NES signals (found only in MDM2) that are responsible for cellular localisation. The acidic domain and zinc finger are known to bind different partners, such as ARF or ribosomal proteins. At the C-terminus of MDM2 and MDM4 there is a RING domain crucial for the dimerisation event and responsible for the E3 ligase activity of the MDM dimers. Based on Fåhraeus and Olivares-Illana (2014).

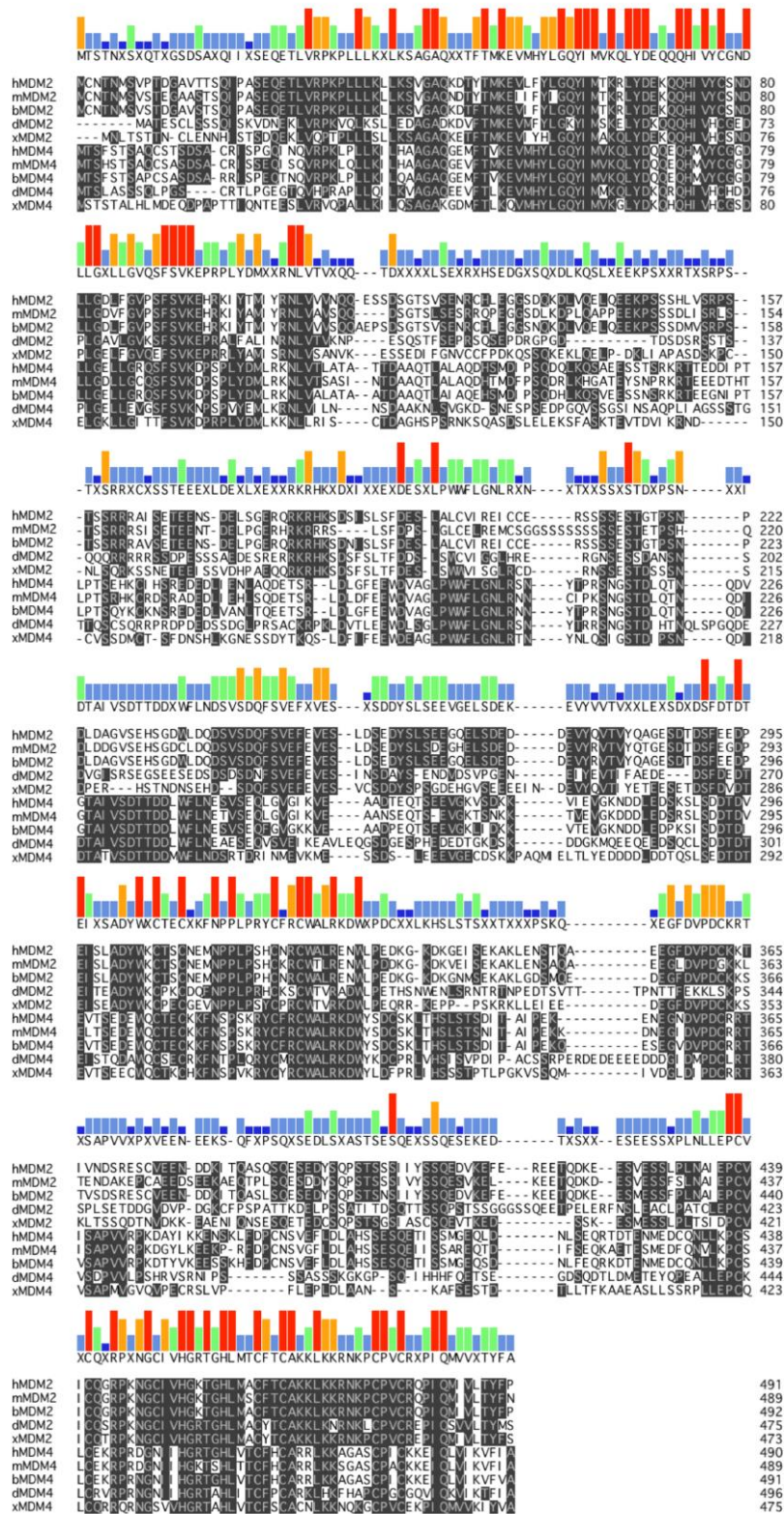


Figure 1.6-2 Sequence comparison between MDM2 and MDM4 from different species

Both MDM2 and MDM4 show a high degree of sequence similarity across different species. Human MDM2 and MDM4 share high homology in the N-terminal p53-binding domain (aa. 25-108 on hMDM2), Zinc finger domain (aa. 290-330 on hMDM2) and RING domain (aa. 436-484 on hMDM2). Identical amino acids are shown in grey boxes. Species abbreviations: h- *Homo sapiens*, m- *Mus musculus*, b- *Bos taurus*, d- *Danio rerio*, x- *Xenopus laevis*.

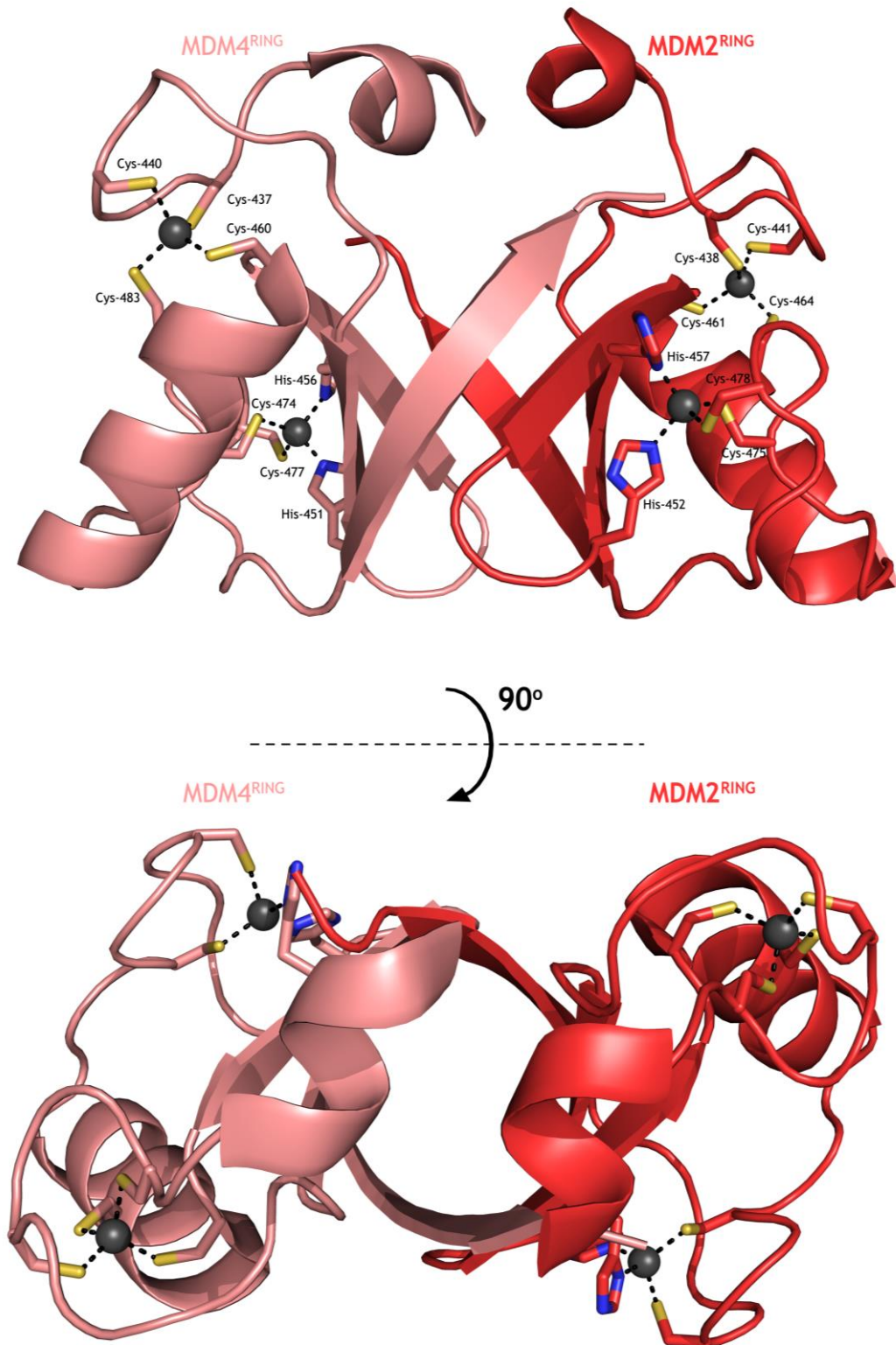


Figure 1.6-3 X-ray structure of MDM2/MDM4 RING hetero-dimer

MDM2/MDM4 RING structure (PDB code 2VJF): MDM2 is presented in red and MDM4 is in salmon. Zinc ions are shown together with cysteine and histidine residues that coordinate them. The 90° rotation around the horizontal axis shows the hydrophobic core as a part of the binding interface between MDM2 and MDM4. Based on Linke *et al.* (2008).

1.6.5 Regulation of MDM2 upon DNA damage

PTMs are the most common regulators of MDM2 activity. The PhosphoSite database specifies more than 70 residues on MDM2 that were shown to be modified by, amongst others, phosphorylation, ubiquitination and acetylation (Hornbeck *et al.*, 2012). Phosphorylation of MDM2 by a wide range of kinases influences its activity, intracellular localisation and molecular association, affecting biological processes such as apoptosis, cell growth and cell cycle regulation. Since MDM2 is mostly described in a relationship to p53 regulation, a set of PTMs which influence MDM2 activity in the context of DNA damage will now be introduced.

- Phosphorylation:

The acidic domain of MDM2 is a target for glycogen synthase kinase 3 β (GSK-3 β) and casein kinases 1 and 2 (CK1, CK2) (Winter *et al.*, 2004; Allende-Vega *et al.*, 2005; Kulikov, Boehme and Blattner, 2005). Phosphorylation of MDM2 by GSK-3 β and CK2 leads to increased inhibition of p53 and conversely, inhibition of these kinases and hypo-phosphorylation of the central region of MDM2 upon ionising radiation leads to p53 stabilisation (Blattner *et al.*, 2002; Winter *et al.*, 2004; Allende-Vega *et al.*, 2005; Kulikov, Boehme and Blattner, 2005).

ATM activation upon DNA damage leads to MDM2 phosphorylation on its C-terminal RING domain (Cheng *et al.*, 2011). Phosphorylation of Ser-395 was shown to impair the nuclear export of p53 and is considered a major regulator of the MDM2-p53 pathway (Maya *et al.*, 2001; Gannon, Woda and Jones, 2012). Interestingly, the same phosphorylation (Ser-395 in MDM2 and Ser-403 in MDM4) event was proposed to activate p53 by switching MDM activity to enhancement of p53 translation under stress conditions (Candeias *et al.*, 2008; Gajjar *et al.*, 2012; Malbert-Colas *et al.*, 2014). Another kinase - Rad3-related kinase (ATR) - phosphorylates human MDM2 at Ser-407 and inhibits the nuclear shuttling of p53 (Shinozaki *et al.*, 2003). ATM-driven phosphorylation of other residues in the proximity of the RING domain (Ser-386, Ser-407, Thr-419, Ser-425, Ser-429) leads to decreased degradation of p53 (Cheng *et al.*, 2009). In 2009 Cheng *et al.* showed that ATM activity prevents MDM2 dimerisation and impairs its ligase activity towards p53 (Cheng *et al.*, 2009). Interestingly, ATM can also target

MDM4 either directly, or indirectly via activation of CHK2 kinase. ATM and CHK2 driven phosphorylation of MDM4 leads to its increased degradation by MDM2, increasing the homodimer pool and resulting in activation of p53 (L. Chen *et al.*, 2005; Okamoto *et al.*, 2005; Pereg *et al.*, 2006).

Finally, protein kinase B (AKT) has dual effects on MDM2 activity. Under normal conditions AKT phosphorylates Ser-166 and Ser-188 and stabilises MDM2, preventing its auto-ubiquitination (Feng *et al.*, 2004). Furthermore, AKT was shown to stabilise MDM4 in a phosphorylation-dependent manner (targeting Ser-367), which in turn leads to further stabilisation of MDM2 (Lopez-Pajares, Kim and Yuan, 2008). However, upon DNA damage AKT inhibits previously mentioned GSK-3 β , leading to hypo-phosphorylation of MDM2 acidic domain and inhibition (Boehme, Kulikov and Blattner, 2008).

- Ubiquitination:

Independent studies showed that DNA damage leads to a drastic decrease in MDM2 stability (Stommel and Wahl, 2004; Itahana *et al.*, 2007; Linares *et al.*, 2007). In 2007 Itahana *et al.* used a murine knock-in model and compared the stability of the mouse WT and C462A MDM2 (Itahana *et al.*, 2007). The C462A (C464 in human) mutation leads to the disruption of the RING finger fold by substituting one of the zinc-coordinating cysteines to alanine. MDM2 C462A does not exhibit ligase activity *in vitro* and cannot relocate p53 *in vivo* (Argentini, Barboule and Wasylyk, 2000; Geyer, Yu and Maki, 2000). Comparison of WT and this MDM2 mutant in the mouse system showed that both have similar half-lives under normal conditions, and the WT turnover is only marginally faster upon irradiation (Itahana *et al.*, 2007). Based on these findings, Itahana *et al.* concluded that MDM2 levels are not only controlled by auto-ubiquitination but also by other E3 ligases under genotoxic stress conditions (Itahana *et al.*, 2007). p300-CBP-associated factor (PCAF) possesses intrinsic E3 ligase activity and ubiquitinates MDM2 for proteasomal degradation (Linares *et al.*, 2007). PCAF knockdown stabilises MDM2 and inhibits p53 activation under DNA damage conditions (Linares *et al.*, 2007). Additional examples of E3s that target MDM2 include the multi-protein ubiquitin ligase complexes SKP1, Cullin, F-box containing complex (SCF) and anaphase promoting complex (APC). Both are

RING-type ligases that are able to mark MDM2 for proteasomal degradation (Inuzuka *et al.*, 2010; He *et al.*, 2014). One example worth mentioning that does not relate to the DNA-damage response, is the activity of NEDD4-1 HECT ligase. NEDD4-1 catalyses the formation of Lys-63 poly-Ub chains on MDM2, which competes with Lys-48 poly-Ub chains built by other E3s and leads to stabilisation of MDM2 in unstressed cells (Xu, Fan and Wang, 2015).

Since ubiquitination plays an important role in controlling MDM2 activity and half-life upon DNA damage, it seems intuitive to anticipate that DUBs (deubiquitinating enzymes) also contribute to the stress response. In unstressed conditions, USP7 binds both MDM2 and MDM4 via its death domain-associated protein 6 (Daxx) domain, leading to their deubiquitination and stabilisation (Cummins and Vogelstein, 2004; Li *et al.*, 2004; Tang *et al.*, 2006). Upon DNA damage Daxx domain is phosphorylated by ATM, which results in dissociation of the MDM2/MDM4-USP7 complex, increased degradation of MDM proteins and p53 activation (Tang *et al.*, 2013). Another DUB shown to target MDM2 is USP15 (Zou *et al.*, 2014). USP15 is often overexpressed in melanoma and colorectal cancer, leading to enhanced MDM2 stabilisation and impairments in p53-driven apoptosis (Zou *et al.*, 2014).

Other Ub-like proteins also influence MDM2 - SUMO and NEDD8 compete with Ub for lysine sites on MDM2, leading to its stabilisation and enhanced degradation of p53 (Buschmann *et al.*, 2000; Watson *et al.*, 2010). Under genotoxic stress conditions there is a decrease in the extent of MDM2 SUMOylation and NEDDylation resulting in MDM2 ubiquitination and activation of p53 (Buschmann *et al.*, 2000; Watson *et al.*, 2010).

1.7 MDM2-ARF-p53 axis

1.7.1 MDM2-p53 interaction

The MDM2 N-terminal hydrophobic domain binds the N-terminal TAD1 domain of p53. This complex is stabilised by multiple Van der Waals interaction between key residues from p53 - Phe-19, Trp-23, and Leu-26 and a hydrophobic cleft in MDM2 composed of the following: Met-50, Leu-54, Leu-57, Gly-58, Ile-61 and Met-62 from $\alpha 2$ helix; Tyr-67, His-73, Val-75, Phe-91 and Val-93 from $\beta 2'$ sheet;

and His-96, Ile-99, Tyr-100 from $\alpha 2'$ helix (Figure 1.7-1) (Kussie *et al.*, 1996). The model of full-length p53 binding to full-length of MDM2 proposes that the interaction between the N-termini of both proteins facilitates further, lower affinity contacts between the p53 central domain and MDM2 acidic domain, which position p53 for ubiquitination (Figure 1.7-2) (Shimizu *et al.*, 2002; Kulikov, Winter and Blattner, 2006; Wallace *et al.*, 2006; Yu *et al.*, 2006).

Depending on its levels, MDM2 either poly- or mono-ubiquitinates p53. High levels of MDM2 lead to p53 poly-ubiquitination and proteasomal degradation, whereas low levels of MDM2 result in p53 mono-ubiquitination, which leads to p53 nuclear export (Rodriguez *et al.*, 2000; Li *et al.*, 2003; Feng *et al.*, 2005; Krummel *et al.*, 2005). Besides marking p53 for degradation, the direct interaction of MDM2 and MDM4 with p53 also inhibits its transcriptional activity by interrupting complex formation between p53 and transcriptional proteins or by disturbing the p53 DNA binding domain (Kruse and Gu, 2009; Cross *et al.*, 2011).

1.7.2 MDM2-ARF interaction

The interaction between ARF and MDM2, and its p53-activating effect was discovered in 1998 by several independent research groups (Kamijo *et al.*, 1998; Pomerantz *et al.*, 1998; Stott *et al.*, 1998; Zhang, Xiong and Yarbrough, 1998). Because of the challenging characteristics of p53, ARF and MDM2, after 20 years we still have limited knowledge on the interplay between these three proteins, with even less understanding of the mechanism governing the MDM2-ARF interaction.

The highly basic nature of ARF is probably responsible for its binding to MDM2. Zhang *et al.* showed that residues 208-491 of MDM2 are sufficient for its interaction with ARF, whereas Stott *et al.* demonstrated that deletion of MDM2 residues 222-437 abolished ARF binding (Stott *et al.*, 1998; Zhang, Xiong and Yarbrough, 1998). Later in 2000, Midgley *et al.* narrowed down the ARF binding region on MDM2 to its acidic domain (residues 210-280), which is the sole domain on MDM2 reported to interact with ARF (Midgley *et al.*, 2000). Similarly to the N37p19ARF peptide, CD and ^1H - ^{15}N NMR spectra suggest that MDM2 210-275 is highly disordered and flexible (Bothner *et al.*, 2001).

The MDM-binding motif on ARF was first narrowed down to exon 1 β (Kamijo *et al.*, 1998; Zhang, Xiong and Yarbrough, 1998). Subsequent studies determined that the first 20 amino acids from the human p14ARF were sufficient for interaction with MDM2 and p53 stabilisation (Figure 1.7-2) (Lohrum *et al.*, 2000; Midgley *et al.*, 2000). Midgley *et al.* tested a series of overlapping, 20-meric peptides from p14 and p19ARF, mapping the required length of ARF for MDM2 binding. Both N20p14ARF and N20p19ARF were able to pull down MDM2 in an ELISA assay. 11-30p19ARF and 21-40p19ARF were also shown to bind MDM2, albeit with lower affinity. Interestingly, an R*FLV**VR motif located at residues 4-7 in human and mouse ARF and residues 21-24 of mouse ARF alone was suggested to be essential for the ARF-MDM2 interaction. N20p14ARF was further shown to stabilise endogenous p53 in U2OS cells and block MDM2-dependent p53 ubiquitination *in vitro*. Finally, Midgley *et al.* showed that N20p14ARF does not interfere with the formation of E1~Ub or E2~Ub *in vitro* (Midgley *et al.*, 2000).

In vitro studies done by Bothner *et al.* showed that upon complex formation in aqueous conditions, two unstructured peptides - N37p19ARF and 210-304 MDM2, form extended, β -stranded structures (Bothner *et al.*, 2001). These oligomeric ARF-MDM2 species were shown to be very stable and resistant to changes in pH, salt concentration, addition of detergents and organic solvents, and even the presence of denaturing agents (4 M urea) (Bothner *et al.*, 2001). Further studies of the β -stranded structures by Sivakolundu *et al.* (2008) showed that the first 9 amino acids of p19ARF are sufficient for the formation of higher-order species with the MDM2 acidic domain (Sivakolundu *et al.*, 2008). They proposed a model in which the ARF-MDM2 oligomers are formed by the electrostatic interactions between Glu and Asp residues from residues 210-304 in MDM2 and Arg residues from N9p19ARF and additionally stabilised by hydrophobic interactions within the core. The ARF-MDM2 sandwich-like structure extends further to form high-molecular weight fibrils, which are suggested to be responsible for the inhibition of MDM2 (Sivakolundu *et al.*, 2008).

1.7.3 ARF-induced stabilisation of p53

Non-competitive binding of ARF and p53 to MDM2 was demonstrated by the assembly of p53-MDM2-ARF complex. Based on this finding, ARF is suggested to influence the MDM2-mediated ubiquitination of p53 in two different ways

(Kamijo *et al.*, 1998; Pomerantz *et al.*, 1998; Stott *et al.*, 1998; Zhang, Xiong and Yarbrough, 1998). Studies done by Weber *et al.* (1999) on MEF cells showed that upon overexpression of N62p19ARF, both ARF and MDM2 localise to the nucleoli, but this is not observed if overexpressed p19ARF does not contain the NoLS sequence (Δ 62p19ARF) (Weber *et al.*, 1999). Based on these data, a model was proposed in which the suggested role of ARF is to localise MDM2 within the nucleolus, where it cannot target p53 for degradation. Further work done by the same group narrowed down the minimum, fully-active sequence of p19ARF to its first 37 residues. Amino acids 1-14 and 26-37 are responsible for binding to MDM2, but also contain the NoLS sequence (residues 26-37). In order to explain how N37p19ARF simultaneously binds MDM2 and induces the relocalisation of the complex to the nucleolus, Weber *et al.* proposed a model in which upon binding to ARF, MDM2 undergoes conformational changes that unmask its cryptic RING-based NoLS (residues 466-473). An explanation of how activation of the NoLS signal located on the RING domain occurred was not provided in this model.

In 2001 Llanos *et al.* proposed a different model for ARF-driven inhibition of MDM2. They looked at endogenous levels of MDM2 in NARF cells (derivatives of the U2OS osteosarcoma) and human diploid fibroblasts under the inducible expression of p14ARF (Llanos *et al.*, 2001). Published data showed that N29p14ARF was sufficient to inhibit the ligase activity of MDM2 and stabilise p53 without pronounced relocalisation of MDM2 to the nucleolus. The model assumes that the basal level of p14ARF in the nucleoplasm is sufficient to target MDM2 and prevent p53 ubiquitination, whereas the substantial surplus of ARF in the nucleolus serves as the “supply” for the nucleoplasmic pool of ARF. This research suggested that the main role of ARF is to directly inhibit the ligase activity of MDM2 without the need for the physical separation between MDM2 and p53 (Llanos *et al.*, 2001).

Notably, we have very limited knowledge on ARF interactions with MDM4. In 2001 Wang *et al.* presented data which suggested that p14ARF is not able to bind MDM4 and its activity is driven solely towards the MDM2 homolog (Wang *et al.*, 2001). Contradicting research was published in successive years, suggesting that p14ARF can directly interact with MDM4 and limit its inhibitory effect on p53 by both translocating it to the nucleus, and redirecting MDM2 ligase activity

towards MDM4 (Jackson, Lindström and Berberich, 2001; Li, Chen and Chen, 2002; Ghosh, Weghorst and Berberich, 2005). As yet, there are no data available to suggest that ARF can inhibit the E3 ligase activity of both MDM2/MDM2 and MDM2/MDM4.

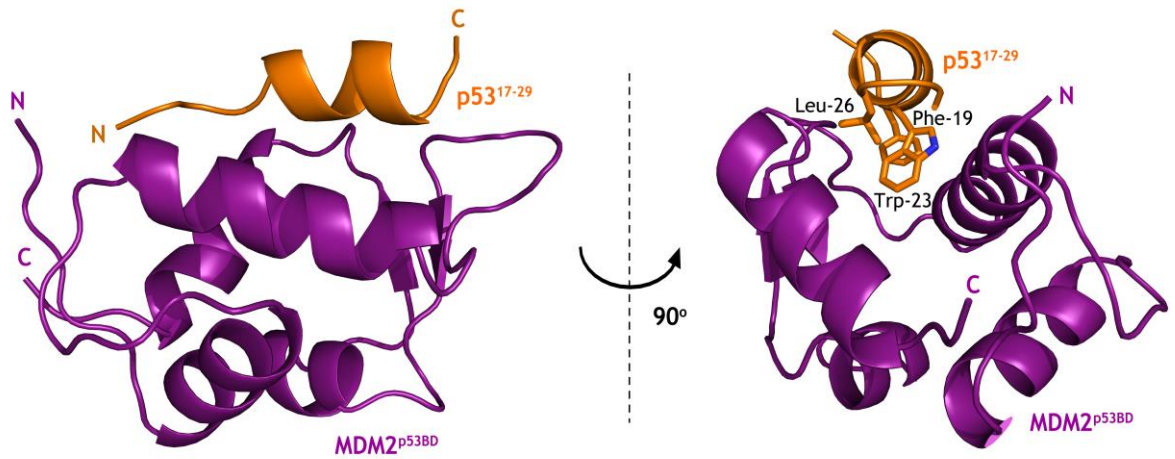


Figure 1.7-1 Structure of the MDM2 p53-binding domain bound to p53 peptide

The MDM2 N-terminal p53-binding domain (shown in magenta) creates a hydrophobic cleft, which can bind the α -helical peptide of p53 (shown in orange). A 90° rotation around the vertical axis shows the critical residues from p53 involved in the interaction with MDM2 hydrophobic pocket (Phe-19, Trp-23 and Leu-26) (PDB code 1YCR). Based on Kussie *et al.*, (1996).

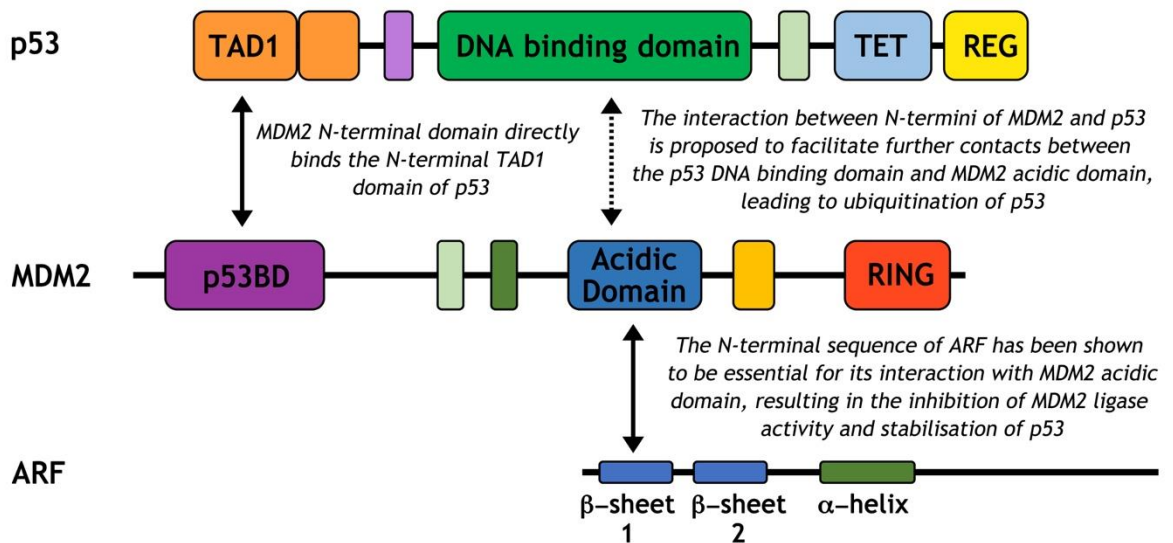


Figure 1.7-2 Schematic representation of the interplay between p53, MDM2 and ARF

The interaction between MDM2 p53 binding domain (p53BD) and p53 TAD1 domain has been first shown by Kussie *et al.* (1996). Furthermore, the model of full-length MDM2-p53 binding proposes that the lower affinity interaction between MDM2 acidic domain and p53 DNA binding domain is triggered, leading to ubiquitination and degradation of p53 (Shimizu *et al.*, 2002; Yu *et al.*, 2006). ARF has been shown to bind to MDM2 acidic domain via its N-terminal sequence, which leads to the stabilisation of p53 (Kamijo *et al.*, 1998; Stott *et al.*, 1998; Midgley *et al.*, 2000). The exact mechanism in which ARF affects the activity of MDM2 remains unknown.

1.7.4 Targeting MDM2-p53 interaction

Lethality of MDM2 null mice at the early embryonic stage emphasises the importance of the tight regulation of MDM2 and p53 levels in cells. A well-characterised single nucleotide polymorphism (SNP) in the MDM2 promoter produced a 3-4-fold increase in mRNA and sensitised mice towards spontaneous tumorigenesis (Bond and Levine, 2007; Post *et al.*, 2010). In contrast, a 50% decrease in MDM2 gene expression led to a significant delay in tumour formation (Alt *et al.*, 2003; Mendrysa *et al.*, 2006; Wang *et al.*, 2006). In nearly 50% of human cancers, p53 inactivation is a characteristic, whereas many WT p53 tumours have defects in maintaining active p53 (Feki and Irminger-Finger, 2004). MDM2 overexpression has been described for most human tumour samples (Momand *et al.*, 1998; Rayburn *et al.*, 2005). MDM2 protein overexpression or gene amplification are most profound in soft tissue sarcomas (i.e. liposarcoma and angiosarcoma), osteosarcomas, glioblastomas, acute lymphocytic leukaemia, as well as a range of carcinomas (i.e. bladder and breast carcinomas) (Stefanou *et al.*, 1998; Zietz *et al.*, 1998; Dei Tos *et al.*, 2000; Gustafsson *et al.*, 2000; Zhou *et al.*, 2000; Lopes *et al.*, 2001; Lukas *et al.*, 2001; O'Campo *et al.*, 2002; Uchida *et al.*, 2002). Upregulation of MDM2 also correlates with poor response to chemotherapy (Rayburn *et al.*, 2005). Multiple studies done in murine models showed that restoration of the WT function of p53 can significantly decrease cancer development and influence survival rate (Martins, Brown-Swigart and Evan, 2006; Ventura *et al.*, 2007; Xue *et al.*, 2007). These findings were further supported by the fact that restoration of WT p53 function leads to apoptosis in transformed cells, whereas untransformed cells undergo growth arrest upon p53 reactivation (Lowe *et al.*, 1993). Taken together, these data suggest that targeting MDM2 and restoring normal p53 levels in WT p53 types of cancer is a potential strategy in cancer treatment.

Targeting MDM2-p53 interactions has been widely used as a potential cancer therapy approach and has been facilitated by the availability of detailed structural data on MDM2-p53 binding. As a result, a number of small compounds have been developed that inhibit p53 binding to MDM2 and lead to p53 stabilisation and activation of pro-apoptotic stimuli in cancer cells. The most potent compounds are known as Nutlins and were discovered by Vassilev *et al.* in 2004 (Vassilev *et al.*, 2004). Nutlin3-a binds the N-terminal domain of MDM2 with

a 90 nM IC₅₀ value and its derivatives - RG7112 and RG7388 - were used in phase I clinical trials (Ding *et al.*, 2013; Vu *et al.*, 2013). The main disadvantage of Nutlin derivatives is high on-target toxicity (i.e. thrombocytopenia and neutropenia) (Andreeff *et al.*, 2016). Another approach undertaken by different groups has been to target MDM2 ligase activity towards p53 (Roxburgh *et al.*, 2012). Compound HLI98s and its homologue HLI373 were designed to target the RING domain of MDM2 and have been proven to restore WT p53 functions in transformed cells, leading to their apoptosis (Yang *et al.*, 2005; Kitagaki *et al.*, 2008). These compounds specifically inhibit p53 polyubiquitination but do not affect MDM2-p53 binding. Unfortunately, they show significant p53-independent functions (Yang *et al.*, 2005). Nonetheless, proof of concept for this approach was provided by another study showing that the usage of the proteasomal inhibitor bortezomib resulted in stabilisation of p53 without affecting its direct interaction with MDM2 (Richardson *et al.*, 2005). This approach mimics the one used in cells in which small molecules such as ARF are used to target MDM2 and stabilise p53 by inhibiting the ligase activity of MDM2 without disrupting MDM2-p53 binding. Moreover, even though ARF inhibits MDM2-dependent p53 polyubiquitination, it still allows for MDM2-driven p53 mono-ubiquitination, as well as MDM2 auto-ubiquitination and degradation *in vivo* (Xirodimas *et al.*, 2001). Unveiling details of the MDM2-ARF interaction would raise unique possibilities for designing ARF-mimetics that are able to reinstate the natural MDM2-p53 cycle in transformed cells.

One of the biggest challenges in designing a drug targeting MDM2 RING is specificity. RING finger domains show high sequence homology and the mechanism of their action (i.e. E2~Ub binding) is well conserved. Interestingly, although ARF does not target the MDM2 close homologue MDM4, some reports suggest that it can inhibit the HECT E3 ligase HUWE1.

1.8 HUWE1

1.8.1 Protein architecture

HUWE1 (also known as ARF-BP1 or MULE) is a ~480 kDa HECT E3 ligase first characterised in 2005 by two groups (Chen *et al.*, 2005; Zhong *et al.*, 2005). HUWE1 contains a set of domains connected by long, flexible regions. Two N-

terminal domains with unknown functions were named ARLD1 and ARDL2 (ARM repeat-like domain; aa 104-374 and 424-815, respectively) by Zhong *et al.*, based on their similarity to Armadillo (ARM) repeats (Zhong *et al.*, 2005). The ARLD domains are followed by a UBA domain (aa 1317-1355), a WWE domain (aa 1612-1692), a BH3 domain (aa 1972-1994) and an NLS signal (aa 2236-2255) (Chen *et al.*, 2005; Zhong *et al.*, 2005). Finally, the C-terminus of HUWE1 contains the catalytic HECT domain (aa 4016-4374) that is responsible for its Ub ligase activity (Figure 1.8-1) (Chen *et al.*, 2005; Zhong *et al.*, 2005). HUWE1 is highly conserved amongst mammals, with more than 90 % sequence identity between human and mouse homologues.

1.8.2 HUWE1 HECT structure

Since HUWE1 is a very big protein (481 kDa) comprising several unstructured regions, structural studies on HUWE1 are particularly challenging. Data available to date include an X-ray structure of the HUWE1 catalytic HECT domain (Pandya *et al.*, 2010). HUWE1 HECT domain comprises two lobes and shows high fold-similarity to the previously characterised structures of HECT domains from E6AP, SMURF2 and WWP1 (Pandya *et al.*, 2010). The N-lobe (residues 3993-4252) contains the E2-binding site (residues 4150-4200), whereas the C-lobe (residues 4259-4374) contains the catalytic cysteine (Cys-4341) (Pandya *et al.*, 2010). The C-lobe of the HUWE1 HECT domain is proximal to the middle of the N-lobe, resulting in a closed, T-shape-like conformation (Pandya *et al.*, 2010). The construct used in these structural studies contains an N-terminal α -helix (α 1) which significantly enhances the thermal stability and rigidity of the HECT domain but does not change the overall fold (Figure 1.8-2). A similar structural element has been found in other HECT E3s and described previously by other groups (Huang *et al.*, 1999; Verdecia *et al.*, 2003). Interestingly, Pandya *et al.* show that the presence of α 1 leads to significant inhibition of HUWE1 catalytic activity towards both auto- and substrate ubiquitination (a 25-fold and 5-fold decrease, respectively) (Pandya *et al.*, 2010).

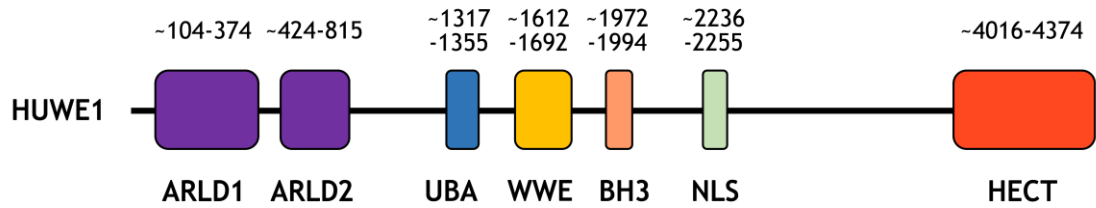


Figure 1.8-1 Domain architecture of HUWE1 protein

HUWE1 consists of nearly 4400 amino acids arranged into a several domains, connected via flexible and unstructured regions. Starting from the N-terminus, HUWE1 contains two ARLD repeats, followed by UBA, WWE and BH3 domains and nuclear localisation signal. At the C-terminus HUWE1 contains the catalytic HECT domain, responsible for its E3 ligase activity.

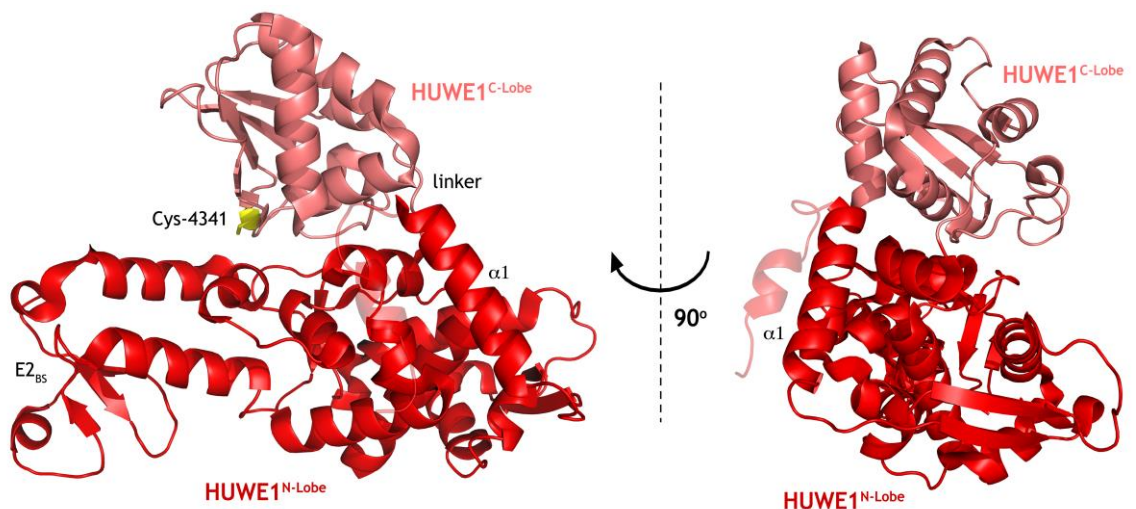


Figure 1.8-2 Structure of HUWE1 HECT domain

The structure of the HUWE1 HECT domain shows high similarity to previously described HECT domains. The N-lobe (shown in red) contains the E2 binding site and is connected to the C-lobe (shown in salmon) via a flexible linker. The C-lobe contains the catalytic cysteine (shown in yellow, with stick representation) and, in this structure, it is positioned in a “closed”, T-shape-like conformation, proximal to the middle of the N-lobe. Additionally, there is an α 1-helix present in the structure, together with an additional sequence being a part of the expression tag (shown as transparent) (PDB code 3H1D). Based on Pandya *et al.* (2010).

1.8.3 HUWE1 role in cell

Chen et al. purified HUWE1 as a major component of the ARF-containing complexes from the H1299 cell line and proposed it to be the primary factor regulating both p53-dependent and independent functions of ARF (Chen *et al.*, 2005). *In vitro* ubiquitination assays showed that a C-terminal fragment of HUWE1 containing the HECT-domain (residues 3760-4374) was inhibited by the N64p14ARF peptide (Chen *et al.*, 2005). Moreover, knockdown of HUWE1 in p53 null H1299 cells led to growth arrest in a manner similar to overexpression of ARF, whereas HUWE1 ablation in WT p53 U2OS cells resulted in p53 stabilisation (Chen *et al.*, 2005). Finally, Chen et al. showed that HUWE1 directly binds and ubiquitinates p53 and this event is inhibited by the N-terminal part of ARF (Chen *et al.*, 2005). The exact mechanism by which ARF binds and inhibits HUWE1 remains unknown.

Zhong et al. identified HUWE1 as a negative regulator of MCL-1 protein (Zhong *et al.*, 2005). MCL-1 (~29 kDa) belongs to the Bcl-2 group of proteins that regulate mitochondrial response to external stimuli. MCL-1 prevents apoptosis after signals such as DNA damage or viral infection (Kozopas *et al.*, 1993; Yang, Kozopas and Craig, 1995; Zhou *et al.*, 1997; Cuconati *et al.*, 2003; Derouet *et al.*, 2004). Actions of pro- and anti-apoptotic proteins lead to homeostasis and provide a means for cellular response depending on external factors. Zhong et al. purified HUWE1 after biochemical fractionation of HeLa cell extracts and identified it as a Ub ligase for MCL-1 (Zhong *et al.*, 2005). Further analysis narrowed down the region sufficient for the direct interaction between HUWE1 and MCL-1 to the BH3 domain on HUWE1 (Zhong *et al.*, 2005). Knock down of HUWE1 in HeLa cells led to the concomitant accumulation of MCL-1 and reduced apoptosis after DNA damage compared with WT HUWE1 cells (Zhong *et al.*, 2005). This research resulted in the HUWE1 classification as a “novel member of BH3-only, proapoptotic family proteins” (Zhong *et al.*, 2005).

Further studies have identified a range of new HUWE1 substrates including the transcriptional repressor CTFC, histone H2AX, proliferating cell nuclear antigen (PCNA), and c-MYC and n-MYC (Adhikary *et al.*, 2005; Qi *et al.*, 2012; Inoue *et al.*, 2013; Atsumi *et al.*, 2015; Choe *et al.*, 2016). Attempts to define the role of HUWE1 in the context of regulation of MYC proteins led to two controversial

conclusions. In 2005 Adhikary et al. proposed that HUWE1 acts as an oncogene by mediating Lys-63 poly-ubiquitination of c-MYC and enhancing its transcriptional activity (Adhikary *et al.*, 2005). However, subsequent work by Zhao et al. and Inoue et al. provided strong evidence that HUWE1 acts as a tumour suppressor in cells (Zhao *et al.*, 2008; Inoue *et al.*, 2013). Zhao et al. showed that HUWE1 poly-ubiquitinates n-MYC with Lys-48-linked chains, thereby influencing optimal neuronal differentiation. Knockout of HUWE1 impaired this process but was rescued by the concomitant depletion of n-MYC (Zhao *et al.*, 2008). Inoue et al. reported that HUWE1 suppresses tumorigenic signals induced by oncogenic RAS by targeting c-MYC bound to MIZ1 and marking it for proteasomal degradation (Inoue *et al.*, 2013). Uncontrolled accumulation of the c-MYC/MIZ1 complex leads to the downregulation of the anti-apoptotic genes *P21* and *P15* (Inoue *et al.*, 2013). Finally, recent studies done by Myant et al. showed that HUWE1 plays an indisputable role as an intestinal tumour suppressor, limiting uncontrolled cell proliferation and reducing DNA damage accumulation (Myant *et al.*, 2017).

1.8.4 Targeting HUWE1 activity

Chen et al. proposed that a therapeutic approach in which HUWE1 is inactivated may be more beneficial than targeting MDM2. Since HUWE1 inactivation leads to growth arrest in p53 null cells and induces apoptosis in a WT p53 background, controlled inactivation of HUWE1 could potentially be used as an anti-tumour treatment in a p53-independent manner (Chen *et al.*, 2005). This approach is further supported by the observation that knockdown of HUWE1 led to p53 stabilisation and apoptosis in human osteosarcoma cells (U2OS), breast carcinoma cells (MCF-7), lung adenocarcinoma cells (A549) and fibroblast (NHF-1) (Chen, Brooks and Gu, 2006). Moreover, HUWE1 was found to be highly overexpressed in breast, colon, lung, prostate, liver and pancreas cancers (Confalonieri *et al.*, 2009; Inoue *et al.*, 2013). Recently HUWE1 was proposed as a therapeutic target in multiple melanoma, since its knockdown led to melanoma cell growth arrest and p53 stabilisation (Crawford and Irvine, 2016).

Ever since ARF was reported to target the activities of both MDM2 and HUWE1, there has been an increasing interest in developing ARF-peptidomimetics as potential drugs. It is essential, though, to understand how a small protein can

tightly regulate two mechanistically different enzymes that both have vital functions in cell development and homeostasis. This would allow for more specific and targeted inhibition of either of the p53-regulating ligases, depending on the genetic background of the disease.

1.9 Objectives of the thesis

The objective of my research is to characterise how p14ARF interacts with two families of E3 ligases, RING and HECT E3 ligases. The family of ARF proteins and their anti-tumour properties were first described more than 20 years ago (Ouelle *et al.*, 1995; Serrano *et al.*, 1996). ARF proteins have a potent inhibitory effect on MDM2 - a protein which is essential for cellular homeostasis. Unfortunately, we still lack information on the fundamentals of the MDM2-ARF interaction. This interaction has potential as a platform for the design of new drugs -that moderate the E3 ligase activity of MDM2. The advantages of inhibiting the MDM2 - E2-Ub interaction, as opposed to disrupting MDM2 RING dimerisation or blocking the direct p53 - MDM2 interaction, were presented by our group in the early 2017 (Nomura *et al.*, 2017). As a result, determining how p14ARF influences the ligase catalytic activity of MDM2 could serve as a potential approach towards tuning MDM2 function in a variety of cancers that retain WT p53. Furthermore, a number of reports suggested that ARF can also influences the activity of HUWE1. The first report on p14ARF binding and inhibiting HECT E3 ligase HUWE1 was published more than 10 years ago, however the mechanism remains elusive (Chen *et al.*, 2005). Understanding the details of ARF-inhibition of two mechanistically different enzymes could be a significant advantage in the field of cancer treatment. For this reason, the objectives of this PhD project were:

- To develop a protocol for purification of an MDM2 construct, which could be implemented in *in vitro* studies to characterise the MDM2 - p14ARF interaction.
- To determine if and how p14ARF influences the catalytic activity of MDM2 via biochemical assays, as well as attempting the crystallisation of the MDM2/p14ARF complex, in order to gain detailed structural information on the interaction between the two proteins.
- To verify whether p14ARF can influence the activity of the HECT E3 HUWE1, as well as to characterise the p14ARF-HUWE1 complex via biochemical assays and structural techniques.

2 MATERIALS AND METHODS

2.1 Materials

- Chemicals and Reagents

NaCl, HCl, NaOH, MgSO₄, Na₂SO₄, KCl, tris(2-carboxyethyl)phosphine (TCEP), dimethyl sulfoxide (DMSO), ammonium persulfate (APS), isopropanol, glycerol, acetic acid, urea, reduced glutathione (GSH), adenosine triphosphate (ATP) and boric acid were purchased from Fisher Chemicals. MgCl₂, imidazole, 2-mercaptoethanol (BME), phenylmethylsulfonyl fluoride (PMSF), PIPES, lysozyme, polyethylene glycols (PEGs), Tween20, TritonX, bovine serum albumin (BSA), tetramethylethylenediamine (TEMED), apyrase and acrylamide/bis-acrylamide were purchased from Sigma-Aldrich. Tris(hydroxymethyl)aminomethane (Tris) and agarose were purchased from Melford. SOB Hanahan's Broth, Dithiothreitol (DTT), Isopropyl β-D-1-thiogalactopyranoside (IPTG), L-arginine, L-lysine, ampicillin, kanamycin and 2-(N-morpholino)ethanesulfonic acid (MES) were purchased from Formedium. Ethanol, methanol and guanidine were purchased from VWR. ZnSO₄ and LiCl were purchased from Fluka.

Ethylenediaminetetraacetic acid (EDTA) was purchased from Roche. Ultrapure water was obtained using the A10 Water Purification System from Millipore (MQ).

- Cloning

Codon-optimised double-stranded DNA fragments and DNA primers were purchased from Integrated DNA Technologies. DNA polymerase kits were purchased from Agilent (PfuUltra II HS) and New England Biolabs (Q5 High-Fidelity Master Mix). Restriction digest enzymes and DNA ligase, together with appropriate buffers, were purchased from New England Biolabs. All PCR reactions were carried out using a Bio-Rad Tetrad 2 Thermal Cycler. pGEX-4T-1 and pRSFDuet-1 vectors, with incorporated TEV protease cleavage sequence, were derived from the commercially available vectors from GE Healthcare and Millipore respectively. Bicistronic pAbl vector was derived from pGEX-4T-1 in Brenda Schulman's lab. pCAL-n vector was purchased from Agilent. Max Efficiency DH5α Competent Cells were purchased from Invitrogen, propagated, and treated chemically to generate a stock of competent cells. Ampicillin- or

kanamycin-containing agar plates for bacterial selection were provided by Molecular Technology Services within the Beatson Institute. Sequencing of the constructs and plasmid DNA purification were carried out by Molecular Technology Services within the Beatson Institute. PCR Purification, miniprep DNA isolation and gel extraction were carried out following the protocols included in the kits purchased from QIAGEN.

- Protein expression and purification

BL21(DE3) were purchased from Stratagene, propagated, and treated chemically to generate a stock of competent cells. *E. coli* LB growth medium was provided by Central Services within the Beatson Institute. Coulter J6-MI and Avanti J-25 centrifuges, as well as JS-4.2 and JA-25.50 rotors were purchased from Beckman Coulter. Cells were lysed using the Microfluidics M-110P microfluidiser or Vibra-Cell VCX 750 Sonicator. The proteins were purified using an ÄKTA Explorer system (GE Healthcare) or by gravity pull-down using the appropriate resin from ABT (Glutathione Sepharose and Ni²⁺ Sepharose) or GE Healthcare Life Sciences (SP Sepharose and Q Sepharose Fast Flow exchange). MonoQ, HiPrep 26/10 desalting and size exclusion columns were purchased from GE Healthcare Life Sciences. A KW-403-4F HPLC column was purchased from Shodex. Thrombin from bovine plasma was purchased from Sigma-Aldrich and purified by heparin affinity chromatography. Vector carrying the TEV protease sequence was obtained from Professor Bottomley's lab (Cabrita *et al.*, 2007). Centrifugal filter units, ultrafiltration membrane discs and Amicon stir cells were purchased from Millipore. Dialysis was conducted using SnakeSkin dialysis tubing from Thermo Fisher Scientific or GeBAflex dialysis tubes from Generon. Small-scale buffer exchange was conducted using Zeba spin desalting columns from Thermo Fisher Scientific. NuPAGE 4-12% Bis-Tris polyacrylamide gels, together with NuPAGE MOPS and MES SDS running buffers were purchased from Invitrogen. InstantBlue Coomassie Protein Stain from Expedeon or the Pierce Silver Stain Kit from Thermo Fisher Scientific were used to visualise the protein bands on SDS PAGE gels. Band intensity quantification was done using an Odyssey CLX imager from Licor Biosciences.

- Biochemical analysis and crystallisation:

p14ARF peptides were purchased from Generon. Protein concentrations were assessed using a DeNovix DS-11 spectrophotometer or Bio-Rad Protein Assay Dye and a Beckman Coulter DU 720 Spectrophotometer. GST capture and amine coupling kits were bought from GE Healthcare Life Sciences. Anti GST-V_{HH} purified protein was purchased from Chromotek. SPR analyses were done using a Biacore T200 from GE Healthcare Life Sciences. Fluorescence polarisation measurements were conducted with a QuantaMaster fluorometer from Photon Technology International. Crystallisation screens were purchased from Molecular Dimensions (Morpheus, PACT premier, ProPlex, MIDASplus, BCS), QIAGEN (The Classics Suite, JCSG+, PEGs, AmSO₄ Suite) and Hampton Research (Index). SWISSCI 3-well crystallisation plates from Hampton Research were set up using a Mosquito Crystal Nanolitre robot from TTP Labtech. Plates were stored and imaged in the ROCK IMAGER from FORMULATRIX.

2.2 Methods

2.2.1 Preparation of competent *E. coli* cells

Competent DH5 α and BL21(DE3) *E. coli* cells were generated by Gary Sibbet. Cells were streaked out from the commercially-bought stock, plated on the agarose gel (with no antibiotic present) and allowed to grow overnight at 37°C. Single colony was used to inoculate 10 ml of SOB medium, which was subsequently incubated overnight at 37°C and used to further propagate the bacterial culture in 2x 500 ml of SOB medium. Once the OD₆₀₀ of the culture reached 0.6, cells were spun down and pellets were incubated on ice. Finally, cells were washed, resuspended and incubated for 1 h in ice-cold TB buffer. Addition of the calcium ions (found in the TB medium in the form of CaCl₂, KCl and MnCl₂) improves the uptake of DNA by cells by attracting negatively charged DNA to the membrane (Dagert and Ehrlich, 1979). DNA is allowed to enter into the cell during the heat shock step. 0.2 ml aliquots of DH5 α and BL21(DE3) cells were snap frozen in liquid nitrogen and stored at -80°C.

TB medium contained: 10 mM PIPES, 60 mM CaCl₂ · 2·H₂O, 250 mM KCl, 55 mM MnCl₂ · 4·H₂O

2.2.2 Subcloning into expression vectors and SDM

Protein sequences of the human MDM2, HUWE1 and p14ARF were obtained from UniProt database (Bateman *et al.*, 2017). Protein domain boundaries were assessed using the secondary structure prediction programs JPred and PSIPRED (McGuffin, Bryson and Jones, 2000; Drozdetskiy *et al.*, 2015). Codon-optimised double-stranded DNA fragments were used as template for PCR reactions. Primers were designed to include the appropriate restriction site with an overhang for cleavage efficiency. Efforts were made to design the primers with a melting temperature above 70°C. An example PCR reaction mix is shown in Table 1. For PCR reactions with PfuUltra II DNA polymerase, the following thermocycler parameters were used: an initial denaturation at 95°C for 3 min; 30-35 extension cycles - 95°C 30 sec, 54°C 30 sec, 72°C 40 sec; a final extension at 72°C for 3 min. Amplified DNA fragments were purified with the Qiagen QIAquick PCR Purification Kit and digested with appropriate restriction enzymes at 37°C for 2 h. Digested products were run on a 1.2 % agarose gel and purified using a Qiagen QIAquick Gel Extraction Kit. Ligation of the purified gene products into previously digested vectors was carried out with Quick Ligase following the manufacturer's protocol. Ligation products were transformed into DH5α cells and 5-10 colonies were selected for DNA miniprepping and sequencing.

In order to generate the I3969A and F3982A constructs of HUWE1, site directed mutagenesis (SDM) was carried out. pAbl vector carrying HUWE1 3900-C sequence was amplified using PfuUltra II DNA polymerase and appropriate primers:

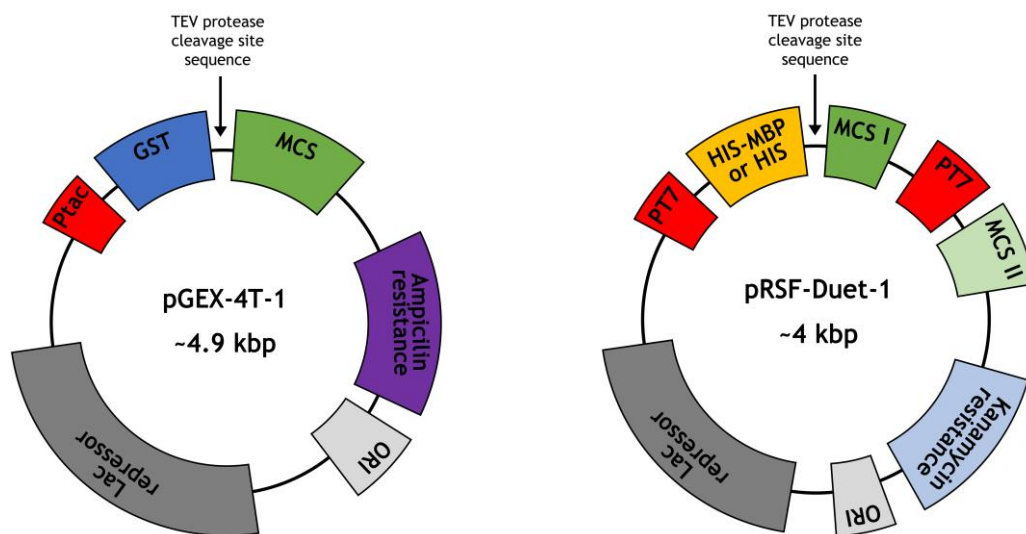
| | |
|-----------------------|--|
| I3969A forward primer | gtcgtgctctgacgcagagcctgattcaacacagtacg |
| I3969A reverse primer | cgtactgtgttgaatcaggctctgcgtcagagcacgac |
| F3982A forward primer | ccaccagaacagcggccggccatccgcta |
| F3982A reverse primer | tagcggatggcccggcctgttctggtgg |

PCR reaction mix, after vector amplification, was incubated with DpnI enzyme at 37°C for 2 h in order to cleave the original vector. DpnI recognises its sequence of interests only when it is methylated - as a result it will cleave the original vector and leave the amplified product carrying the I3969A and F3982A mutations. Reaction mix, purified with the QIAGEN PCR Clean-up kit, was used to transform the DH5 α cells and 5-10 colonies were selected for DNA miniprepping and sequencing.

Details regarding all of the MDM2, p14ARF and HUWE1 constructs, mentioned in this thesis, are listed in Table 2.

Table 1 PfuUltra II HS DNA polymerase 50 μ l-reaction mix

| Component | Stock concentration | Amount per reaction [μ l] | Final concentration |
|--------------------------------|---------------------|--------------------------------|---------------------|
| PfuUltra II reaction buffer | 10X | 5 | 1X |
| dNTP mix | 10 mM /each dNTP | 1 | 0.2 mM /each dNTP |
| DNA template | 100 ng/ μ l | 1 | 2 ng/ μ l |
| Forward primer | 10 μ M | 1 | 0.2 μ M |
| Reverse primer | 10 μ M | 1 | 0.2 μ M |
| DMSO | 100 % | 2.5 | 5 % |
| PfuUltra II HS DNA polymerase | - | 1 | - |
| H ₂ O _{MQ} | - | 37.5 | - |

Figure 2.2-1 *E. coli* expression vectors used in MDM2 and HUWE1 study

pGEX-4T-1 was modified by replacing the thrombin cleavage site with a TEV cleavage site. pRSF-Duet-1 was modified by introducing a TEV protease cleavage sequence between the tag and MCS (multiple cloning site). The pAbo vector was derived from the pGEX-4T-1 backbone by introduction of a second ribosomal binding site followed by an MCS sequence. Plasmid-specific promoters and plasmid-mediated antibiotic resistance sites are indicated.

Table 2 List of constructs described in this thesis

| Construct name | Residues | MW [kDa] | Vector |
|-----------------|-----------|----------|-------------|
| MDM2 FL | 1-491 | 55.2 | pAblo |
| MDM2 210-C | 210-491 | 31.5 | pAblo |
| MDM2 220-C | 220-491 | 30.6 | pAblo |
| MDM2 230-C | 230-491 | 29.7 | pAblo |
| MDM2 240-C | 240-491 | 28.5 | pAblo |
| MDM2 286-C | 361-491 | 23.3 | pAblo |
| MDM2 350-C | 350-491 | 15.9 | pAblo |
| MDM2 361-C | 286-491 | 14.8 | pAblo |
| MDM2 400-C | 400-491 | 10.4 | pAblo |
| MDM2 410-C | 410-491 | 9.3 | pAblo |
| MDM2 428-C | 428-491 | 7.1 | pAblo |
| MDM4 429-C | 429-490 | 6.9 | pAblo |
| p14ARF FL | 1-132 | 13.9 | pRSF-Duet-1 |
| N76p14ARF | 1-76 | 8.4 | pRSF-Duet-1 |
| N56p14ARF | 1-56 | 6.2 | pRSF-Duet-1 |
| N37p14ARF | 1-37 | 4.3 | pRSF-Duet-1 |
| N32p14ARF | 1-32 | 3.8 | pRSF-Duet-1 |
| N20p14ARF | 1-20 | 2.4 | pRSF-Duet-1 |
| 45-64p14ARF | 46-64 | 2.3 | pRSF-Duet-1 |
| 36-55p14ARF | 36-55 | 2.0 | pRSF-Duet-1 |
| 16-32p14ARF | 16-32 | 1.9 | pRSF-Duet-1 |
| 17-32p14ARF | 17-32 | 1.8 | pRSF-Duet-1 |
| HUWE1 FL | 1-4374 | 481.9 | pGEX-4T-1 |
| HUWE1 3753-C | 3753-4374 | 71.4 | pGEX-4T-1 |
| HUWE1 3796-C | 3796-4374 | 66.8 | pGEX-4T-1 |
| HUWE1 3878-C | 3878-4374 | 57.7 | pGEX-4T-1 |
| HUWE1 3900-C | 3900-4374 | 55.3 | pGEX-4T-1 |
| HUWE1 3753-3843 | 3753-3843 | 9.8 | pGEX-4T-1 |
| HUWE1 3843-3902 | 3843-3902 | 6.9 | pGEX-4T-1 |

2.2.3 Protein expression

Vectors carrying the desired DNA sequence were transformed into BL21(DE3) cells. A single colony was used to inoculate 4 ml of LB media with appropriate antibiotic (100 µg/ml of ampicillin or 50 µg/ml of kanamycin). The inoculated medium was incubated overnight at 37°C and transferred into 2 L baffled flasks containing 1 L of pre-warmed sterile LB containing the appropriate antibiotic. For co-expression of two constructs, 10 ml of pre-culture was used with both ampicillin (100 µg/ml) and kanamycin (25 µg/ml) present. 1 L of bacterial culture was used for small-scale test expression and purification and large-scale expressions were conducted using 6 - 100 L of LB, depending on the construct. Cells were incubated in a shaker at 37°C and 200 rpm until the optical density of the culture measured at 600 nm (OD_{600}) reached ~0.3. At this point, the temperature was lowered to 20°C. When the OD_{600} reached a value of 0.6-0.7, expression was induced by adding 1 ml of 0.2 M IPTG per flask. Cells were left shaking at 20°C overnight. Cells were harvested by centrifugation in 1 L centrifuge tubes at 4°C, 4500 g for 15 min using a Beckman JS-4.2 rotor. Cell pellets were resuspended in an appropriate buffer (similar to wash buffer) and transferred into 50 ml conical tubes. PMSF was added to a final concentration of 2.5 mM, and for small-scale test expressions, lysozyme (1 mg/ml) was added as well. Resuspended pellets were frozen in liquid nitrogen and stored at -20°C, -40°C or -80°C.

2.2.4 Protein purification

Buffers for GST-tag protein purification:

Wash buffer: 50 mM Tris-HCl pH 7.6, 200 mM NaCl, 1 mM DTT

Elution buffer: 50 mM Tris-HCl pH 8.0, 200 mM NaCl, 5 mM DTT, 10 mM GSH

Buffers for His-MBP/His-tag protein purification:

Wash buffer: 25 mM Tris-HCl pH 7.6, 200 mM NaCl, 20 mM imidazole, 5 mM BME

Elution buffer: 25 mM Tris-HCl pH 7.6, 200 mM NaCl, 200 mM imidazole, 5 mM BME

Buffers for anion-exchange chromatography:

Buffer A: 50 mM Tris-HCl pH 7-8.5, 1 mM DTT

Buffer B: 50 mM Tris-HCl pH 7-8.5, 1 mM DTT, 1 M NaCl

Buffers for cation-exchange chromatography:

Buffer A: 50 mM MES pH 6-6.5, 1 mM DTT

Buffer B: 50 mM MES pH 6-6.5, 1 mM DTT, 1 M NaCl

Buffers for gravity SP Sepharose pull-down:

Dilution buffer: 50 mM MES pH 6.5, 5 mM DTT

Wash buffer: 50 mM MES pH 6.5, 70 mM NaCl, 5 mM DTT

Elution buffer: 50 mM Tris-HCl pH 8.0, 400 mM NaCl, 5 mM DTT

2.2.4.1 Small-scale purification

Frozen pellets were thawed in cool water and cells were lysed using a Vibra-Cell VCX 750 sonicator set to a 70 % amplitude with 8 pulses of 8 s on and 8 s off.

Lysates were clarified by centrifugation for 20 min at 48200 g in a Beckman JA-25.50 rotor at 4°C. Clarified lysate was decanted into a fresh centrifugation tube and centrifugation repeated under the same conditions. 350 µl of GSH-sepharose or Ni²⁺-resin per litre of bacterial culture was equilibrated with the corresponding wash buffer. Clarified lysate was added to resin equilibrated in wash buffer and gently rocked for 1 h at 4°C. This mixture was transferred to gravity, poly-prep columns (Bio-Rad) and washed until no protein was detectable in the flow-through with Bio-Rad protein dye. Protein was subsequently eluted in 350 µl-fractions with the appropriate elution buffer. Protein concentrations of each fraction were determined using either the DeNovix nano-drop system (Equation 1), where the predicted molar extinction coefficient of a protein was calculated using the ProtParam tool or a Bradford assay with Bio-Rad protein dye, using BSA as a standard (Gasteiger *et al.*, 2005; Bradford, 1976;).

Equation 1 The Beer-Lambert law states that the absorbance value at 280 nm wavelength (A_{280}) is proportional to the protein concentration (conc), where ϵ - molar extinction coefficient, l - light path length (Swinehart, 1962)

$$A = \text{conc} [M] \cdot \epsilon [M^{-1}cm^{-1}] \cdot l [cm]$$

Double pull-down purification protocol was used for co-expression of two different constructs. One of the proteins was expressed with a 6xHis-containing tag (e.g. His-MBP), whereas the second protein was expressed in GST-tagged form. Clarified cell lysate was first equilibrated with Ni²⁺ resin in a manner described above, followed by washing step and elution from the Ni²⁺ beads. Obtained protein sample was subsequently equilibrated with GSH resin. After washing the GSH resin with appropriate buffer, the sample was eluted from the GSH beads and the protein composition was assessed on an SDS-PAGE gel. If two proteins form a complex, their presence should be detectable in both steps of a double pull-down.

Identity of the overexpressed and purified MDM2 and p14ARF construct was confirmed by MS analysis conducted by the Beatson Proteomics facility. Samples were provided in a form of an SDS PAGE gel, where specific protein bands were selected for the analysis in order to confirm their identity.

2.2.4.2 Large-scale purification

Bacterial pellets were thawed in cool water and lysed using a microfluidiser at a pressure of 20000 psi. The volume of beads used for each pull down was estimated based on the protein stability and yield obtained from the small-scale test purification. For example, GST-MDM2 230-C, obtained from 100 L of LB bacterial culture, was pulled down using 40 ml of GSH-sepharose, whereas GST-HUWE1 3796-C, obtained from 6 L of LB culture was pulled down with 10 ml of GSH-sepharose.

Purification of some of the enzymes used in the biochemical assays was conducted by other lab members:

- TEV construct was expressed with a 6xHis tag, incubated with Ni²⁺ resin, and subsequently eluted from the beads with a buffer containing 10% glycerol. Eluted fraction was concentrated, aliquoted, snap frozen in liquid nitrogen and stored at -80°C. TEV was added to the protein of interest at 1:50 (TEV:protein ratio) and incubated overnight at 4°C.

- UBA1 from *Arabidopsis thaliana* was expressed without a tag, incubated with GST-Ub and Mg^{2+} -ATP to form GST-Ub-E1, and subsequently pulled-down using GSH sepharose beads. E1 was eluted from the GST-Ub-E1-GSH sepharose bound complex by using 25 mM DTT to cleave the thioester bond. E1 was further purified using SourceQ anion-exchange chromatography.
- Ubch5B (UBE2D2) was expressed with no tag and purified using SP Sepharose beads followed by cation exchange chromatography with a SourceS column. Contaminant-free fractions were concentrated and loaded onto a HiLoad 26/600 Superdex 75 chromatography column.
- Ub used in the activity assays was expressed with a 6xHis tag and purified by Ni^{2+} -affinity pull down followed by cleavage with TEV protease, Ni^{2+} -affinity pass-back and size exclusion chromatography with a HiLoad 26/600 Superdex 75 column.
- Ubch5B S22R C85K-Ub for SPR analysis was purified by incubation of Ubch5B S22R C85K with UBA1 and 6xHis-Ub, followed by Ni^{2+} -affinity pull down, TEV protease cleavage and purification by SourceS cation exchange chromatography.

2.2.5 Analytical gel filtration and HPLC

The oligomeric state of MDM2 was assessed using a 10/300 GL Superdex 200 analytical gel filtration column with a flow rate of 500 μ l/min and 200 - 300 μ l injected sample volume. This column contains an agarose base matrix with an average bead size of 8.6 μ m and can be used to separate a mixture of molecules with MW below 440 kDa. The preparation of HUWE1 for HPLC-SAXS analysis, as well as estimation of the HUWE1 oligomeric state in the presence of p14ARF were conducted using a Shodex KW-403-4F HPLC column with a flow rate of 160 μ l/min and 50 μ l injected sample volume. This column contains a silica-based matrix and provides high-resolution separation of molecules with MW below 600 kDa.

2.2.6 Denaturing and native gel analysis

SDS-PAGE was used to evaluate protein purification steps, as well as to read-out biochemical assays, including single-turnover lysine discharge and an E3 auto-ubiquitination. Prior to loading on the gel, protein sample was mixed with the 4x NuPAGE LDS loading buffer and incubated at 95°C for 5 min. All SDS-PAGE gels presented in this thesis contain no reducing agent in the NuPAGE LDS loading buffer. MES/SDS running buffer was used for most of the analysis, allowing for an optimal separation of proteins in the MW range of 25-60 kDa. MOPS/SDS was used to visualise the formation of higher-order poly-Ub chains during E3-auto-ubiquitination. SDS-PAGE gels were run for 35 min at 200 V and stained with InstantBlue Coomassie dye, which interacts with the amino and carboxyl groups of proteins. Silver staining was used as an alternative approach to detect very low amounts of protein. Silver ions readily interact with certain protein functional groups (such as carboxyl groups, imidazole and amines) providing a more sensitive method for band detection compared with Coomassie stain. When required, band intensity was quantified using an Odyssey infrared imaging system.

Non-denaturing (native) PAGE was used to determine the oligomeric state of purified fractions of MDM2. Unlike SDS-PAGE, native-PAGE allows for the protein separation based not only on size, but also overall charge. This technique facilitates the distinction between dimeric and oligomeric fractions of MDM2, which are indistinguishable on SDS-PAGE gel. 1xTris-boric Acid pH 8.0 was used as a running buffer at 4°C for 1.5 h at 130 V. Gel composition is shown in Table 3.

Table 3 Reaction mix for the preparation of 4.5% native polyacrylamide gels

| Component | Stock concentration | Amount per 100 ml of gel | Final concentration |
|--------------------------------|---------------------|--------------------------|---------------------|
| Acrylamide/bis-acrylamide | 40 % | 11.2 ml | 4.48 % |
| Tris-boric acid pH 8.0 | 5X | 20 ml | 1X |
| Glycerol | 100 % | 2 ml | 2 % |
| TEMED | 100 % | 82.5 μ l | 0.0825 % |
| APS | 10 % | 500 μ l | 0.5 % |
| H ₂ O _{MQ} | - | 66 ml | - |

2.2.7 Single-turnover lysine discharge assays

Lysine discharge assays were used to assess the potency of E3 enzymes in discharging E2~Ub to free lysine present in solution. Each assay comprises three steps:

1. A pulse step (100 μ l) was used to charge E2 (Ubch5B or Ubch7) with Ub in the presence of E1 (UBA1 from *Arabidopsis thaliana* or UBE1 from *Homo sapiens*). 10X buffer (500 mM Tris-HCl pH 8.0, 500 mM NaCl, 50 mM MgCl₂, 20 mM ATP pH 7.5) was added to provide optimal conditions for enzyme activity (Table 4). Charging of E2 was carried out for 15~20 min either at RT (for Ubch5B) or at 37°C (for Ubch7).
2. A stop solution (60 μ l) containing apyrase and EDTA was prepared and added to the pulse reaction to inhibit E1 and prevent generation of more E2~Ub during the E3-facilitated discharge (Table 5). EDTA chelates the Mg²⁺ ions, and apyrase catalyses the hydrolysis of ATP. Both Mg²⁺ and ATP are required for E1 catalytic activity. After stop solution was added, the reaction was left at RT for ~5-10 min.
3. The chase solution (20 μ l) contained a mixture of E3 and lysine in appropriate buffer conditions (Table 6). A control that contained only buffer and lysine was used to monitor the rate of Ub discharge from E2 without any E3 present.

After the pulse reaction and stop solution were mixed (yielding 160 μl of reaction volume), three aliquots of 48 μl of this mixture were transferred to fresh Eppendorf tubes. 8 μl from each tube was transferred to a new tube with ~4 μl of SDS-containing loading dye - this represents the initial E2-Ub pool available for discharge and is referred to as time '0'. 10 μl of chase solution was added to initiate the lysine discharge reaction. 10 μl aliquots were taken from the reaction at selected time points (Table 7) and added to loading dye to quench the discharge. Proteins were separated using SDS-PAGE and visualised as indicated in figure legends. E2-Ub levels were monitored and compared with the amount present at time 0. Concentrations of reagents in the final mix were as follows: E1 ~400 nM, E2 ~ 7.5 μM , Ub ~ 55 μM , E3 ~ 200-500 nM (depending on the construct), lysine ~ 150 mM.

2.2.8 Auto-ubiquitination assay

Two variants of the auto-ubiquitination assay were implemented to assess the activity of different E3 enzymes. In standard auto-ubiquitination assays, sufficient Ub and E1 were included to continually reload the E2 during the course of the reaction; this type of reaction was used to monitor the rate of poly-Ub chain formation in the presence of E3. Single-turnover auto-ubiquitination assays were used to investigate the rate of poly-Ub chain formation as well as the discharge of Ub from E2 and run in conditions similar to the lysine discharge assay in which E2 cannot be recharged with Ub once E3 is added. For these single-turnover auto-ubiquitination reactions, a pulse reaction was prepared in a manner resembling the lysine discharge assay. Following a 20 min pulse step, EDTA was added to stop the charging of E2. Then E3 was added at concentrations ranging from 2 to 6 μM , depending on the activity of the enzyme. A sample setup for a single-turnover auto-ubiquitination reaction is shown in Table 8. A comparison of reaction schemes for the described assays is shown in Figure 2.2-2.

Table 4 Components of the lysine discharge pulse reaction

| Component | Volume [μ l] | Stock concentration | Final concentration |
|--------------------------------|-------------------|---------------------|---------------------|
| Buffer | 10 | 10X | 1X |
| E1 | 2.5 | 35 μ M | 1 μ M |
| E2 | 5.6 | 255 μ M | 14 μ M |
| Ub | 6.7 | 1640 μ M | 110 μ M |
| NaCl | 4 | 5 M | 200 mM |
| H ₂ O _{MQ} | 71.2 | - | - |

Table 5 Components of the lysine discharge stop solution

| Component | Volume [μ l] | Stock concentration | Final concentration |
|--------------------------------|-------------------|---------------------|---------------------|
| Tris-HCl pH 8.0 | 8 | 1 M | 50 mM |
| NaCl | 4.8 | 5 M | 400 mM |
| EDTA | 8 | 0.5 M | 67 mM |
| Apyrase | 1.6 | 1 U/ μ l | 0.03 U/ μ l |
| H ₂ O _{MQ} | 37.6 | - | - |

Table 6 Components of the lysine discharge chase solution

| Component | Volume [μ l] | Stock concentration | Final concentration |
|--------------------------------|----------------------|---------------------|---------------------|
| E3 | 1-9.2 | - | 200-500 nM |
| Lysine pH 7.6 | 9 | 1.7 M | 0.77 M |
| Tris-HCl pH 8.0 | 1 | 1 M | 50 mM |
| NaCl | 0.8 | 5 M | 200 mM |
| H ₂ O _{MQ} | Top up to 20 μ l | - | - |

Table 7 An example of the time points implemented to compare three independent lysine discharge reactions

| Event | Timer reading | | |
|-----------|---------------|------------|--------------|
| | Reaction 1 | Reaction 2 | Reaction 3 |
| Step 0 | - | - | - |
| Add chase | 0 | 15 s | 30 sec |
| Step 1 | 40 s | 55 s | 1 min 10 sec |
| Step 2 | 1 min 30 s | 1 min 45 s | 2 min |
| Step 3 | 2 min 30 s | 2 min 45 s | 3 min |
| Step 4 | 4 min | 4 min 15 s | 4 min |

Table 8 An example of a single-turnover auto-ubiquitination assay mix

| Component | Volume [μ l] | Stock concentration | Final concentration |
|--------------------------------|----------------------|---------------------|---------------------|
| Buffer | 6 | 10X | 1X |
| E1 | 1.5 | 35 μ M | 1 μ M |
| E2 | 2.8 | 255 μ M | 12 μ M |
| Ub | 2 | 1640 μ M | 55 μ M |
| NaCl | 4 | 5 M | 200 mM |
| EDTA | 3 | 0.5 M | 25 μ M |
| E3 | varying | - | 2-6 μ M |
| H ₂ O _{MQ} | Top up to 60 μ l | - | - |

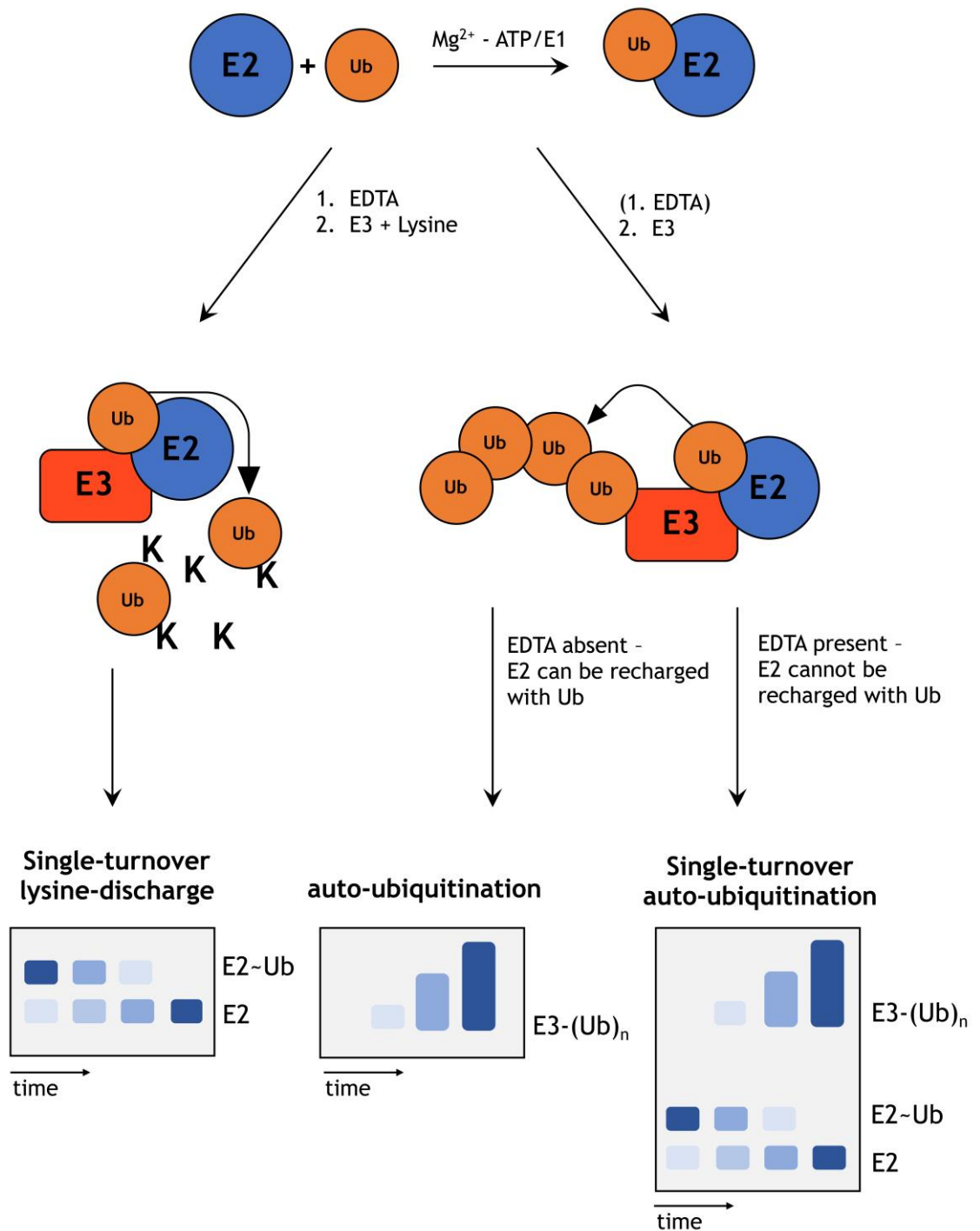


Figure 2.2-2 Comparison of lysine-discharge and auto-ubiquitination reactions

Lysine discharge and auto-ubiquitination reactions both require pre-charging of a selected E2 with Ub. Single-turnover lysine discharge assay allows for monitoring of the Ub discharge from E2 over time in the presence of E3. Each reaction step contains a set amount of E2-Ub which can be visualised on SDS-PAGE gels and is reflected in the intensity of the E2-Ub band. Single-turnover auto-ubiquitination assays allow for controlled poly-Ub chain formation on the surface of E3 by limiting the amount of E2-Ub and are visualised by the simultaneous disappearance of E2-Ub and formation of higher-order E3-(Ub)_n bands on the gel. Standard auto-ubiquitination assays, in which E2 is continuously recharged with Ub, are used to solely monitor formation of E3-(Ub)_n species.

2.2.9 Surface plasmon resonance assay (SPR)

SPR was used to determine the binding affinity between E2-Ub and MDM2. The SPR technique uses the phenomenon of electron movement (plasmon) in the metal surface layer in response to a photon of incident light hitting that surface. The SPR angle at which this movement occurs is dependent on the refractive index of the material near the surface of the metal (i.e. chip coating and captured ligands). As a result, detection is carried out by measuring the changes in reflected light, specifically its intensity and resonance angle shift. Changes in the resonance angle are proportional to the mass of the material bound on the metal layer (i.e. ligand-analyte interaction) (Figure 2.2-3). Resonance Units (RUs) are used as a read-out of the angle shift, where 1RU is equivalent to a 10^{-4} degree angle shift. In SPR experiments, these changes in resonance units are proportional to binding events between analyte and ligand. As a result, SPR allows estimation of binding affinity and kinetics for protein-protein, protein-DNA, receptor-drug etc interactions (Quinn *et al.*, 2000).

Anti-GST nanobodies were coupled to the surface of a CM5 chip. Nanobodies are antigen-specific, heavy chain-only antibodies (Muyldermans, 2013). GST-MDM2 variants were captured at a concentration range of 100-200 $\mu\text{g/ml}$ and purified GST was captured as a control. Ubch5B S22R C85K-Ub was titrated in the running buffer (200 mM NaCl, 25 mM Tris-HCl pH 7.6, 1 mM DTT, 100 $\mu\text{g/ml}$ BSA, 0.005 % Tween20), in incrementing steps from 49 nM to 100 μM . 10 washing cycles were implemented before the analyte was applied, and additional buffer control runs were provided between every 4th cycle of measurements. The experiment was run at RT, with 30 $\mu\text{l/min}$ flow rate, 24 s contact time and 60 s dissociation time. The data were analysed by steady-state affinity analysis using the T200 BioCore Evaluation Software and GrapPad Prism program.

2.2.10 Fluorescence polarisation assay (FP)

Fluorescence polarisation (FP) assays were used to determine the binding affinity between p14ARF and HUWE1. The principle of this technique is based on the correlation between a fluorophore's polarisation and molecular rotation. FP is defined as the difference between fluorescence intensities parallel and perpendicular to the excitation plane (Equation 2). Rapid rotation (and high light

depolarisation) is characteristic for small fluorophore-labelled ligand, whereas upon binding to a substantially bigger partner, the ligand-binding partner complex will show a decrease in rotation rate followed by a decrease in light depolarisation (Figure 2.2-4) (Lea and Simeonov, 2011). The degree of light depolarisation at different stages of titration with the binding partner is used to determine the binding affinity between two components.

Equation 2 Fluorescence polarisation is defined as a difference between fluorescence intensities parallel (I_{\parallel}) and perpendicular (I_{\perp}) to the excitation plane, normalised by the total emission intensity

$$FP = \frac{I_{\parallel} - I_{\perp}}{I_{\parallel} + I_{\perp}}$$

FP measurements were done in a buffer containing 25 mM Tris-HCl pH 7.6, 200 mM NaCl, 1 mM TCEP. N37p14ARF N-terminally labelled with 6-carboxyfluorescein was diluted in 400 μ l of buffer to a concentration of 1 μ M. HUWE1 3796-C (stock concentration of 174 μ M) was titrated into the 6-carboxyfluorescein-N37p14ARF solution starting at 0.5 μ M in two-fold concentration-increasing steps. Relative polarisation at each step was recorded for 100 s. Data were recorded with excitation at 490 nm and emission at 520 nm.

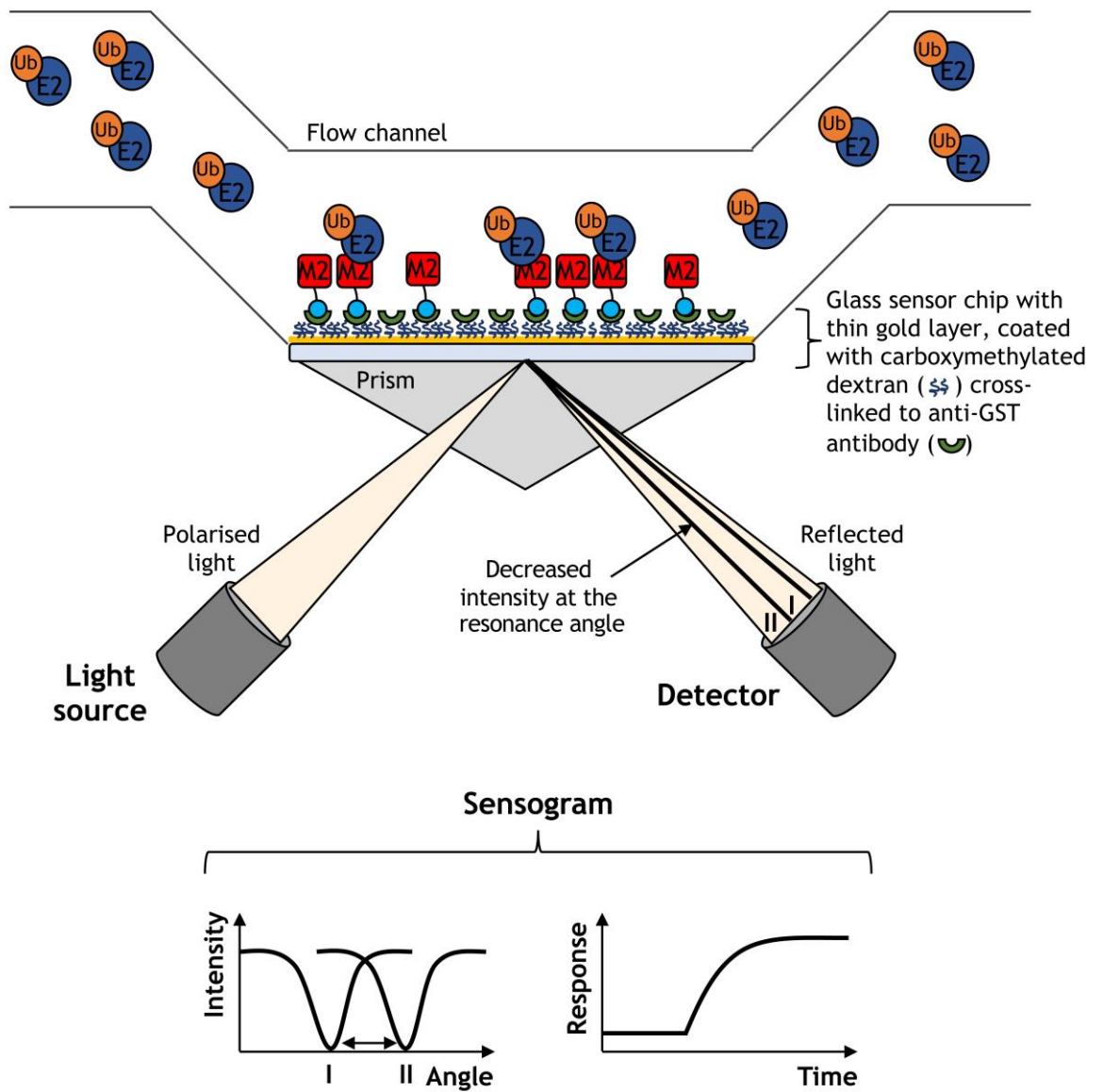


Figure 2.2-3 Principle of the SPR experiment

GST-MDM2 variants were used as ligands and captured on CM5 chips. Several concentrations of UbcH5B-Ub (analyte) were flowed over ligand and the change in refractive index measured. The change in the refracting angle is representative of the change in the mass of the surface material i.e. MDM2-E2-Ub binding. Figure adapted from Cooper (2002).

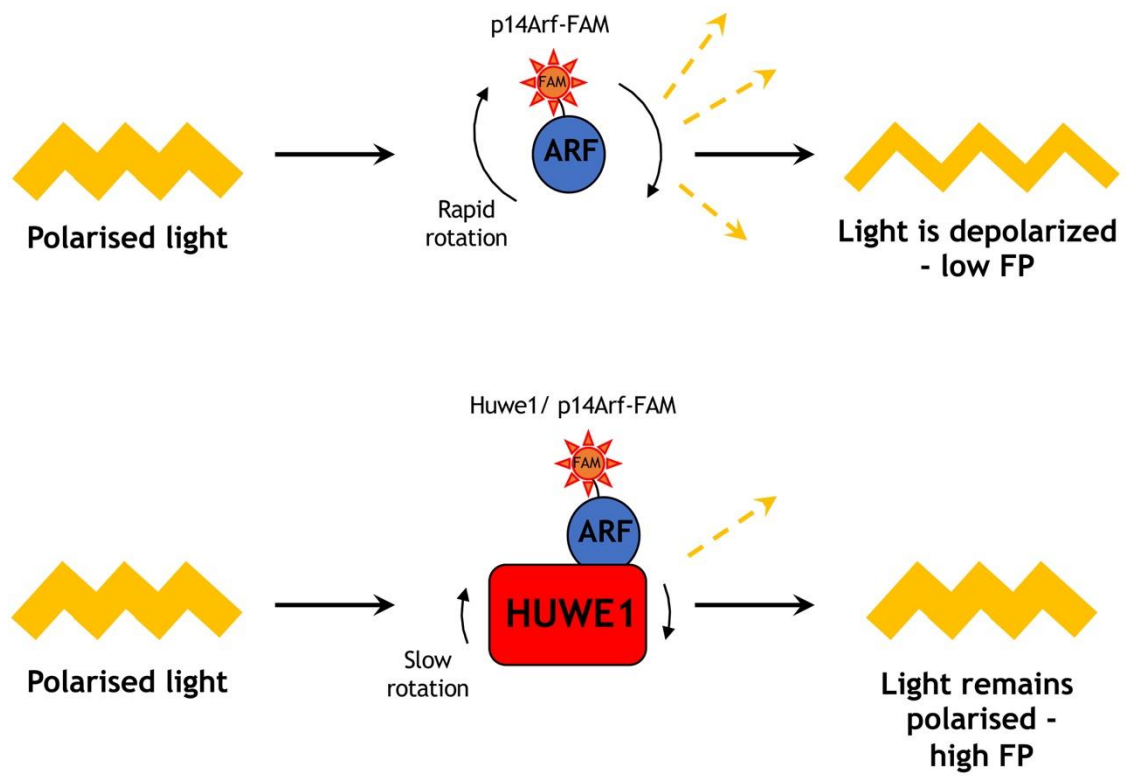


Figure 2.2-4 Principle of the FP experiment

Rapidly rotating fluorescently-labelled small molecules lead to the depolarisation of incident light, resulting in low FP readings. Upon binding to a high-MW partner, rotation slows down, leading to an increase in polarisation of light.

2.2.11 Small angle X-ray scattering (SAXS)

Both X-ray crystallography and SAXS rely on the diffraction of incident X-rays by electrons. SAXS is used to investigate the structural properties of molecules in solution, resulting in the characterisation of their size and shape, as well as providing information on flexibility and aggregation. In a SAXS experiment, a monochromatic X-ray beam is applied to a protein solution and the intensities of the scattered X-rays are recorded (Figure 2.2-5). The same procedure is applied to the buffer, allowing for its subtraction from the sample solution and resulting in the extraction of signal specific to the molecules in solution. The obtained scattering intensity (I) is radially symmetric and is represented as a function of the magnitude of the scattering vector (q) (Equation 3 and Figure 2.2-5) (Kachala, Valentini and Svergun, 2015; Kikhney and Svergun, 2015).

Equation 3 Scattering intensity (q) is a function of the momentum transfer, where λ is the wavelength and θ represents half of the scattering angle

$$q = \frac{(4\pi \cdot \sin\theta)}{\lambda}$$

A particle's molecular weight, radius of gyration (R_g) and maximum dimension (D_{\max}) can be extracted from its experimental scattering pattern. R_g is a mass-weighted average radius of the molecule and is derived using the Guinier approximation (Equation 4). At low q values the Guinier plot of $\log I(q)$ vs q^2 will give a straight line, from which R_g and $I(0)$ can be determined (Kachala, Valentini and Svergun, 2015; Kikhney and Svergun, 2015).

Equation 4 The Guinier approximation provides information on the radius of gyration and intensity value at $q=0$ of a particle in solution

$$I(q) = I(0)\exp\left[-\frac{q^2 \cdot R_g^2}{3}\right]$$

Another way to extract information about a molecule's shape and size is to determine a real space representation $P(r)$ (pair distance distribution function) (Equation 5) by calculating the indirect Fourier transform of the intensity profile. $P(r)$ is typically constrained to be 0 when $r=0$ Å and $r \geq D_{\max}$ (Figure 2.2-6) (Kachala, Valentini and Svergun, 2015; Kikhney and Svergun, 2015).

Equation 5 The $P(r)$ function describes the distances between electrons in the analysed molecule

$$I(q) = \int P(r) \frac{\sin(qr)}{qr} dr$$

Finally, information about a protein's folded state can be extracted from the Kratky plot ($q^2I(q)$ vs q). Analysis of the curve's shape provides insights into globularity and the presence of flexible or unfolded regions (Figure 2.2-6).

2.2.11.1 HPLC-SAXS data collection for HUWE1 constructs

Data were collected at Diamond Light Source beamline B21. 50 μ l of a sample containing HUWE1 construct was run on a Shodex KW-403-4F HPLC column in 25 mM Tris-HCl pH 7.6, 200 mM NaCl, 1 mM TCEP, 5 % DMSO at 160 μ l/min, prior to being exposed to X-ray radiation. N37p14ARF peptide was introduced to HUWE1 3796-C at 6 molar excess and to HUWE1 3900-C at 2 molar excess, to minimise HUWE1 3900-C precipitation. HUWE1 alone and HUWE1/p14ARF complexes were injected at concentrations ranging between 5-7 mg/ml to assure that the peak fractions were sufficiently concentrated to yield strong signals. Data were analysed using the ScÅtter program version 3.1r (*Bioisis: welcome - index*).

2.2.11.2 Generation of the *ab initio* model of HUWE1 3900-C

A reduced dataset, obtained after determination of the Guinier region and analysis of the $P(r)$ distribution function, was used in order to model the shape of HUWE1 3900-C based on its SAXS profile. An initial model was generated using P2 symmetry and the DAMMIF program and was further refined with an implementation of 17 independent runs of the DAMMIN program. The most probable model was chosen and averaged using the DAMAVER package and aligned with the crystal structure of HUWE1 3900-C with SUPCOMB program (Svergun, 1999; Kozin and Svergun, 2001; Volkov and Svergun, 2003; Franke and Svergun, 2009).

2.2.12 X-ray crystallography

Protein X-ray crystallography is used to obtain high-resolution molecular structures. Since diffraction from a single molecule is undetectable, protein

molecules are driven into a crystal form, leading to amplification of the signal. In protein crystals, atoms are periodically and systematically organised, giving rise to a crystal lattice of repeating units. When X-ray beams hit a crystal lattice at a specific angle (θ), a fraction of light undergoes diffraction at the same angle, whereas some will travel through the crystal and interact with subsequent crystal planes. Upon scattering of X-rays from a crystal lattice, peaks of scattered intensity are observed, which correspond to the constructive interference of diffracted waves, giving rise to a diffraction spot (reflection). This phenomenon is described by Bragg's Law and is used to extract information about the crystal (Figure 2.2-7) (Patrick, 2007; Rupp, 2010). The position of each reflection on the detector, reflects the direction in which the particular X-ray beam was diffracted from the crystal, whereas the optical density of the spot corresponds to the intensity of the X-ray beam reaching a given position on the detector (Patrick, 2007; Rupp, 2010). The beam direction is described by a set of three coordinates: h , k and l for each reflection. Those coordinates are used to assign the position of an individual reflection in the reciprocal space, which is the Fourier transform of the atomic positions in the crystal and inversely related to the real space. Finally, each diffracted X-ray is described by a structure-factor equation F_{hkl} , which is a sum of a number of wave equations, one for a diffraction by each atom (Patrick, 2007; Rupp, 2010).

Whilst exposed to X-ray radiation, a crystal is rotated to ensure that data is collected for all angles of incidence on a crystal plane. Initial data processing includes indexing of the diffraction spots, which allows for the identification of the crystal lattice and unit cell dimensions. There are seven crystal lattice systems and each of them is characterised by the smallest repeating unit, referred to as the unit cell. Since the crystal undergoes rotation during measurement, the obtained data set may contain multiple records of a single reflection. These are merged and scaled, resulting in a processed data set. Fourier transform of the two-dimensional diffraction images is used to obtain an electron density model from the collected data (Equation 6) (Patrick, 2007; Rupp, 2010). The equation for the electron density (ρ [$e \cdot \text{\AA}^{-3}$]) is shown below, where V [\AA^3] is the unit cell volume and each F_{hkl} term is a structure factor representing a single reflection:

Equation 6 Electron density as a Fourier sum

$$\rho_{(x,y,z)} = \frac{1}{V} \sum_h \sum_k \sum_l F_{hkl} \cdot e^{-2\pi i(hx+ky+lz)}$$

Two critical parameters need to be known to determine the X-ray structure of the protein - wave amplitude and phase. The amplitude of the diffracted wave is extracted from the intensity, and the phase can be provided by various approaches, such as molecular replacement, isomorphous replacement or anomalous dispersion (Patrick, 2007; Rupp, 2010). Molecular replacement implements an existing structure of a homologous protein as a model, which is then used to determine the placement and orientation of the molecules in the unit cell.

2.2.12.1 HUWE1 3900-C crystal optimisation

Initial screening for crystals of HUWE1 3900-C was performed using 7 different screens (The Classis Suite, PropPLex, Index, JCSG+, Morpheous, PEGs Suite and PACT). HUWE1 3900-C stock was at 290 μ M concentration in a buffer containing: 25 mM Tris-HCl, 200 mM NaCl and 1 mM DTT. Initial crystals were grown using a sitting-drop vapour diffusion, where the hits occurred in the JCSG+ screen in a condition with 24 % w/v PEG1500 and 20 % v/v glycerol. After optimisation, data were collected for crystals of HUWE1 3900-C grown in 21 % w/v PEG3350, 20 % v/v glycerol, Tri-HCl pH 9.0 using a hanging-drop technique.

2.2.12.2 HUWE1 3900-C data collection, processing and refinement

Data were collected at Diamond Light Source beamline I02: $\lambda=0.9795$ Å, 100% transmission, 0.1 s exposure and 0.1° oscillation. 1800 images were collected. Cell content analysis (number of molecules in the asymmetric unit and solvent content) were done using the MATTHEWS_COEF program (Matthews, 1968). The structure was solved by molecular replacement with PHASER using HUWE1 3993-C (PDB code 3H1D) as a search model (McCoy *et al.*, 2007; Pandya *et al.*, 2010). The model was visualised and adjusted using COOT and further refined using PHENIX with non-crystallographic symmetry restraints (Emsley and Cowtan, 2004; Adams *et al.*, 2010). Refined structure was validated using MolProbity

program, where torsion angles, bond lengths and angles, as well as the Van der Waals contacts were evaluated (V. B. Chen *et al.*, 2010).

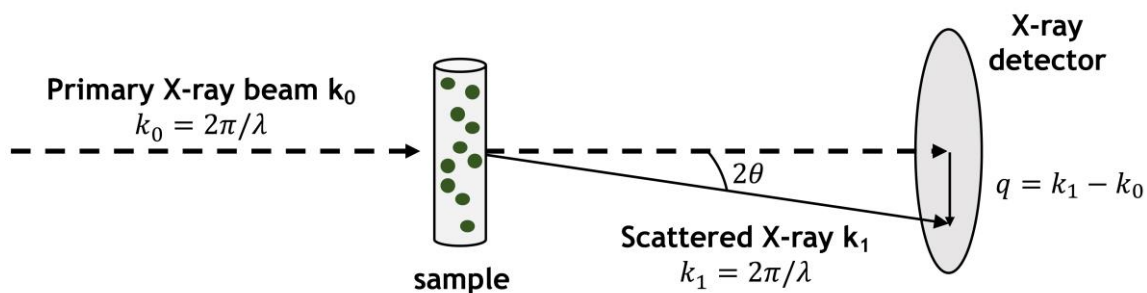


Figure 2.2-5 Schematic representation of a SAXS experiment

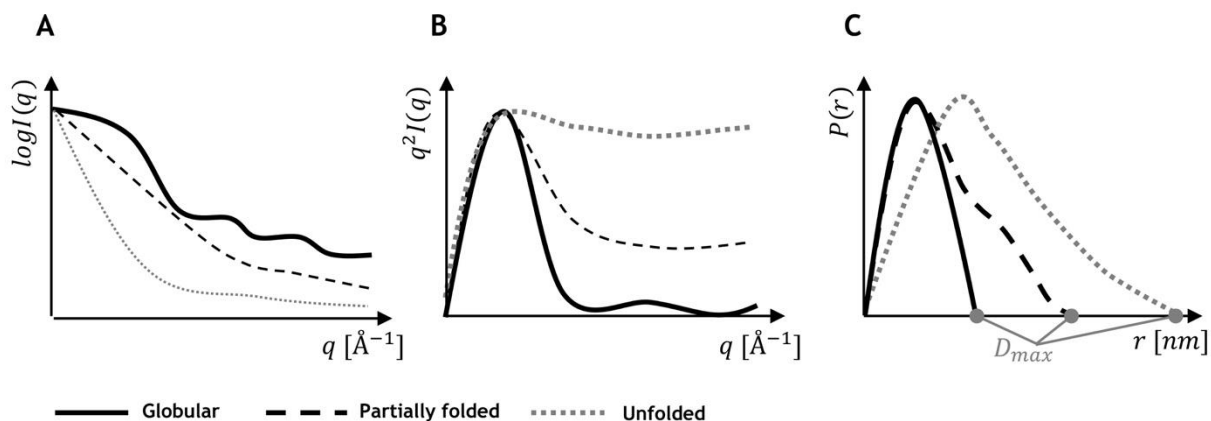


Figure 2.2-6 An example of data obtained from a SAXS experiment

(A) Logarithmic plot of the scattering intensity (I) with respect to the scattering vector (q). (B) A Kratky plot $q^2 I(q)$ vs q provides information on protein compactness. (C) Distance distribution function $P(r)$ provides information on a protein's maximum dimension (D_{\max}).

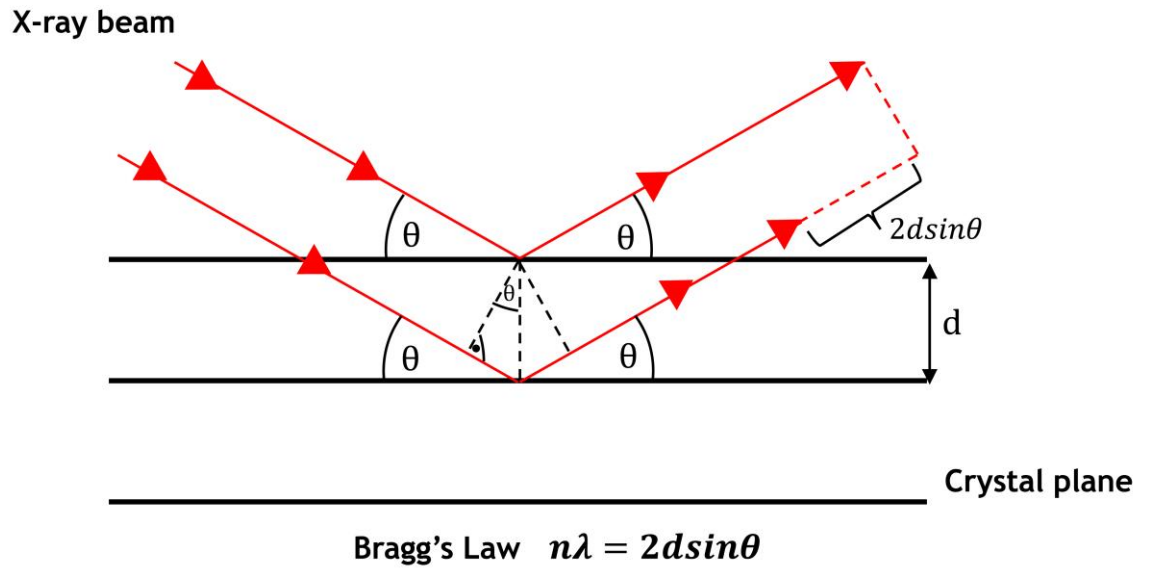


Figure 2.2-7 Bragg diffraction

A diffraction pattern is produced only when X-rays scattered from a crystal plane fulfil the condition for maximum intensity, described by Bragg's Law. λ is the wavelength and θ is the diffraction angle.

3 RESULTS

3.1 Purification of MDM2 constructs

MDM2 has been reported to be a very challenging protein for *in vitro* studies. In 2007, Poyurovsky et al. showed that MDM2 RING domain (residues 400-491), which was expressed and purified from both *E. coli* and insect cells, eluted as a broad peak consistent with oligomers ranging from 100 to 600 kDa during gel filtration chromatography, which correlates with the presence of 5 to 30 copies of MDM2 RING dimer (Poyurovsky *et al.*, 2007). These oligomers were 50 nm in diameter when examined by negative staining electron microscopy and exhibited catalytic activity towards E2-Ub discharge. This study suggested that a supramolecular assembly of the MDM2 RING domain is a biologically relevant mechanism that contributes to stabilisation of the RING-E2-Ub complex. In 2011, Cheng et al showed that full-length MDM2 and a cleaved fragment of the protein (362-C), expressed in mammalian cells (H1299), also eluted at volumes consistent with high-molecular weight oligomers on the gel filtration column (Cheng *et al.*, 2011). Although MDM2 RING domain has the propensity to oligomerise, in both of these studies there was also a peak that eluted at a volume consistent in size with an MDM2 dimer. A former PhD student in our group observed a similar elution profile during purification of MDM2 RING domain on a gel filtration column.

In my studies I wanted to investigate the nature of MDM2-p14ARF interaction. As mentioned in section 1.7.2, ARF has been reported to interact with the acidic domain of MDM2. For this reason, I started my project with exploring the possible protocols for purification of MDM2 constructs that comprised both the RING and acidic domains.

3.1.1 MDM2 acidic domain is required for p14ARF binding

To study the MDM2-p14ARF complex, a variety of MDM2 constructs were cloned and purified. p14ARF 1-56 (referred to as N56p14ARF) was used for the preliminary co-expression experiments to reaffirm the literature-based observation of p14ARF binding to the MDM2 acidic domain (AD). As described earlier (see section 1.6.2), the AD roughly spans residues 210-280 and is followed

by a zinc finger motif (290-335) and C-terminal RING domain (430-490) (Figure 3.1-1). To verify that the AD provides the essential sequence for p14ARF binding, I co-expressed His-MBP-tagged N56p14ARF with GST-tagged MDM2 fragments that contain the RING domain (MDM2 350-C), the RING and zinc finger domains (MDM2 286-C) or all three domains ranging from the AD to the C-terminus (MDM2 230-C) in *E. coli*. The lysate was subjected to Ni²⁺-affinity purification followed by glutathione affinity purification. The eluents from each step were examined using SDS-PAGE to assess the interaction. Neither the RING domain alone (residues 350-C) nor the RING and zinc finger domains (residues 286-C) efficiently pulled down N56p14ARF (Figure 3.1-2 A and B). The fragment of MDM2 that included the AD (residues 230-C) was required to pull down N56p14ARF (Figure 3.1-2 C).

Previous structural studies were performed on the MDM2 AD and N37p19ARF peptide to investigate their interaction (Bothner *et al.*, 2001; Sivakolundu *et al.*, 2008). To investigate how ARF affects MDM2 catalytic activity, I investigated MDM2 constructs containing the AD, zinc finger and RING domains. Below I describe the strategies for purification of MDM2.

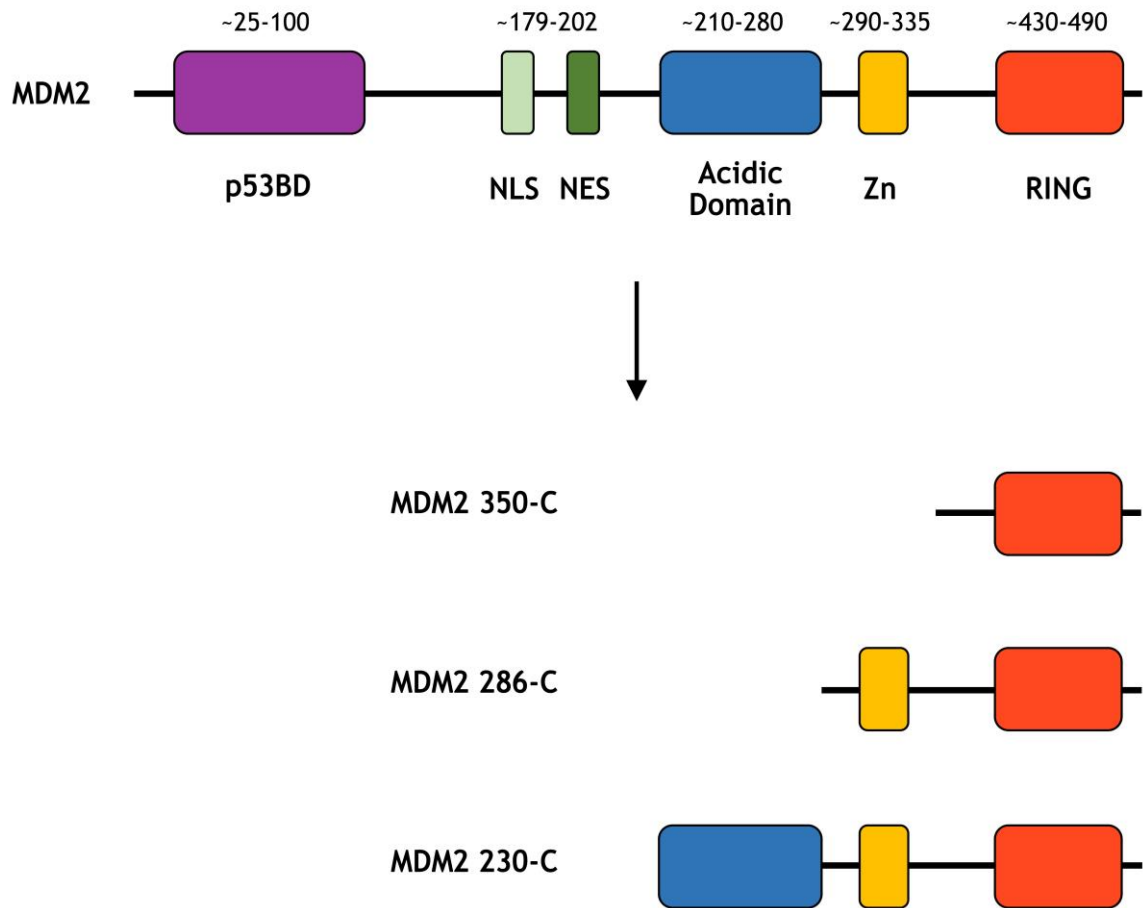


Figure 3.1-1 MDM2 domain architecture and construct design

Schematic representation of MDM2 constructs used to investigate binding to N56p14ARF. MDM2 350-C contains only the catalytic RING domain, MDM2 286-C spans the zinc finger (Zn) motif and RING domain, and MDM2 230-C is composed of the AD, zinc finger and RING domains.

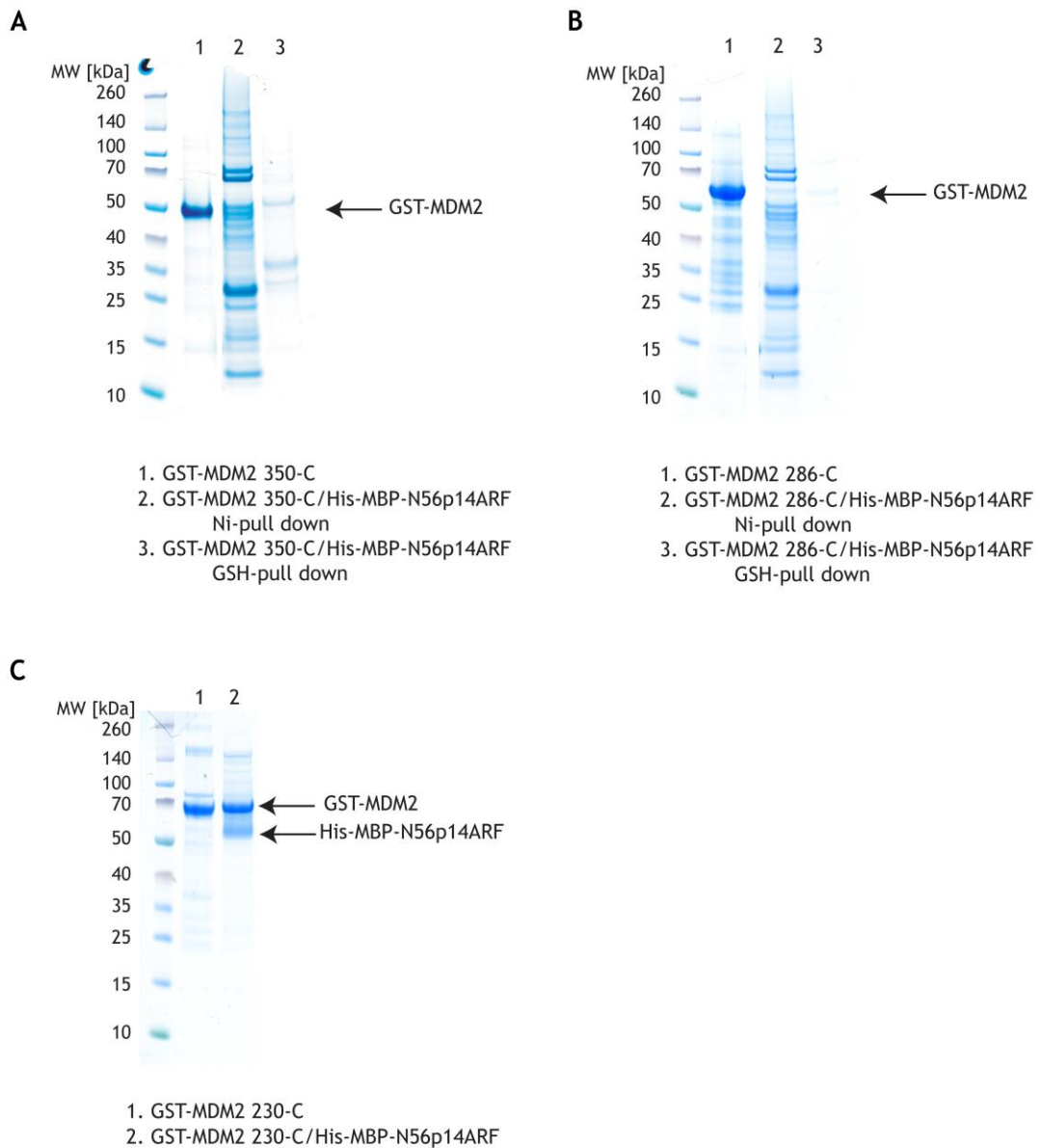


Figure 3.1-2 The AD of MDM2 is required to pull down N56p14ARF

A- SDS-PAGE showing pull-downs of co-expressed GST-tagged MDM2 350-C and His-MBP-N56p14ARF. Lane 1 contains GST-MDM2 350-C purified by glutathione affinity chromatography. Lanes 2 and 3 are the eluents from the first (Ni^{2+} affinity purification) and second (glutathione affinity purification) steps, respectively, of the double pull-down. No GST-tagged MDM2 RING domain (350-C) was detected after the second step, indicating weak or no binding between this fragment of MDM2 and N56p14ARF.

B- SDS-PAGE showing pull-downs of co-expressed GST-tagged MDM2 286-C and His-MBP-N56p14ARF. Lane 1 contains GST-MDM2 286-C purified by glutathione affinity chromatography. Lanes 2 and 3 are the eluents from the first (Ni^{2+} affinity purification) and second (glutathione affinity purification) steps, respectively, of the double pull-down experiment. No GST-tagged MDM2 fragment comprising the zinc finger and RING domains (286-C) was detected after the second step, indicating weak or no binding between this fragment of MDM2 and N56p14ARF.

C- SDS-PAGE showing pull-downs of co-expressed GST-tagged MDM2 230-C and His-MBP-N56p14ARF. Lane 1 contains GST-MDM2 230-C purified by glutathione affinity chromatography. Lane 2 contains GST-MDM2 230-C co-expressed with His-MBP-N56p14ARF purified by Ni^{2+} -affinity followed by glutathione affinity chromatography. Both proteins could be visualised on the Coomassie-stained gel following the double pull-down, indicating binding between MDM2 230-C and N56p14ARF. This result showed that the presence of the AD is required for binding between MDM2 and ARF.

3.1.2 MDM2 240-C forms higher-order oligomers

Research done by a former PhD student showed that the MDM2 RING domain is most stable when expressed with a GST tag, as during the purification of His-MDM2 RING irreversible disulphide bonds were formed. Based on the available literature as well as the expertise of the previous lab member, I investigated the oligomeric state of a range of GST-MDM2 fragments expressed in *E. coli* encompassing the AD to the C-terminus (210-C, 220-C, 230-C and 240-C). Initially I performed small-scale test expressions of these GST-MDM2 constructs and obtained ~500 µg of GST-tagged protein from 1 L of bacterial culture. Subsequently I scaled up the protein production of each of these MDM2 variants to 24 L to obtain sufficient quantities of protein to investigate their oligomeric state by size exclusion chromatography. Below I present the data obtained for the GST-MDM2 240-C construct.

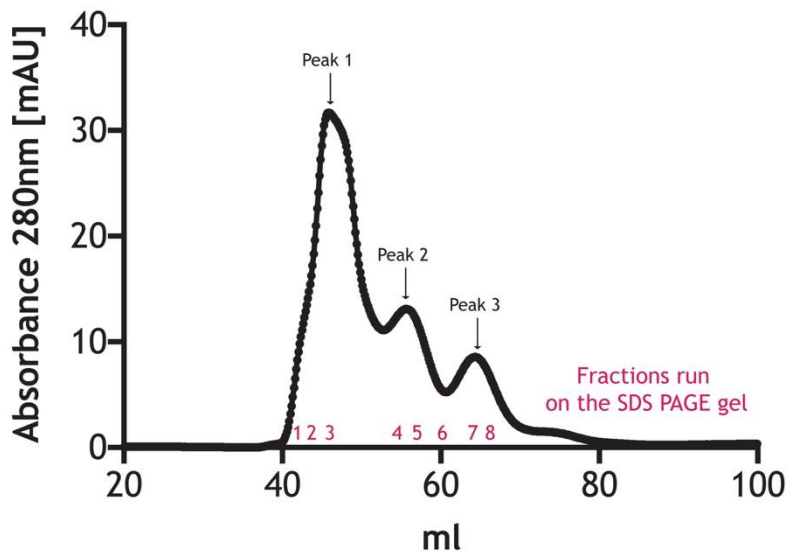
GST-MDM2 240-C was purified by glutathione affinity chromatography. The eluted GST-tagged protein was incubated with TEV protease to cleave the GST-tag, dialysed to remove the glutathione present in the elution buffer and incubated with fresh GSH beads to remove the free GST. Unfortunately, a substantial amount of GST was still present as shown in lane 1 of Figure 3.1-3 B. To investigate the oligomeric state of this MDM2 fragment and separate the fragment from GST, I applied the sample on a 16/600 Superdex 75 size exclusion column (Figure 3.1-3). Mixtures of GST and MDM2-240-C eluted in three overlapping peaks (absorption maxima at 45 ml, 55 ml and 65 ml). Most of the MDM2 was present in the first peak which corresponds to molecular weights (MW) greater than 200 kDa when compared with standards provided by GE Healthcare. The retention volume of the second peak corresponded to a protein with a MW of ~75 kDa and an SDS-PAGE gel confirmed the presence of MDM2 240-C in this peak. The dimeric form of MDM2 240-C has a predicted MW of 57 kDa, suggesting that this peak might primarily comprise dimeric MDM2. The slight discrepancy in MW may arise from MDM2 240-C adopting non-globular conformations. This would affect how MDM2 travels through the column resin compared with globular proteins. It is noteworthy that MDM2 240-C appears bigger on SDS-PAGE than its predicted MW (28.5 kDa for MDM2 240-C monomer). The reason for this phenomenon is not known, but some studies suggest that it may be a result of high content of acidic amino acids in the protein sequence

(Guan *et al.*, 2015). SDS-PAGE revealed that the third peak corresponded to the GST dimer (~50 kDa). These results showed that MDM2 240-C behaves similarly to the RING domain for which most of the protein elutes in the void volume and is consistent with large oligomers, and a small fraction elutes at a later volume consistent with the predicted molecular weight of dimeric MDM2 240-C.

It remains unclear whether the apparent higher molecular species of MDM2 comprise aggregated protein. Preliminary negative staining electron microscopy analyses of the oligomeric peak from full-length MDM2 by another member in the group demonstrated that it displays the characteristics of aggregated protein. Given that dimerisation of the MDM2 RING domain is important for its activity and the structure of MDM2 RING reveals a dimeric configuration, we reasoned that the dimeric fraction eluted from the gel filtration column represents the active MDM2 ligase (Kostic *et al.*, 2006; Uldrijan, Pannekoek and Vousden, 2007; Linke *et al.*, 2008; Nomura *et al.*, 2017). Thus, I aimed to develop strategies to improve the yield and methods for purification of the dimeric fraction of MDM2.

A

Size exclusion elution profile of MDM2



B

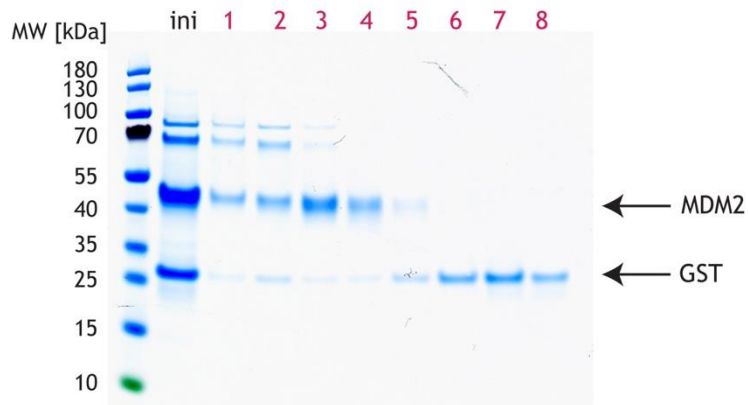


Figure 3.1-3 Oligomerisation of MDM2 240-C construct

A- Elution profile of cleaved MDM2 240-C after glutathione-affinity pass-back on a 16/600 Superdex 75 size exclusion column. MDM2 240-C and GST elute from the column in the form of three overlapping peaks. Elution of the first peak (absorption maximum at 45 ml) begins at a volume corresponding to the void volume of the column, suggesting there is a high molecular weight species of MDM2 240-C in the sample. The second peak elutes at a volume corresponding to the 75 kDa globular protein standard conalbumin, suggesting there is a dimeric species of MDM2 240-C present. The third peak with an absorption maximum at 65 ml elutes at a volume consistent with the MW of GST dimer.

B- SDS-PAGE showing fractions representing the cross-section of the 16/600 Superdex 75 size exclusion elution profile of MDM2 240-C in A. The sample loaded onto the column is labelled as ini.

3.1.3 Examining MDM2 oligomerisation under different expression and buffer conditions

Since the small-scale purification yielded very little MDM2 240-C dimer, two alternative approaches were attempted to increase the proportion of dimeric MDM2.

To potentially increase the proportion of dimeric MDM2 at the stage of protein expression, I purified four small-scale productions of GST-MDM2 240-C expressed in different conditions:

- A standard expression was carried out in which the *E. coli* culture was propagated at 37°C until the OD₆₀₀ reached 0.3. At this point, the temperature was dropped to 20°C and IPTG was added to a final concentration of 200 µM when the OD₆₀₀ reached 0.6. Cells were harvested after overnight incubation at 20 °C.
- To investigate whether slower *E. coli* growth could promote expression of a higher fraction of GST-MDM2 dimer, cultures were propagated at 25°C until the OD₆₀₀ reached 0.3; then the temperature was reduced to 20°C and the culture was induced with 200 µM IPTG when the OD₆₀₀ reached 0.6. Cells were harvested after overnight incubation at 20 °C.
- To investigate if a shorter protein-production phase could produce more dimeric MDM2, a standard expression was carried out but the cells were harvested 2 h after induction with IPTG.
- To investigate whether a more gentle induction could yield more MDM2 dimer, cells were grown and harvested using standard expression conditions but only 1 µM IPTG was used for the induction.

The GST-MDM2 expressed under these four conditions was purified following the small-scale protocol, where GST-tagged protein was eluted from GSH beads after affinity chromatography and the aggregation status was evaluated using an analytical 10/300 Superdex 200 size exclusion column (Figure 3.1-4 A). For each of these expression conditions, the elution profile of GST-MDM2 240-C

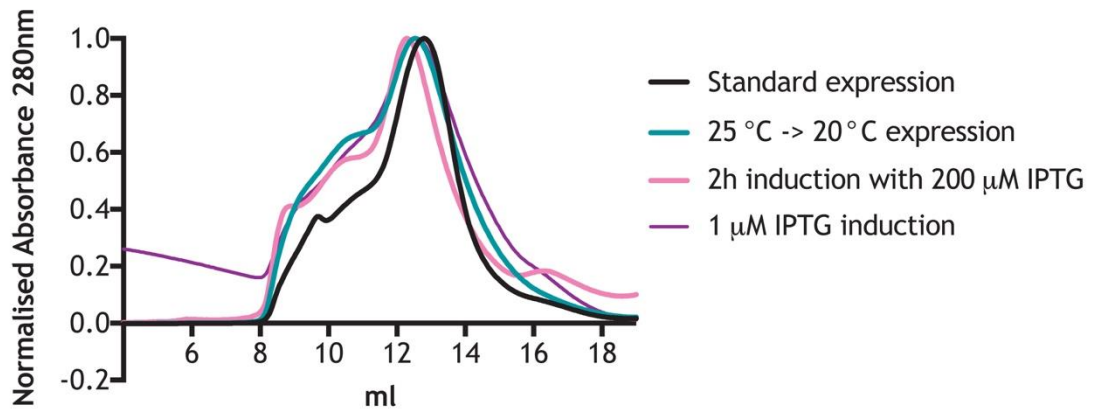
(theoretical MW of a dimer ~100 kDa) was characterised by a broad shoulder beginning to elute at 8 ml which corresponds to the void volume of the column in which the MW of the eluting species are greater than 700 kDa based on the protein standard provided by GE Healthcare. This shoulder overlaps with a second peak with an elution volume of 13 ml, which is consistent with the expected molecular weight of dimeric GST-MDM2 240-C. Unfortunately, none of the expression conditions led to a significant increase in the dimeric fraction of MDM2 compared with the standard expression approach.

Cosolvents can potentially facilitate destabilisation of oligomerised protein species and support the stability of the native counterparts. Kosmotropes (e.g. MgSO_4 , $(\text{NH})_4\text{SO}_4$, Na_2SO_4 , Cs_2SO_4 , KCl) increase the stability of the native state of a protein by increasing the surface tension of solvent and promoting hydration of the native counterpart (Collins and Washabaugh, 1985; Baldwin, 1996). A similar quality has been observed when sugars and polyhydric alcohols (e.g. sucrose, glucose, ethylene glycol, glycerol) are introduced (Timasheff, 1998). Chaotropes (e.g. CaCl_2 , MgCl_2 , LiCl, NaI, NaBr, urea) interact directly with polypeptide chains and thereby decrease the number of interactions that lead to aggregate formation (Edwin, Valkya Sharma and Jagannadham, 2002). In some cases, using L-arginine as a cosolvent prevents protein aggregation although the mechanism is unknown (Das *et al.*, 2007). In addition, detergents (e.g. Tween 20, Nonidet P-40) are often introduced in during protein purification and are well known for facilitating folding during purification of membrane proteins (Zardeneta and Horowitz, 1994).

To investigate whether MDM2 aggregation was reversible, several additives (cosolvents) were tested. Purified oligomeric MDM2 was buffer-exchanged into a range of solutions comprising the standard GSH wash buffer and an additive as listed in Figure 3.1-4 B. Species with MWs above and below 100 kDa were separated by centrifugal ultrafiltration. The same procedure was applied to dimeric and oligomeric MDM2 using additive-free buffer as a reference. Equal volumes of flow-through from each condition were separated by SDS-PAGE. Based on the assumption that dimeric MDM2 (MW 56 kDa) readily passes through the membrane compared with MDM2 aggregate (MW > 200 kDa), an increase in band intensity compared with the oligomeric MDM2 control was expected for

additives that helped to reverse aggregation. None of the introduced additives led to a significant increase in the dimeric form of MDM2 (Figure 3.1-4 B).

A Size exclusion elution profile of GST-MDM2 under different expression conditions



B

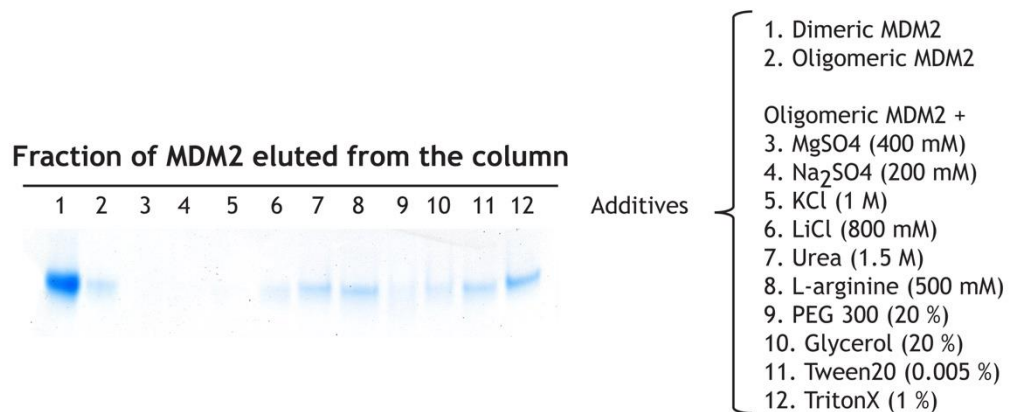


Figure 3.1-4 MDM2 oligomerisation under a variety of expression and buffer conditions

A- Size exclusion profile of GST-MDM2 240-C expressed under different conditions. GST-MDM2 was expressed under different conditions, purified by glutathione-affinity chromatography and loaded onto a 16/600 Superdex 200 column. No increase in the amount of GST-MDM2 240-C dimer was observed.

B- SDS-PAGE showing effects of different additives on oligomerisation of MDM2 240-C. Oligomeric MDM2 240-C was buffer exchanged into a standard GSH wash buffer and mixed with each additive listed on the right panel. The mixture was loaded onto a 100 kDa MW cut-off spin column. Following centrifugation, the flow through was loaded onto an SDS-PAGE gel. If a particular reagent facilitated MDM2 dimerisation, more protein was expected to pass through the 100 kDa membrane compared with the control (lane 2). The same amount and volume of dimeric MDM2 was used as a positive control (lane 1 to verify that the native protein readily passes through the membrane. None of the additives led to a significant increase in MDM2 240-C dimer.

3.1.4 Dimeric MDM2 240-C can be isolated using anion exchange chromatography

The small-scale MDM2 240-C purification described earlier was characterised by a low yield, where only 5-10 % of the initial protein was purified in a dimeric form. Hence, during large-scale productions of this MDM2 construct, unconventional volumes of bacterial culture (80 - 100 L *E. coli* culture) were grown and harvested. Because separation of cleaved MDM2 and GSH proved to be inefficient, I introduced an alternative approach to purification. Instead of eluting GST-MDM2 from the beads and cleaving off the GST-tag in solution, an *in situ* cleavage step was used, where TEV was added to the GSH-bound GST-MDM2 and circulated through the mixture with a peristaltic pump. Free MDM2 was recovered from the flow-through but the presence of heterogenic oligomeric species of MDM2 significantly impeded protein separation by size exclusion chromatography. We postulated that ion exchange chromatography might separate dimer and oligomer based on differences in pI values. MDM2 dimers have a theoretical pI value of approximately 4, suggesting binding to positively-charged resin can occur in higher pH conditions. Oligomerisation of MDM2 might alter the surface net charge compared with dimer, thereby affecting the strength of the oligomer-resin interaction and influencing the salt concentration required for elution. When an oligomer-dimer mixture was applied to a Source Q anion exchange column, two broad overlapping peaks were observed with UV absorption maxima at ~300 mM and ~400 mM NaCl (Figure 3.1-5 A). When these peak fractions were run on an analytical 10/300 Superdex 200 size exclusion column, the first peak eluted after 15 ml on the size exclusion column, which corresponds to an elution volume consistent with the MW predicted for MDM2 240-C dimer (57 kDa) (Figure 3.1-5 D). The second peak from the ion exchange eluted as a broad peak extending from 8 ml to 13 ml on the size exclusion column, suggesting the presence of a mixture of high-MW oligomers (Figure 3.1-5 E). Native-PAGE analysis was implemented to further investigate the aggregation state of the protein in the eluted fractions; differences in migration by native-PAGE were expected only when oligomerisation affected the overall mass/charge ratio of the different species. Fast-travelling, sharp and discrete bands on the native gel were observed for the first peak fractions from the SourceQ column, whereas subsequent fractions produced a slow migrating smear (Figure 3.1-5 C). These results suggested that dimeric MDM2 240-C could be

separated from the oligomeric pool by SourceQ chromatography. To further improve the purity of dimeric MDM2 240-C, the first peak eluted from the SourceQ column was run on a second anion exchange chromatography column (MonoQ) to provide higher resolution for separating dimeric and oligomeric forms of MDM2 (Figure 3.1-6). Peak fractions from the MonoQ elution containing dimeric MDM2 were concentrated, snap frozen in liquid nitrogen and stored at -80°C.

To investigate the effect of p14ARF on the catalytic activity of MDM2, active forms of both purified proteins were required. Lysine discharge assays were implemented to validate MDM2 activity at different stages of the purification procedure. MDM2 was tested in a GST-tagged form, after *in situ* cleavage and after the final anion exchange chromatography purification step. MDM2 was active during all stages of purification as evidenced by the discharge of UbcH5B~Ub within 2 min of the reaction course in the presence of 200 nM of E3 (Figure 3.1-7).

Of all the MDM2 constructs tested, MDM2 230-C showed the highest purity and protein yield after small-scale MDM2/p14ARF double pull-down experiments. Moreover, some reports suggest that the AD of MDM2 stimulates catalytic activity via intramolecular interactions, which in turn enhances p53 ubiquitination. The minimal AD sequence exhibiting these properties was narrowed down to residues 230-260 (Cheng *et al.*, 2014). In my research I wanted to use a construct of MDM2 that would allow me to investigate the nature of MDM2-p14ARF complex with respect to the potential regulation of p53 activity. As a result, MDM2 230-C was selected for further studies on MDM2 activity and its interaction with p14ARF.

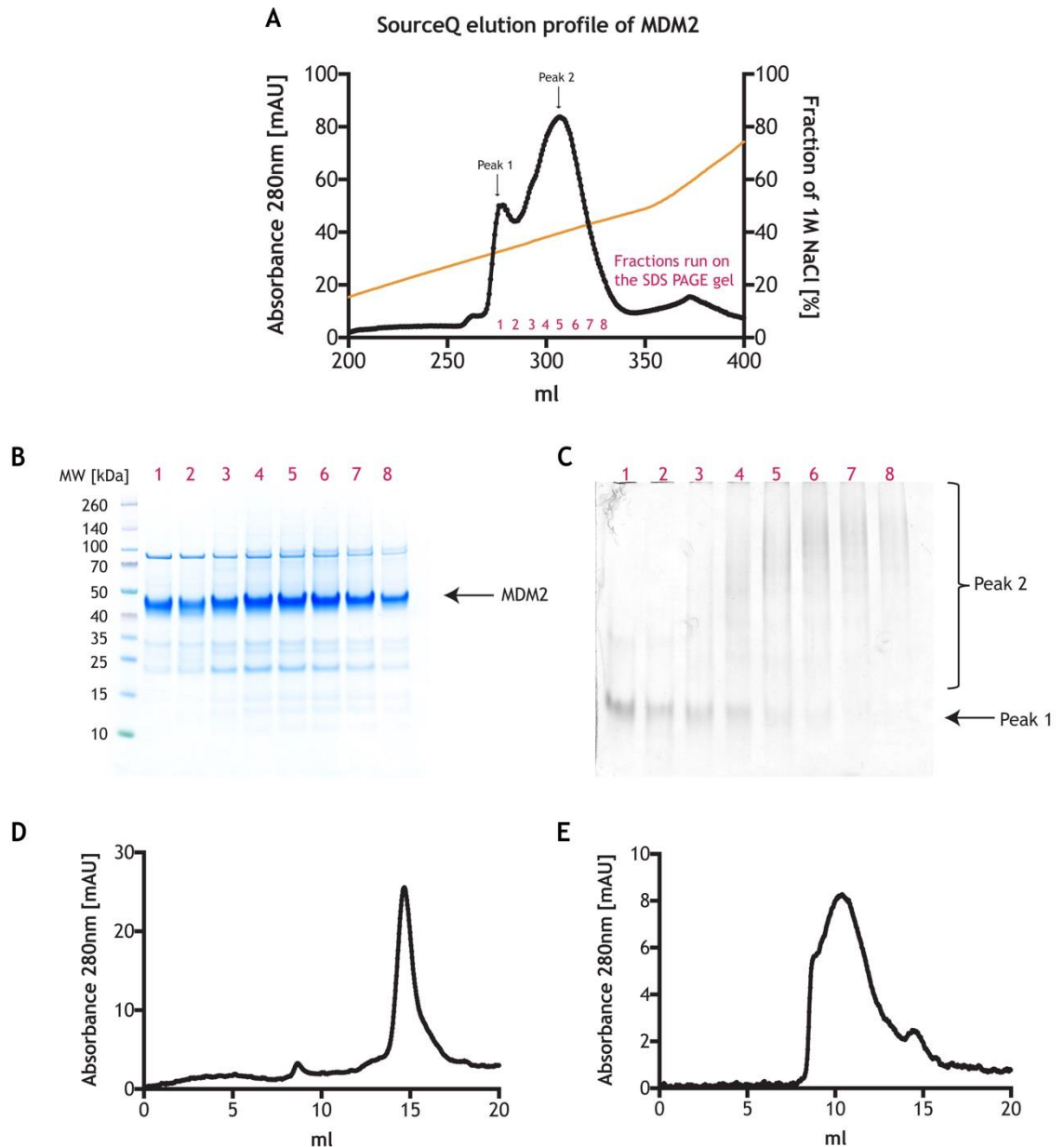


Figure 3.1-5 Purification of MDM2 240-C construct with SourceQ anion exchange chromatography

A- Elution profile of cleaved MDM2 240-C (predicted pI of ~4) loaded onto a SourceQ column. The elution profile for MDM2 240-C was characterised by two broad and overlapping peaks, with absorption maxima at around 300 mM and 400 mM NaCl, respectively.

B- SDS-PAGE showing fractions from both peaks in panel A. MDM2 240-C was present in both overlapping peaks.

C- Native gel of MDM2 240-C from both ion exchange chromatography peaks. MDM2 fractions from the first peak of ion exchange elution ran as a sharp and discrete band, whereas MDM2 fractions from the second peak ran as a "smear" and the defined band from the first peak was fainter or absent.

D- Elution profile of the first peak fraction from the SourceQ column in A loaded onto a 10/300 Superdex 200 column. The peak at 15 ml corresponds to the MW of MDM2 240-C dimer.

E- Elution profile of the second peak fraction from the SourceQ column in A loaded onto a 10/300 Superdex 200 column. Elution of a broad peak begins at ~8 ml, which corresponds to the void volume of the column and is suggestive of the presence of several oligomeric species of MDM2 240-C.

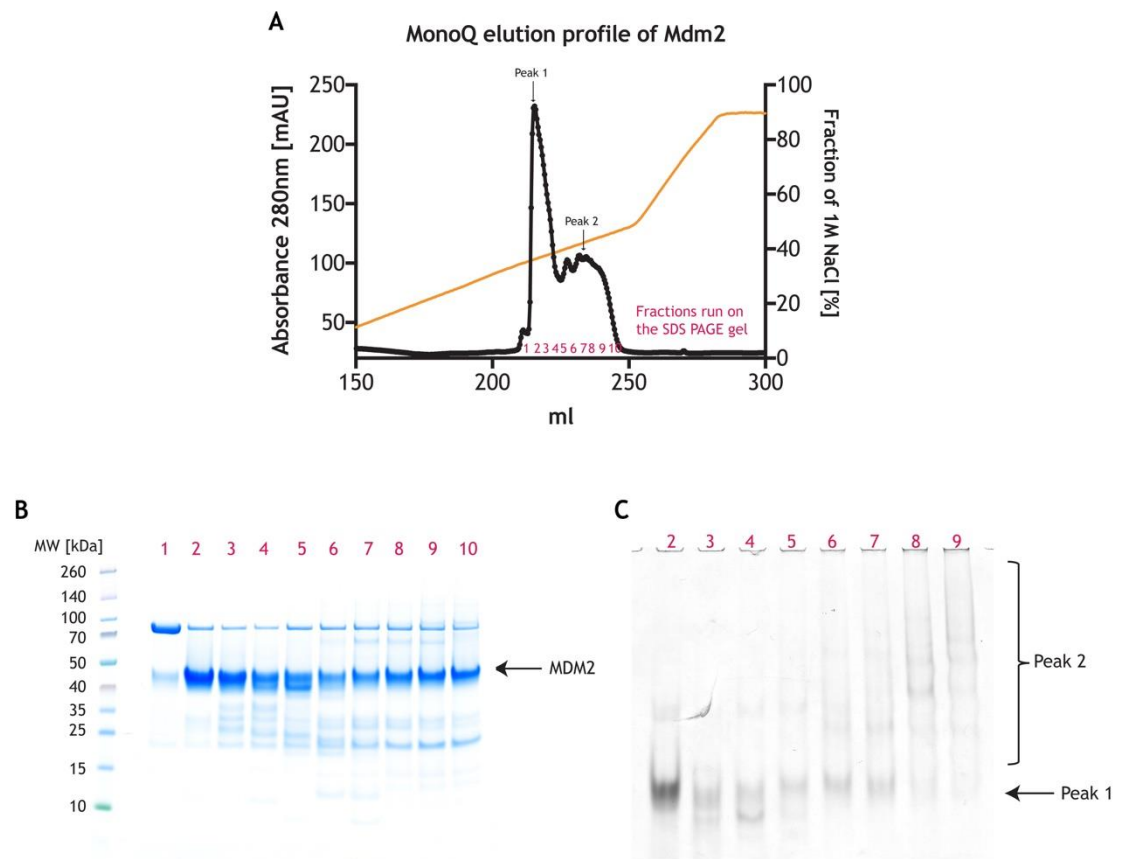


Figure 3.1-6 Purification of MDM2 240-C construct with MonoQ anion exchange chromatography

A- Elution profile from the MonoQ column, which was used after the SourceQ column to provide a higher resolution separation of dimeric and oligomeric species of MDM2 240-C. Dimeric MDM2 was enriched as indicated by the appearance of a sharp peak on the elution profile at ~ 350 mM NaCl, with higher absorbance than the subsequent shoulder/broad peak.

B- The presence of MDM2 240-C in the fractions of the indicated the cross-section of the elution peak in A was confirmed by SDS-PAGE analysis.

C- Enrichment of dimeric MDM2 240-C with respect to total protein was further verified by analysing cross-section fractions on a native-PAGE gel. The sharp and discrete band on the gel corresponds to the defined peak on the MonoQ elution profile.



Figure 3.1-7 Activity of MDM2 240-C at different stages of the purification protocol

SDS-PAGE showing activity of MDM2 construct at various steps of the purification procedure. GST-MDM2 240-C, cleaved protein, as well as the construct purified with anion exchange chromatography discharged UbcH5B-Ub within first 2 min of the reaction time, with 250 nM of E3 present in the reaction. Reactions were performed as described in section 2.2.7.

3.1.5 MDM2 oligomerisation is reversed in the presence of denaturing agents

As described in section 3.1.3, a variety of buffer additives were tested for their positive effect on the formation of MDM2 dimer, but none of them led to a significant increase in the levels of the desired form of the protein. Several studies have described protocols for the refolding of insoluble and aggregated species of proteins into active protein (Morjana, McKeone and Gilbert, 1993; Gorovits, Seale and Horowitz, 1995; Raman, Ramakrishna and Rao, 1996; West, Guise and Chaudhuri, 1997). Moreover, MDM2 RING domain has previously been purified and refolded from inclusion bodies for structural analysis by NMR (Bothner *et al.*, 2001; Sivakolundu *et al.*, 2008).

The phenomenon of protein folding is one of the most baffling problems in biological sciences. The complexity of how a tertiary structure forms from a linear sequence of amino acids was discussed more than 30 years ago by Cyrus Levinthal (Levinthal, 1969). Since then, a series of mechanisms have been proposed to explain the pathway of protein folding including the following: the diffusion-collision theory, in which secondary structures are formed first followed by their coalescence into tertiary structure; the nucleation mechanism in which an initial fold is formed and induces subsequent propagation of the structure; a hydrophobic-collapse mechanism, in which an initial fold is adopted by hydrophobic interactions between amino acids (Wetlaufer, 1973; Karplus and Weaver, 1976; Ptitsyn, 1987; Daggett and Fersht, 2003). The folding pathway of denatured protein has been proposed to follow a funnel-shaped energy landscape, in which intramolecular interactions lead to propagation of the structure through various trajectories of an intermediate state followed by a transition state, and finally yielding the low-energy tertiary fold (Wolynes, Onuchic and Thirumalai, 1995; Dill and MacCallum, 2012). Development of tools allowing for the determination of protein structures led to the classification of primary factors responsible for the formation of a protein fold. Tertiary structure is governed by hydrogen bonds, Van der Waals interactions, electrostatic and hydrophobic interactions, as well as preferred geometry of the protein backbone (Dill, 1990; Dill and MacCallum, 2012). During expression in bacterial systems, protein may be misfolded leading to its aggregation, accumulation in inclusion bodies or degradation. If aggregated protein can be

isolated, different denaturing approaches can be utilised to disrupt the aggregated species, depending on the strength of the applied denaturant. Different chemical compounds have been reported to aid the reversible denaturation of proteins (e.g. alcohols, acids and bases, heavy metals) but the most commonly used agents include urea and guanidinium chloride (GdnHCl). Urea has been reported to facilitate protein unfolding in two ways: it has been shown to create hydrogen bonds with polar NH and CO peptide groups, blocking intramolecular hydrogen bonds and destabilising β -sheets; moreover, urea has been proposed to alter water structure and influence protein solvation state, leading to exposure of the protein's hydrophobic core (Wingfield, 1995; Bennion and Daggett, 2003). The drawback of urea usage comes from the fact that over time it decomposes into ammonium cyanate, which readily reacts with lysine side chains, leading to their carbamylation and neutralisation (Wingfield, 1995). Guanidinium ions have been reported to target α -helices by coating amino acid residues with planar and aliphatic side chains (Wingfield, 1995; Camilloni *et al.*, 2008; Lim, Rosgen and Englander, 2009). GdnHCl was shown to yield a higher refolding efficiency when compared with equivalent concentrations of urea (West, Guise and Chaudhuri, 1997). Protein refolding using chemical compounds assumes that the denatured protein can be redirected into its "native" fold following a folding trajectory after the denaturant is removed from the system. Several guidelines are available on implementation of urea and/or GdnHCl in protein refolding. Based on these guidelines, I developed a protocol for the refolding of oligomeric MDM2 230-C and assessed whether refolding could convert MDM2 230-C oligomer into dimer.

MDM2 230-C obtained from a large-scale expression was applied onto a Source Q anion exchange column. Protein from the first peak was purified following the protocol described in Section 3.1.4 and yielded sample which was used as a standard for dimeric species of MDM2 230-C. Fractions corresponding to the second, broad peak from the ion exchange were pooled, diluted, re-applied onto a SourceQ column, and eluted with a sharp salt gradient to concentrate the protein. This strategy resulted in the complete recovery of the protein as compared with other concentrating techniques (Figure 3.1-8). 10X buffer containing 250 mM Tris-HCl pH 7.6, 1.5 M NaCl, 10 mM TCEP, 100 μ M ZnSO₄ was prepared ahead of the refolding experiment. ZnSO₄ was present in order to

provide Zn ions required for the formation of the active RING domain fold. Oligomeric MDM2 230-C was diluted with water, 10X buffer (yielding 1X concentration) and the desired amount of 8 M urea or 8 M GdnHCl (yielding 0-6 M final concentration) and incubated for 90 min on ice. The denaturing agent was removed rapidly using a Zeba spin desalting column. An abrupt replacement of the denaturant has been reported to be advantageous over slow dialysis or dilution since prolonged presence of intermediate concentrations of urea or GdnHCl can facilitate aggregation during protein refolding (De Bernardez Clark, 1998). Finally, 200 μ l of refolded MDM2 230-C was loaded onto an analytical 10/300 Superdex 200 size exclusion column to assess its oligomeric state.

As seen in Figure 3.1-9, increasing concentrations of urea in the denaturing solution led to an increase in the amount of MDM2 dimer compared with oligomer. Quantification of the dimeric and oligomeric peaks of MDM2 at each of the urea concentrations showed that refolding from 6 M of urea yielded 2.72 times more MDM2 dimer compared with oligomer. Compared with other methodologies I tried, a substantial amount of MDM2 dimer was recovered using this technique. Because GdnHCl is reportedly more efficient at protein refolding, I next tested whether refolding from 6 M GdnHCl yielded more MDM2 dimer than refolding from 6 M urea. GdnHCl was only marginally better than urea based on quantification of the dimer / oligomer ratio (3.47 for GdnHCl vs 2.72 for urea) as shown Figure 3.1-10. Next, I assessed whether the refolded protein retains activity by performing lysine discharge assays. Purity and composition of each sample was first analysed on an SDS-PAGE gel (Figure 3.1-11). Oligomeric MDM2 refolded from 6 M urea or 6 M GdnHCl discharged E2-Ub faster as compared with the oligomeric control, but was slower when compared with dimeric MDM2 purified from the first peak of SourceQ chromatography (Figure 3.1-8). The presence of oligomeric species in refolded MDM2 samples as shown on the size exclusion chromatograms (Figure 3.1-10) might contribute to the reduced activity observed as compared with MDM2 dimer purified by ion exchange chromatography. It is noteworthy that E2-Ub is labile and will discharge slowly even in the absence of E3. To ensure that the discharge of Ub from E2 was not caused by the residual presence of denaturant in solution, I investigated the effects of buffers used during refolding on the lysine discharge assay. Standard 1X buffer without MDM2 present was subjected to the refolding treatment and

used in the lysine discharge assay. As seen in Figure 3.1-12 B, none of the buffer conditions stimulated the discharge of E2-Ub. These data demonstrate that refolded MDM2 dimer is active, more so than the oligomeric fraction of MDM2.

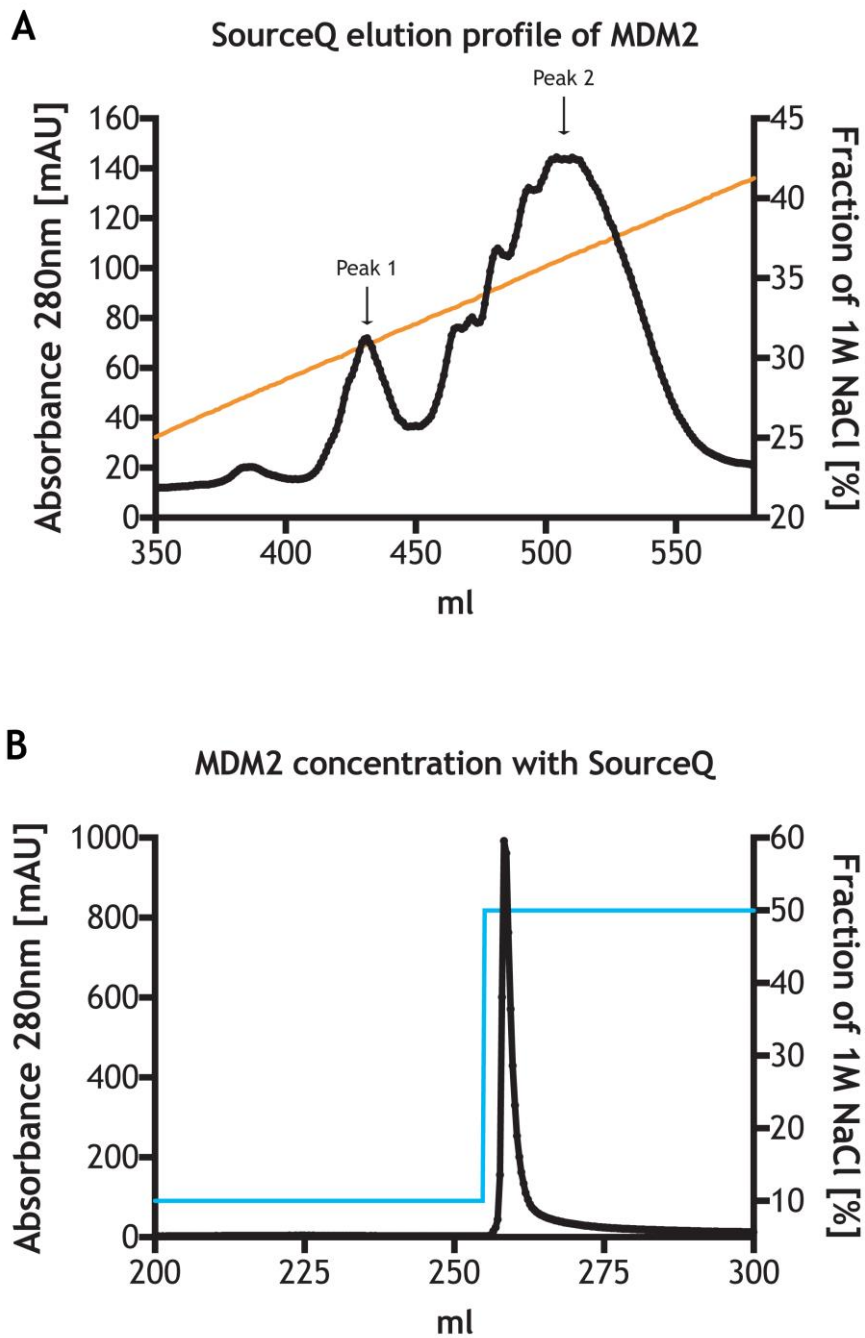


Figure 3.1-8 Purification of the oligomeric fraction of MDM2 230-C

A- Elution profile showing separation of dimeric and oligomeric MDM2 230-C with SourceQ chromatography. The first peak was used as a standard for the dimeric form of the protein. The second peak was concentrated and used in the refolding experiment.

B- Elution profile showing concentration of the second peak from panel A using SourceQ chromatography. The second peak in panel A was loaded onto a SourceQ column and eluted with a sharp gradient to concentrate the protein.

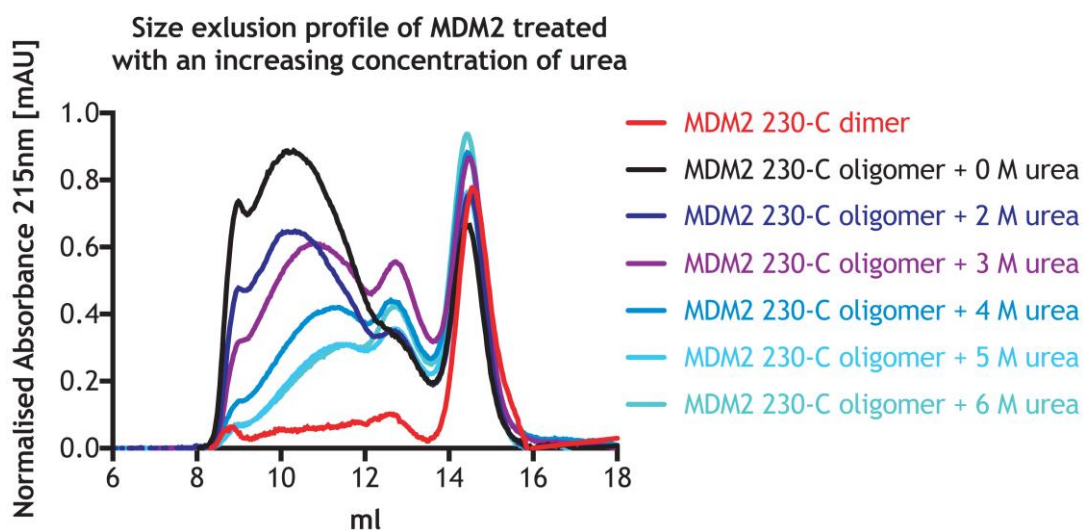


Figure 3.1-9 The effect of different urea concentrations on MDM2 230-C refolding

A range of urea concentrations was tested for efficiency in refolding of the oligomeric fraction of MDM2 230-C. Disappearance of the oligomeric peak and an increase in the dimeric peak height were observed with increasing concentrations of urea. The first peak from the SourceQ column was used as a standard for dimeric MDM2 230-C.

Table 9 Increase in dimeric species of MDM2 during refolding experiment

| Concentration of the denaturant | MDM2 concentration [mg/ml] | Oligomer peak absorbance [mAU] | Dimer peak absorbance [mAU] | Dimer / Oligomer ratio ¹ |
|---------------------------------|----------------------------|--------------------------------|-----------------------------|-------------------------------------|
| 0 M | 0.34 | 48 | 36 | 0.75 |
| 2 M urea | 0.3 | 44 | 52 | 1.18 |
| 3 M urea | 0.36 | 57 | 81 | 1.42 |
| 4 M urea | 0.36 | 39 | 82 | 2.10 |
| 5 M urea | 0.31 | 31 | 72 | 2.32 |
| 6 M urea | 0.32 | 39 | 106 | 2.72 |
| 6 M GdnHCl | 0.35 | 38 | 132 | 3.47 |

¹For simplicity, dimer to oligomer ratio was determined based on the peak absorbance

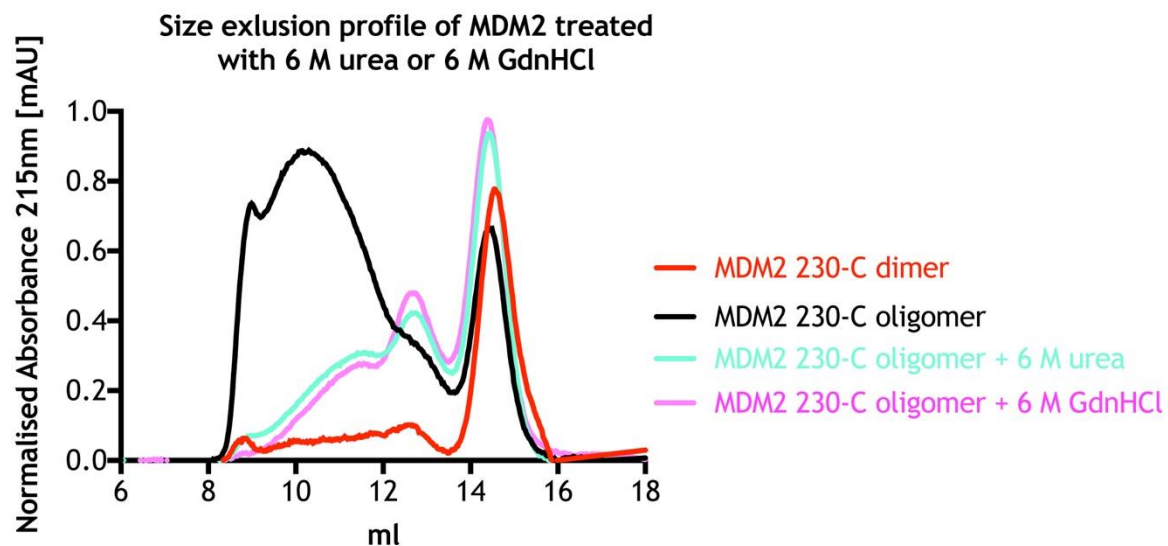


Figure 3.1-10 Comparison of urea and GdnHCl in the refolding experiment

The efficiency of 6 M GdnHCl or urea in refolding MDM2 230-C. GdnHCl gave a slight advantage over urea. Based on these results and because GdnHCl is more stable in solution, it was chosen for subsequent refolding experiments.

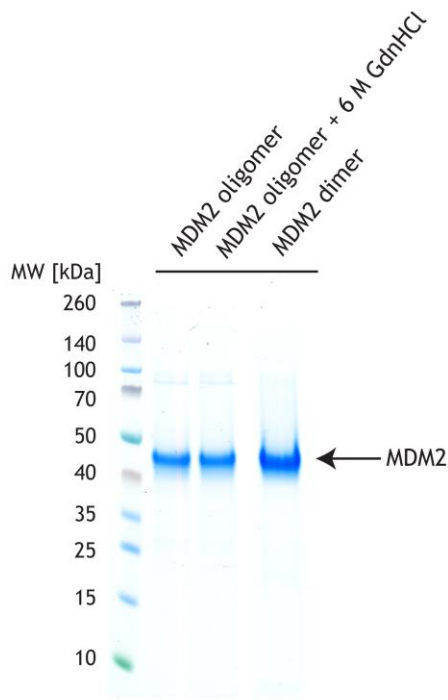


Figure 3.1-11 Purity of MDM2 230-C samples used in lysine discharge assays

The purity of dimeric, oligomeric and refolded MDM2 230-C was examined on an SDS-PAGE gel.

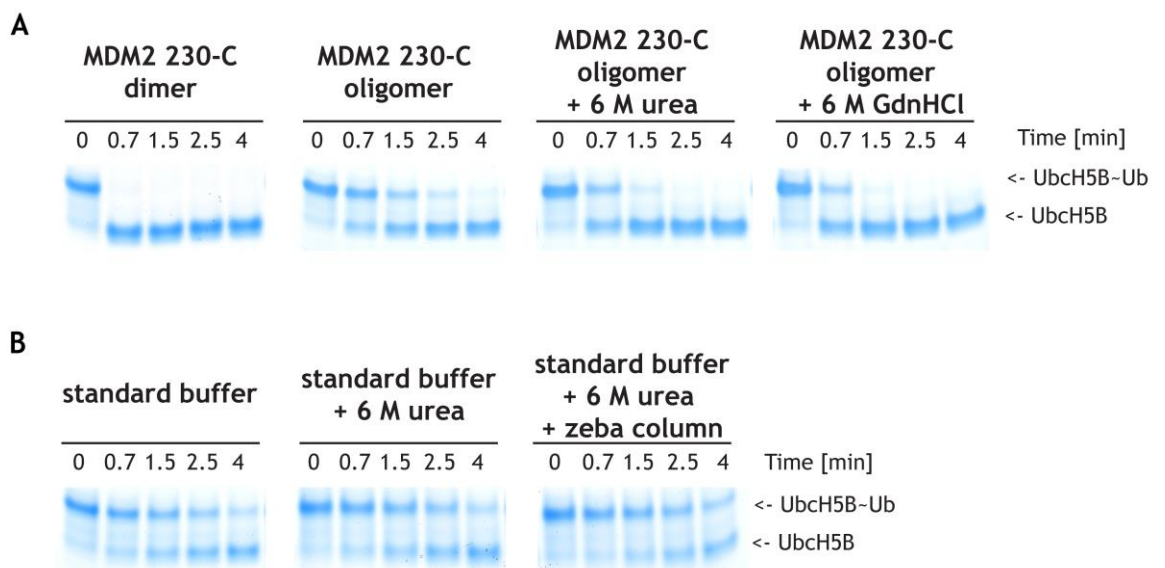


Figure 3.1-12 Activity of refolded MDM2 230-C

A- SDS-PAGE showing activity of oligomeric MDM2 230-C refolded with 6 M urea or 6 M GdnHCl in discharging Ubch5B~Ub. Oligomeric and dimeric MDM2 230-C purified from peak 1 and 2 of SourceQ chromatography, respectively, were used as benchmarks. MDM2 obtained after refolding from urea or GdnHCl showed an increase in ability to discharge Ubch5B~Ub as compared with the oligomeric fraction. Reactions were performed as described in section 2.2.7, using 250 nM indicated E3.

B- SDS-PAGE showing that various buffer conditions used during refolding had no effect on Ubch5B~Ub discharge.

Next, I included the refolding step in the large-scale protein production of MDM2 230-C. MDM2 230-C was purified using a SourceQ column as described in Section 3.1.4. Fractions containing both dimeric and oligomeric MDM2 were pooled together, concentrated with a sharp gradient on a SourceQ column (Figure 3.1-8 B) and incubated with previously described buffer containing 6 M GdnHCl. After 90 min of incubation on ice, MDM2 was buffer exchanged to 1X buffer using a HiPrep 26/10 desalting column and subsequently loaded onto a 26/600 Superdex 200 size exclusion column. The elution profile resembled the one obtained in the small-scale test - a broad peak appeared with an absorption maximum at 150 ml and was followed by a sharp peak at a retention volume of 180 ml. The first peak contained oligomeric MDM2, whereas the second peak contained the dimeric MDM2 (Figure 3.1-13). MDM2 230-C fractions from the second peak were pooled and concentrated by application onto a MonoQ column eluted with a sharp gradient. This MDM2 230-C was subsequently re-assessed on the same size exclusion column to check whether concentration and / or salt concentration affected dimer stability. Unfortunately, most of the protein eluted in the form of a higher-order MW species (Figure 3.1-13). It seems that during concentration, dimeric MDM2 forms higher oligomers.

Given the challenges in improving the yield of dimeric MDM2 as described above, I re-focused my efforts on characterising MDM2-p14ARF complexes using small-scale expression tests and dimeric MDM2 purified as described in section 3.1.4.

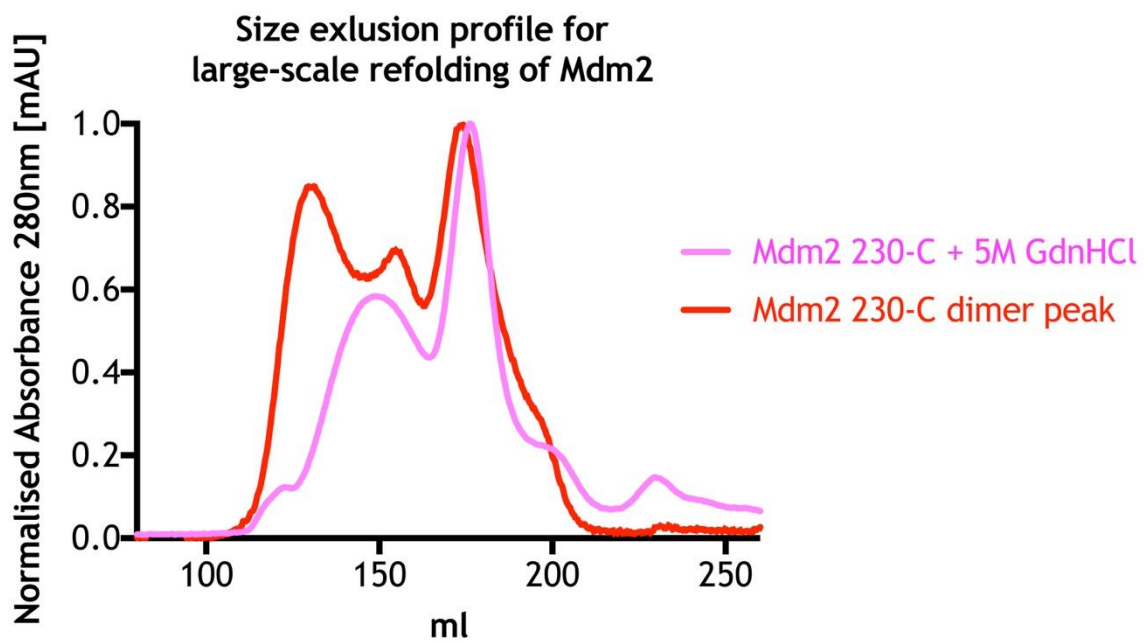


Figure 3.1-13 Large-scale refolding of MDM2 230-C

Elution profile of refolded MDM2 230-C on a 26/600 Superdex 200 size exclusion column. The magenta profile corresponds to MDM2 230-C obtained after refolding from 5 M GdnHCl; Second peak obtained from that run, was pooled, concentrated and reloaded on the same column (red elution profile).

3.1.6 Discussion

In conclusion, I have developed a protocol which allowed me to isolate the dimeric fraction of MDM2 230-C. I have also shown that the oligomerisation event affects the catalytic potency of MDM2. Isolated dimer of MDM2 230-C showed higher activity towards Ubch5B-Ub discharge, compared with its oligomeric counterpart (Figure 3.1-12). Moreover, I have developed a refolding protocol, which indicated that the oligomerisation of MDM2 can be reversed in the presence of denaturing agents, leading to an increased catalytic activity of the protein (Figure 3.1-12). This further conferred the observation that the ligase activity of MDM2 is dependent of its oligomeric state. The initial purification tests of MDM2 240-C indicated that the cleaved protein obtained after the affinity chromatography purification step displayed similar activity to the purified MDM2 240-C dimer (Figure 3.1-7). It is noteworthy that the cleaved MDM2 240-C contained a mixture of dimer and oligomer and this particular reaction was not optimised, but merely served to check whether the protein was active. Subsequently a more detailed purification was developed to separate MDM2 230-C dimer and oligomer and confirmed that the dimeric form was more active. Finally, another member of our group investigated the nature of the full-length MDM2 using negative staining electron microscopy and showed that the oligomeric fraction contains a substantial portion of aggregated protein. This might be caused by a fraction of protein being misfolded during expression, resulting in formation of aggregates. Based on our structural and biochemical characterisation of MDM2 RING homo- and heterodimer, active MDM2 homodimer and MDM2/MDM4 heterodimer requires RING domain dimerisation to bind and activate E2~Ub for catalysis (Nomura *et al.*, 2017). It seems likely that oligomerisation might impede or occlude E2~Ub binding thereby reducing the activity.

The phenomenon of MDM2 oligomerisation was previously described by other groups, who used insect and mammalian cells to produce MDM2. This suggests that MDM2 oligomerisation is an inherent characteristic of the overexpressed protein and is independent of the implemented expression system. Poyurovsky *et al.* studied the behaviour of the RING domain of MDM2 (400-C) and proposed that its oligomerisation is driven by the hydrophobic C-terminal residues of MDM2 (residues 485-491) (Poyurovsky *et al.*, 2007). Based on this hypothesis, MDM2

needs to dimerise before forming higher order oligomers, as abrogation of the dimerisation capacity of MDM2 eliminates further formation of oligomers. Extensive oligomerisation of MDM2 RING (428-C) was also described by a previous lab member, suggesting that the catalytic domain of MDM2 may be responsible for its supramolecular assembly. These data agrees with the study published by Cheng et al. in 2001 in which deletion of the C-terminal RING domain from full-length MDM2 construct decreased the formation of MDM2 oligomers (Cheng *et al.*, 2011). It is worth mentioning that Cheng et al. also showed that there is a substantial difference in the amount of the oligomerised protein between MDM2 constructs comprising residues 410-C and 361-C (Cheng *et al.*, 2011). This suggests that even though the RING domain is possibly the main driver of MDM2 oligomerisation, the extent of oligomerisation also depends on other regions of MDM2. In 2014 Cheng et al. suggested that the AD of MDM2 can bind the RING domain, possibly via electrostatic interactions (Cheng *et al.*, 2014). This indicates that MDM2 is capable of forming various inter- and intramolecular interactions, which possibly contribute to oligomerisation.

Interestingly, Poyurovsky et al. suggested that MDM2 oligomerisation is a biologically relevant event, as the high-MW species of the protein exhibited catalytic activity (Poyurovsky *et al.*, 2007). This hypothesis does not agree with my observations; however, it is possible that the oligomeric species of MDM2 230-C show different potency towards Ub transfer compared with oligomerised MDM2 400-C. Moreover, the oligomeric RING domain used by Poyurovsky et al. in the *in vitro* auto-ubiquitination assay may also contain the dimeric, active species of the protein, resulting in detectable formation of poly-Ub species.

It is important to consider that the work mentioned here, done by myself and other groups, looked only at overexpressed MDM2. Regardless of the expression system, MDM2 analysis is carried out at concentrations higher than that of endogenous protein. We lack knowledge on the oligomerisation state of endogenous MDM2 in cells. It is possible that the extensive oligomerisation, witnessed by us and other research groups, is an artificially induced state resulting from an abrupt overproduction of the protein. This hypothesis is supported by the oligomerisation observed after refolded MDM2 230-C dimer was concentrated. However, *in vivo*, MDM2 is known to be widely post-translationally

modified. If endogenous MDM2 also undergoes oligomerisation, there might a mechanism employed involving post-translational mechanisms to regulate oligomerisation. In 2009 and 2011 Cheng et al. published results of their extensive research on ATM-driven phosphorylation of MDM2 (Cheng *et al.*, 2009, 2011). They showed that upon γ irradiation of 293T cells, MDM2 is phosphorylated at residues positioned close to the RING domain, and this event is a result of ATM kinase activity. Phosphorylation of 6 residues (Ser-386, Ser-395, Ser-407, Thr-419, Ser425 and Ser-429) decreased oligomerisation of MDM2 362-C purified from SJSA cells, as evaluated by size exclusion chromatography. This indicates that post-translational modifications can influence the oligomeric state of MDM2. However, in these studies Cheng at al. examined the oligomeric state of the RING domain only. Consequently, it is not known if the activity of ATM results in an increase in the amount of full-length MDM2.

In conclusion, purification protocols I developed allowed me to isolate dimeric MDM2 230-C, which was used in subsequent studies to investigate MDM2 - p14ARF complex. MDM2 is a very challenging protein to examine *in vitro* due to its prominent oligomerisation. Even though some reports suggest that particular PTMs could decrease the oligomerisation of MDM2, we lack the knowledge on how specific modifications of MDM2 would influence its function, especially in the context of MDM2-p14ARF complex formation. Finally, as described in section 1.3-4, MDM2 from different species shows the highest sequence identity within well-defined domains (i.e. p53BD, AD, RING), whereas less sequence similarity is observed for the remaining parts of the protein. It is likely that site-directed mutagenesis studies, informed by a comparison of MDM2 sequences from different organisms, might yield a more stable construct of the full-length protein.

3.2 Biochemical characterisation of MDM2-p14ARF complexes

In the early 2000s a number of independent groups published work detailing ARF-MDM2 interactions. Midgley et al. implemented an ELISA to determine the sequence of p14ARF required for MDM2 binding (Midgley *et al.*, 2000). They proposed that the first 20 amino acids of p14ARF are sufficient for binding and inhibiting MDM2 and also reported that GFP-tagged p14ARF 1-20 led to an increase in the endogenous levels of p53 in MCF7 and U2OS cells, as well as decrease in the MDM2-dependent p53 ubiquitination *in vitro* (Midgley *et al.*, 2000). Lohrum et al. further supported these findings, showing that p14ARF 1-22 binds and re-localises MDM2 to the nucleolus of MCF7 and U2OS cells (Lohrum *et al.*, 2000). They also suggested that a second, low-affinity MDM2-binding site may be encoded in Exon 2 of the p14ARF locus (Lohrum *et al.*, 2000). Kriwacki's group looked at the interaction between human MDM2 and p19ARF, putting forward a theory that two segments of p19ARF (1-14 and 26-37) are required for binding to two independent sites on MDM2 (AD and RING), leading to the nucleolar localisation of MDM2 and cell cycle arrest of MEFs (Weber *et al.*, 2000). This group subsequently focused on the conserved motif - R*FLV**VR, present in the first 37 amino acids of both p14ARF and p19ARF and published an NMR structure of N37p19ARF (Bothner *et al.*, 2001; DiGiammarino *et al.*, 2001). Moreover, in 2001 Llanos et al. found that overexpression of N29p14ARF in NARF cells and human diploid fibroblast leads to stabilisation of p53 without nucleolar relocalisation of MDM2 (Llanos *et al.*, 2001). A more detailed literature review on the MDM2-ARF-p53 axis can be found in section 1.7.

Based on these reports, we hypothesised that ARF exhibits inhibitory effects on MDM2 by initially binding with high-affinity to the AD and then by low affinity to the RING domain, which in turn leads to the inhibition of ligase activity and possibly re-localises the complex to the nucleolus. For this reason, I wanted to validate the minimal sequence of p14ARF required to reduce ligase activity of MDM2 using biochemical activity assays in order to purify MDM2/p14ARF complex suitable for structural studies.

3.2.1 p14ARF constructs design

Analysis of p14ARF sequence with secondary structure prediction programs suggested that the protein is highly disordered, with only three secondary structure motifs present. Two β -strands have been linked to residues 1-14 and 19-28, which are followed by an α -helix (residues 40-54) (McGuffin, Bryson and Jones, 2000; Drozdetskiy *et al.*, 2015) (Figure 3.2-1). Based on these analyses, as well as the available literature, I created a range of p14ARF constructs that were used for initial characterisation of p14ARF-MDM2 complexes:

- N20p14ARF (2.4 kDa) contains the first conserved acidic motif and is located within the first predicted β -strand.
- 17-32p14ARF (1.8 kDa) contains the second conserved acidic motif and is located within the second predicted β -strand.
- N37p14ARF (4.3 kDa) spans both acidic motifs and the two β -strands mentioned above.
- N56p14ARF (6.2 kDa) is the longest construct, which spans the N-terminal sequence of ARF and is predicted to contain the two aforementioned β -strands followed by an α -helix.

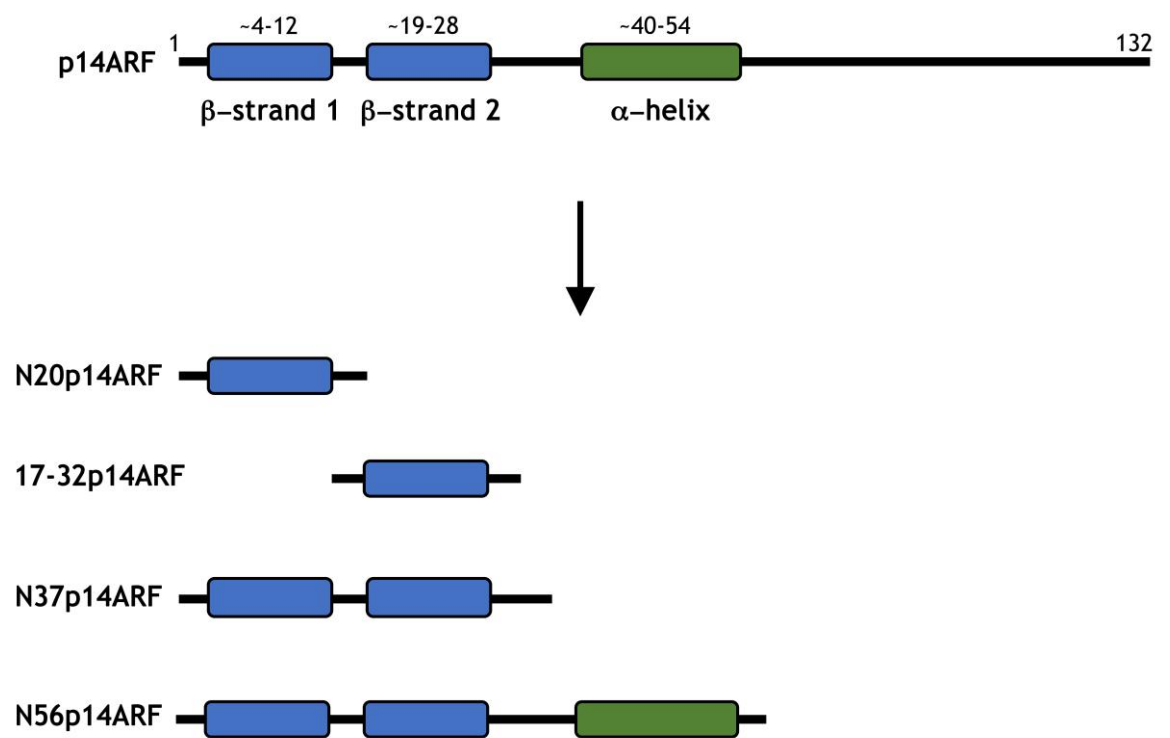


Figure 3.2-1 p14ARF predicted domain architecture and construct design

Schematic representation of p14ARF constructs generated for MDM2 230-C binding analysis. Constructs were designed based on secondary structure prediction analysis. Both N20p14ARF and 17-32p14ARF comprise sequences predicted to span independent β -strand; N37p14ARF comprises both β -strands, and N56p14ARF contains both β -strands and an additional sequence predicted to have a helical fold.

3.2.2 p14ARF constructs bind MDM2 230-C

To validate which fragment of p14ARF is responsible for binding to MDM2 230-C, I co-expressed both proteins with various tag systems and performed small-scale double pull-down tests. GST-MDM2 was tested for binding to His-MBP-p14ARF and His-p14ARF constructs, whereas His-MBP-MDM2 binding to CBP-p14ARF variants was investigated. As seen in Figure 3.2-2, MDM2 230-C was easily detectable in all of the conditions, suggesting direct binding to all p14ARF constructs. However, because all the p14ARF sequences are characterised by a low MW, their detection was problematic in the case of small tag systems (His-tag MW~1.2 kDa; CBP-tag MW~3 kDa) (Figure 3.2-2 B and C). In contrast, addition of a high-MW tag (MBP MW ~42 kDa) to p14ARF greatly facilitated its identification using SDS-PAGE (Figure 3.2-2 A). Although the His-MBP-N56p14ARF band was less sharp and defined compared with other p14ARF constructs, all of the conditions suggest formation of a complex between ARF and MDM2.

3.2.3 p14ARF affects MDM2 catalytic activity *in vitro*

After confirming that all of the created p14ARF constructs are able to bind and pull-down MDM2, I wanted to test how p14ARF constructs affect MDM2 activity. For this purpose, I performed lysine discharge assay, where I tested the influence of His-MBP-p14ARF on the activity of GST-MDM2 230-C. As shown on Figure 3.2-3, GST-MDM2 230-C stimulated the discharging Ubch5B-Ub as compared with the negative control, in which no E3 was present in the reaction. In contrast, all purified GST-MDM2 230-C/His-MBP-p14ARF complexes led to decreased activity. The most pronounced effect on GST-MDM2 230-C was provided by N56p14ARF and N37p14ARF, in which the disappearance of the Ubch5B-Ub band was comparable to the negative control. Both N20p14ARF and 17-32p14ARF also reduced the activity of GST-MDM2 230-C, but the effect was less pronounced as compared with the longer p14ARF constructs.

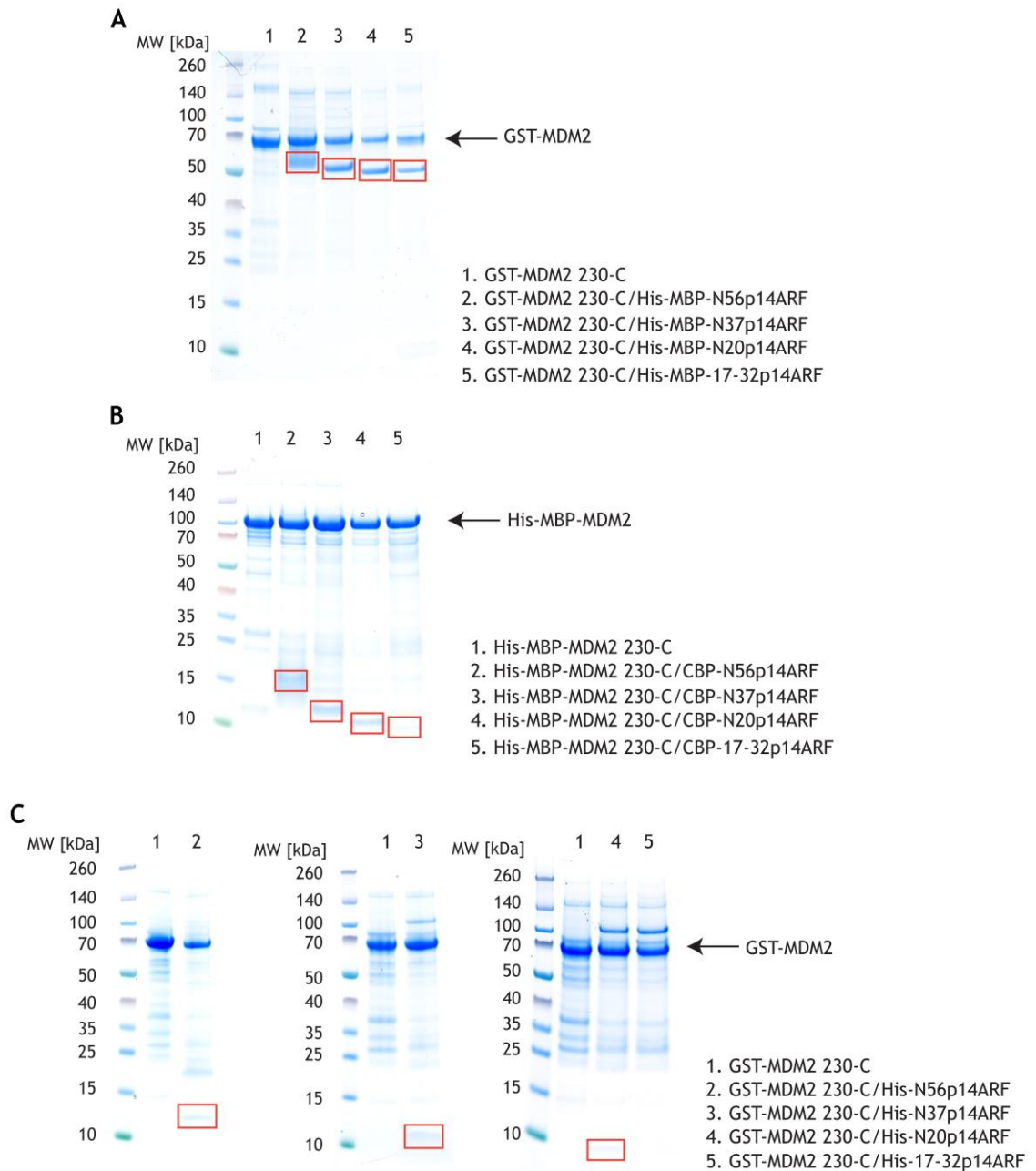


Figure 3.2-2 Double pull-down of MDM2 230-C and p14ARF variants

A- SDS-PAGE showing double pull-down of GST-MDM2 230-C with different His-MBP-p14ARF constructs. GST-MDM2 230-C was co-expressed with each His-MBP-p14ARF construct. Lysates were subjected to Ni^{2+} -resin purification followed by GSH-Sepharose purification. All His-MBP-p14ARF constructs pulled down GST-MDM2 230-C. Red squares indicate different His-MBP-p14ARF constructs.

B- SDS-PAGE showing double pull-down of GST-MDM2 230-C with different CBP-p14ARF constructs. GST-MDM2 230-C was co-expressed with CBP-p14ARF constructs. Lysates were subjected to calmodulin-resin purification followed by GSH-Sepharose purification. All CBP-p14ARF constructs pulled down GST-MDM2 230-C. Red squares indicate different CBP-p14ARF constructs.

C- SDS-PAGE showing double pull-down of GST-MDM2 230-C with different His-p14ARF constructs. GST-MDM2 230-C was co-expressed with His-p14ARF constructs. Lysates were subjected to Ni^{2+} -resin purification followed by GSH-Sepharose purification. Despite the small MW of His-p14ARF peptides, GST-MDM2 230-C was present after double pull-down indicating that it binds all His-p14ARF constructs. Red squares indicate different His-p14ARF constructs.

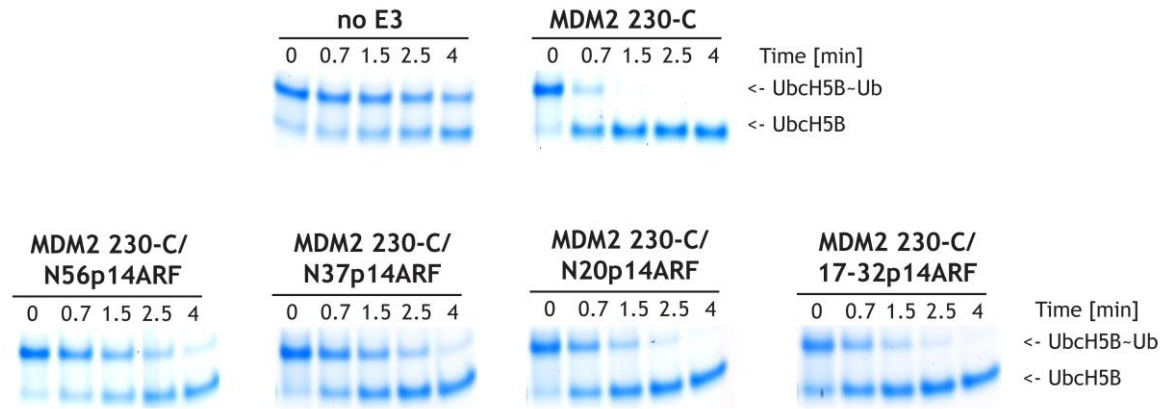


Figure 3.2-3 Influence of p14ARF constructs on MDM2 catalytic activity

The effect of p14ARF constructs on MDM2 230-C catalytic activity was assessed with lysine discharge assay. GST-MDM2 230-C discharged Ubch5B-Ub rapidly, whereas the presence of His-MBP-N56p14ARF or His-MBP-N37p14ARF greatly reduced the discharge of Ubch5B-Ub. Similarly, His-MBP-N20p14ARF and His-MBP-17-32p14ARF also reduced the activity of MDM2 230-C. Reactions were performed as described in section 2.2.7, using 300 nM indicated E3.

The lysine discharge assay probes how MDM2 RING domain binds Ubch5B-Ub and optimises the thioester bond for transfer of Ub to free lysine. In contrast, in autoubiquitination assays the accessibility of acceptor lysines on the E3 and on other substrates in the reaction influence the activity. Therefore, defects observed in Ubch5B-Ub discharge in the presence of p14ARF suggest that p14ARF somehow inhibits the ability to bind and prime E2-Ub for transfer. How p14ARF achieves this when it binds to the AD region of MDM2, which is distal from the RING domain, is intriguing. We hypothesised a model whereby the high-affinity p14ARF interaction with the MDM2 AD triggers a conformational change that blocks the E2-Ub binding surface of the RING domain.

To investigate whether p14ARF constructs can impede the binding between MDM2 RING and E2-Ub, I performed SPR analyses to investigate the binding affinity of GST-MDM2 230-C with Ubch5B S22R C85K-Ub in the presence and absence of His-MBP-p14ARF constructs. All GST-MDM2 230-C/His-MBP-p14ARF complexes were co-expressed in *E. coli* and purified by double pull-down as described earlier. Sensograms and binding curves for each of the ligands are shown in Figure 3.2-4 and K_d values are listed in Table 10.

Table 10 K_d for interactions between GST-MDM2 230-C / His-MBP-p14ARF variants and Ubch5B S22R C85K-Ub

| Immobilised protein | K_d [μM] | Binding diminution (fold) |
|------------------------------------|-------------------------|---------------------------|
| GST-MDM2 230-C | 39 | |
| GST-MDM2 230-C/His-MBP-N56p14ARF | 71 | 1.8 |
| GST-MDM2 230-C/His-MBP-N37p14ARF | 78 | 2 |
| GST-MDM2 230-C/His-MBP-N20p14ARF | 55 | 1.4 |
| GST-MDM2 230-C/His-MBP-17-32p14ARF | 87 | 2.2 |

The results showed that the presence of various His-MBP-p14ARF sequences reduced the affinity of GST-MDM2 230-C for Ubch5B S22R C85K-Ub by ~2-fold. Based on the differences observed in the lysine discharge assays (Figure 3.2-3), I was anticipating a greater effect. This discrepancy in effects might be due to conformational constraints introduced by the SPR technique. For SPR, GST-

MDM2/His-MBP-p14ARF constructs were captured on the chip surface using a GST-specific antibody. Immobilising the complex on the chip surface might limit conformational freedom. Furthermore, given both GST and MDM2 RING can dimerise, immobilisation could additionally limit the MDM2 conformation, depending on how the GST-tag binds the anti-GST-antibody. Lastly, the MBP-tag introduced to assist visualisation is large and may potentially block conformational changes, especially when the complex is immobilised. Nonetheless, the binding studies support the hypothesis that p14ARF binding likely induces a conformational change that blocks the E2-Ub binding site on the RING domain.

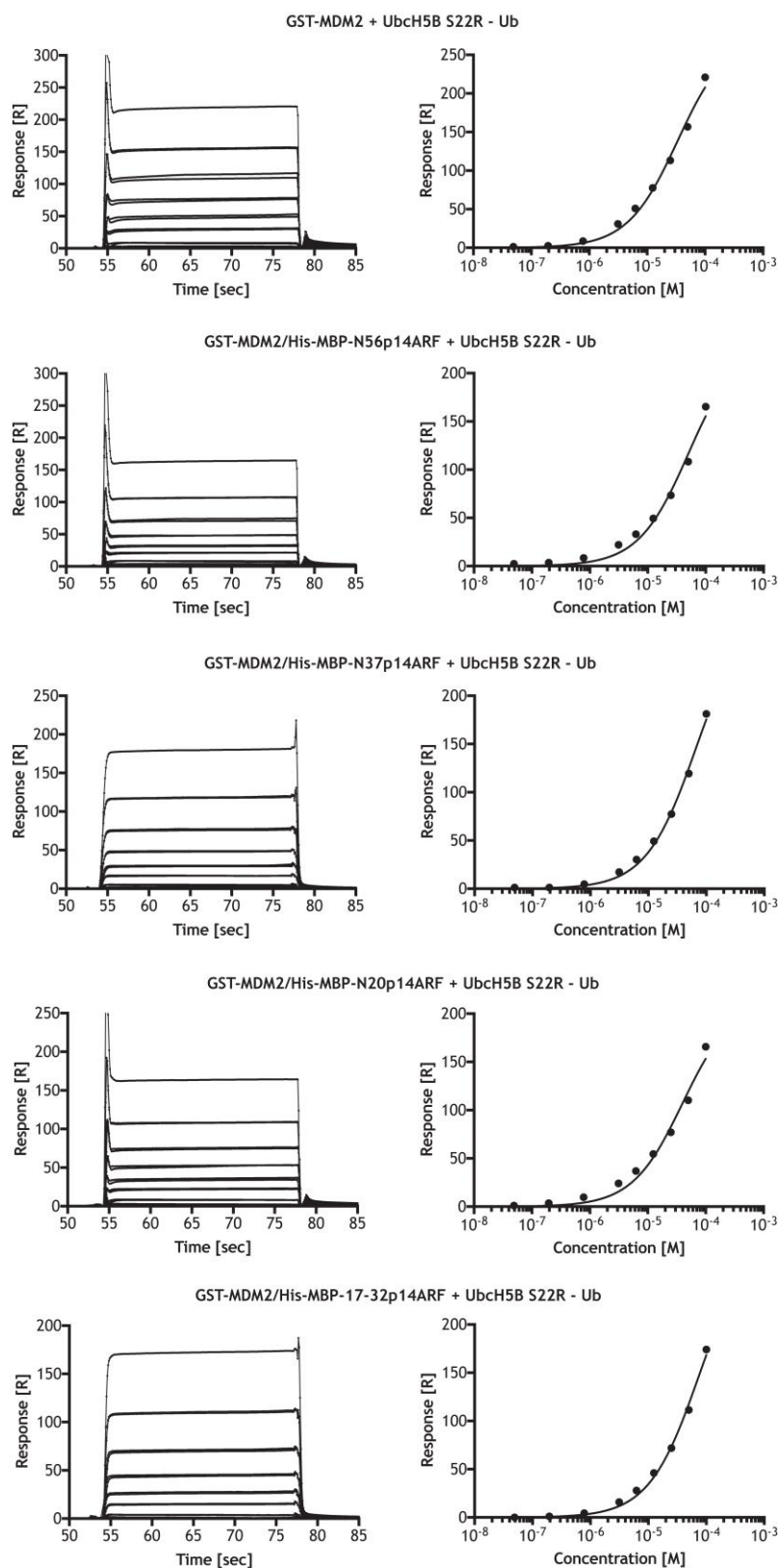


Figure 3.2-4 SPR analysis of the binding affinity between GST-MDM2 230-C/His-MBP-p14ARF variants and UbCh5B-Ub complex

Representative sensograms (left) and binding curves (right) for GST-MDM2 230-C and GST-MDM2 230-C/His-MBP-p14ARF variants in the presence of UbCh5B S22R-Ub. The S22R mutant of UbCh5B was used to eliminate the backside binding of Ub to UbCh5B. The presence of p14ARF resulted in a modest, ~2-fold decrease in the binding affinity between MDM2 230-C and UbCh5B-Ub. The experiments were performed in duplicate.

3.2.4 MDM2/p14ARF complex purification is hindered by its extensive oligomerisation

To investigate the mechanism of MDM2 inhibition by p14ARF using structural studies, I attempted to purify MDM2 230-C/p14ARF complex. Even though I experienced great difficulties isolating dimeric MDM2 230-C, I decided to first co-express GST-MDM2 230-C with His-MBP-p14ARF for these studies. Domains that are predicted to be intrinsically unstructured quite often hinder protein purification, leading to their aggregation (Bondos and Bicknell, 2003). Even though both MDM2 AD and p14ARF are predicted to be highly disordered, we hypothesised that they may fold properly upon complex formation (Bondos and Bicknell, 2003). We maintained use of MBP-tagged p14ARF because it facilitated protein analysis using SDS-PAGE. In addition, MBP-tags have been used to aid protein solubility and crystallisation. For these reasons, a construct was created where His-MBP-N56p14ARF was expressed without a TEV protease cleavage sequence after MBP (referred to as MBP*). Treatment with TEV was expected to produce MDM2 230-C/His-MBP*-N56p14ARF complex. These constructs were co-expressed in 100 L of bacterial culture and purified by following the MDM2 purification protocol described in section 3.1.4.

SDS-PAGE analysis of the MDM2 230-C/His-MBP*-N56p14ARF complex after *in situ* cleavage of the GST-tag is shown in Figure 3.2-5 A. The complex was subsequently purified using a SourceQ column. GST-MDM2 230-C/His-MBP*-N56p14ARF complex eluted from the SourceQ column as two overlapping peaks that both contained MDM2 230-C and His-MBP*-N56p14ARF as observed using SDS-PAGE analysis (Figure 3.2-5 A and B). To investigate the oligomerisation state of the complex, the eluted fractions were applied onto a 16/600 Superdex 200 size exclusion column (Figure 3.2-6 A and B). The first peak from the SourceQ column eluted in the form of two overlapping peaks with absorption maxima at ~65 ml and ~80 ml. Column specification provided by the GE Healthcare for a standard run with the same sample load and flow rate indicates the presence of proteins with estimated MWs' of 150 kDa and 30 kDa, respectively. The ~65 ml peak correlates with the MW of MDM2 230-C/His-MBP*-N56p14ARF complex (160 kDa) and both proteins were evident when fractions from the peak were analysed by SDS-PAGE (Figure 3.2-6 C). The second peak from the SourceQ column was characterised by a very broad and heterogeneous elution profile on the size

exclusion column. Nevertheless, SDS-PAGE analysis confirmed the presence of both proteins. The 65 ml retention volume is characterised by the presence of both proteins at a 1:1 ratio as judged by the equal band intensity on SDS-PAGE. This experiment confirmed that MDM2 230-C and N56p14ARF form a stable complex, and both proteins remain bound during ion exchange and size exclusion chromatography. Unfortunately, separation of the dimeric MDM2 230-C/His-MBP*-N56p14ARF complex proved to be extremely challenging. Having experienced great difficulties purifying the MDM2/p14ARF complex, I decided to purify both proteins individually and then assemble the complex.

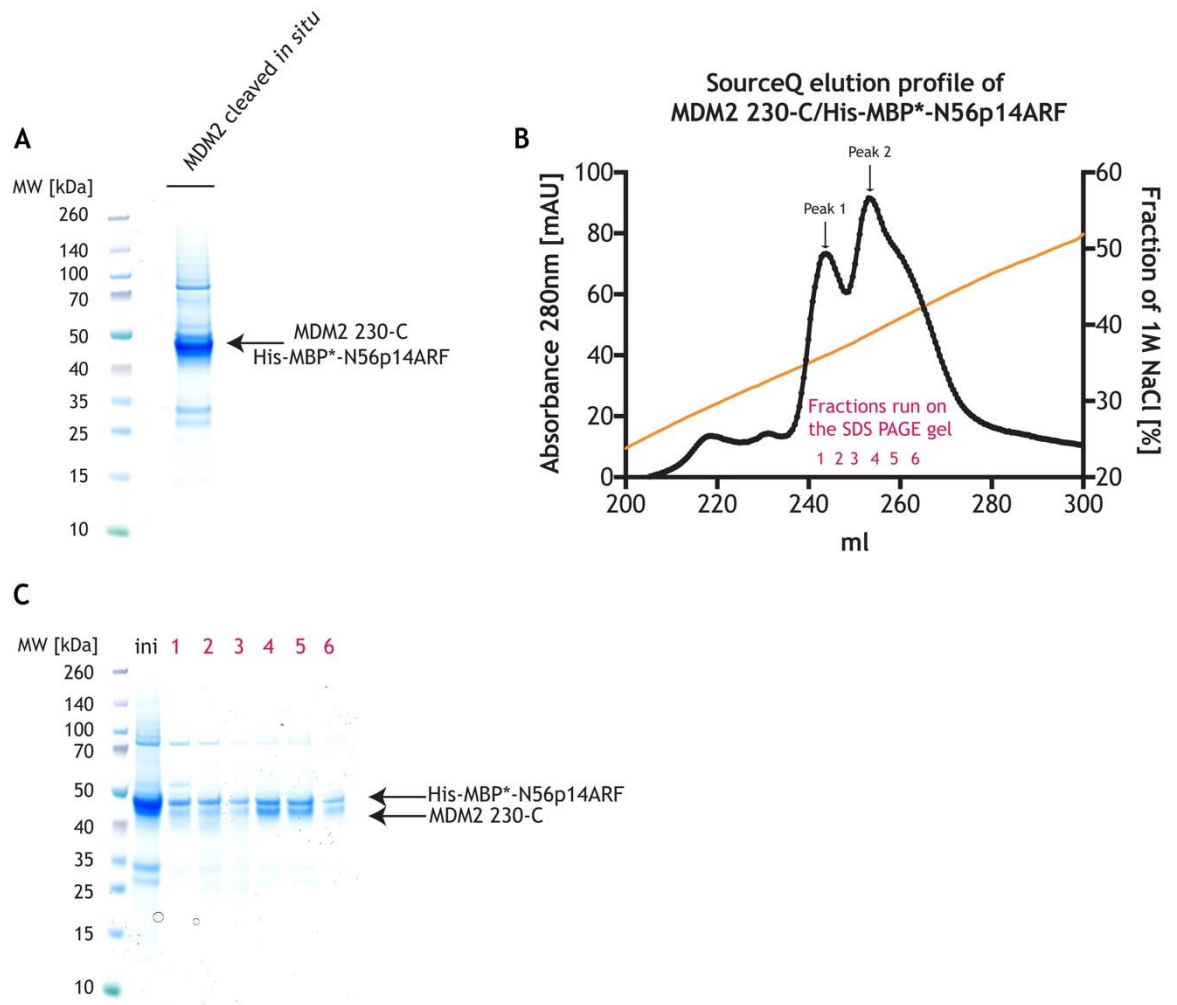


Figure 3.2-5 Purification of MDM2 230-C/His-MBP*-N56p14ARF complex with SourceQ chromatography

A- SDS-PAGE showing MDM2 230-C/His-MBP*-N56p14ARF complex. The first step of the GST MDM2 230-C/His-MBP*-N56p14ARF complex purification involved Ni²⁺-affinity purification followed by GSH-sepharose-affinity purification. The complex was eluted from the GSH-sepharose column by an *in-situ* cleavage with TEV protease. Cleaved MDM2 230-C/His-MBP*-N56p14ARF was analysed on an SDS-PAGE gel. MDM2 230-C and His-MBP*-N56p14ARF bands overlapped but were resolved as shown in panel C when less protein was loaded.

B- SourceQ elution profile of MDM2 230-C/His-MBP*-N56p14ARF complex. The elution profile was characterised by the presence of two overlapping peaks with absorption maxima at 360 mM and 400 mM NaCl.

C- SDS-PAGE showing the presence of MDM2 230-C and His-MBP*-N56p14ARF in both peaks from SourceQ elution in panel B. The sample loaded onto the column is labelled as ini.

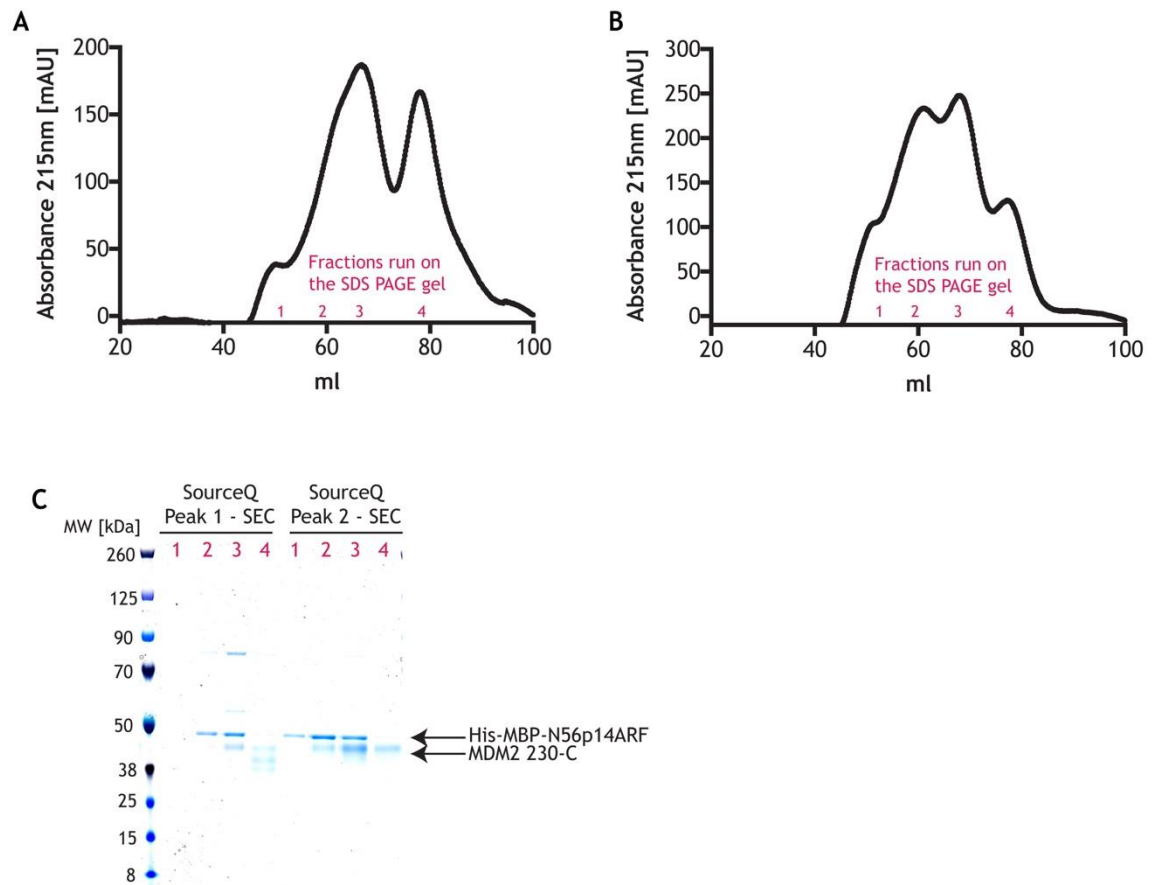


Figure 3.2-6 Purification of MDM2 230-C/His-MBP*-N56p14ARF complex by size exclusion chromatography

A- Size exclusion profile of MDM2 230-C/His-MBP*-N56p14ARF complex eluted in the first peak of the SourceQ column run in Figure 3.2-5 panel B. MDM2 230-C / His-MBP*-N56p14ARF were analysed on a 16/600 Superdex 200 size exclusion column. The first peak from the source Q column was characterised by the presence of two, main overlapping peaks, with absorption maxima at 65 ml and 80 ml.

B- Size exclusion profile of MDM2 230-C/His-MBP*-N56p14ARF complex eluted from the second peak of the SourceQ column run in Figure 3.2-5 panel B. The elution profile showed the presence of 4 overlapping peaks with absorption maxima at ~50 ml, 60 ml, 65 ml and 80 ml.

C- SDS-PAGE showing the peak fractions from the size exclusion chromatography profiles shown in panels A and B. MDM2 230-C/p14ARF complex was primarily present in the second peak of the SourceQ elution and was characterised by a retention volume of 65 ml on the 16/600 Superdex 200 column.

3.2.5 p14ARF alone does not express in a soluble form

As I have previously determined that His-MBP-N56p14ARF binds and inhibits MDM2, I initially decided to purify this construct of p14ARF. Surprisingly, a Ni²⁺ affinity pull down experiment showed no detectable expression of His-MBP-N56p14ARF but large amounts of protein corresponding to His-MBP alone were evident (Figure 3.2-7). It is likely that expression of p14ARF on its own is toxic and unfavourable, whereas co-expression with a binding partner like MDM2 leads to formation of a stable complex (Rosano and Ceccarelli, 2014). A secondary structure prediction of the His-MBP-N56p14ARF construct suggested that the N-terminus of MBP, together with the TEV cleavage sequence, form an unstructured and flexible linker that may also impede the expression of the p14ARF sequence (Yu *et al.*, 2017). More comprehensive analysis (e.g. Western blotting) would be required in order to confidently verify lack of p14ARF expression in the soluble form, as the SDS PAGE gel in Figure 3.2-7 was only analysed with Coomassie stain.

Because expression and purification of MDM2/p14ARF complex and p14ARF alone are extremely challenging, we decided to focus on two new approaches to investigate the nature of the MDM2-p14ARF interaction:

- We acquired a synthetic peptide of p14ARF, which was solubilised and added to the previously purified dimeric MDM2 230-C to form MDM2/p14ARF complex.
- We created “fusion constructs” of ARF and MDM2, in which p14ARF and MDM2 are expressed as one construct, ensuring production of a 1:1 complex.

The following sections describe these approaches and their outcomes in more detail.

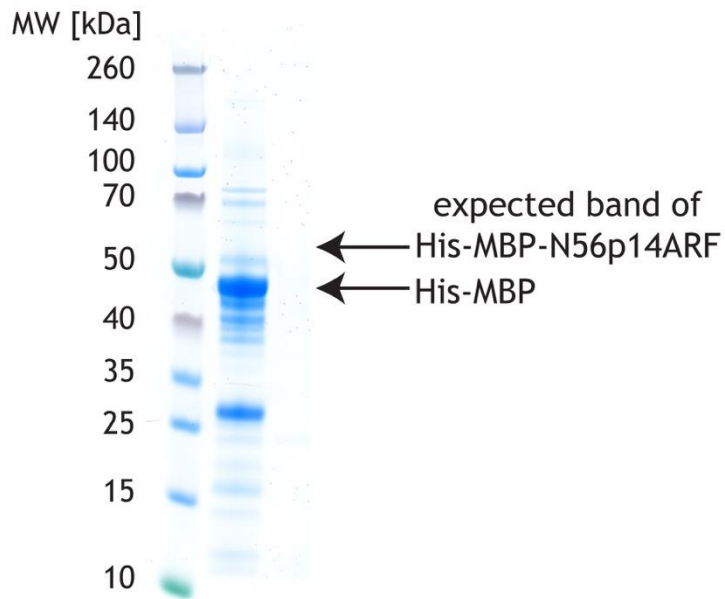


Figure 3.2-7 Test expression of N56p14ARF construct

SDS-PAGE showing Ni²⁺-pull down of His-MBP-N56p14ARF construct. There was no detectable expression of His-MBP-N56p14ARF, but a predominant band corresponding to His-MBP alone was detected. Figure 3.2-2 A, lane 2 indicates that the band corresponding to MBP-N56p14ARF should appear above the 50 kDa marker.

3.2.6 N37p14ARF peptide inhibits MDM2 ligase activity

Because expression of p14ARF constructs did not yield suitable or any quantity of soluble protein, we purchased synthetic p14ARF peptide. We intended to introduce this peptide directly to purified MDM2 to form MDM2-p14ARF complex. Because peptide synthesis may be affected by length and sequence complexity, we decided to focus on the first 37 amino acids of ARF. My earlier work showed that this fragment is as potent as N56p14ARF in inhibiting MDM2 activity (Figure 3.2-3). N37p14ARF peptide (referred to as N37p14ARF) is very basic (predicted pI~12) and hydrophobic. Initial attempts to solubilise the peptide in a number of buffers revealed that the peptide was insoluble in aqueous-based buffers; the peptide formed a white precipitate. Following the guidelines for solubilising peptides provided by Generon, I tested a range of solvents to minimise N37p14ARF precipitation. Suggested additives, such as ethanol and acetic acid, did not improve the solubility of the peptide. The only solvent that solubilised the N37p14ARF peptide was DMSO. DMSO may lead to the formation of sulfoxides and disulfides if methionine, cysteine or tryptophan are present in the peptide sequence (Tam *et al.*, 1991). To prevent formation of sulfoxides and disulfides, I diluted N37p14ARF peptide in the presence of 1 mM TCEP. Small aliquots of 5 mM N37p14ARF were snap frozen in liquid nitrogen and stored at -80°C after dissolving in 100 % DMSO. Another solvent that was suggested for solubilising hydrophobic peptides is 4-8 M GdnHCl and urea, and I was able to successfully solubilise N37p14ARF in GdnHCl as well.

To assemble MDM2/p14ARF complex, I added an excess of N37p14ARF dissolved in DMSO or GdnHCl to MDM2 230-C (~20 μ M) at 6:1 molar ratio to ensure saturation of p14ARF binding site on MDM2. Upon mixing the two components, a strong white precipitate formed immediately. After centrifugation, there was no protein detected in the supernatant suggesting that both components precipitated. Addition of DMSO or GdnHCl alone did not cause any visible precipitation of MDM2. Precipitation was also observed for lower MDM2:p14ARF molar ratios (e.g. 1:5 and 1:4), but when the two components were mixed at 1:1 molar ratio, no precipitation was observed. Therefore, I prepared MDM2 230-C/N37p14ARF complex at a 1:1 molar ratio and assessed the effect of p14ARF on MDM2 activity.

To ensure that none of the N37p14ARF-driven effects were artefacts resulting from disulfide bond formation, I performed assays with N37p14ARF peptide diluted in 6 M GdnHCl. To rule out solvent effects, all experiments were accompanied by a control, where equivalent concentrations of DMSO or GdnHCl were introduced to MDM2 without N37p14ARF present. I purified MDM2 constructs including GST-MDM2 230-C, which contains the AD and RING domain, and GST-MDM2 428-C, which only contains the RING domain. Moreover, I also generated heterodimers comprising GST-MDM2 230-C/His-MDM4 429-C and GST-MDM2 428-C/His-MDM4 429-C by co-expressing both proteins in *E. coli* and purifying complexes using Ni²⁺-affinity followed by GSH-sepharose affinity chromatography. I tested the effects of N37p14ARF by performing lysine discharge assays. Addition of N37p14ARF reduced Ubch5B-Ub discharge catalysed by both GST-MDM2 230-C and GST-MDM2 428-C (Figure 3.2-8 A and B). Interestingly, addition of N37p14ARF did not inhibit the activity of GST-MDM2 230-C/His-MDM4 429-C and GST-MDM2 428-C/His-MDM4 429-C complexes. (Figure 3.2-8 C and D). These results showed that N37p14ARF specifically inhibits MDM2 ligase activity. Notably, even the RING domain alone (MDM2 428-C) was inhibited, suggesting that N37p14ARF can potentially bind the RING domain to block E2-Ub binding. That N37p14ARF had no effect on the corresponding MDM2/MDM4 constructs suggests that certain features present in the homodimer are required for N37p14ARF binding.

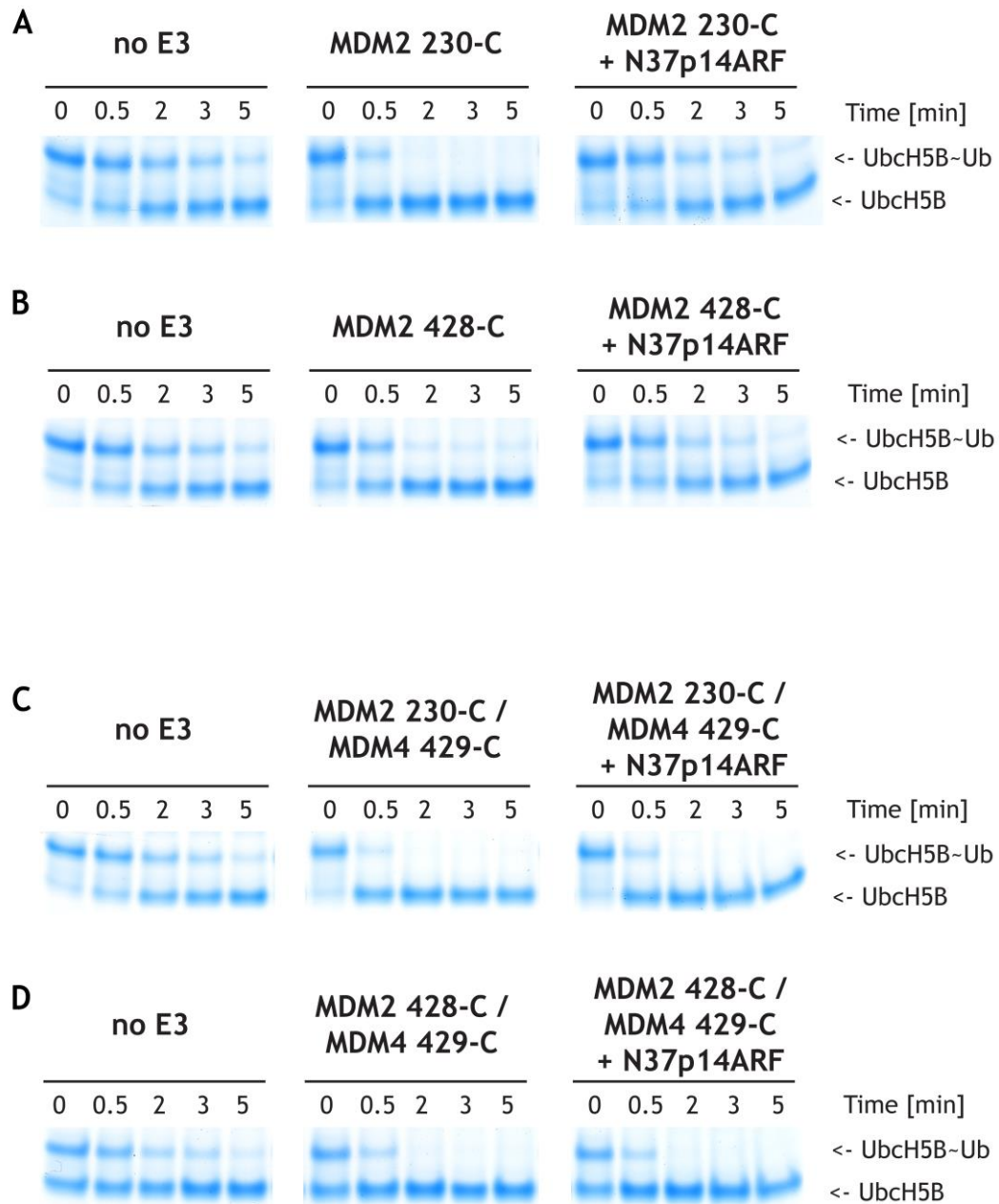


Figure 3.2-8 N37p14ARF peptide influences the activity of MDM2 homodimer but not MDM2/MDM4 heterodimer

All GST-MDM2 and GST-MDM2/His-MDM4 constructs were incubated with N37p14ARF at a 1:1 ratio for 1h at 4°C. For reactions without E3, an equivalent volume of the solvent (GdnHCl) was added.

A and B- SDS-PAGE showing the effect of N37p14ARF on Ubch5B~Ub discharge catalysed by GST-MDM2 230-C and GST-MDM2 428-C, respectively. Reactions were performed as described in section 2.2.7, using 250 nM indicated E3.

C and D- SDS-PAGE showing the effect of N37p14ARF on Ubch5B~Ub discharge catalysed by GST-MDM2 230-C/His-MDM4 429-C and GST-MDM2 428-C/His-MDM4 429-C, respectively. Reactions were performed as described in section 2.2.7, using 500 nM indicated E3.

3.2.7 N37p14ARF peptide induces MDM2 oligomerisation

The oligomerisation state of MDM2 affects its catalytic activity - larger oligomers are less active than MDM2 homodimer (Figure 3.1-12); based on these findings, I wanted to investigate whether N37p14ARF peptide affected the oligomeric state of MDM2. For this purpose, I incubated dimeric MDM2 230-C (see section 3.1.4) with N37p14ARF at a 1:1 ratio and applied the sample onto a Shodex KW-403-4F HPLC column, which provides higher resolution sample separations than the Superdex columns. Dimeric and oligomeric fractions of MDM2 incubated with DMSO or GdnHCl alone were used as standards. As seen in Figure 3.2-9 A, oligomeric and dimeric MDM2 230-C eluted from the HPLC column after 13 min and 16 min respectively. The elution profile of dimeric MDM2 230-C incubated with N37p14ARF peptide is characterised by a broad peak with an absorption maximum at ~13 min, overlapping with peaks in the oligomeric MDM2 230-C elution profile, followed by a second, much smaller peak, appearing after 16 min of the elution. This result suggests that ARF peptide induces oligomerisation of MDM2. I further assessed the effect of N37p14ARF on dimeric MDM2 230-C by native-PAGE analysis. As shown in Figure 3.2-9 B, when N37p14ARF was added to MDM2 230-C dimer, the discrete MDM2 230-C band disappeared and a high MW smear similar to that observed for the oligomeric fraction of MDM2 appeared (see Figure 3.1-5 C). Together these results show that N37p14ARF induces MDM2 oligomerisation.

Based on my earlier refolding success, I next investigated whether refolding MDM2/N37p14ARF complex reduces oligomerisation. I performed small-scale refolding experiments using oligomeric MDM2 230-C (see section 3.1.5) in the presence and absence of N37p14ARF, where N37p14ARF was first dissolved in 6 M GdnHCl-containing buffer and then mixed with oligomeric MDM2 at 4:1 molar ratio in the presence of GdnHCl. Under denatured conditions, there was no precipitation upon mixing even at this higher molar ratio. Upon removal of GdnHCl by Zeba desalting column, there was no sign of precipitation. The sample was loaded on a 10/300 Superdex gel filtration to assess the effect of N37p14ARF. The elution profile showed a pronounced oligomerisation of MDM2 as compared with the sample treated in the absence of N37p14ARF (Figure 3.2-10 A) suggesting that refolding does not alter N37p14ARF-induced MDM2 oligomerisation. Interestingly, SDS-PAGE analysis showed the presence of a

smearly high MW band in the refolded MDM2/N37p14ARF sample (Figure 3.2-10 B). Mass spectroscopic analysis of this band confirmed the presence of N37p14ARF peptide. Lastly, I assessed the activity of the refolded MDM2/N37p14ARF complex by lysine discharge assays. As shown in Figure 3.2-11, oligomerised MDM2 230-C alone showed an increase in activity after refolding, whereas inclusion of N37p14ARF in the refolding mix greatly reduced MDM2 230-C activity. Together, these results show that N37p14ARF induces MDM2 230-C oligomerisation, leading to reduced ligase activity.

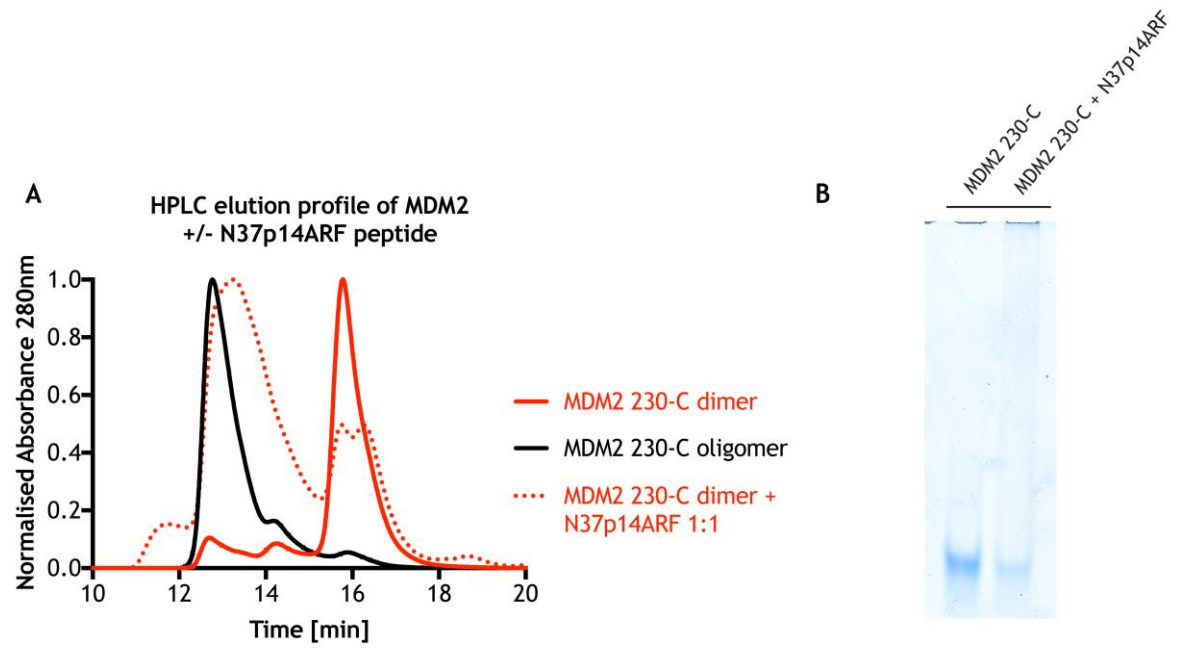
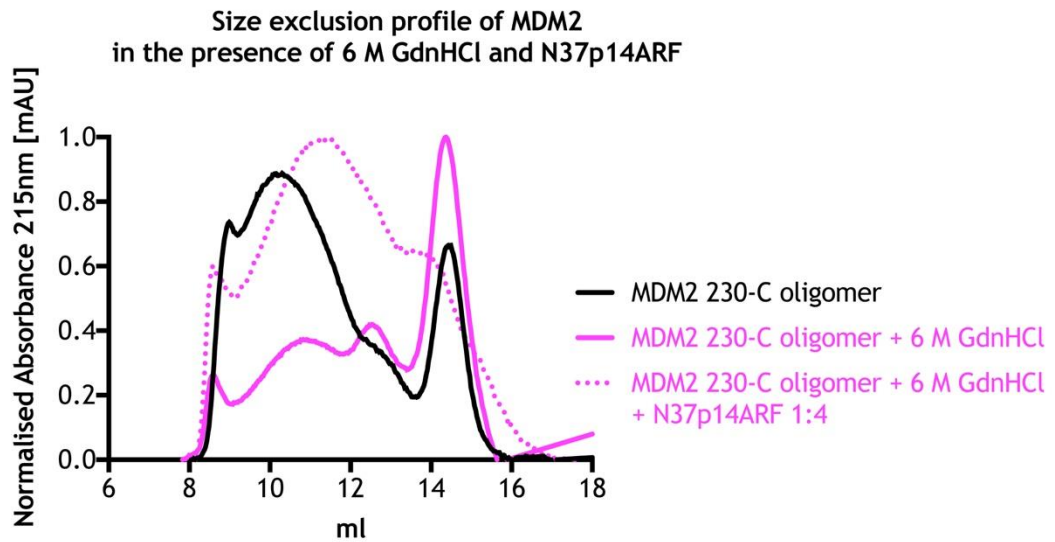


Figure 3.2-9 N37p14ARF peptide induces MDM2 oligomerisation

A- HPLC elution profile of MDM2 230-C in the presence and absence of N37p14ARF. Oligomeric and dimeric fractions of MDM2 230-C and dimeric MDM2 230-C mixed with N37p14ARF at 1:1 molar ratio were loaded on a Shodex KW-403-4F HPLC column.

B- Native-PAGE showing dimeric MDM2 230-C and dimeric MDM2 230-C mixed with N37p14ARF at 1:1 molar ratio.

A



B

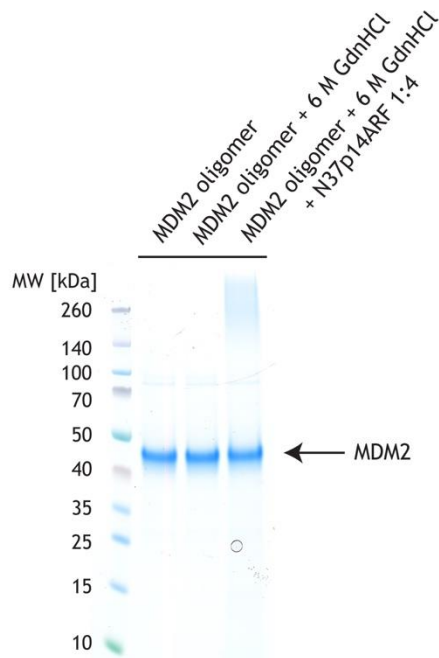


Figure 3.2-10 Oligomerisation of MDM2/p14ARF complex is not reversible following denaturation in GdnHCl and refolding

A- Size exclusion elution profile of oligomeric MDM2 230-C refolded in the presence and absence of N37p14ARF. Oligomeric MDM2 230-C and refolded MDM2 following treatment with GdnHCl in the presence and absence of N37p14ARF were loaded on a 10/300 Superdex 200 size exclusion column.

B- SDS-PAGE showing oligomeric MDM2 230-C alone and refolded from treatment with GdnHCl in the presence and absence of N37p14ARF.

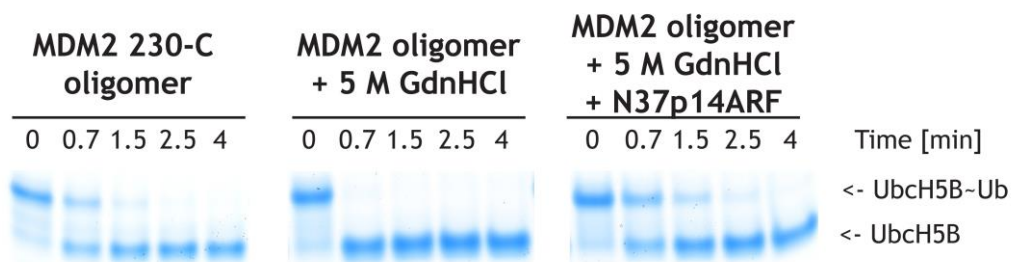


Figure 3.2-11 SDS-PAGE showing the activity of refolded MDM2 230-C/N37p14ARF complex

SDS-PAGE showing the lysine discharged assays used to assess the activity of oligomeric MDM2 230-C alone and refolded from treatment with GdnHCl in the presence and absence of N37p14ARF. Reactions were performed as described in section 2.2.7, using 200 nM indicated E3.

3.2.8 Fusion construct facilitates purification of ARF-MDM2 complex

Thus far, assembly of MDM2-p14ARF complex has been hampered by low yields and complexities introduced by MDM2 oligomerisation coupled with p14ARF peptide induced oligomerisation. Although I developed a protocol for isolating and purifying MDM2 dimer, I was unable to express and purify any fragment of p14ARF alone. Only two methods have yielded complexes - mixing p14ARF peptide with MDM2 dimer and co-expressing MDM2 230-C/His-MBP*-p14ARF. N37p14ARF peptide is hydrophobic and is likely to be unstructured in solution as reported previously (Bothner *et al.*, 2001; Sivakolundu *et al.*, 2008). It is unclear how N37p14ARF induces MDM2 230-C oligomerisation and we cannot exclude the possibility that N37p14ARF can self-oligomerise together with MDM2 230-C due to its high hydrophobic content. The size exclusion profile of MDM2 230-C/His-MBP*-p14ARF complex (Figure 3.2-6) showed a small fraction of this complex seemingly eluted as a dimer, suggesting that this possibility was not correct. Thus, we decided to generate a complex using p14ARF-MDM2 fusion constructs, in which both proteins are expressed at a 1:1 ratio in a single polypeptide chain.

The first construct I generated consisted of p14ARF fused to the N-terminus of MDM2 210-C. The rationale for this construct was to introduce enough flexibility between the two proteins to allow p14ARF to bind the AD of MDM2. The N56p14ARF sequence was fused to the N-terminus of MDM2 210-C with a linker consisting of eight repeats of a GGSG sequence (hereafter referred to as N56p14ARF~~MDM2 210-C; ~~ indicates the linker). Moreover, two thrombin cleavage sequences were introduced at each end of the linker to allow for the complete removal of any restraints between two proteins (Figure 3.2-12). The N56p14ARF~~MDM2 210-C construct was cloned into the pAbl expression vector, which allowed for its expression in a GST tagged form and subsequent removal of the GST tag with TEV protease. Expression and purification of GST-N56p14ARF~~MDM2 210-C construct was tested in two independent semi large-scale expression experiments (~30 L of *E. coli*).

In the first test I purified GST-N56p14ARF~~MDM2 210-C (66 kDa) by GSH-Sepharose affinity purification. The presence of a GST-tag on N56p14ARF after thrombin cleavage enabled the monitoring of the binding between p14ARF and

MDM2. SDS-PAGE analysis confirmed the presence of GST-N56p14ARF--MDM2 210-C after GSH-Sepharose affinity purification (Figure 3.2-13), but the intensity of the band corresponding to the GST-tag alone was equally strong, indicating that expression of GST-N56p14ARF--MDM2 210-C may be problematic. Next, I assessed whether both GST and the linker could be removed by addition of TEV and thrombin proteases, respectively. Addition of TEV protease to GST-N56p14ARF--MDM2 210-C resulted in the disappearance of the band previously correlated to the GST-tagged fusion construct with an increase in the GST band intensity, as well as the appearance of the N56p14ARF--MDM2 210-C (41 kDa) (Figure 3.2-13). This indicated that GST could be readily removed from the construct. Incubation of GST-N56p14ARF--MDM2 210-C with thrombin resulted in the formation of GST-N56p14ARF (33 kDa) and MDM2 210-C (32 kDa), which were easily visualised by SDS-PAGE (Figure 3.2-13). To investigate the oligomeric state, I applied GST-N56p14ARF--MDM2 210-C onto an analytical 10/300 Superdex 200 size exclusion column. The GST-N56p14ARF--MDM2 210-C elution profile was characterised by the presence of two peaks. The first peak eluted between 8 ml and 16 ml and the second peak eluted at ~17 ml (Figure 3.2-14 A). SDS-PAGE analysis confirmed the presence of GST-N56p14ARF--MDM2 210-C in the first peak and free GST in the second peak (Figure 3.2-14 B). The elution profile of GST-N56p14ARF--MDM2 210-C treated with thrombin was similar to the uncleaved protein (Figure 3.2-14 A). Moreover, SDS-PAGE showed that upon removal of the linker, GST-N56p14ARF and MDM2 210-C co-elute, (Figure 3.2-14 C) suggesting that N56p14ARF and MDM2 210-C form a stable complex.

My second protein purification test focused on isolating a GST-free version of the complex. GST-N56p14ARF--MDM2 210-C was first purified by GSH-sepharose-affinity chromatography and cleaved *in situ*, which resulted in the formation of free N56p14ARF--MDM2 210-C. Next the sample was applied onto the 16/600 Superdex 200 size exclusion chromatography column. The elution profile was characterised by a sharp peak appearing at a retention volume equal to 40 ml and descending into a long, broad shoulder (Figure 3.2-15 A). SDS-PAGE showed that N56p14ARF--MDM2 210-C was present in fractions across the peak (Figure 3.2-15 B). A 40 ml retention volume on this column corresponds to MWs above 400 kDa according to specifications provided by GE Healthcare. Further attempts to purify the dimeric fraction of N56p14ARF--MDM2 210-C were unsuccessful.

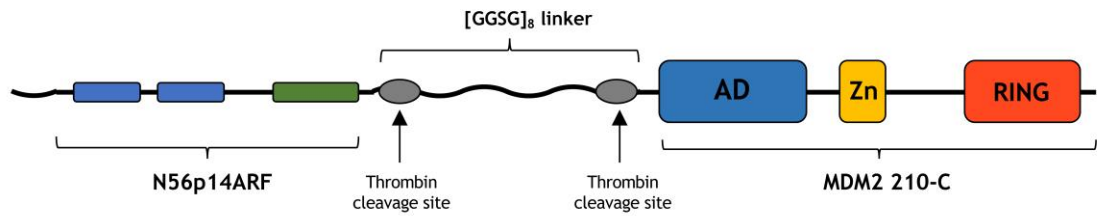


Figure 3.2-12 Architecture of the N56p14ARF~MDM2 210-C construct

The designed fusion construct consists of the N56p14ARF sequence linked to MDM2 210-C via a flexible linker. Two thrombin cleavage sequences were introduced to ensure complete separation of p14ARF and MDM2 upon removal of the linker. The construct was cloned into the pAlo vector, resulting in the expression of GST-tagged N56ARF~MDM2 210-C, where a TEV cleavage sequence was present between the GST and p14ARF.

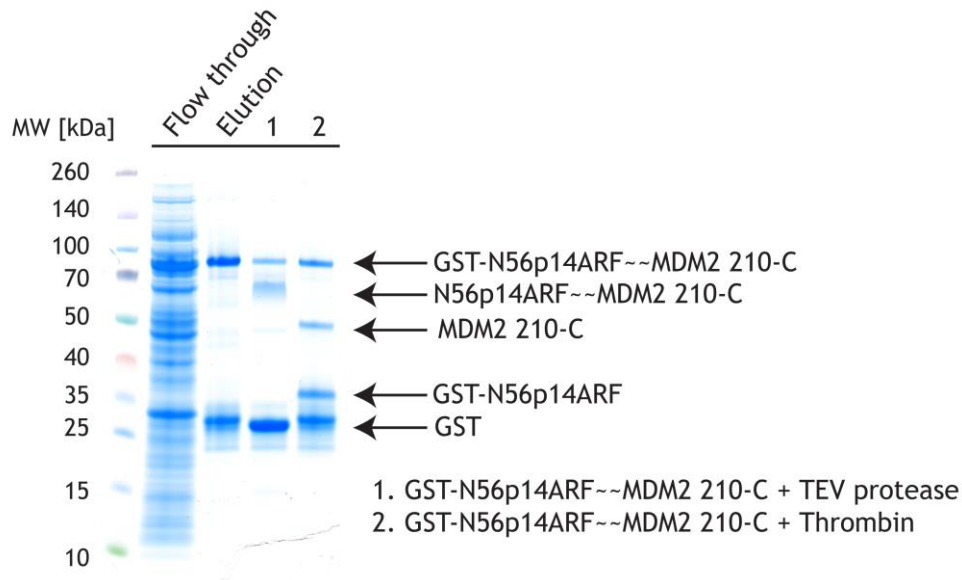


Figure 3.2-13 SDS-PAGE showing GST-N56p14ARF~MDM2 210-C and cleavage by TEV and thrombin proteases

Protein excluded from the GSH resin during washing is shown in the first lane. GST-N56p14ARF~MDM2 210-C (66 kDa) eluted from GSH beads is shown in the second lane. Addition of TEV to the eluted sample resulted in a decrease in intensity of the GST-N56p14Ar~MDM2 210-C band, an increase in the intensity of the GST band, and the appearance of a band corresponding to the MW of N56p14ARF~MDM2 210-C (41 kDa). Addition of thrombin to GST-N56p14ARF~MDM2 210-C produced GST-N56p14ARF (33 kDa) and MDM2 210-C (32 kDa).

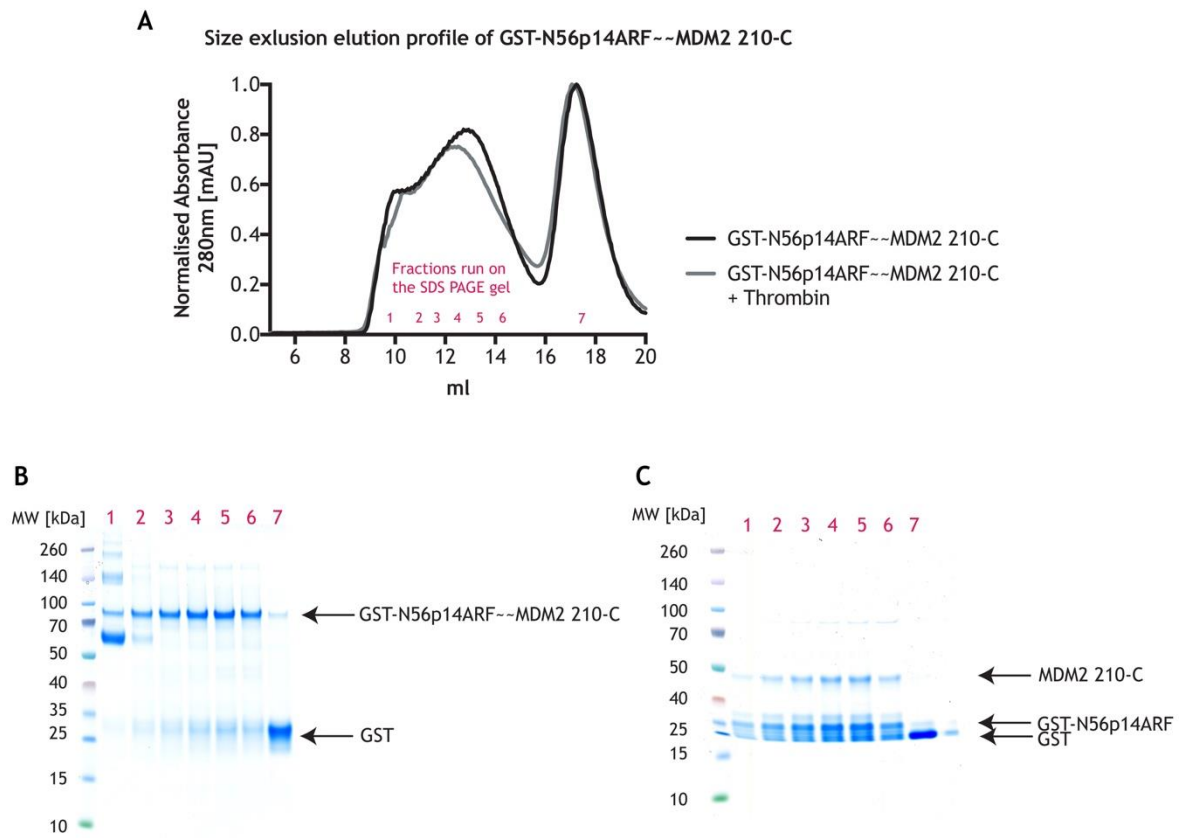
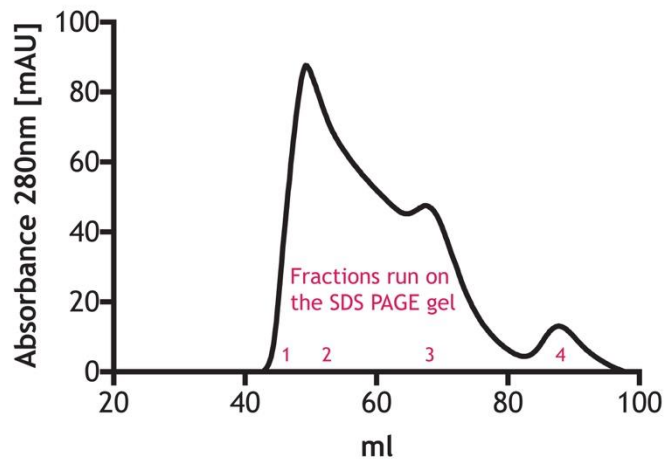
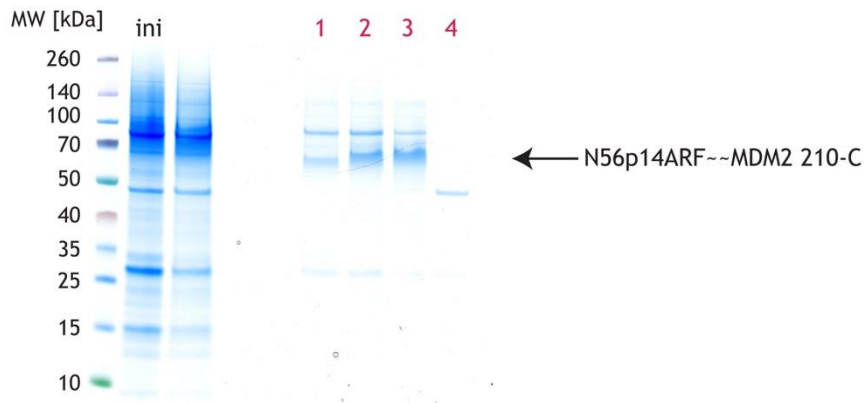


Figure 3.2-14 Size exclusion elution profile of GST-N56p14ARF--MDM2 210-C following treatment with thrombin

A- Elution profile of GST-N56p14ARF--MDM2 210-C treated with and without thrombin on a 10/300 Superdex 200 size exclusion column. A broad peak covering elution volumes from 8-16 ml was previously linked to the presence of high MW oligomeric species of MDM2 (see Figure 3.1-5 D and E, Figure 3.1-9 and Figure 3.2-10 A).

B- SDS-PAGE analysis of fractions eluted from GST-N56p14ARF--MDM2 210-C run shown in A confirmed the presence of the protein of interest in the first, broad peak. A sharp peak at ~17 ml of the retention volume contained GST alone.

C- SDS-PAGE analysis of the eluted samples from GST-N56p14ARF--MDM2 210-C treated with thrombin. Both GST-N56p14ARF and MDM2 210-C bands were present in the first broad peak.

A Size exclusion elution profile of N56p14ARF~~MDM2 210-C**B****Figure 3.2-15** Size exclusion elution profile of N56p14ARF~~MDM2 210-C

A- Elution profile of N56p14ARF~~MDM2 210-C on a 16/600 Superdex 200 size exclusion column.

B- SDS-PAGE analysis confirmed the presence of N56p14ARF~~MDM2 210-C in the broad peak in panel A. First lane (marked as "ini") represents sample obtained after *in situ* cleavage of the GST-N56p14ARF~~MDM2 210-C construct, prior to application on the size exclusion chromatography column.

3.2.9 p14ARF-MDM2 RING fusion constructs confirms ARF-driven inhibition of MDM2 ligase activity

I have shown that the presence of the AD of MDM2 is required for the formation of a stable p14ARF-MDM2 complex. However, the N37p14ARF peptide study showed that p14ARF directly inhibits the activity of MDM2 RING domain. Since I did not observe an interaction between MDM2 RING domain alone and p14ARF using a double-pull down, I speculated that p14ARF likely binds MDM2 RING domain with weak affinity. To study the effect of p14ARF on MDM2 RING domain without using synthetic p14ARF peptide, I generated various constructs of p14ARF fused to MDM2 RING domain. Based on N37p14ARF synthetic peptide inhibiting MDM2 activity to the same extent as MBP-N56p14ARF, I focused my investigation on the effects of p14ARF N-terminal residues on MDM2 RING domain. I generated several GST-tagged constructs in which residues 1-32 of p14ARF were linked to the N-terminus of MDM2 350-C (shown in Figure 3.2-16). All of these constructs were expressed and purified by glutathione sepharose-affinity column. The eluted fractions showed the expected full-length GST-tagged fusion constructs along with other contaminants, including GST alone (Figure 3.2-17). To assess the effects of p14ARF on MDM2 activity, I performed lysine discharge assays. Given that the purity of each fusion variant was different, I standardised their concentration by measuring the intensity of the GST-p14ARF-MDM2 350-C band using the LI-COR imaging system and then correlated the actual protein concentration with the intensity of the GST-MDM2 350-C control (Figure 3.2-17). GST-MDM2 350-C rapidly discharged UbCh5B-Ub within the first minute, whereas the presence of N32p14ARF fusion resulted in a decrease in the disappearance of UbCh5B-Ub (Figure 3.2-18 A). Interestingly, very little or no inhibition was detected when N32p14ARF was fused to MDM2 350-C in complex with His-MDM4 429-C, indicating that N32p14ARF selectively inhibits the RING domain of MDM2 homodimer (Figure 3.2-18 B). This observation was further supported by SPR analysis, where upon introduction of N32p14ARF, GST-MDM2 350-C displayed ~7-fold weaker binding affinity for UbCh5B-Ub than GST-MDM2 350-C alone. In contrast, GST-MDM2 350-C/His-MDM4 429-C and GST-N32p14ARF-MDM2 350-C/His-MDM4 429-C exhibited similar affinities for UbCh5B-Ub (Table 11 and Figure 3.2-19; ~1.4 fold difference). Next, I investigated the effects of shorter p14ARF fragments on MDM2 RING activity. N14p14ARF and 16-32p14ARF, containing the first and second β -strands of ARF, respectively, were

fused to the N-terminus of MDM2 350-C. Interestingly, neither of these shorter p14ARF fusion constructs affected MDM2 activity (Figure 3.2-20). Sequence alignment of p14ARF and p19ARF showed several conserved residues at the N-terminus of ARF protein (section 1.4.2). Notably, two conserved R*FLV**VR motifs (motif 1 consists of R3, F5 and V7; motif 2 consists of R21, F23 and V25) were identified. A fusion construct bearing alanine substitutions of these six amino acids was generated (R3A, F5A, V7A, R21A, F23A, V25A, referred to as 6ALA). GST-N32p14ARF-6ALA-Mdm 350-C displayed similar activity as GST-MDM2 350-C alone, suggesting that these motifs are important for p14ARF-mediated inhibition of MDM2 RING domain activity (Figure 3.2-20).

Table 11 Effects of N32p14ARF on the K_d for interactions between Ubch5B S22R C85K-Ub and MDM2 homodimer or MDM2/MDM4 heterodimer

| Immobilised protein | K_d [μ M] | Binding diminution (fold) |
|---|------------------|---------------------------|
| GST-MDM2 350-C | 21 | |
| GST-N32p14ARF-MDM2 350-C | 150 | 7.1 |
| GST-MDM2 350-C/His-MDM4 429-C | 52 | |
| GST-N32p14ARF-MDM2 350-C/His-MDM4 429-C | 75 | 1.4 |

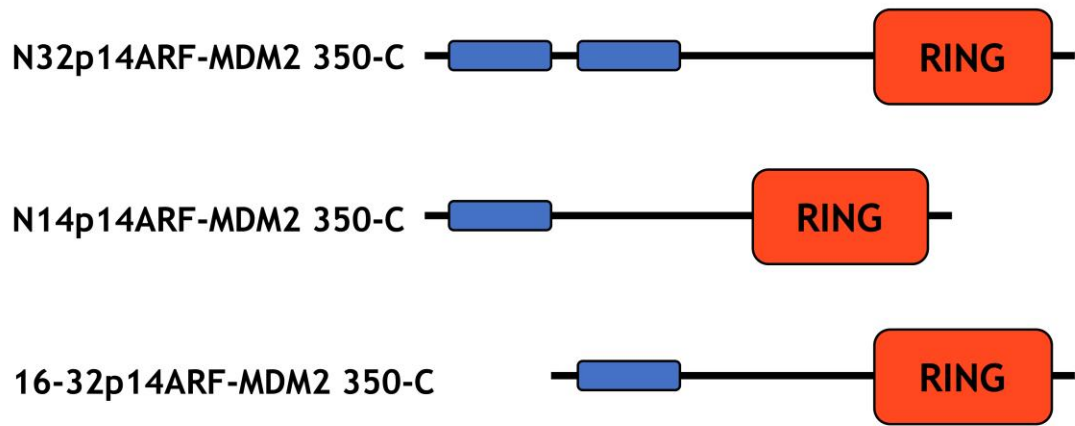


Figure 3.2-16 Schematic diagram of the p14ARF-MDM2 350-C constructs

Several p14ARF-MDM2 350-C fusion constructs were generated. N32p14ARF contains the two β -strands whereas N14p14ARF and 16-32p14ARF contain only one β -strand. p14ARF sequences were fused directly to the N-terminus of MDM2 350-C. All of the constructs were cloned into the pAbl vector and expressed with an N-terminal GST tag.

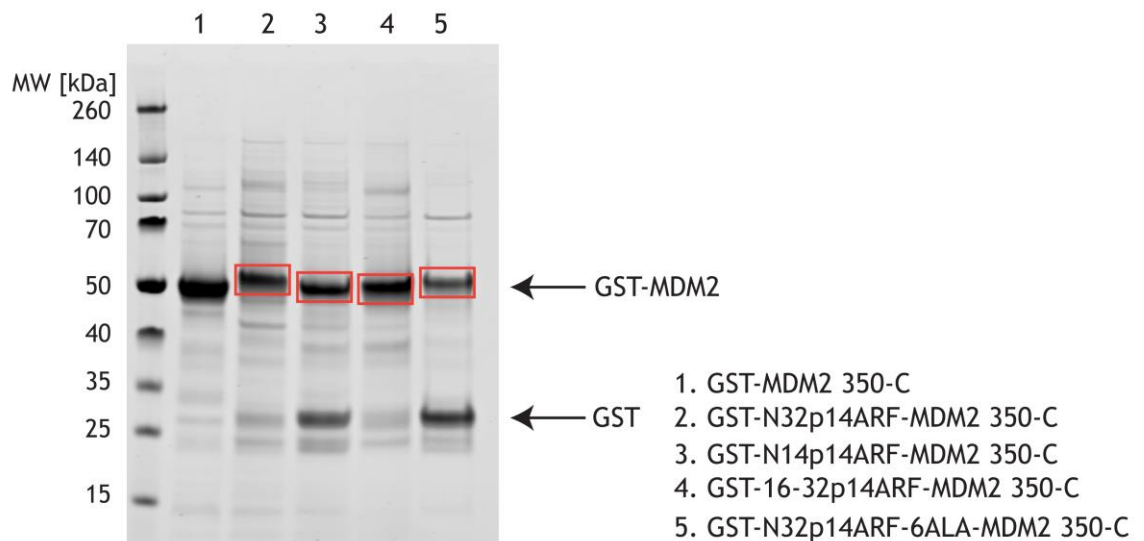


Figure 3.2-17 Determination of GST-p14ARF-MDM2 350-C construct concentration

GST-p14ARF-Mdm 350-C constructs eluted from the GSH resin were analysed by SDS-PAGE. The intensities of the bands corresponding to the constructs of interest (shown in red boxes) were measured and compared with that of the GST-MDM2 350-C to normalise the protein concentration.

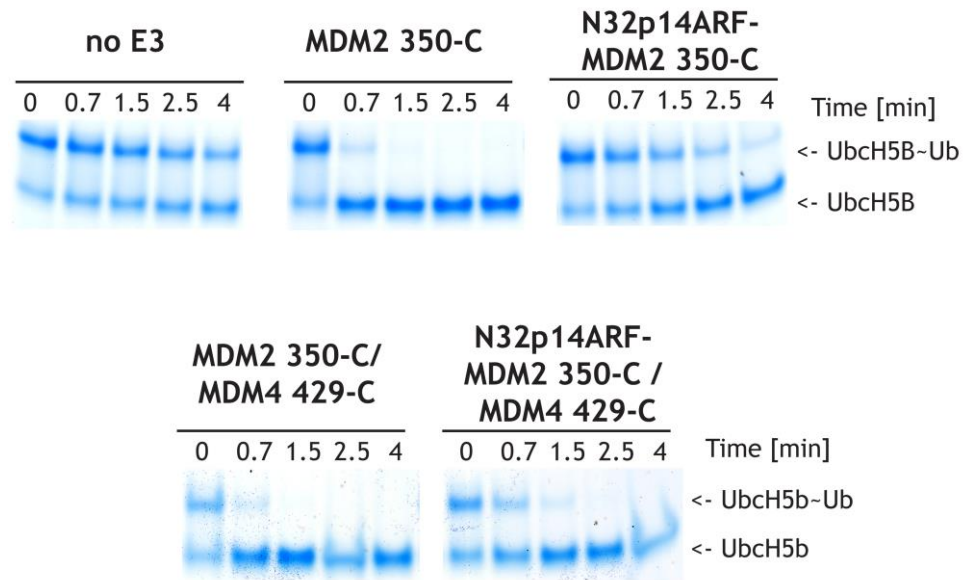


Figure 3.2-18 SDS-PAGE showing the effect of N32p14ARF fusion on the activity of MDM2 homodimer and MDM2/MDM4 heterodimer

SDS-PAGE showing the lysine discharge assays, performed in order to evaluate the activity of GST-N32p14ARF-MDM2 350-C and GST-N32p14ARF-MDM2 350-C/His-MDM4 429-C constructs. Reactions were performed as described in section 2.2.6, using 250 nM MDM2 homodimer and 500 nM MDM2/MDM4 heterodimer.

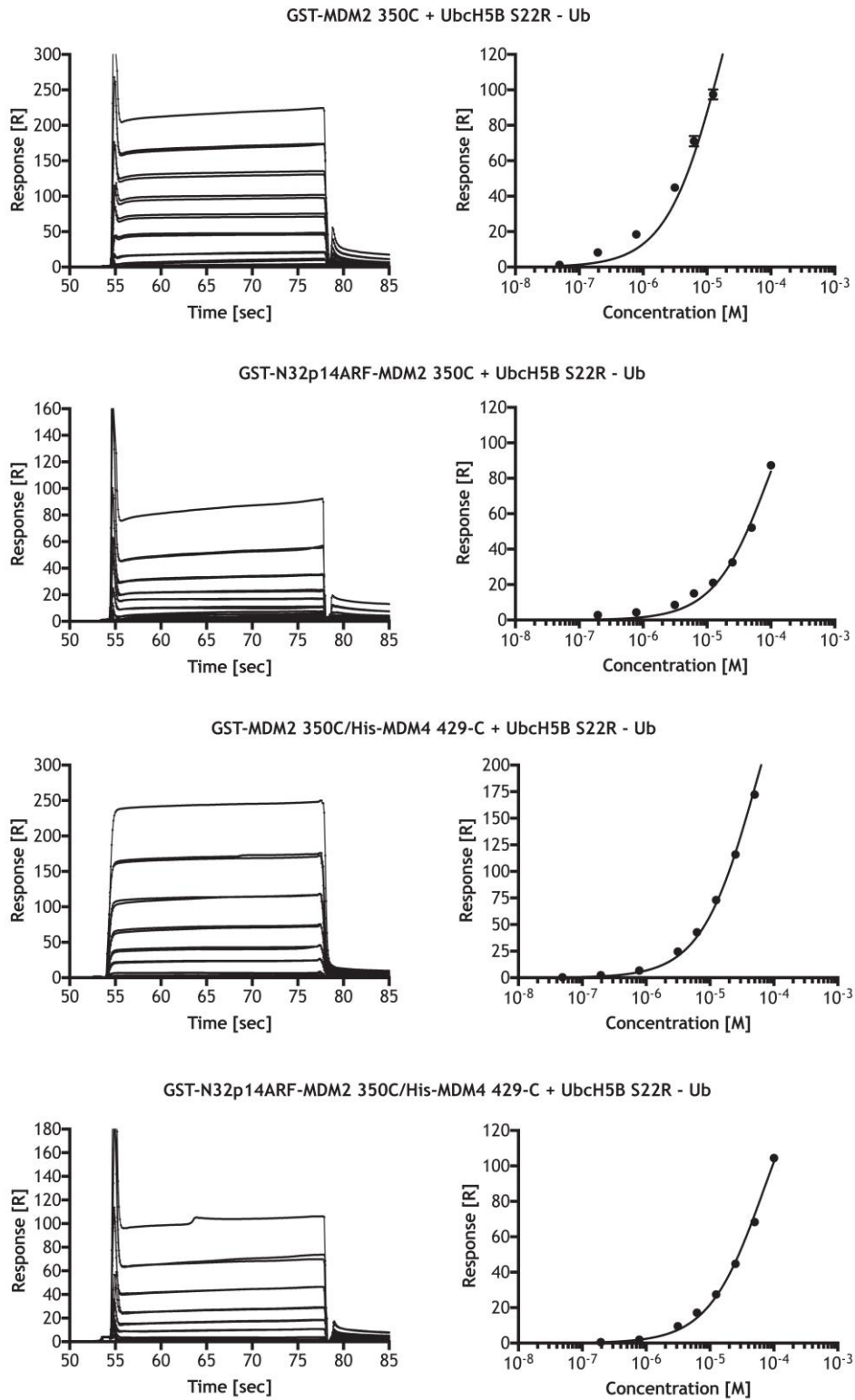


Figure 3.2-19 SPR analysis of the effect of N32p14ARF fusion on the binding affinity between GST MDM2 350-C and Ubch5B-Ub

Representative sensograms (left) and binding curves (right) for GST-MDM2 350-C, GST-N32p14ARF-MDM2 350-C, GST-MDM2 350-C/His-MDM4 429-C and GST-N32p14ARF-MDM2 350-C/His-MDM2 429-C in the presence of Ubch5B S22R-Ub. The experiments were performed in duplicate.

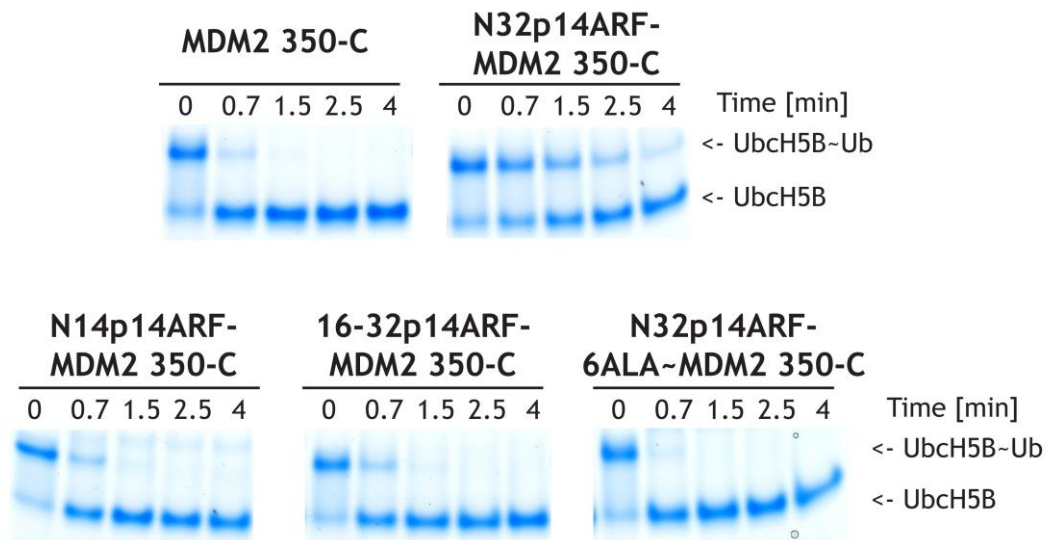


Figure 3.2-20 SDS-PAGE showing the effect of p14ARF fusion variants on the activity of GST-MDM2 350-C

SDS-PAGE showing the lysine discharge assays, performed in order to evaluate the activity of GST-p14ARF-MDM2 350-C variants. Reactions were performed as described in section 2.2.6, using 250 nM indicated E3.

3.2.10 Discussion

In conclusion, I have shown that p14ARF influences the ligase activity of MDM2 homodimer, and the presence of two R*FLV**VR motifs is required for that event. Lysine discharge assay, using MDM2 and p14ARF variants co-expressed in *E. coli*, showed that introduction of His-MBP-N37p14ARF or His-MBP-N56p14ARF results in a decreased potency of GST-MDM2 230-C towards Ub_{CH5B}-Ub discharge (Figure 3.2-3). Moreover, I have shown that His-MBP-N20p14ARF and His-MBP-17-32p14ARF, containing single β -strands with the R*FLV**VR motif, can also bind and pull-down GST-MDM2 230-C (Figure 3.2-2). Lysine discharge showed that HIS-MBP-17-32p14ARF influences the catalytic activity of GST-MDM2 in a manner similar to HIS-MBP-N20p14ARF, however the inhibitory effect is not as pronounced as the one driven by N56p14ARF or N37p14ARF (Figure 3.2-3). This observation was further supported by the studies with N37p14ARF peptide, as well as the generation of p14ARF-MDM 350-C fusion constructs. Moreover, my data are with the report published in 2000 by Weber *et al.*, which showed that both β -strands of p19ARF (each containing the R*FLV**VR motif), can bind MDM2, suggesting that ARF contacts MDM2 via two independent binding sites within the N37p19ARF sequence (Weber *et al.*, 2000).

As there is no information on how ARF can influence the ligase activity of MDM2, I decided to first focus on the minimal p14ARF sequence that exhibits an inhibitory effect on MDM2. For this reason, I implemented N37p14ARF peptide in my studies, as the bacterial expression of p14ARF constructs proved to be very challenging. Unfortunately, N37p14ARF peptide was characterised by very poor solubility and initial tests on complex formation showed precipitation upon addition of N37p14ARF to dimeric MDM2 230-C. I managed to overcome the extensive precipitation by incubating dimeric MDM2 230-C with N37p14ARF in the presence of 6 M GdnHCl, followed by buffer exchange to remove GdnHCl. Using this procedure, I found that N37p14ARF peptide inhibits the activities of MDM2 230-C and MDM2 RING alone in the lysine discharge assay (Figure 3.2-8).

To further verify whether p14ARF can directly influence the catalytic domain of MDM2, I also created p14ARF-MDM2 RING fusion constructs. Fusion construct could overcome the low-affinity interaction between p14ARF and RING domain. Fusion of N32p14ARF was able to influence the catalytic activity of MDM2 350-C

and this effect was abolished upon disruption of the conserved R*FLV**VR motif (Figure 3.2-20). Furthermore, a ~7-fold decrease in the MDM2 - Ubch5B-Ub binding affinity in the presence of N32p14ARF was observed by SPR (Figure 3.2-19). Fusion of the single- β -strand containing constructs of p14ARF did not affect the catalytic activity of MDM2, suggesting that both β -strands of p14ARF are required in order to influence the activity of MDM2. Finally, both N37p14ARF peptide and the fusion constructs showed a mild effect on MDM2/MDM4 activity and E2-Ub binding, suggesting that the homodimeric feature of MDM2 is essential for p14ARF to exert its effect.

The lysine discharge assay measured the reactivity of the Ubch5B-Ub thioester bond that is independent of lysine position on the substrate as free lysine was used as the substrate. Therefore, the activity is directly attributed to how the RING domain binds and activates Ubch5B-Ub to facilitate catalysis. The decrease in activity observed in the MDM2 RING domain alone in the presence of p14ARF suggests that p14ARF might interfere with the catalytic domain of MDM2 by blocking the E2-Ub binding site. Basing on the obtained data, we conceived two possible models of p14ARF-driven inhibition of MDM2:

- Given that p14ARF does not pulldown the MDM2 RING domain efficiently, we postulated that a high-affinity p14ARF interaction with the AD could trigger substantial rearrangements in the overall fold of the MDM2 C-terminus. This could cause the RING domain to “fold back” onto the AD and this interaction could be bridged by low-affinity RING - ARF binding. Involvement of the RING domain in the p14ARF-AD interaction would in turn prevent its binding to E2-Ub (Figure 3.2-21).
- Size exclusion chromatography showed that N37p14ARF peptide induces extensive oligomerisation of dimeric MDM2 230-C leading to decreased activity (Figure 3.2-10 and Figure 3.2-11). We don't know if the MDM2 - p14ARF complex oligomerisation is a biologically relevant event, or whether it is driven by the hydrophobic nature of p14ARF peptide, which alone could form higher-order oligomers in aqueous conditions. Interestingly, in 2003 Menendez et al. analysed H1299 cell lysate with native-PAGE gel and suggested that endogenous p14ARF forms high MW

oligomers (Menéndez *et al.*, 2003). Based on these results, it seems likely that p14ARF could inhibit MDM2 by inducing oligomerisation that blocks the E2~Ub binding site.

In 2001, Bothner *et al.* presented an NMR analysis of the MDM2 AD (210-304) and N37p19ARF peptides, which revealed that both are unstructured and flexible in aqueous conditions (Bothner *et al.*, 2001). However, upon MDM2 AD - N37p19ARF complex formation, a significant transition towards β -sheets was observed in 2D NMR spectra (Bothner *et al.*, 2001). Size exclusion analysis of MDM2 210-304 - N37p19ARF complex showed formation of high MW oligomers rather than bimolecular species (Bothner *et al.*, 2001). Authors suggested that the MDM2 AD - ARF interaction is driven by both electrostatic and hydrophobic interactions. The R*FLV**VR motif contains alternating charged (R) and hydrophobic residues (FLV), which in a linear conformation would be found on both sides of a β -strand, giving rise to a “hydrophobic face” and a “charged face” on the peptide. Bothner *et al.* further suggested that the same arrangement of acidic and hydrophobic amino acids can be found in two separate segments of the AD of MDM2 corresponding to residues 235-259 and 270-289 (Bothner *et al.*, 2001; Sivakolundu *et al.*, 2008). Based on these findings, they proposed a model where alternating electrostatic and hydrophobic interactions between two β -sheets of p19ARF and two segments of MDM2 AD lead to the formation of high MW “sandwich-like” species. This model of p19ARF-driven oligomerisation of the MDM2 AD is consistent with the oligomerisation of MDM2 230-C I observed in the presence of p14ARF peptide; however, because my construct of MDM2 is significantly longer than the one used by Bothner *et al.*, it is impossible to stipulate whether p19ARF-driven oligomerisation of MDM2 210-304 and p14ARF-driven oligomerisation of MDM2 230-C are both controlled by the same mechanism.

In summary, I have shown that the most pronounced inhibition of MDM2 arises from the implementation of both R*FLV**VR motifs, which can be found in N37p14ARF and N56p14ARF. Furthermore, I have shown that N37p14ARF peptide is inducing oligomerisation of MDM2. We do not know whether the simultaneously observed decrease in the ligase activity of MDM2 is a result of the oligomerisation process itself or a direct p14ARF - RING interaction. In the near

future I would like to investigate the oligomerisation status of the p14ARF-MDM2 350-C fusion constructs, as well as other p14ARF-RING fusions (e.g. MDM2/MDM4, RNF38), in order to determine whether the formation of higher-order MW species directly links to the loss of the catalytic activity of the enzyme. Finally, as we have shown that inhibiting the MDM2 - E2-Ub interaction can serve an advantageous therapeutical approach, we started a collaboration with Professor Sachdev Sidhu, where we implement the phage-display technique to discover peptide sequences which can specifically bind the RING domain of MDM2, leading to its inhibition (McLaughlin and Sidhu, 2013; Arita *et al.*, 2016; Nomura *et al.*, 2017).

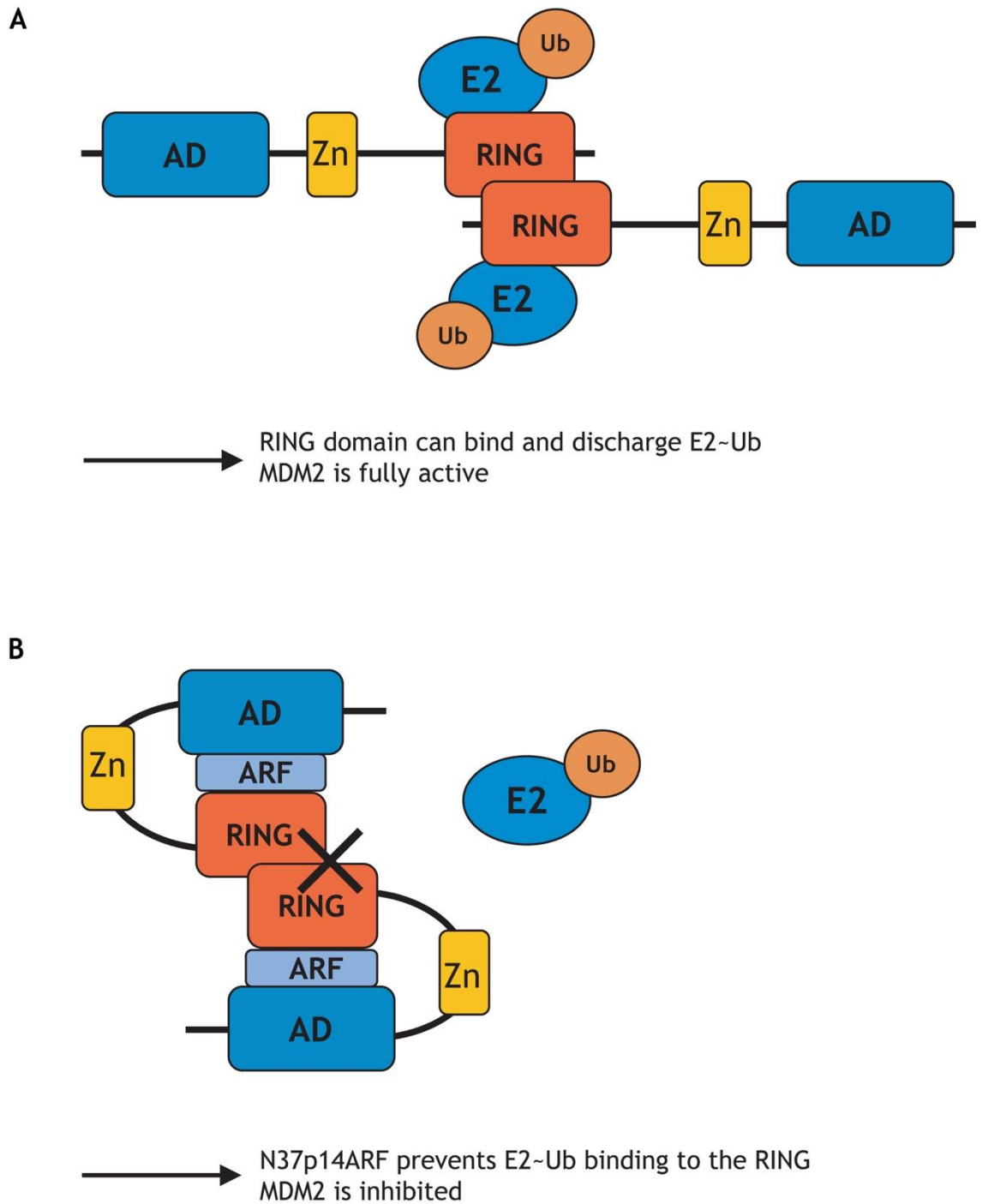


Figure 3.2-21 Possible model of MDM2 inhibition driven by p14ARF

A- In the absence of p14ARF, MDM2 RING dimer is able to bind and discharge E2-Ub.

B- p14ARF binding to the AD of MDM2 triggers a conformational change, where the RING domain folds back towards the AD and that interaction is bridged by the presence of p14ARF. As a result, the RING domain is inhibited and no longer able to bind E2-Ub.

3.3 Structural and biochemical characterisation of HUWE1-p14ARF complexes

In 2005 Chen et al. identified HUWE1 as a binding partner of p14ARF using a pull-down coupled with mass spectrometry analysis (Chen *et al.*, 2005). They showed that GST-p14ARF binds ³⁵S-labelled HUWE1 1015-4374 but not HUWE1 1-1014 and that the N-terminal fragment of ARF encompassing residues 1-64 was required for interaction. Notably, deletion of the first 14 residues of p14ARF greatly compromised the HUWE1 interaction. Chen et al. further showed that *in vitro* autoubiquitination activity of GST-HUWE1 3760-4374 was impaired in the presence of p14ARF 1-64. Similarly, GST-HUWE1-driven ubiquitination of FLAG-p53 was diminished upon introduction of p14ARF 1-64 (Chen *et al.*, 2005). Unfortunately, since the publication of this work, only a limited number of studies have investigated how HUWE1 and ARF interact with each other and the mechanism of ARF-driven HUWE1 inhibition.

p14ARF is best known for its inhibitory effect on MDM2, which leads to p53 stabilisation. The study showed that p14ARF could also influence HUWE1 activity leading to p53 stabilisation (Chen *et al.*, 2005). Strikingly, the N-terminus of p14ARF is essential for its inhibitory effect on both MDM2 and HUWE1. In this chapter, I investigate how p14ARF binds and inhibits HUWE1 activity.

3.3.1 Purification of HUWE1 constructs

3.3.1.1 HUWE1 construct design

Chen et al. showed that the C-terminal fragment of HUWE1 (aa 3760-4374) is sufficient for binding of p14ARF in a manner that inhibits E3 ligase activity (Chen *et al.*, 2005). Based on these data, I decided to focus my research on C-terminal constructs of HUWE1 that comprise the HECT domain and p14ARF-binding region. Because of its size and predicted disordered regions, bacterial expression, purification and crystallisation of full-length HUWE1 would be very challenging. As the only domain identified in the HUWE1 3760-C is the C-terminal HECT domain, I implemented secondary structure prediction analysis to aid in the design of HUWE1 constructs. Based on these predictions, HUWE1 3753-C (71 kDa), HUWE1 3796-C (67 kDa), HUWE1 3833-C (63 kDa), HUWE1 3878-C (58 kDa)

and HUWE1 3900-C (55 kDa) were generated and used in initial purification and activity tests.

3.3.1.2 GST-HUWE1 purifies readily

All HUWE1 constructs expressed readily in *E. coli*. To establish a strategy for protein purification, I cloned HUWE1 3753-C into pGEX-4T-1 and pRSFDuet-1 vectors containing an N-terminal GST and His-tag, respectively. GST-HUWE1 was cleaved *in situ* whereas His-HUWE1 was eluted from Ni²⁺ resin and purified in the His-tagged form. I implemented a SourceQ anion exchange column following the affinity step of protein purification, as the theoretical pI of HUWE1 3753-C is 5.3, suggesting it will bind positively charged resin at neutral pH or higher. The SourceQ elution profile of HUWE1 cleaved *in situ* showed a defined and sharp peak at 220 mM NaCl (Figure 3.3-1 A). Peak fractions were concentrated and applied on the 16/600 Superdex 200 size exclusion column (Figure 3.3-1 B). The size exclusion elution profile consisted of two peaks. The first peak appeared at a retention volume of 40 ml with a broad shoulder. A retention volume of 40 ml corresponds to the void volume and likely indicates the formation of higher MW oligomers of the protein. The second peak eluted after 80 ml consistent with protein with a MW of ~50 kDa based on the column calibration specifications provided by GE Healthcare. SDS-PAGE analysis confirmed the presence of HUWE1 in both peaks (Figure 3.3-1 C). Fortunately, the peaks did not overlap so I was able to separate and concentrate the non-oligomerised species of HUWE1.

The anion exchange chromatogram of His-HUWE1 was characterised by the presence of a broad and heterogeneous peak spanning concentrations of NaCl ranging from 170 mM to 380 mM (Figure 3.3-2 A). SDS-PAGE analysis confirmed the presence of His-HUWE1 and other higher MW bands. These higher MW bands seemingly resulted from intermolecular disulfide bond formation between HUWE1 molecules (Figure 3.3-2 B). In our group, we frequently observe that Ni²⁺-affinity purification promotes disulfide bond formation in proteins that contain cysteine residues. The ability of Ni²⁺ to catalyse oxidation of thiols is well-documented (Bagiyan *et al.*, 2003). Because of this disulfide bond formation, HUWE1 constructs were expressed in pGEX-4T-1 vector, purified by glutathione-affinity chromatography, cleaved with TEV protease *in situ*, and further purified by SourceQ and size exclusion chromatography.

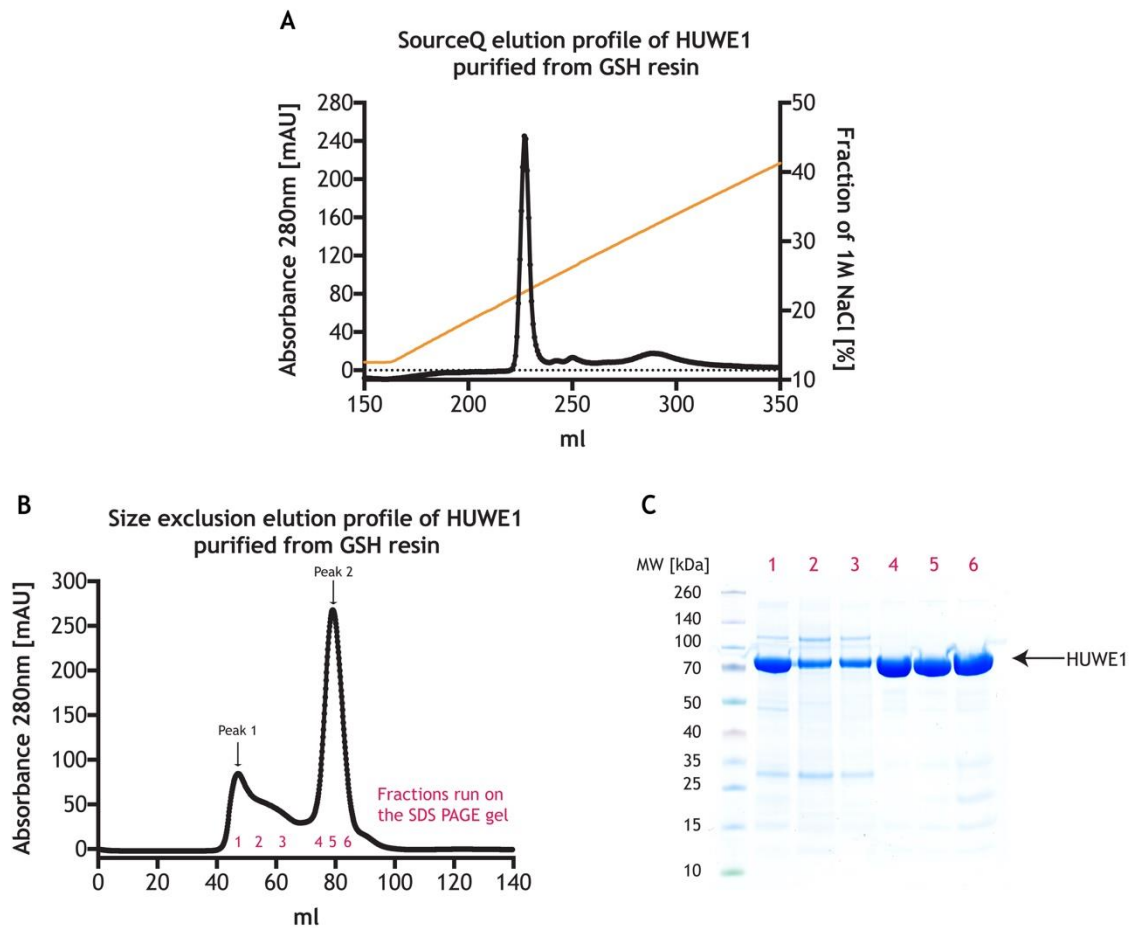


Figure 3.3-1 Purification of pGEX-4T-1-expressed HUWE1 3753-C

A- SourceQ elution profile of HUWE1 3753-C. HUWE1 3753-C obtained after *in situ* cleavage with TEV protease was applied to a SourceQ anion exchange column. The elution profile was characterised by the presence of a sharp peak, which eluted at ~220 mM NaCl.

B- Size exclusion profile of HUWE1 3753-C. Peak fractions from A were pooled and concentrated then applied to a 16/600 Superdex 200 size exclusion column.

C- SDS-PAGE showing fractions representing the cross-section of the 16/600 Superdex 200 size exclusion elution profile of HUWE1 3753-C in B.

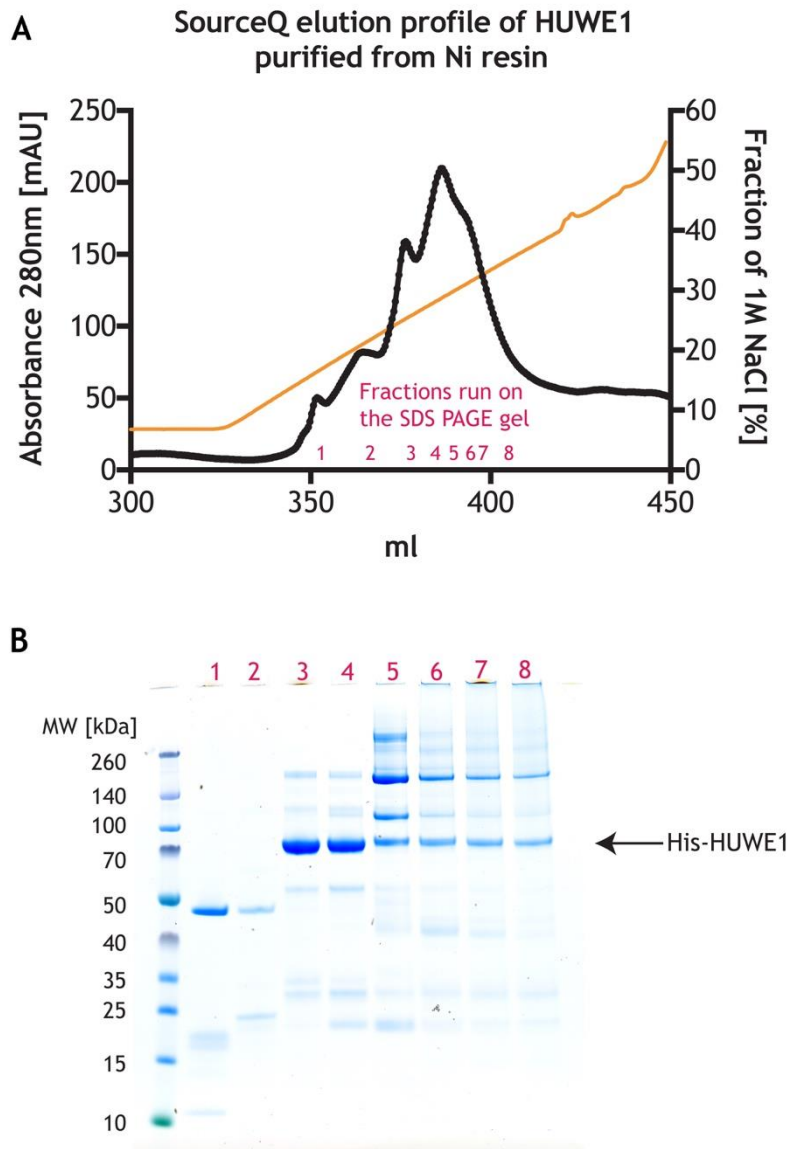


Figure 3.3-2 Purification of His-tagged HUWE1 3753-C expressed in pRSFDuet-1

A- SourceQ elution profile of His-HUWE1 3753-C. His-HUWE1 3753-C obtained after Ni²⁺-affinity purification was applied to a SourceQ anion exchange column. The elution profile was characterised by the presence of a broad and heterogeneous peak that spanned NaCl concentrations ranging from 170 mM to 380 mM.

C- SDS-PAGE showing fractions representing the cross-section of the SourceQ anion exchange elution profile of His-HUWE1 3753-C in A.

3.3.2 HUWE1 constructs show high *in vitro* activity

Section 1.3 of the Introduction highlights the main differences between RING and HECT E3s. RING E3s catalyse the direct transfer of Ub from E2 to lysine residues on substrates; we model this reaction *in vitro* using lysine discharge assays, in which we add copious amounts of free lysine to a reaction and monitor the disappearance of E2~Ub complex using SDS-PAGE. In contrast, HECTs catalyse substrate ubiquitination in two steps. First, Ub is transferred from E2 to the catalytic cysteine on the C-lobe of the E3 and then it is conjugated to a lysine residue on a substrate. Because of this two-step mechanism, lysine discharge assays are unsuitable for monitoring differences in E3 activity - if transfer of Ub from the E3 catalytic cysteine to substrate is slower than the formation of E3~Ub, then a reduction in the rate of the first step of the catalytic reaction may not be observed. Hence, to evaluate the activity of HUWE1 constructs, I performed single-turnover auto-ubiquitination assays. In these assays, I pre-charged E2 with Ub, stopped the E1-E2 transthiolation reaction with EDTA and then added HUWE1. HUWE1 activity was monitored by the appearance of a HUWE1-Ub ladder and the simultaneous disappearance of E2~Ub. Figure 3.3-3 shows that all purified HUWE1 constructs are similarly active as demonstrated by the fast formation of poly-ubiquitinated HUWE1 and the disappearance of E2~Ub. It is noteworthy that this assay does not allow for the direct comparison of the activity of different HUWE1 constructs because the constructs have different numbers of lysines; both the numbers and the accessibility of these lysine sites may influence the rate of HUWE1 autoubiquitination.

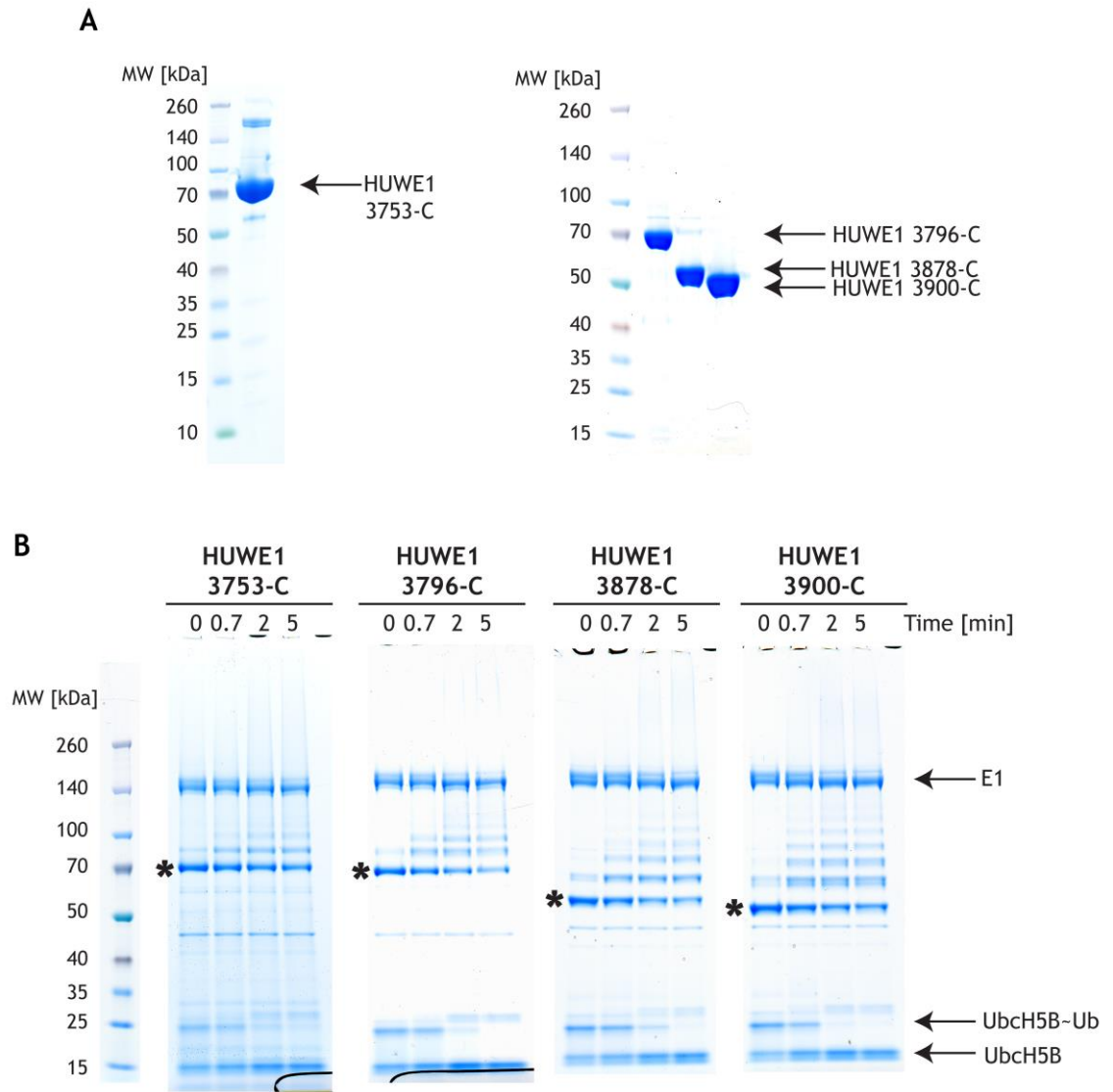


Figure 3.3-3 Activity of HUWE1 constructs

A- SDS-PAGE was used to evaluate the purity of HUWE1 constructs.

B- SDS-PAGE showing single-turnover autoubiquitination catalysed by different HUWE1 constructs. Reactions were performed as described in section 2.2.8. An asterisk denotes non-ubiquitinated HUWE1. Assays were performed using 6 μ M of the indicated E3.

3.3.3 HUWE1 pulls down N56p14ARF

Chen et al. showed that residues 1-64 of p14ARF (referred to as N64p14ARF) are sufficient to bind and influence the activity of HUWE1 3760-C (Chen *et al.*, 2005). Based on these findings, I first investigated whether N56p14ARF, used in the MDM2 studies, is able to bind and pull down the HUWE1 constructs I had cloned. I co-expressed GST-HUWE1 constructs with His-MBP-N56p14ARF and performed Ni²⁺-affinity followed by glutathione-affinity chromatography to assess whether a complex formed. All steps including Ni²⁺ resin wash and elution, followed by GSH resin wash and elution are shown in Figure 3.3-4 A. SDS-PAGE analysis showed that all GST-HUWE1 constructs were present with His-MBP-N56p14ARF after double pull-down. However, I noticed that the band intensities of the proteins eluted from GSH resin were stronger than His-MBP-N56p14ARF even after Ni²⁺-affinity step. To ensure that GST-HUWE1 did not bind non-specifically to the Ni²⁺ resin, I performed two independent pull-downs of GST-HUWE1 constructs, using either GSH or Ni²⁺ resin. Figure 3.3-4 B shows that all GST-HUWE1 variants bound to the Ni²⁺ resin. Thus, an alternate tagging system was required to assess complex formation using a double pull down assay.

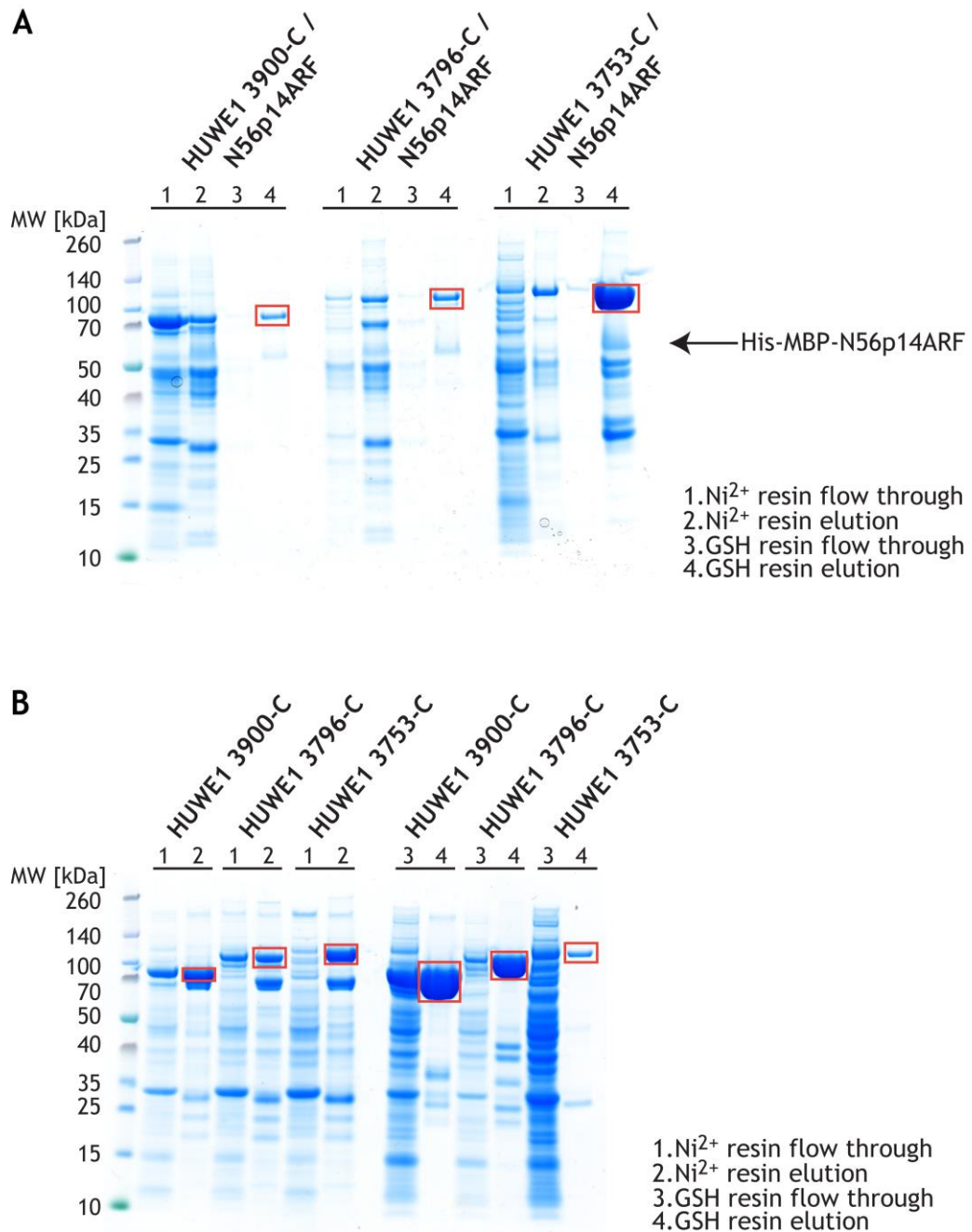


Figure 3.3-4 His-MBP-N56p14ARF can pull down GST-HUWE1

A- SDS-PAGE showing Ni²⁺ and GSH resin pull down of GST-HUWE1 variants co-expressed with His-MBP-N56p14ARF. Lysates were applied to Ni²⁺ resin, washed and eluted as described in section 2.2.3.1. Lane 1 contains unbound protein and lane 2 contains protein eluted from Ni²⁺ resin. The eluted fraction from Ni²⁺ resin was applied onto glutathione-affinity resin, wash and eluted as described in section 2.2.3.1. Lane 3 contains unbound protein and lane 4 contains protein eluted from glutathione-affinity resin. Red boxes indicate GST-HUWE1 variants and an arrow indicates the expected His-MBP-N56p14ARF bands.

B- SDS-PAGE showing GST-HUWE1 variants eluted from Ni²⁺ and GSH resin. Lysates were applied to Ni²⁺ or GSH resin. Lane 1 contains unbound protein and lane 2 contains protein eluted from Ni²⁺ resin. Lane 3 contains unbound protein and lane 4 contains protein eluted from GSH-affinity resin.

3.3.4 N37p14ARF peptide induces oligomerisation of HUWE1 constructs

As there was no additional literature-based information on the minimal p14ARF sequence required to bind and modulate HUWE1 activity, I decided to test whether the N37p14ARF peptide, which I used in MDM2 studies, could interact with HUWE1. To investigate whether N37p14ARF peptide could influence the activity of HUWE1 variants, I mixed N37p14ARF dissolved in 8 M GdnHCl with a range of different concentrations of HUWE1 variants. After experiencing great difficulties with introducing p14ARF peptide to MDM2, I started by mixing HUWE1 and N37p14ARF at 1:1 ratio and gradually increased the peptide concentration. After I had reached the maximum concentration of ARF possible at which no precipitation was observed, I microcentrifuged the sample and buffer exchanged it to remove GdnHCl from the solution. Modest precipitation was observed in the sample containing HUWE1 3753-C when N37p14ARF was added at a 6-fold excess, but no precipitation was observed in the sample where HUWE1 3796-C was mixed with N37p14ARF even at a 1:6 molar ratio. For HUWE1 3900-C, slight precipitation was observed when N37p14ARF was added at 2-fold excess and heavy precipitation occurred with an increasing molar ratio of N37p14ARF. I confirmed that HUWE1 was present in the precipitated fraction of the solution by SDS-PAGE (Figure 3.3-6). All of the experiments described in this section were done using the samples of HUWE1/p14ARF peptide obtained after removal of the precipitant. To determine whether p14ARF peptide influences the oligomeric state of HUWE1, all HUWE1 variants were incubated with a 6-fold excess of N37p14ARF, centrifuged, buffer-exchanged into 25 mM Tris-HCl pH 7.6, 200 mM NaCl, 1 mM TCEP and subsequently applied onto a Shodex KW-403-4F HPLC column. As a control, HUWE1 variants in the absence of N37p14ARF were treated with the same volume of GdnHCl as those with peptide and subjected to the same protocol prior to application to the HPLC column. Figure 3.3-5 shows HPLC elution profiles of HUWE1 3753-C, HUWE1 3796-C and HUWE1 3900-C in the presence and absence of N37p14ARF. All HUWE1 variants alone eluted after ~17 min. When compared with the BioRad MW standard elution from the same column, the 17 min retention time indicated the presence of a sample with MW between 100~50 kDa. After incubation with N37p14ARF, peaks from runs with HUWE1 3753-C and HUWE1 3796-C shifted to ~13 min retention time, which corresponds to protein with a MW of ~670 kDa. No peak shift was observed for

HUWE1 3900-C after introduction of N37p14ARF. I also investigated effects of N37p14ARF on HUWE1 variants when N37p14ARF was present at lower molar ratios. I mixed HUWE1 3796-C with N37p14ARF at molar ratios of 1:0.5 and 1:1. Figure 3.3-7 shows that introduction of N37p14ARF at lower molar ratios led to broadening of the HUWE1 peak and the appearance of a shoulder with a retention time beginning at 12 min and ending at 16 min. These results suggest that low molar ratios of N37p14ARF might affect HUWE1 conformation and lead to peak broadening. As the N37p14ARF molar ratio increases, HUWE1 likely forms the higher MW oligomers.

In the subsequent experiments, I focused on one HUWE1 variant that binds N37p14ARF (3796-C) and one that does not (3900-C).

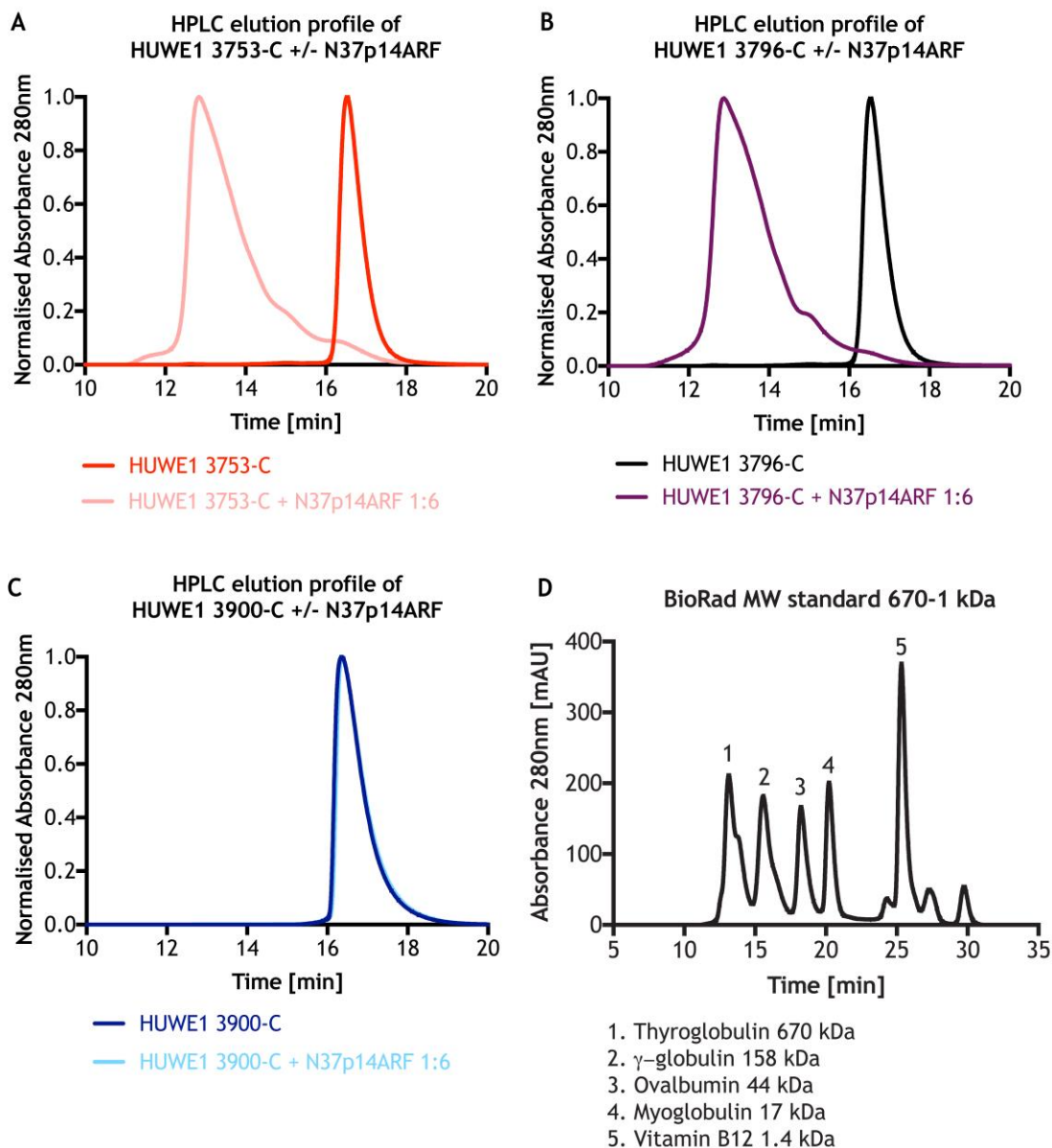


Figure 3.3-5 N37p14ARF induces oligomerisation of selected HUWE1 constructs

HUWE1 constructs were mixed with N37p14ARF peptide dissolved in GdnHCl at a 1:6 molar ratio of protein to peptide. Spun-down and buffer-exchanged samples were further loaded onto a Shodex KW-403-4F HPLC column. HUWE1 incubated with GdnHCl alone was used as a control.

A- Elution profile of HUWE1 3753-C in the presence (pink) and absence (red) of N37p14ARF.

B- Elution profile of HUWE1 3796-C in the presence (purple) and absence (black) of N37p14ARF.

C- Elution profile of HUWE1 3900-C in the presence (cyan) and absence (blue) of N37p14ARF.

D- Elution profile of BioRad MW standard. BioRad MW standard was loaded on the Shodex KW-403-4F HPLC column.

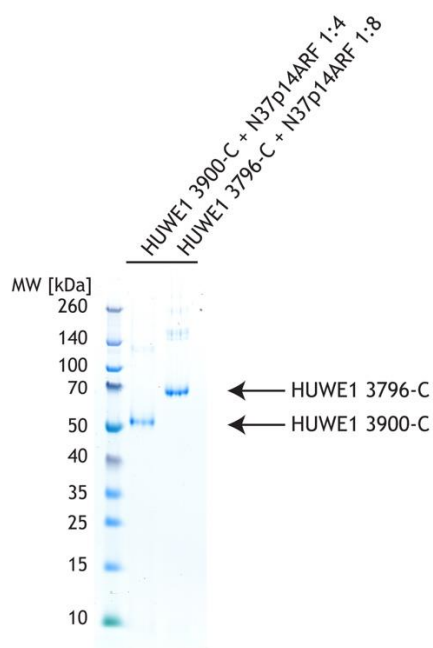


Figure 3.3-6 HUWE1 is found in the insoluble fraction of the HUWE1/N37p14ARF complex

HUWE1 3796-C was mixed with N37p14ARF peptide at 1:8 molar ratio, whereas HUWE1 3900-C was mixed with N37p14ARF peptide at 1:4 ratio. Samples were spun down, precipitates were dissolved in 8 M GdnHCl and analysed on the SDS PAGE gel.

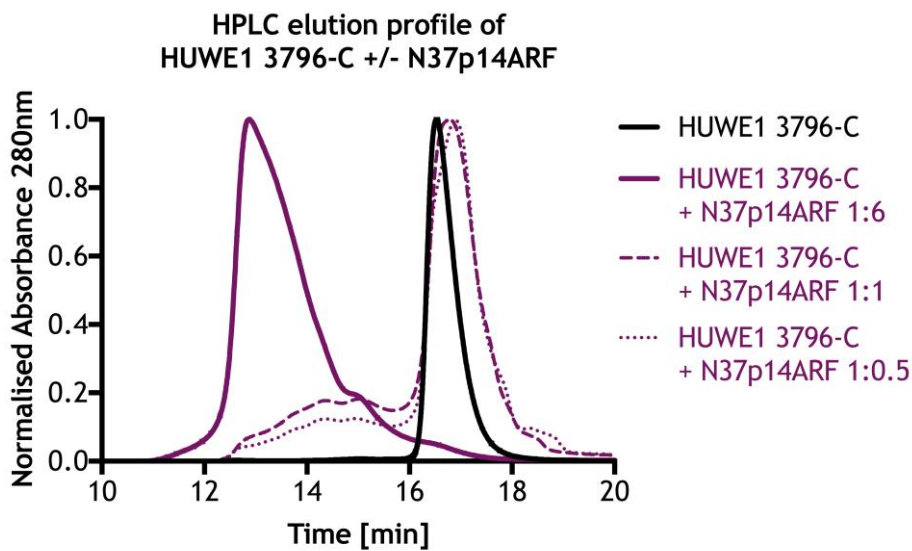


Figure 3.3-7 HPLC elution profile of HUWE1 3796-C mixed with lower molar ratios of N37p14ARF

HUWE1 3796-C was mixed with N37p14ARF peptide dissolved in GdnHCl at indicated molar ratios of protein to peptide. Spun-down and buffer-exchanged samples were further loaded onto a Shodex KW-403-4F HPLC column. HUWE1 3796-C incubated with GdnHCl alone was used as a control.

3.3.5 HUWE1 3796-C binds N37p14ARF with low micro-molar affinity

There is no information in the literature on the binding affinity between p14ARF and HUWE1. To assess the binding affinity between HUWE1 and p14ARF, I obtained N37p14ARF peptide labelled with 6-carboxyfluorescein (FAM-N37p14ARF) at the N-terminus and performed fluorescence polarisation assays (described in the section 2.2.9) to determine the K_d for the HUWE1 3796-C interaction with N37p14ARF. FAM-N37p14ARF was present at a concentration of 1 μM and HUWE1 3796-C was added in 2-fold incrementing steps ranging from 0.5 μM to 8 μM . Fluorescence polarisation of the sample was measured at each step for 100 s (Figure 3.3-8 A) and obtained values were plotted against HUWE1 concentration to estimate the K_d value (Figure 3.3-8 B). The binding affinity was estimated by a nonlinear regression and one-site binding model using GraphPad Prism. The K_d for the interaction between HUWE1 3796-C and FAM-N37p14ARF was determined to be $\sim 1\mu\text{M}$.

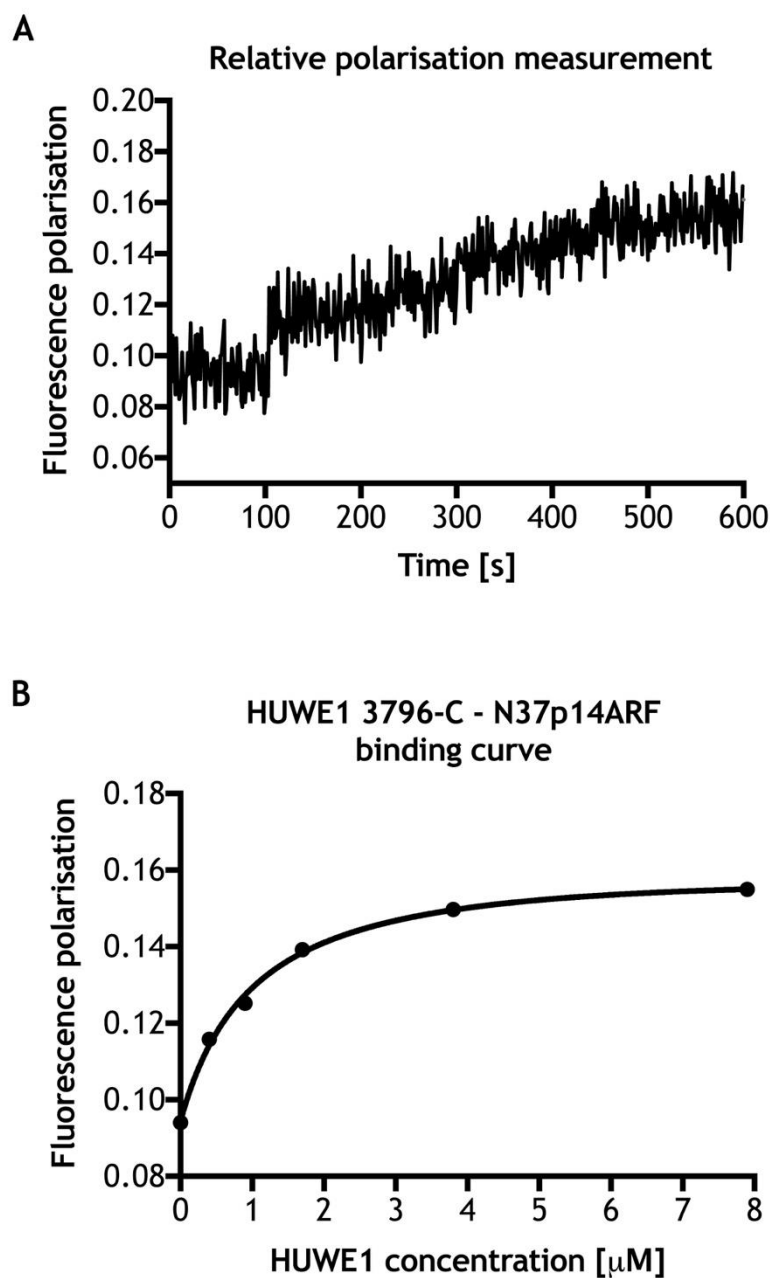


Figure 3.3-8 Binding affinity between HUWE1 3796-C and FAM-N37p14ARF

A- FAM-N37p14ARF peptide was diluted to $1\mu\text{M}$ and the fluorescence polarisation was measured. Since ARF peptide has a low MW, fast tumbling will result in high light depolarisation and low polarisation value. Upon incremental addition of HUWE1 and formation of a high-MW p14ARF-HUWE1 complex, the tumbling of FAM-N37p14ARF slows down, resulting in a decrease of light depolarisation and higher polarisation values. The fluorescence polarisation was measured for 100 s at each step and averaged.

B- The obtained values from A were used to estimate the K_d for the HUWE1- FAM-N37p14ARF interaction. The binding affinity was determined by a nonlinear regression and one-site binding model using GraphPad Prism.

3.3.6 N37p14ARF does not influence HUWE1 activity

I next assessed how N37p14ARF affected HUWE1 enzymatic activity. I prepared HUWE1 3796-C/N37p14ARF complex at a 1:6 molar ratio by applying the methodology described in section 3.3.4 and investigated catalytic activity using single-turnover auto-ubiquitination assays. I tested the activity of HUWE1 3796-C in the presence of two different E2s, Ubch5B and Ubch7. As I mentioned in section 1.3 of the Introduction, little is known about the mechanism of E2-Ub selectivity by E3s. Different families of HECT E3s have been reported to preferentially interact with either Ubch5B or Ubch7 (Schwarz, Rosa and Scheffner, 1998).

For activity assays, HUWE1 3796-C and HUWE1 3796-C/N37p14ARF complex were analysed by SDS-PAGE to ensure that there was no significant difference in the amount of E3 present after mixing N37p14ARF or GdnHCl and buffer exchange (Figure 3.3-9 A). Both HUWE1 3796-C and HUWE1 3796-C/N37p14ARF complex showed enzymatic activity in the presence of Ubch5B (Figure 3.3-9 B). There was no noticeable difference in the rate of the disappearance of the Ubch5B-Ub band in when N37p14ARF was present, but the HUWE1 autoubiquitination pattern was different. In the presence of N37p14ARF, a “smeary” pattern was observed at later time points indicative of the formation of longer poly-Ub chains. HUWE1 displayed a slower activity overall when Ubch7 was used as the E2 as compared with Ubch5B. As observed for Ubch5B, N37p14ARF had no observable effect on the rate of disappearance of the Ubch7-Ub band and the appearance of ubiquitinated HUWE1 (Figure 3.3-9 C). These results suggest that N37p14ARF does not inhibit the catalytic machinery of HUWE1 but likely alters HUWE1 conformation, thereby changing the accessibility of lysine sites on HUWE1 leading to different patterns of poly-Ub chain formation.

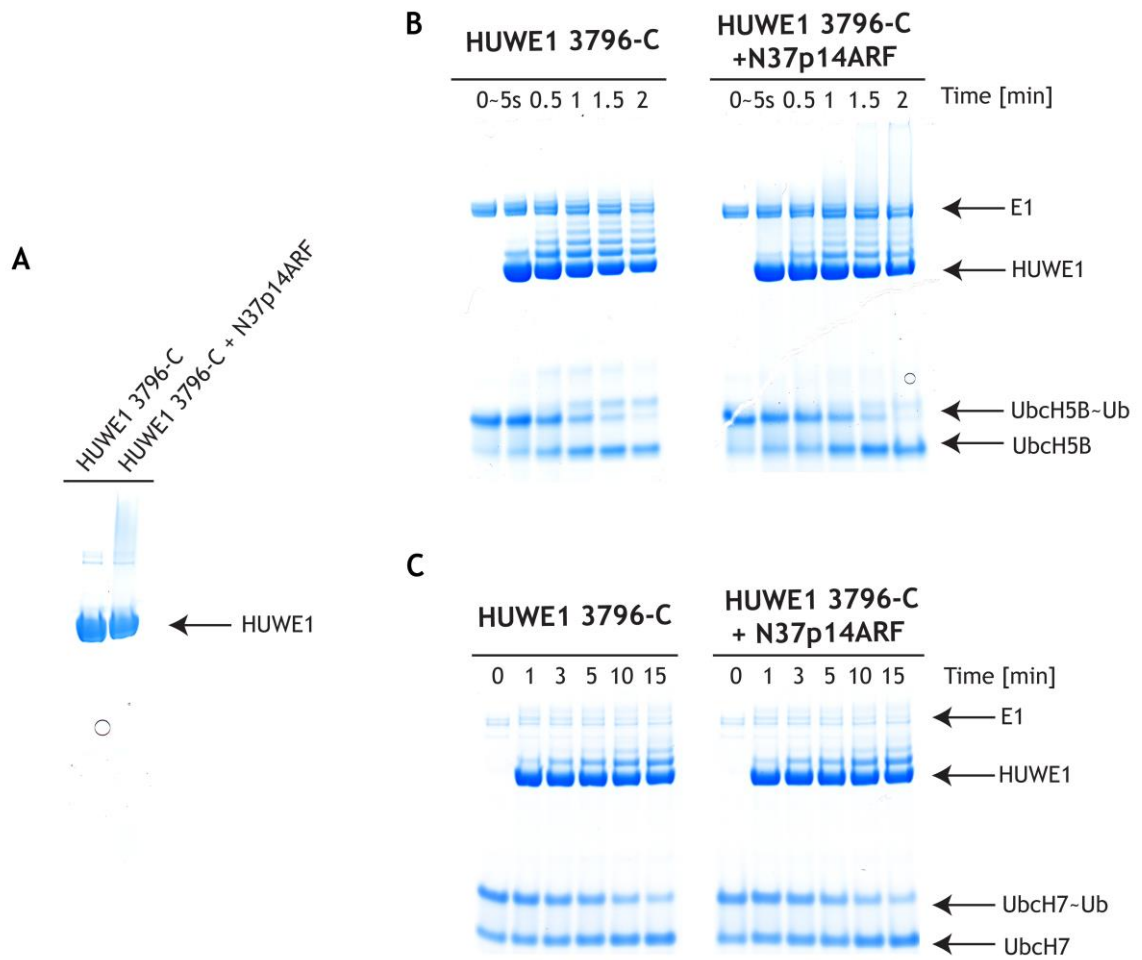


Figure 3.3-9 Effect of N37p14ARF on HUWE1-catalysed Ub transfer

A- SDS-PAGE showing HUWE1 3796-C and HUWE1 3796-C/N37p14ARF complex. The concentrations of HUWE1 3796-C and HUWE1 3796-C/N37p14ARF complex after buffer exchange were determined with Bradford assay and equal amounts of protein were loaded on the SDS-PAGE to ensure the same amount of HUWE1 was used in the assay.

B- SDS-PAGE showing single turnover autoubiquitination catalysed by HUWE1 3796-C and HUWE1 3796-C/N37p14ARF complex using UbcH5B~Ub. Reactions were performed as described in section 2.2.7, using 6 μ M of the indicated E3.

C- SDS-PAGE showing single turnover autoubiquitination catalysed by HUWE1 3796-C and HUWE1 3796-C/N37p14ARF complex using UbcH7~Ub. Reactions were performed as described in section 2.2.7, using 6 μ M of the indicated E3.

3.3.7 Structural analysis of the HUWE1 – N37p14ARF complexes

Because the HUWE1 constructs expressed and purified readily I was able to implement two different approaches for the structural characterisation of HUWE1 alone and in complex with p14ARF. To characterise the effects of N37p14ARF on HUWE1, I performed SEC SAXS analysis and performed crystallisation trials on HUWE1 alone and in complex with p14ARF.

3.3.7.1 SAXS analysis reveals heterogenous oligomerisation of HUWE1 3796-C upon p14ARF binding

Details regarding sample preparation for SEC SAXS analysis can be found in the section 2.2.10.1 of the Materials and Methods.

SEC SAXS has an advantage in that it separates protein components including different oligomeric species on an HPLC SEC column first before the sample is analysed by SAXS. All HUWE1 samples were run on a Shodex KW-403-4F HPLC column before being subjected to X-ray radiation. Proteins were run on the HPLC column at 160 $\mu\text{l}/\text{min}$ flow rate. 591 frames were collected for HUWE1 3796-C alone and in the presence of N37p14ARF and 281 frames were collected for HUWE1 3900-C alone and in the presence of N37p14ARF. Obtained signal plots were used to select the frames corresponding to buffer or to protein. As buffer migrates through the column slower than protein, efforts were made to select frames following protein peak elution and data collection for buffer subtraction. Using this approach minimised differences arising from buffer contributions across all samples. Selection of the frames corresponding to the protein peak was facilitated by the analysis of the R_g (radius of gyration) values for each frame. R_g describes the distribution of a protein's mass around its centre of gravity and peaks from homogenous samples are characterised by near constant values of R_g . ScÅtter software allowed me to either average selected peak frames, which were then subjected to buffer subtraction, or subtract the buffer and analyse each peak frame separately, which greatly facilitated the analysis of HUWE1 3796-C/N37p14ARF sample (*Bioisis: welcome - index*). Subtracted data were analysed for differences in protein shape and dimensions (R_g and D_{max} values), as well as for the presence of aggregation and to assess the folded state (intensity plot, Kratky plot and $P(r)$ distribution).

HUWE1 3796-C alone eluted from the HPLC column as a sharp and defined peak at ~17 min retention time as described previously. The homogeneous nature of the sample was visualised on the signal plot, where the signal corresponding to the protein was characterised by a sharp and symmetrical peak with R_g values fluctuating around 35 Å (Figure 3.3-10 A). Frames with the highest integral ratio of signal to background were selected, averaged and subjected to buffer subtraction. HUWE1 3796-C mixed with N37p14ARF at 1:6 molar ratio eluted from the HPLC column in the form of a broad peak at a retention time of ~13 min as described previously. The signal plot corresponding to the HUWE1 3796-C/N37p14ARF complex was also characterised by the presence of an asymmetrical peak. Strikingly, R_g values for the peak frames ranged from ~125 Å to ~60 Å, indicating a heterogeneous mixture (Figure 3.3-10 B). As the R_g values differed significantly across the signal plot, I decided to analyse three separate parts of the signal plot to provide more detailed information on the oligomeric species of HUWE1 3796-C/N37p14ARF complex present in the peak. Selected frames (marked 1, 2 and 3) were subjected to buffer subtraction and analysed separately to obtain protein dimension and folded state data (Figure 3.3-10 B). Both HUWE1 3900-C alone and in the presence of 6 molar excess of N37p14ARF were characterised by a retention volume of ~17 min on the HPLC column and a symmetrical signal plot with uniform R_g values. As a result, peak frames were averaged and subjected to buffer subtraction (Figure 3.3-11 A and B).

The obtained scattering curves were first analysed at very small scattering angles using the Guinier approximation. Guinier analysis results in a linearisation of the obtained scattering data in the region where the scattering angle is close to zero. This allows for the determination of the R_g and intensity at zero scattering angle ($I(0)$). Manual Guinier analysis requires two steps: removal of the non-linear points from the starting, low- q region of the scattering curve, followed by limiting the maximum q value to satisfy the $q \cdot R_g < 1.3$ limit. The $q \cdot R_g < 1.3$ is a constraint developed by Feigin and Svergun, which ensures that the derived parameters are within 10% of the real value, as the Guinier analysis is an approximation of the scattering curve, imposing approximation errors on the derived values (Feigin and Svergun, 1989). Guinier analysis for HUWE1 3796-C and HUWE1 3900-C is shown in Figure 3.3-12 and Figure 3.3-13, respectively, and the obtained R_g values for each of the HUWE1 samples are shown in Table 12.

This type of analysis is also very useful in evaluating the presence of protein aggregation, which produces a non-linear dependence of $\ln[I(q)]$ vs q^2 . This behaviour was not observed for either HUWE1 construct or the HUWE1 3796-C/N37p14ARF complex, suggesting that the high-MW peak observed by HPLC of the HUWE1 3796-C/N37p14ARF complex is not aggregated. After determining the Guinier region for each of the analysed samples, I scaled the data and compared \log_{10} intensity and Kratky plots for HUWE1 alone and in the presence of N37p14ARF. Scattering curves ($\log I(q)$ vs q) contain information about the shape of the analysed protein, whereas Kratky plots ($q^2 \cdot I(q)$ vs q) indicate the folded state of the sample. The $P(r)$ distribution function describes the paired-set of all distances between all electrons within the protein structure and is a useful tool for visualising conformational changes. The $P(r)$ distributions were determined by choosing a D_{\max} value that yields a smooth and positive distribution. The data were refined after further trimming to ensure that no negative values were present and no undulations were found in the distribution function. The procedure was repeated until the obtained data were consistent with the underlying distribution defined by the D_{\max} value. The obtained D_{\max} values for each of the HUWE1 samples are shown in Table 12.

Table 12 R_g and D_{\max} values obtained from SAXS analysis of HUWE1 / N37p14ARF complexes

| Construct | R_g [Å] | D_{\max} [Å] |
|--------------------------|-----------|----------------|
| HUWE1 3796-C | 35 | 141 |
| HUWE1 3796-C/N37p14ARF 1 | 117 | 441 |
| HUWE1 3796-C/N37p14ARF 2 | 81 | 304 |
| HUWE1 3796-C/N37p14ARF 3 | 70 | 239 |
| HUWE1 3900-C | 35 | 111 |
| HUWE1 3900-C/N37p14ARF | 34 | 111 |

The obtained R_g value for HUWE1 3796-C was 35 Å, whereas the obtained R_g values for the cross-section of the HUWE1 3796-C/N37p14ARF peak ranged from 70 Å to 117 Å. Similarly, a substantial increase in the D_{\max} value was observed upon addition of N37p14ARF to HUWE1 3796-C: HUWE1 alone was characterised by maximum dimension of to 141 Å, whereas the D_{\max} values for the cross

section of the HUWE1 3796-C/N37p14ARF peak ranged from 239 Å to 441 Å. This suggests that upon addition of N37p14ARF, HUWE1 3796-C forms heterogeneous oligomers. Furthermore, the shape of the $\log_{10}I(q)$ plot for HUWE1 3796-C indicates the presence of a folded, globular-like protein. A dramatic change in the scattering curve is observed upon addition of N37p14ARF peptide. Three separate frames from the HUWE1 3796-C/N37p14ARF signal plot suggested the presence of elongated, “rod-like” species when scattering curve data was compared with those for HUWE1 3796-C alone (Figure 3.3-14 A). My initial hypothesis proposed that HUWE1 3796-C unfolded upon N37p14ARF binding, but the normalised Kratky plot analysis showed that HUWE1 3796-C and different species of HUWE1 3796-C/N37p14ARF exhibit a high degree of protein folding with no signs of aggregation or sample unfolding (Figure 3.3-14 B). This type of Kratky plot is useful in determining the state of the protein in solution, with an implementation of a semi-quantitative approach. The plot is generated by multiplying the q vector by the protein’s R_g value, as well as by multiplying the $I(q)$ by $(q \cdot R_g)^2$. Additionally, $I(q)$ value is divided by the experiment’s $I(0)$ in order to normalise for particle mass (Rambo and Tainer, 2011; Receveur-Brechot and Durand, 2012). Peak at value of ~ 1.1 will be observed for samples which fulfil the Guinier approximation. Figure 3.3-14 B suggests that HUWE1 3796-C resembles a globular protein, however upon introduction of N37p14ARF it becomes asymmetric or flexible (Receveur-Brechot and Durand, 2012).

In contrast, no apparent change in the R_g and D_{max} values were observed for HUWE1 3900-C alone and in the presence of N37p14ARF. Both HUWE1 3900-C and HUWE1 3900-C/N37p14ARF had R_g values of ~ 35 Å and D_{max} values of 111 Å. This suggests that N37p14ARF does not bind this HUWE1 construct or does not induce HUWE1 3900-C oligomerisation. Further analysis of the scattering curves for both samples showed nearly identical curves, indicating that the protein is folded and globular-like (Figure 3.3-15 A). Similarly, normalised Kratky plots for HUWE1 3900-C and HUWE1 3900-C/N37p14ARF were indistinguishable and indicated the presence of a folded globular-like protein with no signs of aggregation (Figure 3.3-15 B).

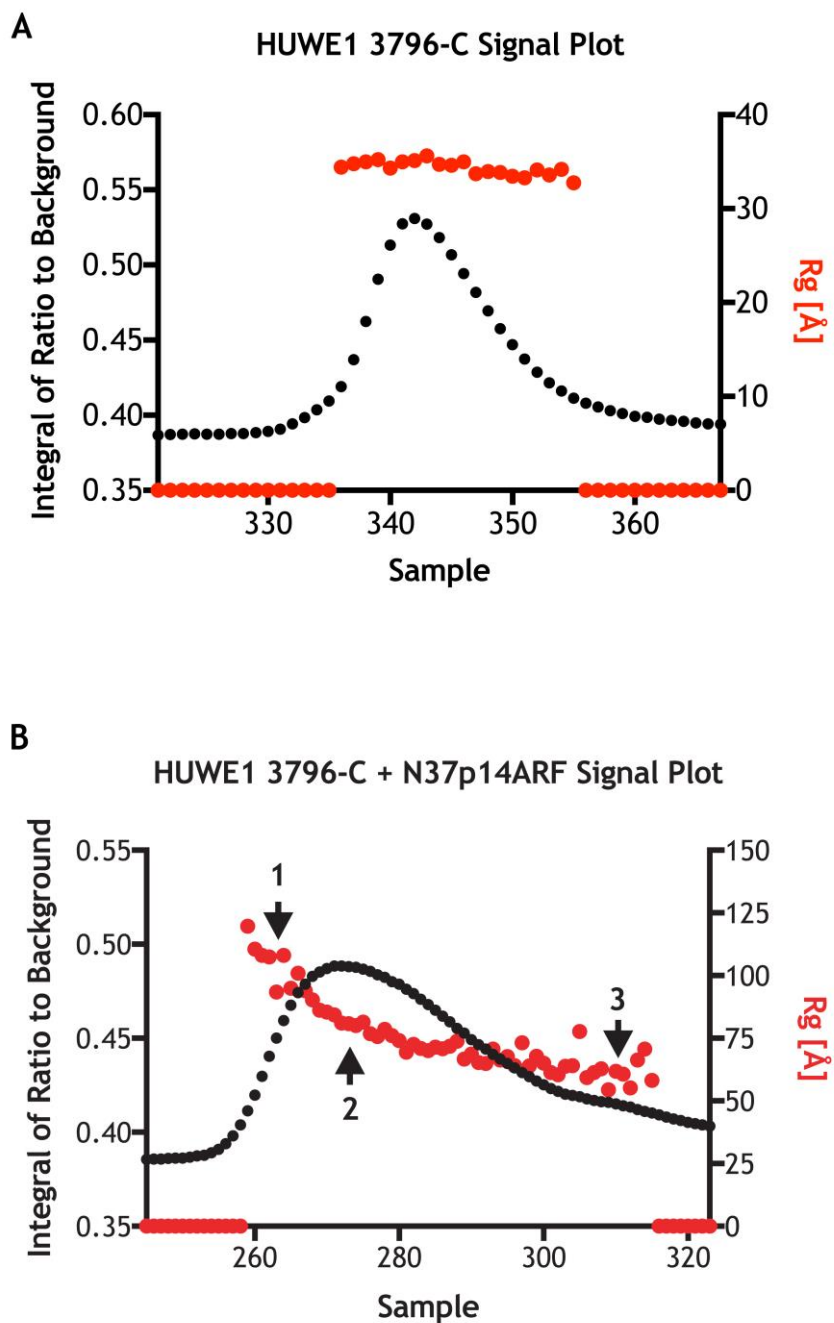


Figure 3.3-10 Signal plots for HUWE1 3796-C and HUWE1 3796-C / N37p14ARF obtained after SEC SAXS

A- Signal plot peak for HUWE1 3796-C.

B- Signal plot peak for HUWE1 3796-C/N37p14ARF. To allow for the analysis of this peak, I separately characterised three different frames of the HUWE1 / ARF signal plot, marked here as 1, 2 and 3.

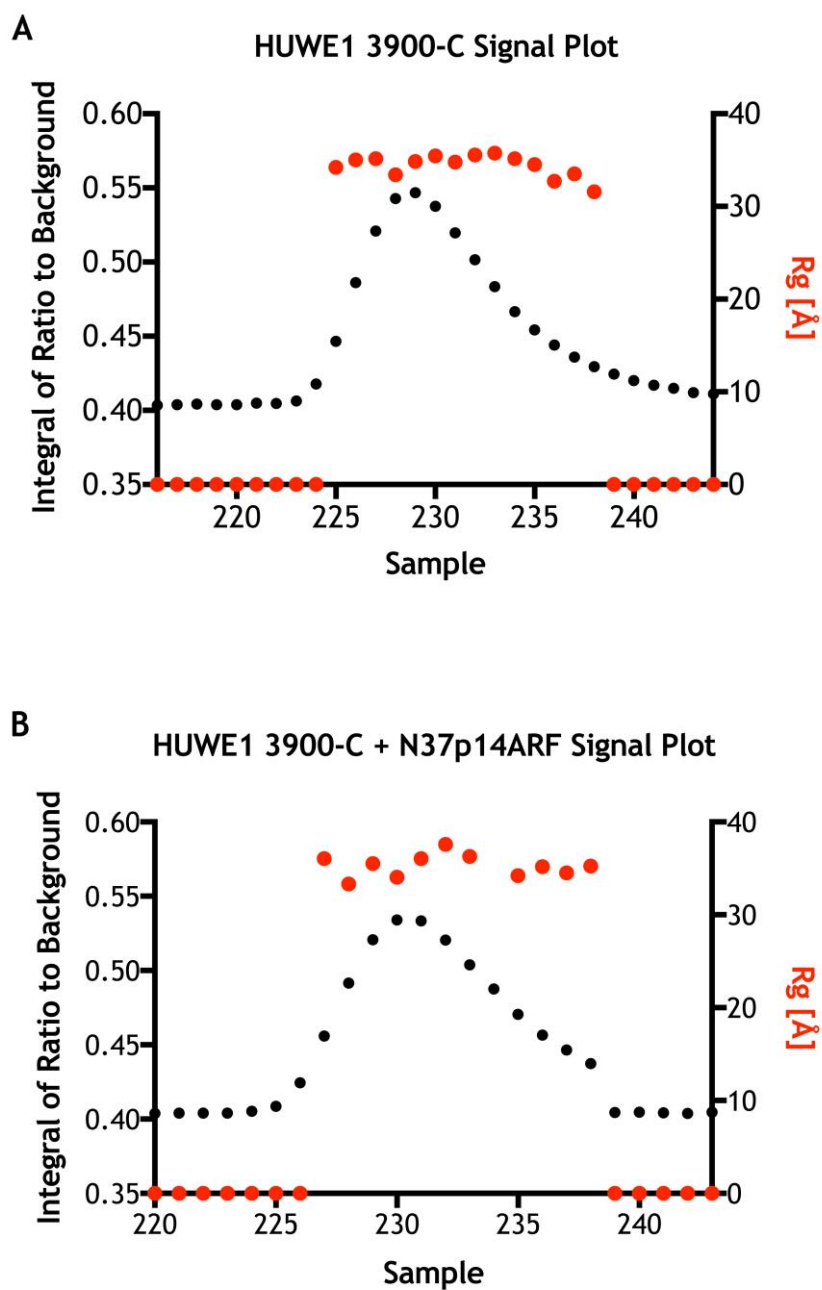


Figure 3.3-11 Signal plots for HUWE1 3900-C and HUWE1 3900-C/N37p14ARF obtained after SEC SAXS

A- Signal plot peak for HUWE1 3900-C.

B- Signal plot peak for HUWE1 3900-C/N37p14ARF.

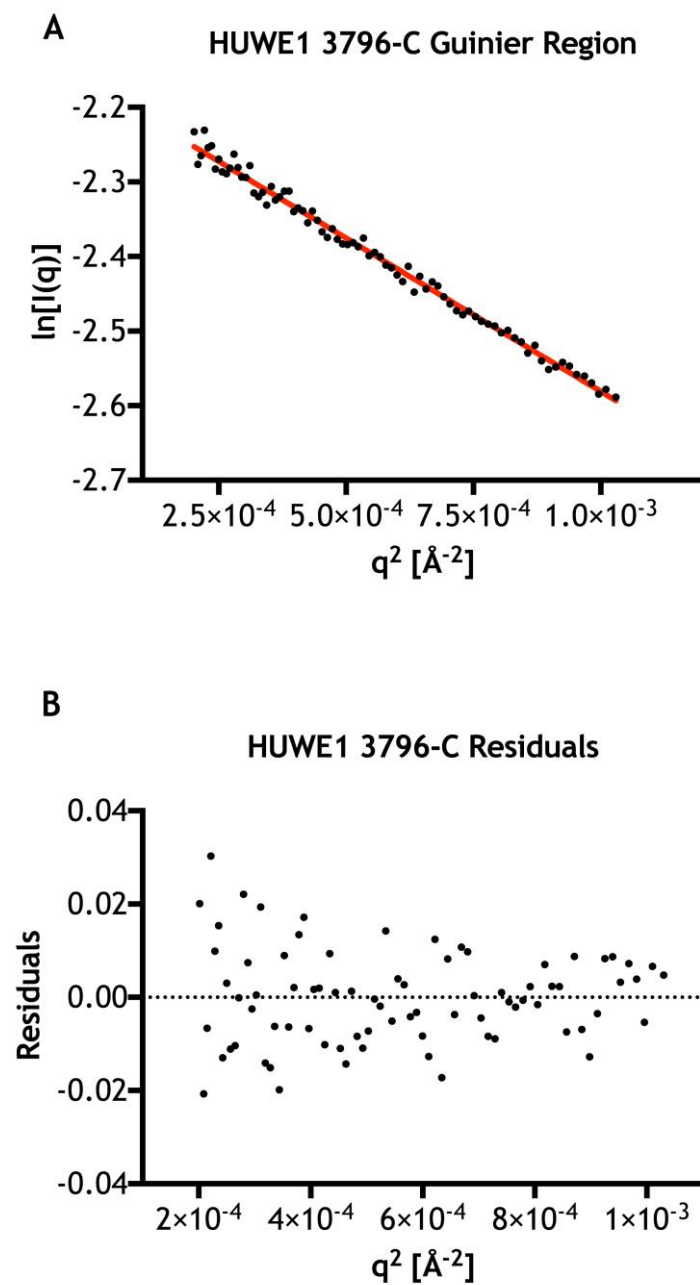


Figure 3.3-12 Guinier analysis for HUWE1 3796-C

A- Linearisation of the scattering data for HUWE1 3796-C in the region where the scattering angle is close to zero.

B- Residuals of the fit shown in figure A.

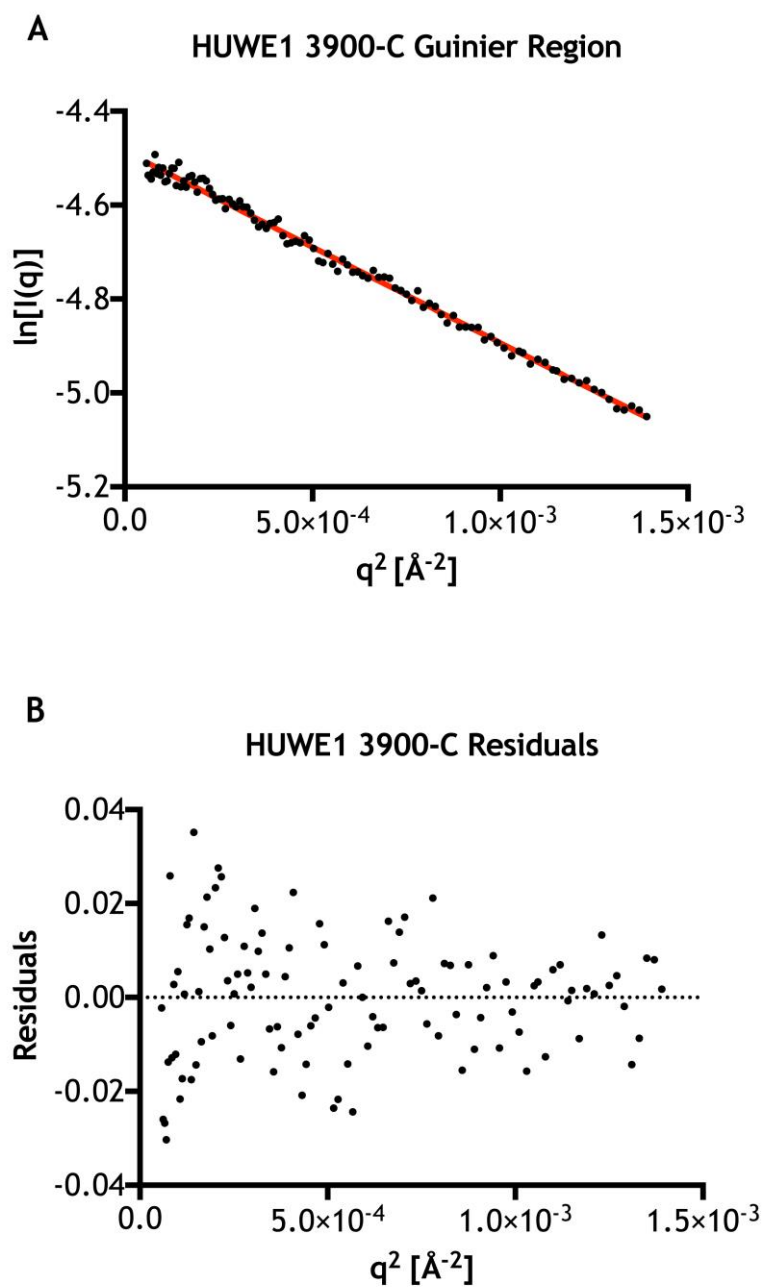


Figure 3.3-13 Guinier analysis for HUWE1 3900-C

A- Linearisation of the scattering data for HUWE1 3900-C in the region where the scattering angle is close to zero.

B- Residuals of the fit shown in figure A.

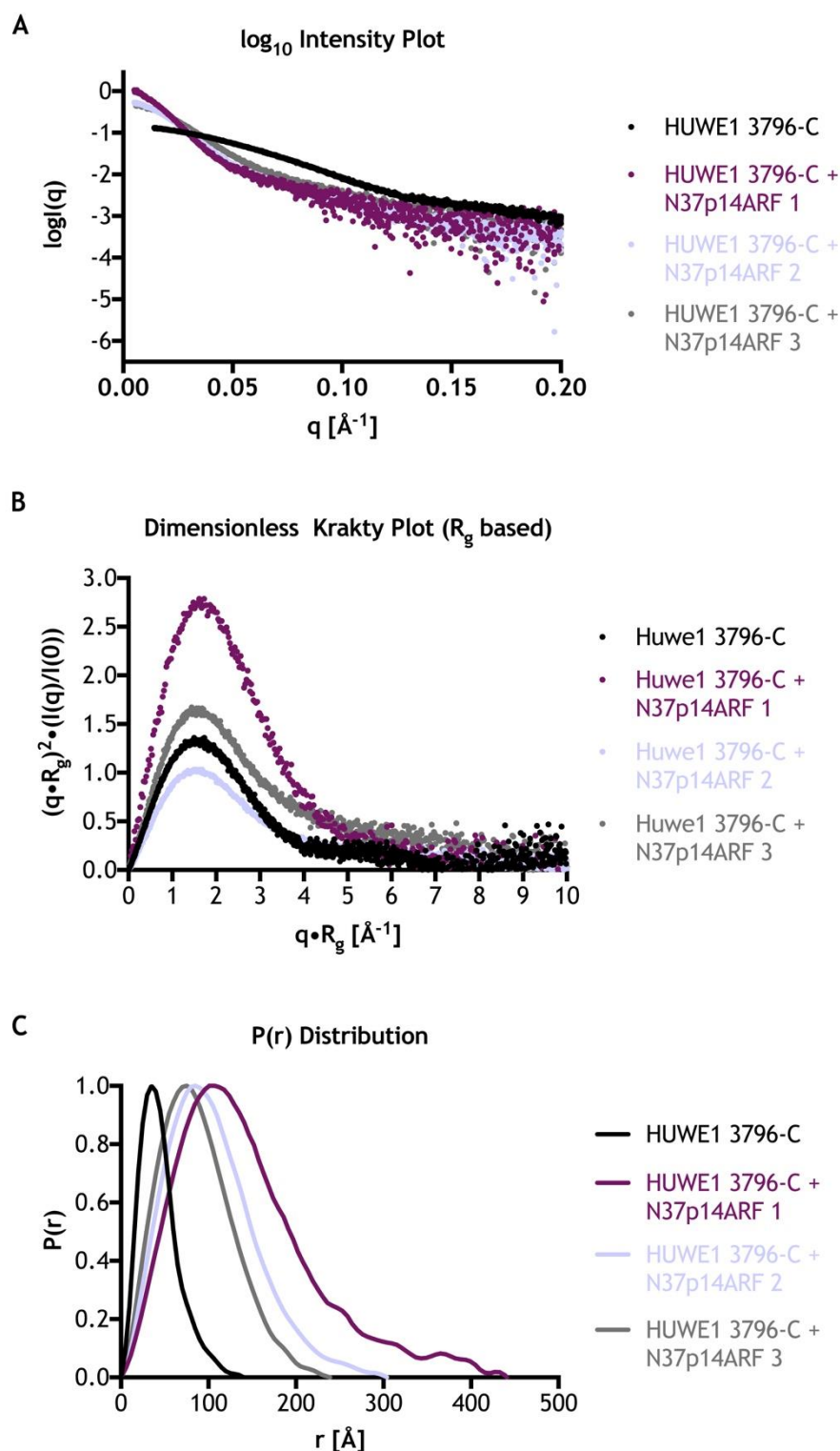


Figure 3.3-14 Analysis of the SEC SAXS data obtained for HUWE1 3796-C +/- N37p14ARF peptide

A- Comparison of scattering curves for HUWE1 3796-C and three different frames of HUWE1 3796-C/ N37p14ARF.

B- Comparison of Kratky plots for HUWE1 3796-C and three different frames of HUWE1 3796-C / N37p14ARF.

C- $P(r)$ distribution function analyses were used to determine D_{max} values for HUWE1 3796-C and each frame of HUWE1 3796-C / N37p14ARF.

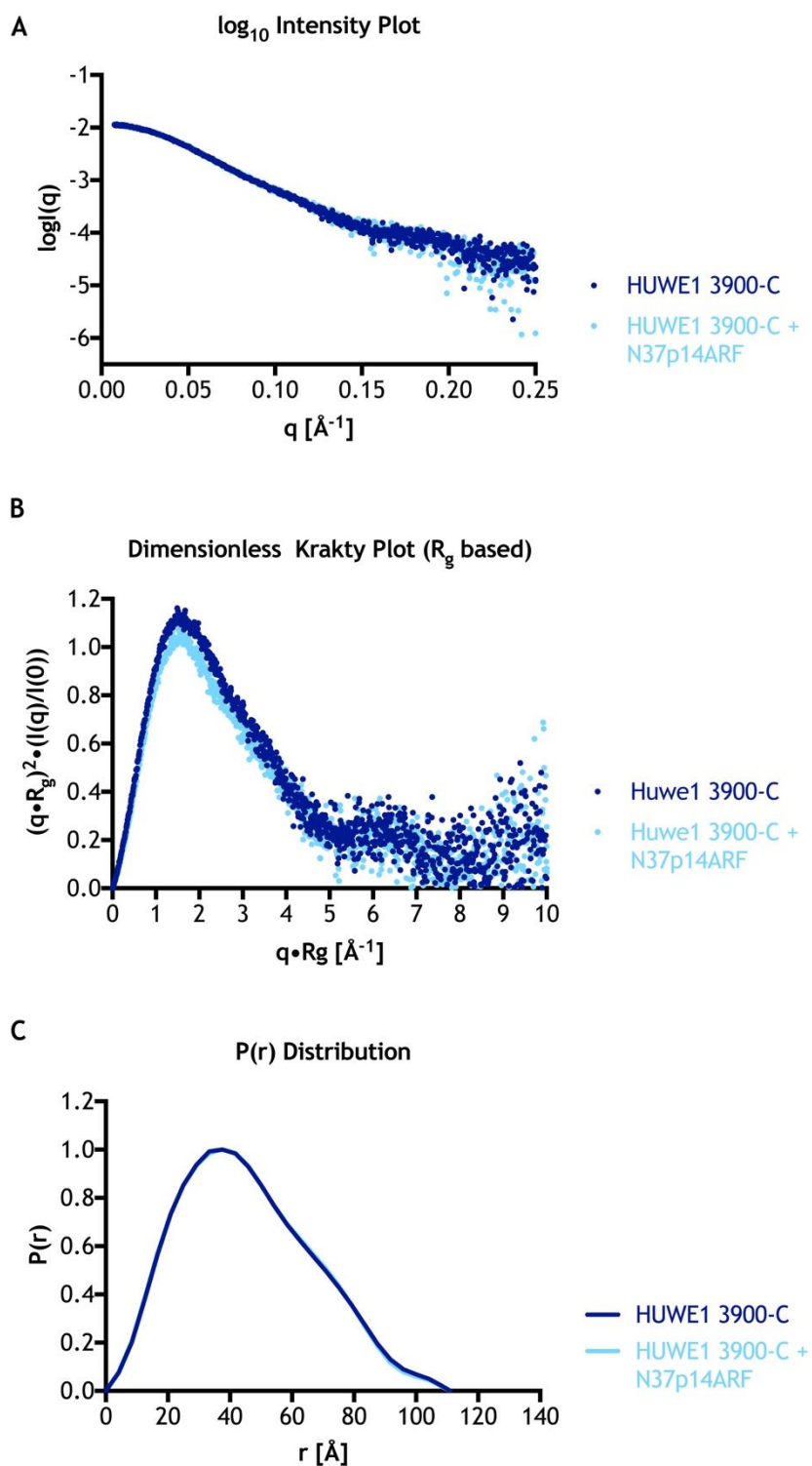


Figure 3.3-15 Analysis of the SEC SAXS data obtained for HUWE1 3900-C +/- N37p14ARF peptide

A- Comparison of scattering curves for HUWE1 900-C and HUWE1 3900-C/ N37p14ARF.

B- Comparison of Kratky plots for HUWE1 3900-C and HUWE1 3900-C/ N37p14ARF.

C- $P(r)$ distribution function analyses were used to determine a D_{max} value for each of the HUWE1 3900-C samples.

3.3.7.2 Crystallisation of HUWE1

I applied various approaches to crystallise HUWE1/N37p14ARF complex. One strategy involved crystallisation trials in which N37p14ARF peptide was added to a range of HUWE1 constructs at 1:4, 1:2, 1:1 and 1:0.5 ratios. Alternatively, crystallisation trials were set up from concentrated HPLC fractions of HUWE1/N37p14ARF complex. Unfortunately, no crystals of HUWE1/N37p14ARF complex were obtained. HUWE1 3900-C was included in these trials and fortuitously crystallised in one of the tested conditions. These crystals have a tetragonal shape and diffracted above 7 Å. Further condition optimisation yielded crystals that diffracted to a resolution of ~3 Å. The structure was determined and refined as described in the Methods (section 2.2.12.2). The final model contains residues 3953-4336 with residues 3900-3952 and 4337-C missing due to no observable electron density. The data collection and refinement statistics are shown in Table 13.

The HUWE1 3900-C structure comprises the catalytic HECT domain and contains an additional 41 amino acids at the N-terminus not present in the structure of HUWE1 3993-C published in 2010 by Pandya *et al.* (Pandya *et al.*, 2010). There are two molecules (designated A and B) of HUWE1 3900-C in the asymmetric unit that adopt similar conformations, and superimposition of C α atoms yields a root mean square deviation (RMSD) value of 0.67 Å. The N-terminal 41 residues form an α -helical turn (helix1A aa 3983-3992) and an α -helix (helix2A aa 3958-3972) in molecule A and two α -helices in molecule B (helix1B aa 3978-3991 and helix2B aa 3954-3970) (Figure 3.3-16 A). These helices from molecules A and B form an asymmetric dimer in which helix2B is oriented toward the C-lobe of the HECT domain from molecule A. The contacts between the two molecules and the positioning of both helices within each subunit mainly involve hydrophobic interactions (Figure 3.3-17). Helix1B of is stabilised by intramolecular hydrophobic contacts involving Leu-4241, Val-3966, Leu-3992, Ile-3989 and Phe-3982 (Figure 3.3-17 A). There is a hydrophobic core at the dimer interface formed by Leu-3966 and Leu-3970 from molecule B and Leu-3966, Ile-3969, Leu-3985 from molecule A (Figure 3.3-17 B). The HECT domains from each subunit adopt a “T-shape” conformation in which the C-lobe is positioned in proximity to the middle of the N-lobe (Figure 3.3-16 B). The HECT domain of molecule B adopts a conformation similar to the HECT domain in HUWE1 3993-C and

superposes with an RMSD of ~ 1.2 Å for all C α atoms (Figure 3.3-18) (Pandya *et al.*, 2010). No comparison was made with molecule A because residues 4162-4193, which span the E2 binding site, could not be built into the model due to missing electron density. Interestingly, both molecules show higher conformation similarity within their C-lobes (RMSD of ~ 0.2 Å for C α atoms, Figure 3.3-18 B), as opposed to their N-lobes (RMSD of ~ 0.8 Å for C α atoms, Figure 3.3-18 B). One of the largest deviations between the structures is the E2 binding site (Figure 3.3-18 B). An extensive comparison of E2-binding sites from various HECT structures in the presence and absence of E2 by Zhang *et al.* revealed that the E2-binding site is mobile (Zhang *et al.*, 2016). Whether the E2-binding site conformation in HUWE1 3900-C results from crystal packing or represents a biologically relevant conformation is unknown.

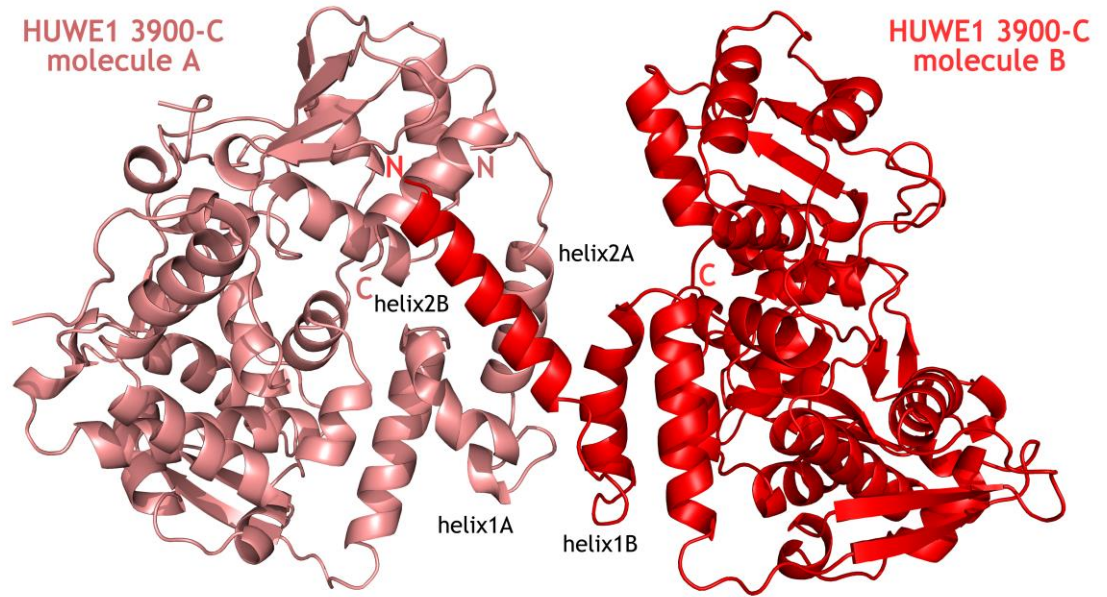
Shortly after I obtained the HUWE1 3900-C structure, Sander *et al.* published a nearly identical structure of HUWE1 (3951-C) that superposes with an RMSD of ~ 0.2 Å for all C α atoms (Figure 3.3-19). Sander *et al.* also observed an asymmetric dimer formed via the N-terminal helices and validated its functional significance (Sander *et al.*, 2017). In the dimer interface, the N-terminal helix of one HUWE1 subunit (helix2B on Figure 3.3-16 A) contacts the C-lobe of the second HUWE1 subunit, thereby locking the C-lobe in a fixed conformation. Moreover, Sander *et al.* showed that the C-terminal end of HUWE1, which contains the catalytically relevant “-4 Phe” residue, is buried at the dimer interface (Sander *et al.*, 2017). In my structure, the contact between N-terminal helix of one HECT subunit with the C-lobe of the second HECT subunit is present, but the C-termini of both HUWE1 subunits could not be modelled due to missing electron density. For a HECT domain to catalyse Ub transfer, the C-lobe must rotate between two different conformations for the E2-E3 transthiolation and the E3-substrate Ub transfer reactions (see section 1.3.2). Based on these observations, Sander *et al.* proposed that in the dimeric state, HUWE1 3951-C is auto-inhibited, as it has only one functional HECT domain. When they substituted residues Phe-3982 and Ile-3969 within the hydrophobic core of the dimer interface to alanine, the full catalytic activity of HUWE1 was recovered (Sander *et al.*, 2017). They also identified an “activation segment” (residues 3843-3896) that has a similar sequence to helix1 (residues 3978-3991) and showed that in the presence of this sequence, HUWE1 forms a monomer. They

proposed that this activation segment binds helix1 via intra-molecular interactions to reverse auto-inhibition. Interestingly, Sander et al. suggested that p14ARF exerts its inhibitory effect on HUWE1 by binding to the activation segment and promoting formation of dimeric auto-inhibited HUWE1 (Sander *et al.*, 2017). They further showed that residues 45-75 of p14ARF bind the activation segment of HUWE1 and inhibit activity.

Table 13 X-ray crystallographic data collection and refinement statistics. Values in the brackets correspond to the highest resolution shell.

| Data Collection | |
|--------------------------------------|-------------------------|
| Wavelength [Å] | 0.9795 |
| Space group | <i>P</i> 6 ₃ |
| Cell dimensions | |
| a, b, c [Å] | 177.71, 177.71, 105.40 |
| α, β, γ [°] | 90, 90, 120 |
| Resolution [Å] | 39.56 - 2.66 |
| R _{merge} | 0.144 (2.251) |
| I/σ(I) | 13.2 (1.4) |
| CC _{1/2} | 1.0 (0.4) |
| Completeness [%] | 100 (100) |
| Multiplicity | 10.1 (9.7) |
| Refinement | |
| Reflections used | 69735 |
| R _{work} /R _{free} | 0.2202/0.2488 |
| No. of non-hydrogen atoms | 6620 |
| Water molecules | 90 |
| Average B factors | |
| Protein | 75.6 |
| Solvent | 62.8 |
| RMSD from ideality | |
| Bonds [Å] | 0.0093 |
| Angles [°] | 1.124 |
| Ramachandran statistics | |
| Favoured [%] | 97.72 |
| Disallowed [%] | 0 |
| MolProbity clash score | 6.2 |

A



B

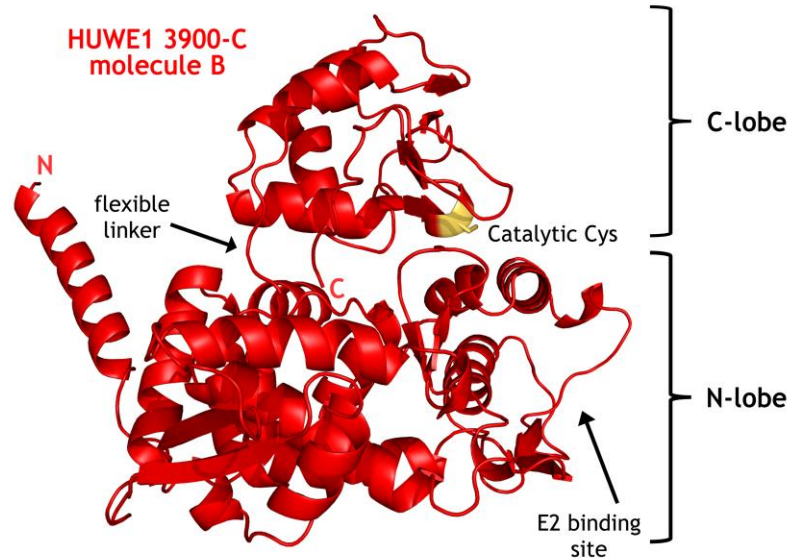


Figure 3.3-16 Crystal structure of HUWE1 3900-C

A- Overall structure of HUWE1 3900-C. Two HUWE1 molecules, A and B, are coloured in pink and red, respectively. The HUWE1 3900-C structure contains an additional 41 amino acids at the N-terminus as compared with HUWE1 3993-C (Pandya *et al.*, 2010), These residues form two helices, helix1 and helix2, as indicated.

B- Structural organisation of the HECT domain of molecule B. The catalytic cysteine is shown in yellow; The E2-binding site and the flexible linker connecting N- and C-lobes are indicated.

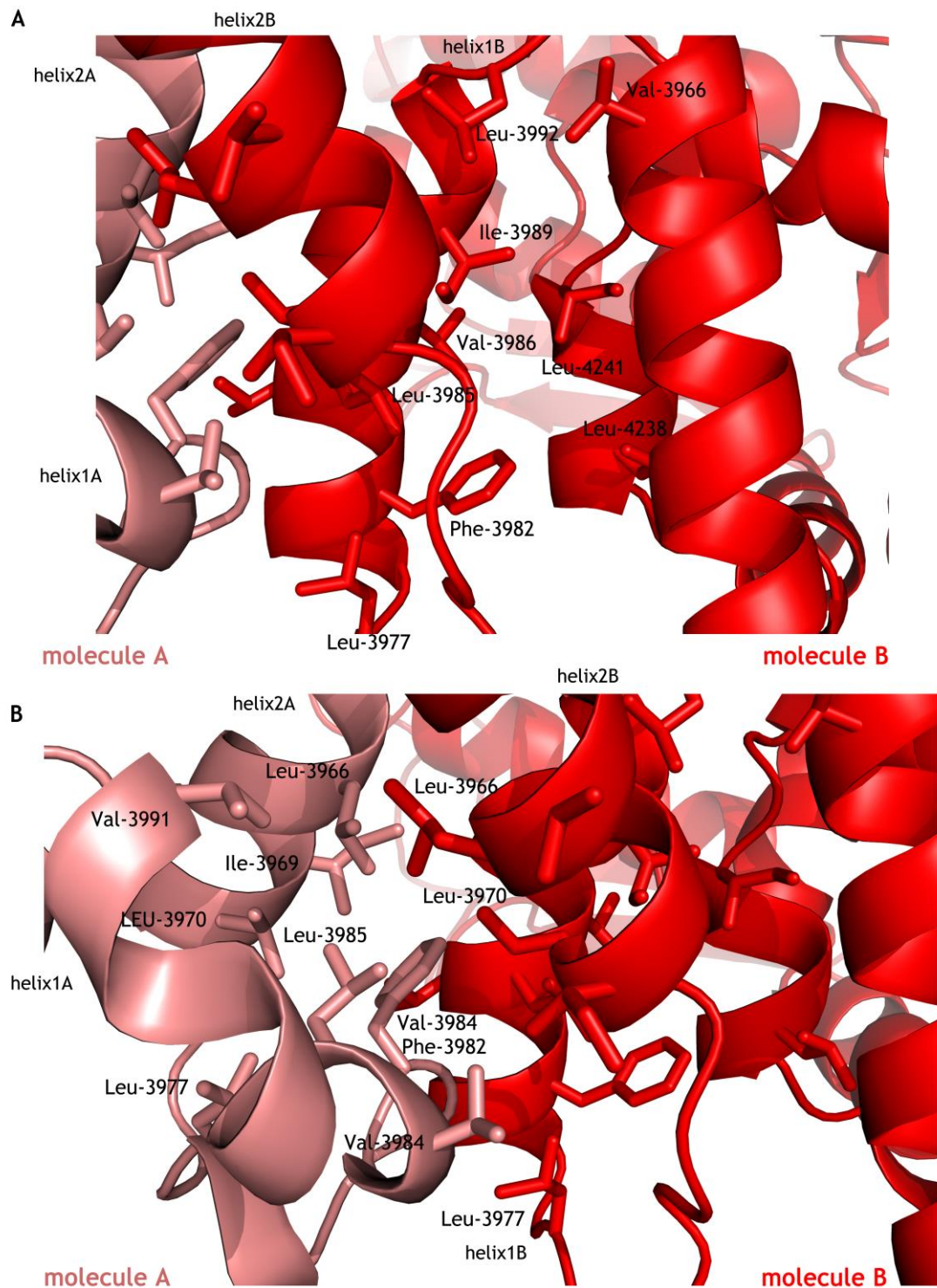


Figure 3.3-17 Hydrophobic contacts stabilise the HUWE1 dimer

A- Close-up view of helix1B and helix2B from HUWE1 molecule B. Residues that form hydrophobic interactions and stabilise helix1B in molecule B are labelled.

B- Close-up view of the HUWE1 dimer interface. Helix1B from molecule B forms hydrophobic interactions with helix1A and helix2A from molecule A.

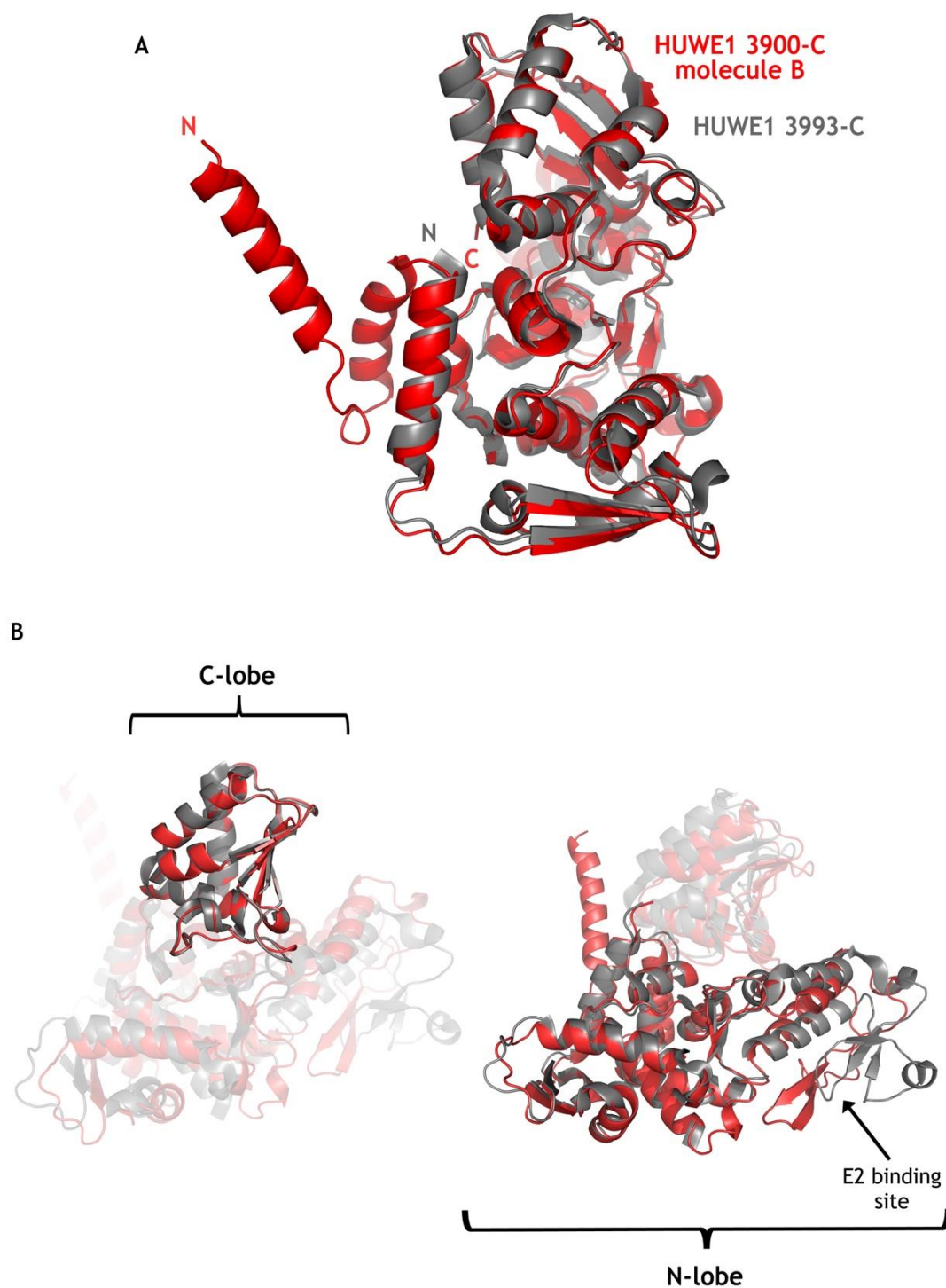


Figure 3.3-18 Superimposition of HUWE1 3900-C and HUWE1 3993-C

A,B – Two different views of superimposed structures of HUWE1 3900-C molecule B and HUWE1 3993-C (PDB code 3H1D) (Pandya *et al.*, 2010). HUWE1 3900-C molecule B is in red and HUWE1 3993-C is in grey. Figure B shows the superposition of either C-lobes or N-lobes alone, to emphasise the real differences between two structures.

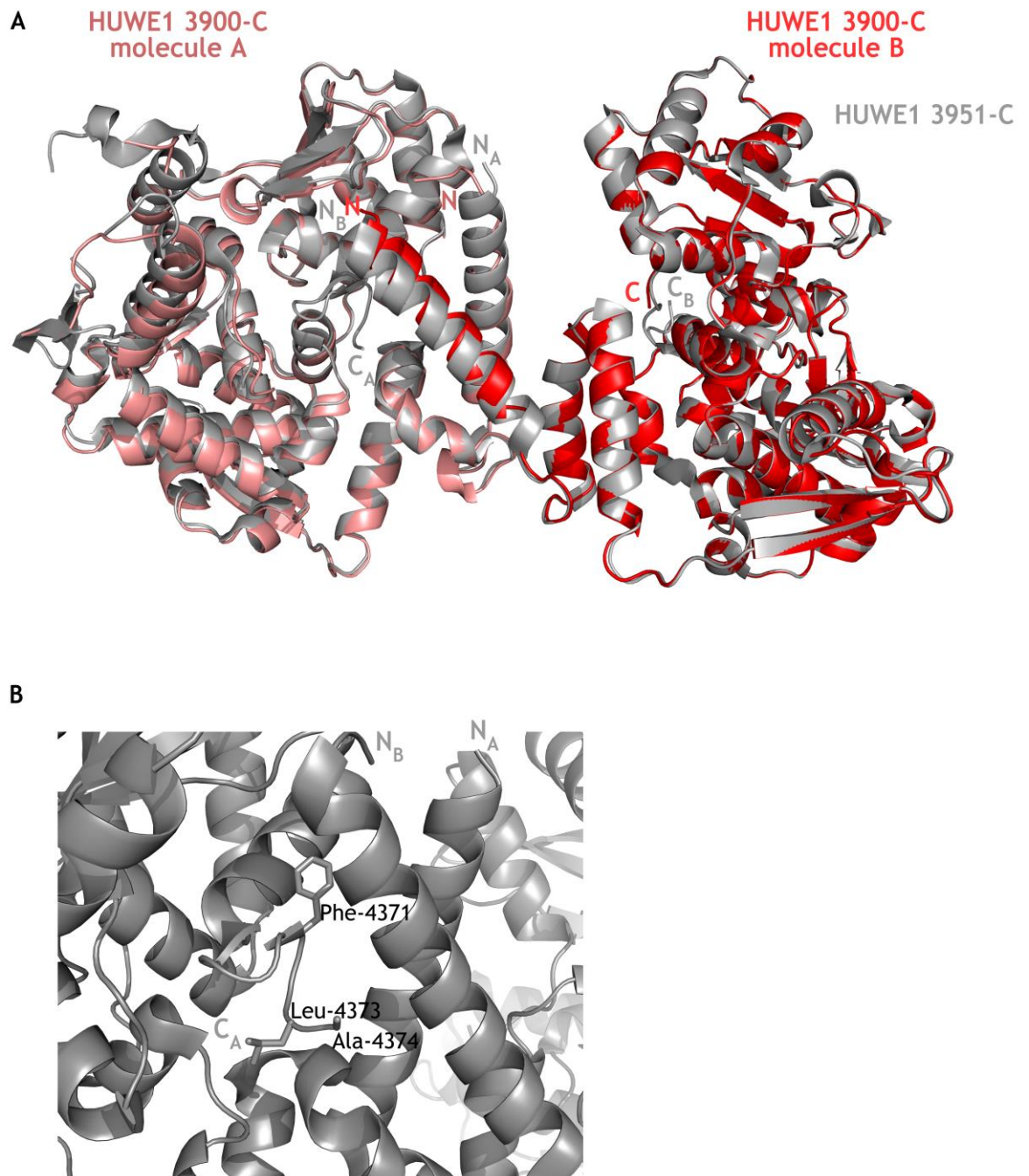


Figure 3.3-19 Superimposition of HUWE1 3900-C and HUWE1 3951-C

A- Superimposed structures of HUWE1 3900-C and HUWE1 3951-C (PDB code 5LP8) (Sander *et al.*, 2017). HUWE1 3900-C is in red and HUWE1 3951-C is in grey.

B- Close up of the dimer interface in HUWE1 3951-C (PDB code 5LP8). The C-terminal tail from one subunit contacts $\alpha 2$ at the N-terminus of the second subunit. Hydrophobic residues from the C-terminal tail including the “-4 Phe residue” are shown as sticks (Sander *et al.*, 2017).

3.3.8 HUWE1 3900-C dimerises in solution

Sander et al. proposed that an activation segment spanning residues 3843-3896 of HUWE1 is important for blocking dimerisation. Based on these findings, my 3900-C and 3796-C HUWE1 constructs should be a dimer and monomer, respectively, in solution. To investigate whether HUWE1 3900-C dimerises in solution, I compared HPLC elution profiles of HUWE1 3900-C and HUWE1 3796-C. As shown in Figure 3.3-20 A, both HUWE1 variants eluted from HPLC column at retention times of ~16 min with the HUWE1 3900-C peak eluting marginally earlier than HUWE1 3796-C. The predicted MW of a HUWE1 3900-C monomer is ~12 kDa smaller than that of HUWE1 3796-C (67 kDa). Despite being smaller, HUWE1 3900-C eluted slightly earlier from the HPLC size exclusion column, suggesting that it has a larger mass or is more elongated than HUWE1 3796-C. To investigate further, I generated an ab initio model of HUWE1 3900-C using the scattering curve obtained from the SAXS experiment. This model was superimposed with the crystal structure of dimeric HUWE1 3900-C and the calculated envelope of the “in solution” HUWE1 3900-C fits the dimeric X-ray structure, suggesting that HUWE1 3900-C forms a dimer in solution (Figure 3.3-20 B). To investigate whether dimerisation of HUWE1 3900-C could be reversed by disrupting the hydrophobic interface, I generated I3969A and F3982A variants of HUWE1 3900-C and compared their HPLC elution profiles with wild-type HUWE1 (Figure 3.3-21). Both HUWE1 3900-C I3969A and F3982A eluted at retention times of ~18 min, whereas wild-type HUWE1 eluted at a retention time of ~17 min. This suggested that introduction of a single point mutation at the dimer interface could induce a change in the MW of HUWE1. Previous studies showed that monomeric HUWE1 has increased catalytic activity compared with the dimer (Sander *et al.*, 2017). To investigate if HUWE1 3900-C I3969A and F3982A were more active than wild-type, I performed single-turnover auto-ubiquitination assays and found that all three variants showed similar rates of poly-Ub chain formation and disappearance of the Ub_{CH5B}-Ub band (Figure 3.3-22). Moreover, direct comparison of the potency of HUWE1 3796-C and HUWE1 3900-C towards Ub_{CH5B}-Ub and Ub_{CH7}-Ub discharge did not show an observable difference in their activities (Figure 3.3-23). Collectively, my results suggest that HUWE1 3900-C forms a dimer in solution based on HPLC and SAXS data and substitution of I3969A or F3982A alters its size as shown on HPLC

elution profiles. However, dimeric HUWE1 3900-C does not appear to be auto-inhibited.

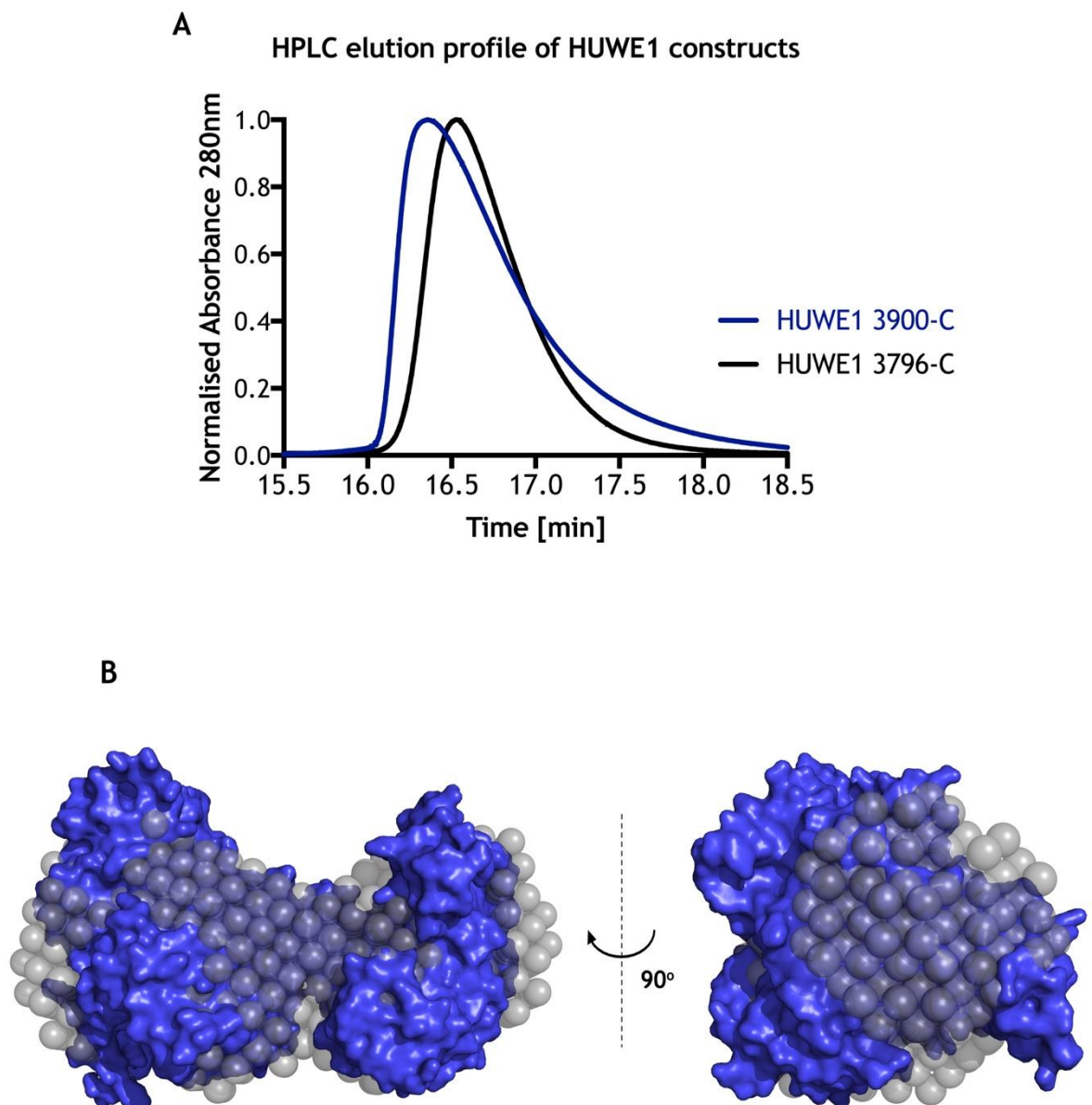


Figure 3.3-20 HUWE1 3900-C dimerises in solution

A- Comparison of the HPLC elution profiles of HUWE1 3796-C and HUWE1 3900-C. Samples were loaded onto a Shodex KW-403-4F HPLC column.

B- Superposition of the crystallised HUWE1 3900-C dimer surface (blue) and the *ab initio* model calculated from the HUWE1 3900-C scattering curve in solution (grey). The envelope obtained from solution scattering is in agreement with the dimer model of the protein obtained from the X-ray crystallography studies.

HPLC elution profile of HUWE1 3900-C variants

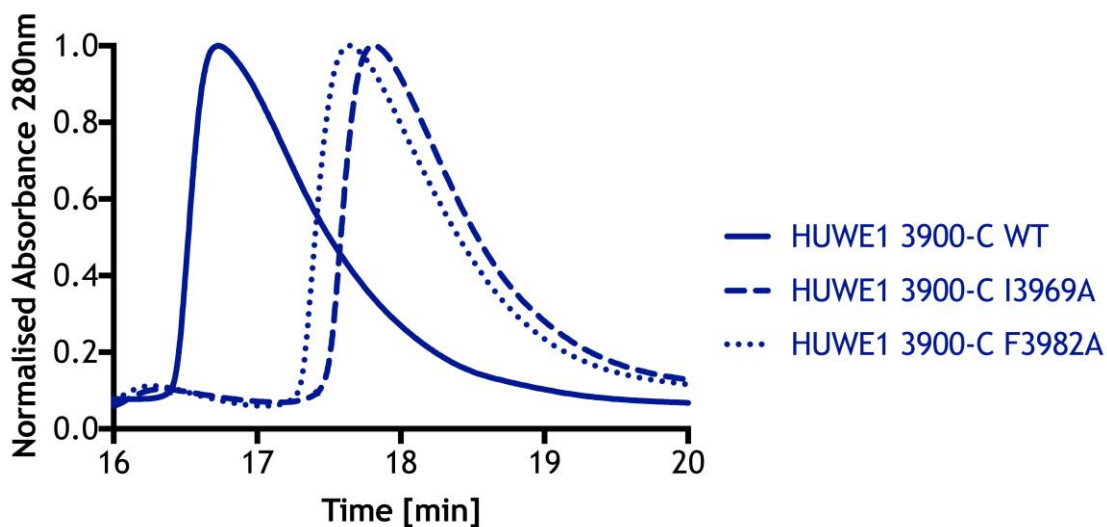


Figure 3.3-21 HUWE1 3900-C dimerisation can be reversed by disrupting the hydrophobic dimer interface

HPLC elution profiles of HUWE1 3900-C WT, I3969A and F3982A. Samples were loaded onto a Shodex KW-403-4F HPLC column.

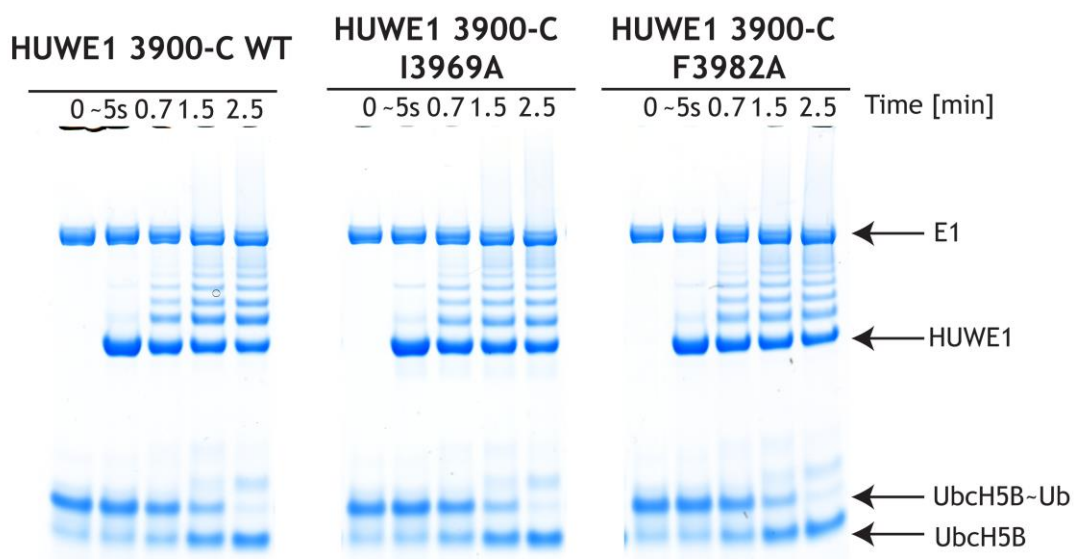


Figure 3.3-22 The dimerisation state of HUWE1 3900-C does not influence its catalytic activity

SDS-PAGE gels showing single-turnover auto-ubiquitination assays of HUWE1 3900-C variants with UbcH5B-Ub. Reactions were performed as described in section 2.2.8, with a 4 μ M concentration of each indicated E3.

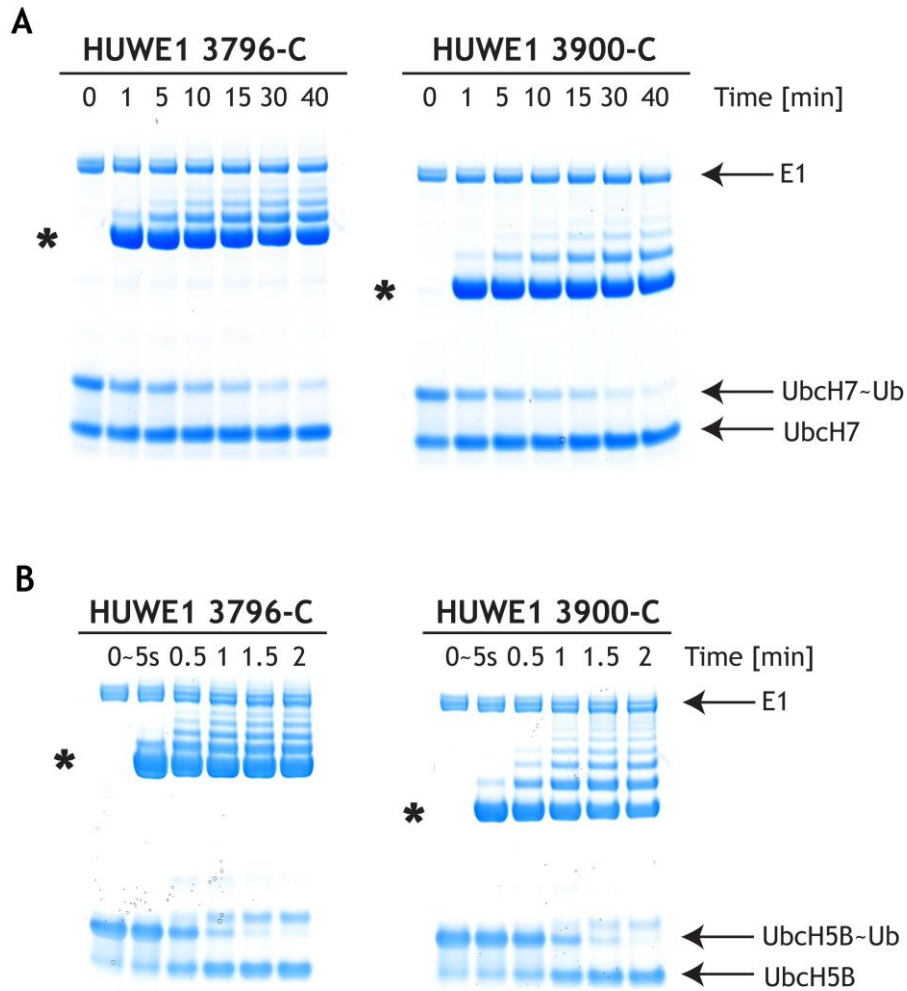


Figure 3.3-23 Activation segment does not influence the activity of HUWE1 3796-C

SDS-PAGE gels showing single-turnover auto-ubiquitination assays of HUWE1 3796-C and HUWE1 3900-C using (A) UbcH7~Ub and (B) UbcH5B~Ub. An asterisk marks the band corresponding to the non-ubiquitinated HUWE1 variant used in each assay. Reactions were performed as described in section 2.2.8, with a 6 μ M concentration of each indicated E3.

3.3.9 p14ARF does not influence HUWE1 catalytic activity

Sander et al. suggested that residues 45-75 (referred to as 45-75p14ARF) of p14ARF are required to inhibit HUWE1 activity (Sander *et al.*, 2017). Importantly, these residues are not present in N37p14ARF, which did not inhibit HUWE1 activity in my assays (Figure 3.3-9). To investigate whether the suggested fragment of p14ARF binds and inhibits HUWE1 activity, I performed double pull-down experiment. The predicted isoelectric point of the activation segment of HUWE1 (residues 3843-3896) is 4.0, suggesting this part of the protein is very acidic. On the other hand, p14ARF is very basic, having a theoretical pI value of ~12.5. This suggests that the interaction between HUWE1 and ARF might be driven by electrostatic interactions. To examine whether N37p14ARF (pI ~12.3) and 45-75p14ARF (pI ~12.6) can bind HUWE1, I generated two constructs of HUWE1 spanning residues 3753-3843 and 3843-3902. Both have low predicted pIs (~4.4 and ~4.2 respectively) but only HUWE1 3843-3902 contains the reported activation segment. Both GST-tagged HUWE1 constructs were co-expressed with His-MBP variants of p14ARF (Figure 3.3-24). N76p14ARF and the previously investigated N56p14ARF were used as controls. Appropriate measures were used to ensure that GST-HUWE1 variants did not bind Ni²⁺ resin non-specifically. GST-HUWE1 3753-3843 and GST-HUWE1 3843-3902 pulled down all His-MBP p14ARF constructs, suggesting that the activation segment is not the sole fragment of HUWE1 responsible for p14ARF binding. Since I confirmed that 45-75p14ARF binds HUWE1, I assessed whether it can inhibit HUWE1 ligase activity. I ordered three new synthetic peptides of p14ARF: 36-55p14ARF (which contains the previously mentioned α -helix of p14ARF), 45-64p14ARF (which was used in the study published by Sander et al.) and N76p14ARF, which incorporates all the p14ARF sequence present in the previously mentioned p14ARF peptides. All of the peptides were dissolved in 8 M GdnHCl to a final concentration of 5 mM and introduced to HUWE1 3796-C at a 1:6 molar ratio. No precipitation was observed for any of the peptides. The HUWE1 3796-C activity in the presence of these p14ARF variants was assessed using single-turnover auto-ubiquitination assays. None of these peptides affected the rates of the disappearance of Ub₅-Ub or poly-Ub chain formation, suggesting that p14ARF does not inhibit HUWE1 activity (Figure 3.3-25). I also investigated whether any of these p14ARF peptides induce HUWE1 oligomerisation. HUWE1 3796-C was incubated with a 6-

fold molar excess of each p14ARF peptide and subsequently applied onto the HPLC column. Addition of N76p14ARF or 36-55p14ARF resulted in the formation of a high MW peak with a retention time of 13 min, similar to that observed with the addition of N37p14ARF (Figure 3.3-26). In contrast, addition of 45-64p14ARF peptide resulted in a less pronounced disappearance of the HUWE1 3796-C peak and formation of a broad and heterogenous peak with a retention time of ~14 min.

N76p14ARF peptide was visible as a discrete band on SDS-PAGE gels, and I used this to my advantage to investigate whether N76p14ARF peptide co-elutes with HUWE1 3796-C on an HPLC column. HUWE1 3796-C was mixed with N76p14ARF peptide at a 1:1 ratio, and applied onto the HPLC column. BSA incubated in a 1:1 molar ratio with N76p14ARF was used as a control. Addition of N76p14ARF to HUWE1 3796-C led to the appearance of a heterogeneous peak with a retention time spanning from 12-15 min (Figure 3.3-27 A) whereas this peptide had no effect on the elution profile of BSA (Figure 3.3-27 B). The protein concentration in each fraction obtained from the HPLC was measured and all of the protein-containing samples were run on SDS-PAGE gels, which were stained with silver to detect N76p14ARF peptide (Figure 3.3-28). The small peak that formed upon addition of N76p14ARF peptide contained both HUWE1 3796-C and the majority of N76p14ARF peptide. A small amount of N76p14ARF could be detected in the major HUWE1 3796-C peak. The intensities of the bands, corresponding to HUWE1 on the gel B and C (Figure 3.3-28), differ due to longer developing procedure applied to gel C. Together, my results show that p14ARF binds HUWE1 3796-C and induces HUWE1 oligomerisation but does not influence HUWE1 activity.

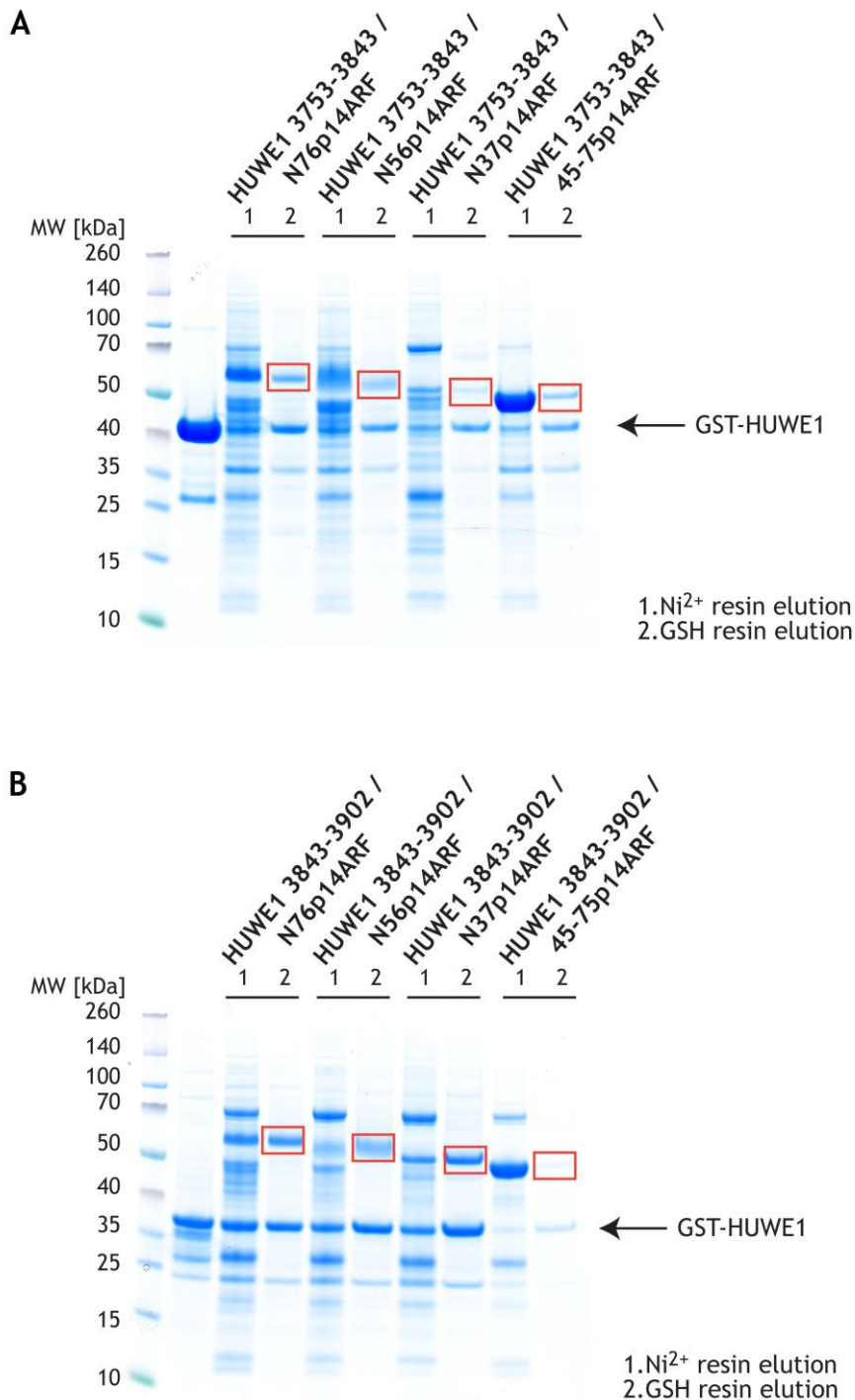


Figure 3.3-24 HUWE1 3753-3843 and HUWE1 3843-3902 bind several fragments of p14ARF

A- SDS-PAGE gel showing double pull-down of GST-HUWE1 3753-3843 with different His-MBP-p14ARF constructs. Cell lysates were subjected to Ni²⁺-resin purification followed by GSH-Sepharose purification. GST-HUWE1 3753-3843 pulled down all His-MBP-p14ARF constructs. Red squares indicate different His-MBP-p14ARF constructs. The first lane shows GST-HUWE1 3753-3843 alone.

B- SDS-PAGE gel showing double pull-down of GST-HUWE1 3843-3902 with different His-MBP-p14ARF constructs. Cell lysates were subjected to Ni²⁺-resin purification followed by GSH-Sepharose purification. GST-HUWE1 3843-3902 pulled down all His-MBP-p14ARF constructs. Red squares indicate different His-MBP-p14ARF constructs. The first lane shows GST-HUWE1 3843-3902 alone.

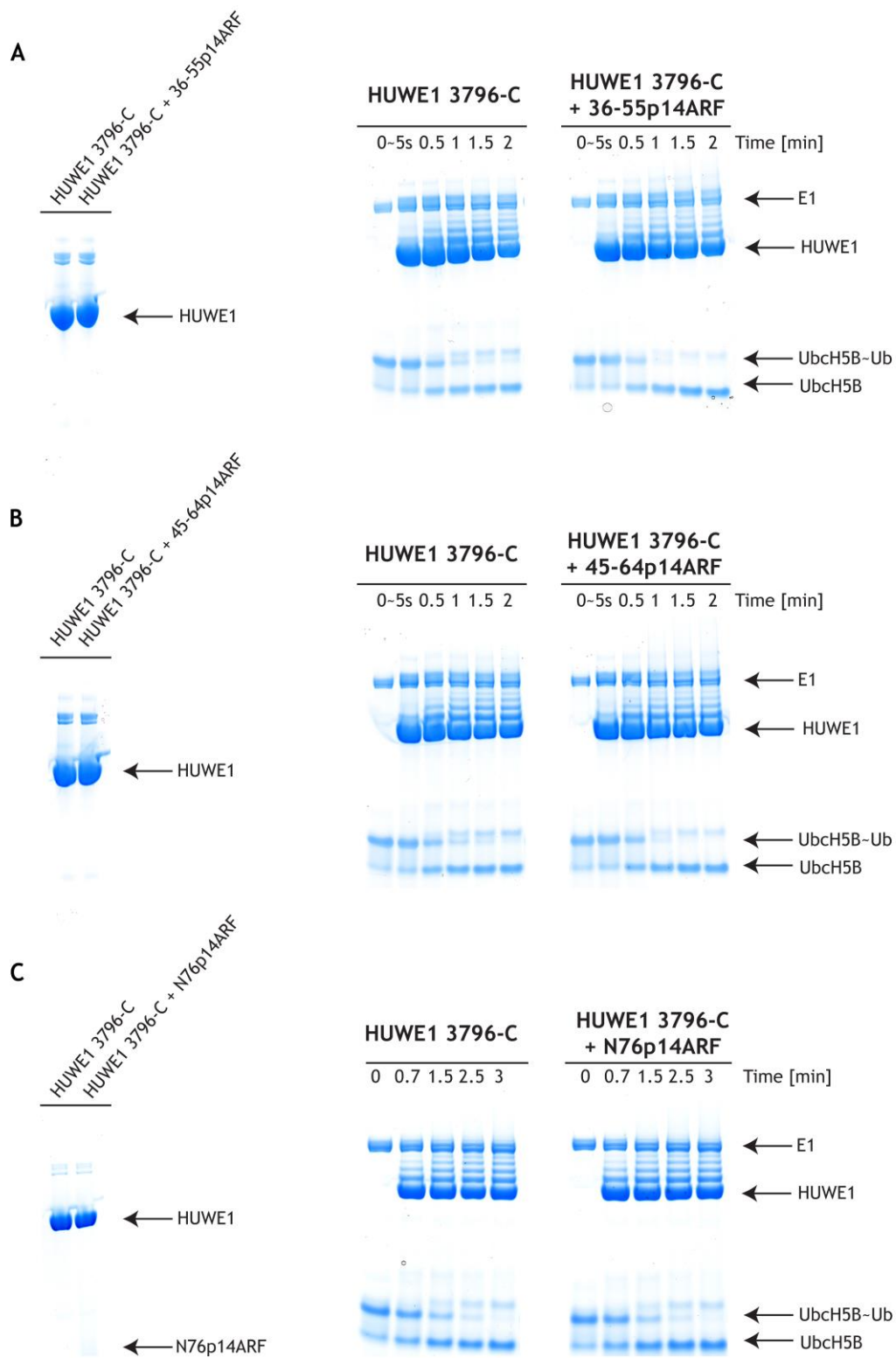


Figure 3.3-25 p14ARF variants do not influence HUWE1 catalytic activity

SDS-PAGE gels showing single-turnover auto-ubiquitination assays of HUWE1 3796-C in the presence of a 6-molar excess of different p14ARF peptides (A– 36-55p14ARF; B- 45-64p14ARF; C- N76p14ARF). HUWE1 3796-C in the presence and absence of each p14ARF peptide was first analysed by SDS-PAGE to ensure that equal amounts of E3 were used in each reaction (left hand side of each panel). HUWE1 3796-C showed similar potency towards Ubch5B-Ub discharge and poly-Ub chain formation independent of the presence of p14ARF peptides: (A) 36-55p14ARF; (B) 45-64p14ARF; (C) N76p14ARF. Reactions were performed as described in section 2.2.8, using 6 μ M of HUWE1 3796-C.

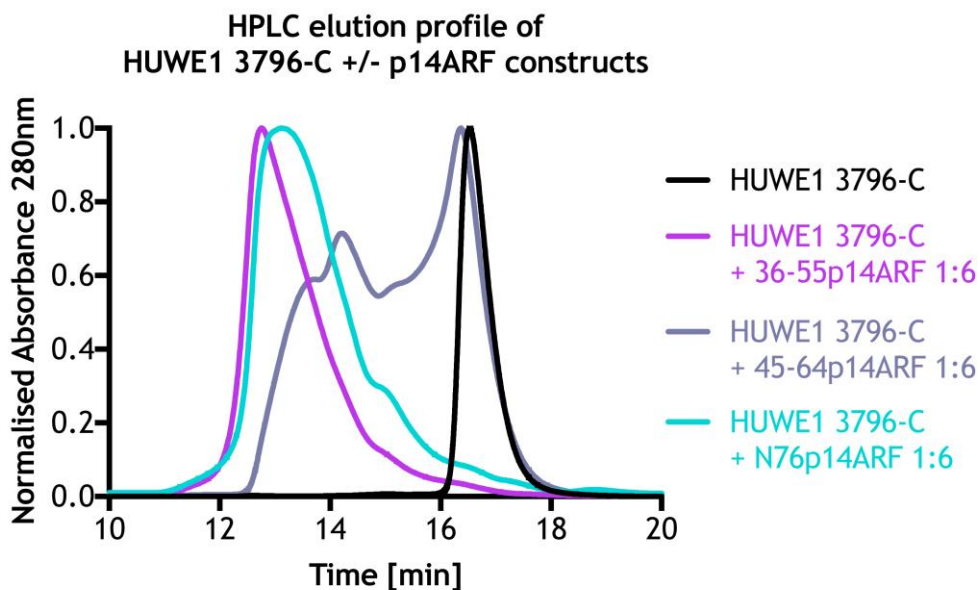


Figure 3.3-26 p14ARF variants induce oligomerisation of HUWE1 3796-C

HPLC elution of HUWE1 3796-C (in black) in the presence of a 6-molar excess of different p14ARF peptides. 36-55p14ARF (in magenta) and N76p14ARF (in cyan) induced formation of a high-MW species of HUWE1 3796-C in a manner similar to N37p14ARF whereas 45-64p14ARF induced formation of a broad heterogeneous peak. Samples were loaded onto a Shodex KW-403-4F HPLC column.

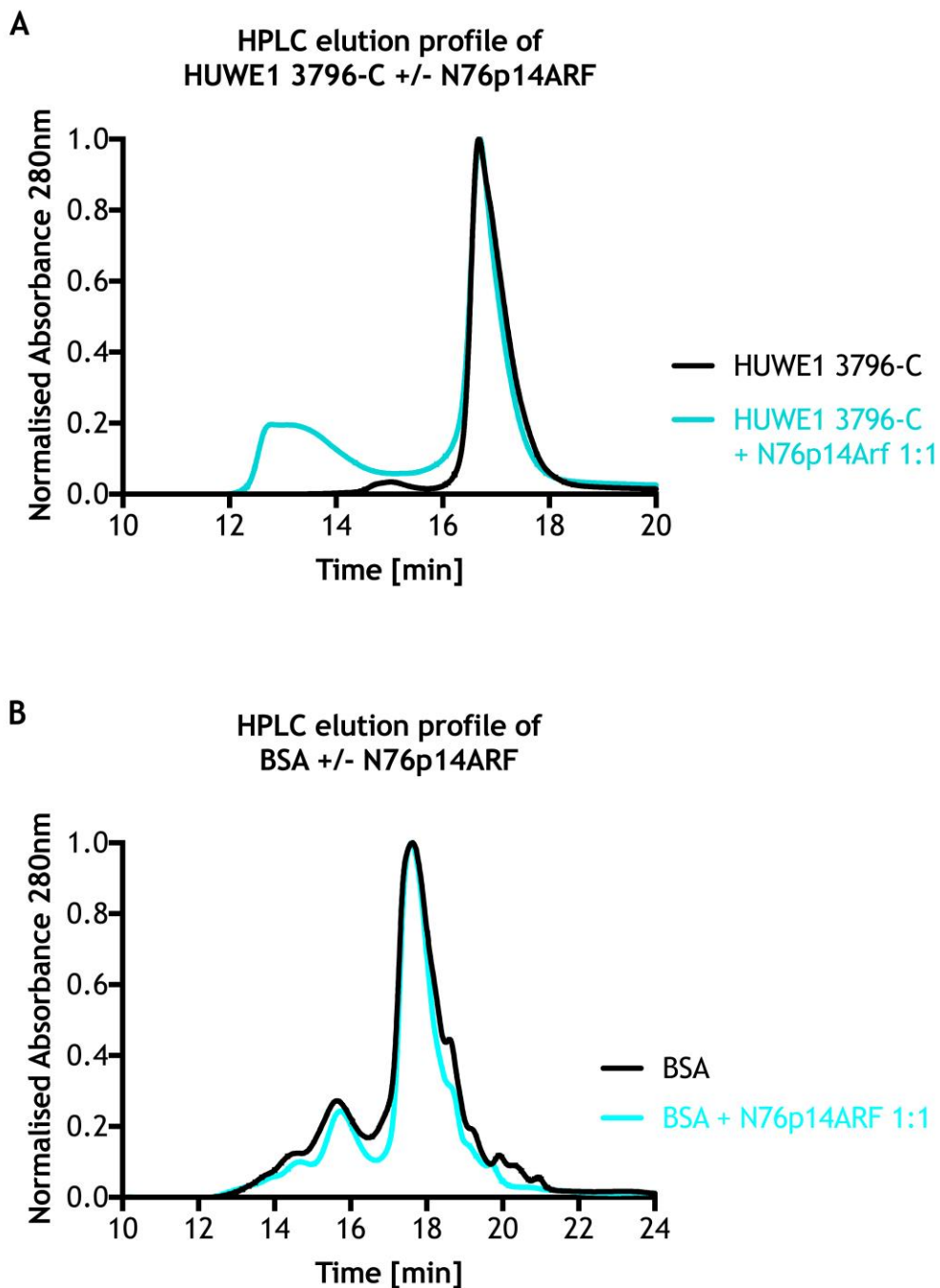


Figure 3.3-27 HPLC elution profiles of HUWE1 3796-C and BSA incubated with a 1:1 molar ratio of N76p14ARF

A- HPLC elution profile of HUWE1 3796-C in the presence of an equimolar amount of N76p14ARF.

B- HPLC elution profile of BSA in the presence an equimolar amount of N76p14ARF.

Samples were loaded onto a Shodex KW-403-4F HPLC column.

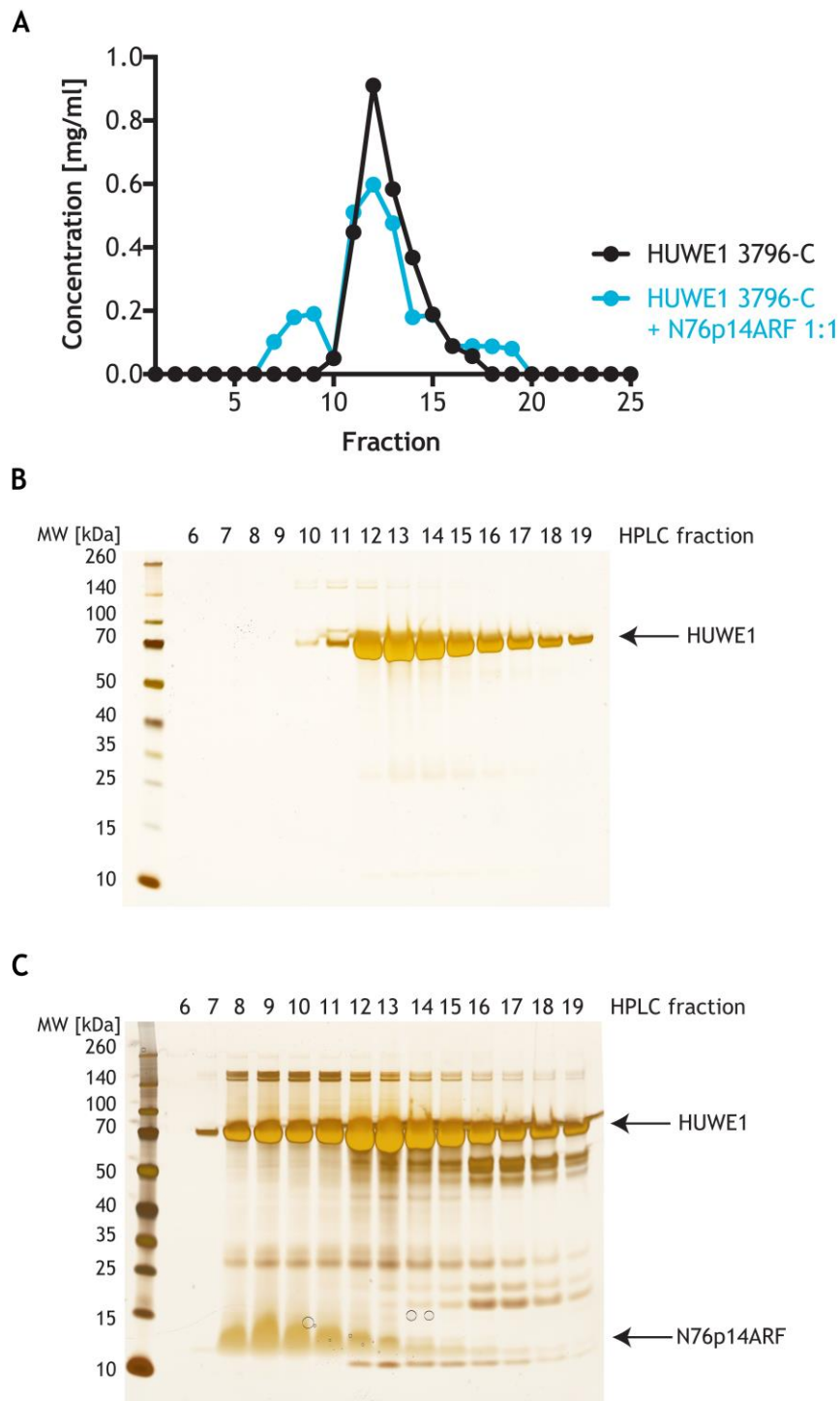


Figure 3.3-28 N76p14ARF coelutes with HUWE1 3796-C in the high-MW peak

A- Protein concentration in each fraction obtained after HPLC analysis of HUWE1 3796-C in the presence and absence of N76p14ARF was measured.

B- SDS-PAGE gel analysis of fractions 6 – 19 obtained after HPLC analysis of HUWE1 3796-C shows that HUWE1 localises predominantly in fractions 12, 13 and 14, which correspond to a sharp peak on the HPLC elution profile.

C- SDS-PAGE gel analysis of fractions 6 – 19 obtained from HPLC of HUWE1 3796-C / N76p14ARF complex shows that upon introduction of the p14ARF peptide, a fraction of HUWE1 elutes earlier (fractions 8 – 11) together with N76p14ARF.

3.3.10 Discussion

In conclusion, I have shown that p14ARF can bind HUWE1. This interaction results in the formation of high-MW species of HUWE1. However, the oligomerisation event does not influence the catalytic activity of the HECT E3 ligase.

Initially, I attempted GST-HUWE1/His-MBP-N56p14ARF double pull-down experiments but these were inconclusive in determining the sequence of HUWE1 responsible for p14ARF binding. For this reason, I used N37p14ARF peptide to investigate binding to two HUWE1 constructs encompassing residues 3796-C and 3900-C. Little or no precipitation was observed when the peptide was titrated into the longer construct, but HUWE1 3900-C showed noticeable precipitation in the presence of a 2 molar excess of ARF peptide. Because HUWE1 3796-C could “withstand” higher concentrations of N37p14ARF compared with HUWE1 3900-C, I was able to use a fluorescence polarisation assay to determine the binding affinity between HUWE1 3796-C and FAM-N37p14ARF peptide. FAM-N37p14ARF peptide binds to HUWE1 3796-C with a K_d of 1 μ M. The HPLC analysis of the HUWE1/N37p14ARF peptide sample, obtained after removal of any precipitant from the solution, showed that N37p14ARF peptide induces oligomerisation of HUWE1 3796-C. At the same time, no change in the elution profile of HUWE1 3900-C was observed. The heterogeneous nature of the oligomeric peak of HUWE1 3796-C obtained after introduction of N37p14ARF peptide was further confirmed using SAXS. Protein oligomers were characterised by D_{max} values ranging from 239 Å to 441 Å and R_g values ranging from 70 Å to 117 Å after introduction of N37p14ARF peptide. For comparison, HUWE1 3796-C alone is characterised by D_{max} and R_g values of 141 Å and 35 Å, respectively. However, no change in the size of HUWE1 3900-C was observed after introduction of N37p14ARF peptide, where D_{max} (111 Å) and R_g (35 Å) remained constant. Although N37p14ARF peptide binds HUWE1 3796-C and induces extensive oligomerisation, I saw no inhibition of HUWE1 3796-C catalytic activity in the presence of the peptide. Single-turnover auto-ubiquitination assays showed that the potency of HUWE1 3796-C towards discharge of Ub_{CH5B}-Ub or Ub_{CH7}-Ub is not affected by the presence of N37p14ARF peptide. However, higher-order poly-Ub chains are generated at later time points upon introduction of the peptide. The change in the ubiquitination pattern and formation of a “smear”

could be a result of HUWE1 3796-C undergoing conformational changes or oligomerisation, which may influence the number and positioning of accessible lysine residues.

I set up extensive crystallisation screens with different HUWE1 variants in the presence and absence of N37p14ARF peptide to attempt to elucidate how the two form a complex. Only HUWE1 3900-C alone produced crystals, which diffracted to ~ 3 Å resolution after optimisation. There were two copies of HUWE1 3900-C in the asymmetric unit, which formed an asymmetrical dimer. My HUWE1 3900-C structure revealed positions of 41 amino acids compared with the structure of HUWE1 3993-C previously published in 2010 by Pandya et al. These residues form α -helices that comprise the dimer interface - the N-terminal α -helix of one molecule (molecule B) faces away from the HECT domain and points towards the C-lobe of the other molecule (molecule A) (Pandya *et al.*, 2010). The interface between molecule A and B is stabilised by hydrophobic interactions. Shortly after I obtained my HUWE1 structure, Sander et al. published a nearly identical structure of HUWE1 3951-C, proposing that the observed HUWE1 dimer is a biologically relevant, auto-inhibited state of HUWE1 (Sander *et al.*, 2017). Using size exclusion chromatography, they showed that HUWE1 3951-C dimerisation can be prevented by substituting two residues - Phe-3982 and Ile-3969 - to alanine. They showed that the F3982A and I3969A variants of HUWE1 exhibit higher activity in *in vitro* auto-ubiquitination assays, as well as in *in vivo* substrate ubiquitination assays, compared to wild-type protein. They further propose that residues 3843-3896 of HUWE1 form an activation segment that prevents the HUWE1 dimer formation, thereby increasing its catalytic activity. Using size exclusion chromatography, they showed that HUWE1 constructs containing the activation segment elute at a volume consistent in MW with a monomer. Furthermore, they showed that these constructs of HUWE1 exhibit higher activity towards substrate ubiquitination *in vivo* compared with HUWE1 constructs lacking the activation segment. Finally, Sander et al. proposed that p14ARF peptide, comprising residues 45-75 (45-75p14ARF), can bind the activation segment of HUWE1, thereby locking the protein in an auto-inhibited state (Sander *et al.*, 2017).

My HUWE1 3796-C contains the activation segment sequence, whereas HUWE1 3900-C does not. HUWE1 3900-C (55 kDa) was characterised by an earlier elution from the HPLC column than HUWE1 3796-C (67 kDa), which suggests that it is forming a bigger complex in solution when compared with HUWE1 3796-C. Dimerisation of HUWE1 3900-C was also confirmed by a SAXS-derived *ab initio* model, which superimposed on the X-ray structure of the protein. The F3982A and I3969A mutants of HUWE1 3900-C showed a significant shift on the HPLC elution profile compared with WT HUWE1 3900-C consistent with disruption of the dimer interface. However, I did not observe a difference in HUWE1 3900-C catalytic activity upon disruption of the dimer, where each of the HUWE1 3900-C variants showed comparable potency in E2~Ub discharge and poly-Ub chain formation. Similarly, there was no difference in activity when I investigated the rate of E2~Ub discharge catalysed by HUWE1 3796-C and HUWE1 3900-C. To validate whether the N37p14ARF peptide I used is simply lacking the inhibitory sequence, we purchased different p14ARF peptides (36-55p14ARF, 45-64p14ARF and N76p14ARF) and investigated their effect on HUWE1 3796-C. None of these p14ARF peptides influenced the overall catalytic activity of HUWE1 3796-C in single-turnover auto-ubiquitination assays. Sander et al. investigated the effect of 45-75p14ARF peptide on different constructs of HUWE1 using ubiquitination assays and detecting Ub with Western blots (Figure 3.3-29). Sander et al. used as much as a 15-fold excess of p14ARF peptide. At most, I used a molar excess of 6-fold; hence, the quantity of peptide may not have been sufficient to trigger an inhibitory effect on HUWE1 3796-C. Unfortunately, higher concentrations of p14ARF peptides resulted in precipitation of HUWE1 in my hands. Notably, Figure 3.3-29 shows that even at 15-fold excess 45-75p14ARF moderately inhibited HUWE1 constructs.

In summary, I have shown that even though N37p14ARF binds HUWE1 3796-C with low- μ M affinity, it does not influence the catalytic activity of the HECT domain. Moreover, HUWE1 3900-C dimerises in solution and this event is driven by hydrophobic interactions between N-terminal residues of the subunits. In contrast to the literature, my results suggest that this is not an auto-inhibitory mechanism. It is possible that the HUWE1 3900-C dimer is the most energetically stable conformation of this fragment of HUWE1, whereas introduction of additional N-terminal residues drives HUWE1 towards a monomeric state. The

importance of the activation segment is questionable in light of the fact that all of the HUWE1 constructs described here encompass only the C-terminal part of the full-length protein; we cannot anticipate how the remaining ~3760 residues of HUWE1 influence its structure and activity.

I believe that we still did not unequivocally confirm that p14ARF is able to influence HUWE1 catalytic activity. For this reason, in the near future I want to generate BH3-containing constructs of HUWE1, together with various forms of p14ARF that can be used in *in vivo* assays to investigate the influence of p14ARF on HUWE1-driven ubiquitination of MCL-1.

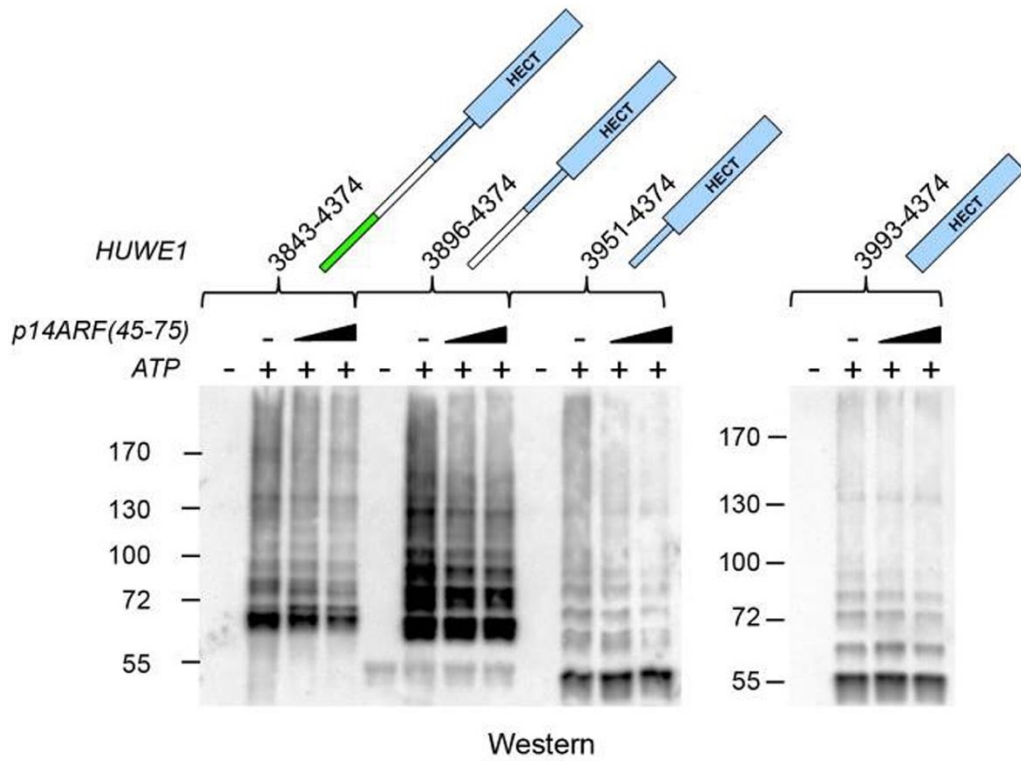


Figure 3.3-29 Figure from Sander *et al.* (2017), showing 45-75p14ARF-driven inhibition of various HUWE1 constructs

Auto-ubiquitination assays were conducted with 45-75p14ARF at 15 and 75 μ M concentration, and 100 nM E1, 3 μ M UbcH7, 5 μ M HUWE1, 100 μ M Ub, 3 mM ATP, and 8 mM $MgCl_2$. Reactions were performed in 25 mM HEPES, pH 7.7 at 37 $^{\circ}$ C for 15 min. Schematic diagrams of HUWE1 fragments are shown on top in which the activation segment is coloured green and the HECT domain and inhibitory α -helix, are coloured blue.

4 CONCLUDING REMARKS

E3 ligases are challenging drug targets owing to a highly conserved Ub transfer mechanism and similarities in the E3-E2-Ub interactions. As a result, lack of specificity and off-target toxicity are two of the biggest challenges to the development of new inhibitors. During my PhD, I have learnt that p14ARF shows remarkable specificity towards inhibition of MDM2. Even the MDM2/MDM4 heterodimer, which structurally and mechanistically resembles the MDM2 homodimer, is not affected by p14ARF. This result shows that direct and specific inhibition of E3 ligases with small peptides is possible and is a mechanism employed by cells.

Studies on the mechanism of p14ARF-induced inhibition of RING and HECT ligases were challenging, due to extensive oligomerisation of MDM2/p14ARF and HUWE1/p14ARF complexes. Although addition of p14ARF peptide led to a formation of higher-MW species of both MDM2 and HUWE1, p14ARF affects RING and HECT E3 ligases differently. Even though we do not know whether p14ARF influences MDM2 activity by directly interacting with the RING domain, or by inducing formation of higher-order oligomers, the presence of p14ARF resulted in decreased catalytic potency of MDM2 towards UbCH5B-Ub discharge. Based on these results, we used a phage display assay to identify novel peptide sequences that specifically interact with the MDM2 homodimer or the MDM2/MDM4 heterodimer and modulate their E3 ligase activity. This effect would resemble the action of p14ARF in cells and could be used to design MDM2-specific peptidomimetics, thereby broadening our capabilities in targeting MDM2 in the context of WT p53 environment.

There are two reports that show that p14ARF directly influences the activity of HUWE1 but more extensive research needs to be conducted in order to verify whether p14ARF can indeed inhibit a HECT E3 ligase. My results are in contradiction to the findings published by Sonja Lorenz's group. These contradictory findings suggest that our current understanding of the activity and mechanism of HUWE1 enzyme is incomplete. *In vitro* studies of HUWE1 focus on the C-terminal end of the protein due to the extraordinarily large size of the protein. In my opinion, cell-based assays could provide a more comprehensive approach towards assessing if and how p14ARF interacts with HUWE1. Strong

emphasis should be put on investigating a HUWE1 construct that can interact with its binding partners (such as MCL) and promote their degradation. My work shows that p14ARF-driven oligomerisation of HUWE1 did not affect its ligase activity, but influenced the number and positioning of accessible lysine residues, which resulted in the change of HUWE1 auto-ubiquitination pattern. It is possible that p14ARF affects HUWE1 catalytic activity by spatially rearranging the HECT and substrate binding domains, which could influence HUWE1 substrate ubiquitination potency.

The presence of heterogeneous mixtures of higher-order oligomers and poor solubility dramatically impeded studies owing to a lack of suitable quantities of a homogeneous sample for crystallisation trials. As a result, implementation of different structural techniques, such as cryo-electron microscopy, might be more suitable for studying MDM2/p14ARF and HUWE1/p14ARF complexes.

Protein oligomerisation and aggregation have been widely associated with the development of a range of pathologies, such as Alzheimer's disease, Parkinson's disease, type II diabetes and various types of cancers (Chiti and Dobson, 2006; Invernizzi *et al.*, 2012). On the other hand, a number of reports suggest that protein aggregation can also be employed for beneficial purposes, for example during programmed necrosis, storage of secretory peptides or the formation of stress granules (Gilks, 2004; Maji *et al.*, 2009; Li *et al.*, 2012). Proteins with regions that primarily contain aliphatic or hydrophobic residues (valine, leucine, isoleucine, phenylalanine, tyrosine and tryptophan), or are characterised by an alternating sequence of charged and non-polar amino acids, have been recognised to be aggregation-prone (Broome and Hecht, 2000; Monsellier *et al.*, 2008). Yet these features are used during protein folding to establish hydrophobic cores (Rousseau, Serrano and Schymkowitz, 2006; Hartl, Bracher and Hayer-Hartl, 2011). This dual nature creates a fine balance between protein folding and aggregation. Interestingly, these aggregation-prone regions are also frequently involved in the formation of a ternary complex (Castillo and Ventura, 2009; Pechmann *et al.*, 2009). MDM2 (acidic domain), HUWE1 (activation segment) and p14ARF contain regions that are characterised by an alternating sequence of charged and aliphatic residues and have been reported to be indispensable for complex formation. Whether oligomerisation of MDM2 and

HUWE1 in the presence of p14ARF peptide is a biologically relevant phenomenon is unknown. Protein aggregation has been shown to be highly dependent on concentration, and it is possible that the p14ARF-driven formation of higher-order oligomers of MDM2 and HUWE1 is an artefact resulting from studying complexes at concentrations exceeding biological levels (Pappu *et al.*, 2008; Cohen *et al.*, 2012). Moreover, studying proteins *in vitro*, in the absence of the natural cell environment, can decrease the stability of a protein's "native" state and drive it towards more energetically favourable, aggregated or oligomerised states (Jahn and Radford, 2008). Cells employ various mechanisms to prevent protein aggregation, including but not limited to the following: they employ chaperones, which may protect aggregation-prone segments of a protein or use specific compartments during protein production to ensure that protein is held within a certain environment and possible complex formation is regulated by the cell (Gershenson and Gierasch, 2011; Hartl, Bracher and Hayer-Hartl, 2011; Pastore and Temussi, 2012).

To decipher how p14ARF influences the activity of MDM2 and possibly HUWE1, efforts need to be made to develop an approach which will allow us to study these complexes *in vivo*. Some of the techniques that could be implemented for this purpose include transmission electron microscopy (TEM) and Förster resonance energy transfer (FRET) (Gershenson and Gierasch, 2011; Miyazaki *et al.*, 2016).

List of References

Abida, W. M. and Gu, W. (2008) 'p53-dependent and p53-independent activation of autophagy by ARF', *Cancer Research*. NIH Public Access, 68(2), pp. 352-357. doi: 10.1158/0008-5472.CAN-07-2069.

Adams, P. D. *et al.* (2010) 'PHENIX: A comprehensive Python-based system for macromolecular structure solution', *Acta Crystallographica Section D: Biological Crystallography*. International Union of Crystallography, 66(2), pp. 213-221. doi: 10.1107/S09074444909052925.

Adhikary, S. *et al.* (2005) 'The ubiquitin ligase HectH9 regulates transcriptional activation by Myc and is essential for tumor cell proliferation', *Cell*, 123(3), pp. 409-421. doi: 10.1016/j.cell.2005.08.016.

Allende-Vega, N. *et al.* (2005) 'Phosphorylation of the acidic domain of Mdm2 by protein kinase CK2', *Molecular and Cellular Biochemistry*, 274(1-2), pp. 85-90. doi: 10.1007/s11010-005-3074-4.

Alt, J. R. *et al.* (2003) 'Mdm2 haplo-insufficiency profoundly inhibits Myc-induced lymphomagenesis', *EMBO Journal*. European Molecular Biology Organization, 22(6), pp. 1442-1450. doi: 10.1093/emboj/cdg133.

Andreeff, M. *et al.* (2016) 'Results of the phase I trial of RG7112, a small-molecule MDM2 antagonist in leukemia', *Clinical Cancer Research*, 22(4), pp. 868-876. doi: 10.1158/1078-0432.CCR-15-0481.

Appella, E. and Anderson, C. W. (2001) 'Post-translational modifications and activation of p53 by genotoxic stresses', *European Journal of Biochemistry*, 268(10), pp. 2764-2772. doi: 10.1046/j.1432-1327.2001.02225.x.

Araki, S. *et al.* (2010) 'TGF- β 1-induced expression of human Mdm2 correlates with late-stage metastatic breast cancer', *Journal of Clinical Investigation*, 120(1), pp. 290-302. doi: 10.1172/JCI39194.

Argentini, M., Barboule, N. and Wasyluk, B. (2000) 'The contribution of the RING

- finger domain of MDM2 to cell cycle progression', *Oncogene*. Nature Publishing Group, 19(34), pp. 3849-3857. doi: 10.1038/sj.onc.1203737.
- Arita, Y. *et al.* (2016) 'Rapid isolation of peptidic inhibitors of the solute carrier family transporters OATP1B1 and OATP1B3 by cell-based phage display selections', *Biochemical and Biophysical Research Communications*, 473(2), pp. 370-376. doi: 10.1016/j.bbrc.2016.01.050.
- Atsumi, Y. *et al.* (2015) 'ATM and SIRT6/SNF2H Mediate Transient H2AX Stabilization When DSBs Form by Blocking HUWE1 to Allow Efficient γ H2AX Foci Formation', *Cell Reports*, 13(12), pp. 2728-2740. doi: 10.1016/j.celrep.2015.11.054.
- Badciong, J. C. and Haas, A. L. (2002) 'MdmX is a RING finger ubiquitin ligase capable of synergistically enhancing Mdm2 ubiquitination', *Journal of Biological Chemistry*. American Society for Biochemistry and Molecular Biology, 277(51), pp. 49668-49675. doi: 10.1074/jbc.M208593200.
- Bae, B. Il *et al.* (2005) 'p53 mediates cellular dysfunction and behavioral abnormalities in Huntington's disease', *Neuron*, 47(1), pp. 29-41. doi: 10.1016/j.neuron.2005.06.005.
- Bagiyan, G. A. *et al.* (2003) 'Oxidation of thiol compounds by molecular oxygen in aqueous solutions', *Russian Chemical Bulletin*. Kluwer Academic Publishers-Plenum Publishers, 52(5), pp. 1135-1141. doi: 10.1023/A:1024761324710.
- Baldwin, R. L. (1996) 'How Hofmeister ion interactions affect protein stability', *Biophysical Journal*. The Biophysical Society, 71(4), pp. 2056-2063. doi: 10.1016/S0006-3495(96)79404-3.
- Barak, Y. *et al.* (1993) 'Mdm2 Expression Is Induced By Wild Type P53 Activity', *The EMBO journal*. European Molecular Biology Organization, 12(2), pp. 461-8. Available at: <http://www.ncbi.nlm.nih.gov/pubmed/8440237> (Accessed: 27 April 2018).
- Barak, Y. *et al.* (1994) 'Regulation of mdm2 expression by p53: Alternative

promoters produce transcripts with nonidentical translation potential', *Genes and Development*, 8(15), pp. 1739-1749. doi: 10.1101/gad.8.15.1739.

Barlow, P. N. *et al.* (1994) 'Structure of the C3HC4 domain by ¹H-nuclear magnetic resonance spectroscopy: A new structural class of zinc-finger', *Journal of Molecular Biology*, 237(2), pp. 201-211. doi: 10.1006/jmbi.1994.1222.

Bateman, A. *et al.* (2017) 'UniProt: The universal protein knowledgebase', *Nucleic Acids Research*. Oxford University Press, 45(D1), pp. D158-D169. doi: 10.1093/nar/gkw1099.

Ben-Saadon, R. *et al.* (2006) 'The Polycomb Protein Ring1B Generates Self Atypical Mixed Ubiquitin Chains Required for Its In Vitro Histone H2A Ligase Activity', *Molecular Cell*, 24(5), pp. 701-711. doi: 10.1016/j.molcel.2006.10.022.

Bennion, B. J. and Daggett, V. (2003) 'The molecular basis for the chemical denaturation of proteins by urea', *Proceedings of the National Academy of Sciences*. National Academy of Sciences, 100(9), pp. 5142-5147. doi: 10.1073/pnas.0930122100.

De Bernardez Clark, E. (1998) 'Refolding of recombinant proteins', *Current Opinion in Biotechnology*, pp. 157-163. doi: 10.1016/S0958-1669(98)80109-2.

Bertwistle, D., Sugimoto, M. and Sherr, C. J. (2004) 'Physical and Functional Interactions of the Arf Tumor Suppressor Protein with Nucleophosmin/B23', *Molecular and Cellular Biology*. American Society for Microbiology, 24(3), pp. 985-996. doi: 10.1128/MCB.24.3.985-996.2004.

den Besten, W. *et al.* (2005) 'Myeloid leukemia-associated nucleophosmin mutants perturb p53-dependent and independent activities of the Arf tumor suppressor protein', *Cell cycle (Georgetown, Tex.)*, 4(11), pp. 1593-1598. doi: 2174 [pii].

Bioisis: welcome - index (no date). Available at:

<http://www.bioisis.net/welcome> (Accessed: 16 July 2018).

- Blattner, C. *et al.* (2002) 'Hypophosphorylation of Mdm2 Augments p53 Stability', *MOLECULAR AND CELLULAR BIOLOGY*, 22(17), pp. 6170-6182. doi: 10.1128/MCB.22.17.6170-6182.2002.
- Boehme, K. A., Kulikov, R. and Blattner, C. (2008) 'p53 stabilization in response to DNA damage requires Akt/PKB and DNA-PK', *Proceedings of the National Academy of Sciences*, 105(22), pp. 7785-7790. doi: 10.1073/pnas.0703423105.
- Bond, G. L. and Levine, A. J. (2007) 'A single nucleotide polymorphism in the p53 pathway interacts with gender, environmental stresses and tumor genetics to influence cancer in humans', *Oncogene*. Nature Publishing Group, 26(9), pp. 1317-1323. doi: 10.1038/sj.onc.1210199.
- Bondos, S. E. and Bicknell, A. (2003) 'Detection and prevention of protein aggregation before, during, and after purification.', *Analytical biochemistry*, 316(2), pp. 223-31. Available at: <http://www.ncbi.nlm.nih.gov/pubmed/12711344> (Accessed: 9 August 2018).
- Borden, K. L. *et al.* (1995) 'The solution structure of the RING finger domain from the acute promyelocytic leukaemia proto-oncoprotein PML', *The EMBO journal*, 14(7), pp. 1532-1541. Available at: <http://www.ncbi.nlm.nih.gov/pubmed/7729428> (Accessed: 12 April 2018).
- Borer, R. A. *et al.* (1989) 'Major nucleolar proteins shuttle between nucleus and cytoplasm', *Cell*, 56(3), pp. 379-390. doi: 10.1016/0092-8674(89)90241-9.
- Bornstein, G., Ganoth, D. and Hershko, A. (2006) 'Regulation of neddylation and deneddylation of cullin1 in SCFSkp2 ubiquitin ligase by F-box protein and substrate', *Proceedings of the National Academy of Sciences*, 103(31), pp. 11515-11520. doi: 10.1073/pnas.0603921103.
- Bothner, B. *et al.* (2001) 'Defining the molecular basis of Arf and Hdm2 interactions', *Journal of Molecular Biology*. Academic Press, 314(2), pp. 263-277. doi: 10.1006/jmbi.2001.5110.
- Bourdon, J. (2014) 'p53 isoforms change p53 paradigm', *Molecular & Cellular*

Oncology. Taylor & Francis, 1(4), pp. 1-2. doi: 10.4161/23723548.2014.969136.

Bradford, M. M. (1976) 'A rapid and sensitive method for the quantitation of microgram quantities of protein utilizing the principle of protein-dye binding', *Analytical Biochemistry*. Academic Press, 72(1-2), pp. 248-254. doi: 10.1016/0003-2697(76)90527-3.

Breitaud, S. *et al.* (2007) 'p53-dependent neuronal cell death in a DJ-1-deficient zebrafish model of Parkinson's disease', *Journal of Neurochemistry*, 100(6), pp. 1626-1635. doi: 10.1111/j.1471-4159.2006.04291.x.

Broome, B. M. and Hecht, M. H. (2000) 'Nature disfavors sequences of alternating polar and non-polar amino acids: Implications for amyloidogenesis', *Journal of Molecular Biology*, 296(4), pp. 961-968. doi: 10.1006/jmbi.2000.3514.

Brown, C. J. *et al.* (2008) 'The electrostatic surface of MDM2 modulates the specificity of its interaction with phosphorylated and unphosphorylated p53 peptides', *Cell Cycle*, 7(5), pp. 608-610. doi: 10.4161/cc.7.5.5488.

Brzovic, P. S. *et al.* (2003) 'Binding and recognition in the assembly of an active BRCA1/BARD1 ubiquitin-ligase complex', *Proceedings of the National Academy of Sciences*, 100(10), pp. 5646-5651. doi: 10.1073/pnas.0836054100.

Brzovic, P. S. *et al.* (2006) 'A Ubch5/ubiquitin noncovalent complex is required for processive BRCA1-directed ubiquitination', *Molecular Cell*, 21(6), pp. 873-880. doi: 10.1016/j.molcel.2006.02.008.

Buetow, L. *et al.* (2015) 'Activation of a Primed RING E3-E2-Ubiquitin Complex by Non-Covalent Ubiquitin', *Molecular Cell*, 58(2), pp. 297-310. doi: 10.1016/j.molcel.2015.02.017.

Buetow, L. and Huang, D. T. (2016) 'Structural insights into the catalysis and regulation of E3 ubiquitin ligases', *Nature Reviews Molecular Cell Biology*. Nature Publishing Group, 17(10), pp. 626-642. doi: 10.1038/nrm.2016.91.

Buschmann, T. *et al.* (2000) 'SUMO-1 modification of Mdm2 prevents its self-

ubiquitination and increases Mdm2 ability to ubiquitinate p53', *Cell*, 101(7), pp. 753-762. doi: 10.1016/S0092-8674(00)80887-9.

Busuttil, V. *et al.* (2010) 'NF- κ B inhibits T-cell activation-induced, p73-dependent cell death by induction of MDM2', *Proceedings of the National Academy of Sciences*, 107(42), pp. 18061-18066. doi: 10.1073/pnas.1006163107.

Cabrita, L. D. *et al.* (2007) 'Enhancing the stability and solubility of TEV protease using in silico design', *Protein Science*. Wiley-Blackwell, 16(11), pp. 2360-2367. doi: 10.1110/ps.072822507.

Calabrò, V. *et al.* (2002) 'The human MDM2 oncoprotein increases the transcriptional activity and the protein level of the p53 homolog p63', *Journal of Biological Chemistry*, 277(4), pp. 2674-2681. doi: 10.1074/jbc.M107173200.

Camilloni, C. *et al.* (2008) 'Urea and guanidinium chloride denature protein L in different ways in molecular dynamics simulations', *Biophysical Journal*. The Biophysical Society, 94(12), pp. 4654-4661. doi: 10.1529/biophysj.107.125799.

Candeias, M. M. *et al.* (2008) 'p53 mRNA controls p53 activity by managing Mdm2 functions', *Nature Cell Biology*, 10(9), pp. 1098-1105. doi: 10.1038/ncb1770.

Cappadocia, L. and Lima, C. D. (2018) 'Ubiquitin-like Protein Conjugation: Structures, Chemistry, and Mechanism', *Chemical Reviews*, 118(3), pp. 889-918. doi: 10.1021/acs.chemrev.6b00737.

Carr, S. M., Munro, S. and Thangue, N. B. La (2012) 'Lysine methylation and the regulation of p53', *Essays In Biochemistry*, 52, pp. 79-92. doi: 10.1042/bse0520079.

Castillo, V. and Ventura, S. (2009) 'Amyloidogenic regions and interaction surfaces overlap in globular proteins related to conformational diseases', *PLoS Computational Biology*. Edited by R. Nussinov. Public Library of Science, 5(8), p. e1000476. doi: 10.1371/journal.pcbi.1000476.

Chang, C. J., Freeman, D. J. and Wu, H. (2004) 'PTEN regulates Mdm2

expression through the P1 promoter', *Journal of Biological Chemistry*. American Society for Biochemistry and Molecular Biology, 279(28), pp. 29841-29848. doi: 10.1074/jbc.M401488200.

Checler, F. and Alves Da Costa, C. (2014) 'P53 in neurodegenerative diseases and brain cancers', *Pharmacology and Therapeutics*, 142(1), pp. 99-113. doi: 10.1016/j.pharmthera.2013.11.009.

Checler, F. and Da Costa, C. A. (2014) 'Interplay between parkin and p53 governs a physiological homeostasis that is disrupted in parkinson's disease and cerebral cancer', *Neurodegenerative Diseases*, 13(2-3), pp. 118-121. doi: 10.1159/000354075.

Chen *et al.* (2005) 'ARF-BP1/mule is a critical mediator of the ARF tumor suppressor', *Cell*, 121(7), pp. 1071-1083. doi: 10.1016/j.cell.2005.03.037.

Chen, D. *et al.* (2010) 'Transcription-independent ARF regulation in oncogenic stress-mediated p53 responses', *Nature*. Nature Publishing Group, 464(7288), pp. 624-627. doi: 10.1038/nature08820.

Chen, D. *et al.* (2013) 'Differential effects on ARF stability by normal versus oncogenic levels of c-Myc expression', *Molecular Cell*, 51(1), pp. 46-56. doi: 10.1016/j.molcel.2013.05.006.

Chen, D., Brooks, C. L. and Gu, W. (2006) 'ARF-BP1 as a potential therapeutic target', *British Journal of Cancer*, 94(11), pp. 1555-1558. doi: 10.1038/sj.bjc.6603119.

Chen, D., Yoon, J. B. and Gu, W. (2010) 'Reactivating the ARF-p53 axis in AML cells: By targeting ULF', *Cell Cycle*, 9(15), pp. 2946-2951. doi: 10.4161/cc.9.15.12355.

Chen, L. *et al.* (2005) 'ATM and Chk2-dependent phosphorylation of MDMX contribute to p53 activation after DNA damage', *EMBO Journal*, 24(19), pp. 3411-3422. doi: 10.1038/sj.emboj.7600812.

- Chen, L. and Chen, J. (2003) 'MDM2-ARF complex regulates p53 sumoylation', *Oncogene*. Nature Publishing Group, 22(34), pp. 5348-5357. doi: 10.1038/sj.onc.1206851.
- Chen, V. B. *et al.* (2010) 'MolProbity: All-atom structure validation for macromolecular crystallography', *Acta Crystallographica Section D: Biological Crystallography*, 66(1), pp. 12-21. doi: 10.1107/S0907444909042073.
- Chen, Z. *et al.* (2017) 'A Tunable Brake for HECT Ubiquitin Ligases', *Molecular cell*. Elsevier, 66(3), pp. 345-357. doi: 10.1016/j.molcel.2017.03.020.
- Cheng, Q. *et al.* (2009) 'ATM activates p53 by regulating MDM2 oligomerization and E3 processivity', *EMBO Journal*, 28(24), pp. 3857-3867. doi: 10.1038/emboj.2009.294.
- Cheng, Q. *et al.* (2011) 'Regulation of MDM2 E3 Ligase Activity by Phosphorylation after DNA Damage', *Molecular and Cellular Biology*, 31(24), pp. 4951-4963. doi: 10.1128/MCB.05553-11.
- Cheng, Q. *et al.* (2014) 'Autoactivation of the MDM2 E3 ligase by intramolecular interaction.', *Molecular and cellular biology*. American Society for Microbiology, 34(15), pp. 2800-10. doi: 10.1128/MCB.00246-14.
- Chi, X. Z. *et al.* (2009) 'Runt-related transcription factor RUNX3 is a target of MDM2-mediated ubiquitination', *Cancer Research*, 69(20), pp. 8111-8119. doi: 10.1158/0008-5472.CAN-09-1057.
- Chiti, F. and Dobson, C. M. (2006) 'Protein Misfolding, Functional Amyloid, and Human Disease', *Annual Review of Biochemistry*. Annual Reviews, 75(1), pp. 333-366. doi: 10.1146/annurev.biochem.75.101304.123901.
- Choe, K. N. *et al.* (2016) 'HUWE1 interacts with PCNA to alleviate replication stress', *EMBO reports*, 17(6), pp. 874-886. doi: 10.15252/embr.201541685.
- Christensen, D. E., Brzovic, P. S. and Klevit, R. E. (2007) 'E2-BRCA1 RING interactions dictate synthesis of mono- or specific polyubiquitin chain linkages',

Nature Structural and Molecular Biology, 14(10), pp. 941-948. doi: 10.1038/nsmb1295.

Ciechanover, A., Elias, S. and Heller, H. (1980) 'Characterization of the heatstable polypeptide of the ATP-dependent proteolytic system from reticulocytes', *Journal of Biological Chemistry*, 255(16), pp. 7525-7528. Available at: <http://www.ncbi.nlm.nih.gov/pubmed/6249802> (Accessed: 14 January 2019).

Cocchetti, P. *et al.* (2008) 'The CK2 phosphorylation of catalytic domain of Cdc34 modulates its activity at the G1 to S transition in *Saccharomyces cerevisiae*', *Cell Cycle*, 7(10), pp. 1391-1401. doi: 10.4161/cc.7.10.5825.

Cohen, P. (2002) 'The origins of protein phosphorylation', *Nature Cell Biology*. Nature Publishing Group, 4(5), pp. 127-130. doi: 10.1038/ncb0502-e127.

Cohen, S. I. A. *et al.* (2012) 'From macroscopic measurements to microscopic mechanisms of protein aggregation', *Journal of Molecular Biology*, pp. 160-171. doi: 10.1016/j.jmb.2012.02.031.

Collins, K. D. and Washabaugh, M. W. (1985) 'The Hofmeister effect and the behaviour of water at interfaces', *Quarterly Reviews of Biophysics*, 18(4), pp. 323-422. doi: 10.1017/S0033583500005369.

Colombo, E. *et al.* (2006) 'Delocalization and destabilization of the Arf tumor suppressor by the leukemia-associated NPM mutant', *Cancer Research*. American Association for Cancer Research, 66(6), pp. 3044-3050. doi: 10.1158/0008-5472.CAN-05-2378.

Confalonieri, S. *et al.* (2009) 'Alterations of ubiquitin ligases in human cancer and their association with the natural history of the tumor', *Oncogene*, 28(33), pp. 2959-2968. doi: 10.1038/onc.2009.156.

Cooper, M. A. (2002) 'Optical biosensors in drug discovery', *Nature Reviews Drug Discovery*. Nature Publishing Group, 1(7), pp. 515-528. doi: 10.1038/nrd838.

- Craig, A. L. *et al.* (1999) 'Novel phosphorylation sites of human tumour suppressor protein p53 at Ser20 and Thr18 that disrupt the binding of mdm2 (mouse double minute 2) protein are modified in human cancers.', *The Biochemical journal*, 342(1), pp. 133-141. doi: 10.1042/0264-6021:3420133.
- Crawford, L. and Irvine, A. E. (2016) 'The E3 Ubiquitin Ligase HUWE1 Is a Potential Therapeutic Target for Multiple Myeloma', *Blood*, 128(22), p. 240. Available at: <http://www.bloodjournal.org/content/128/22/240?ssoc-checked=true> (Accessed: 8 May 2018).
- Cross, B. *et al.* (2011) 'Inhibition of p53 DNA binding function by the MDM2 protein acidic domain', *Journal of Biological Chemistry*, 286(18), pp. 16018-16029. doi: 10.1074/jbc.M111.228981.
- Cuconati, A. *et al.* (2003) 'DNA damage response and MCL-1 destruction initiate apoptosis in adenovirus-infected cells', *Genes and Development*, 17(23), pp. 2922-2932. doi: 10.1101/gad.1156903.
- Cummins, J. M. and Vogelstein, B. (2004) 'HAUSP is required for p53 destabilization', *Cell Cycle*, 3(6), pp. 689-692. doi: 10.4161/cc.3.6.924.
- Dagert, M. and Ehrlich, S. D. (1979) 'Prolonged incubation in calcium chloride improves the competence of Escherichia coli cells.', *Gene*, 6(1), pp. 23-8. Available at: <http://www.ncbi.nlm.nih.gov/pubmed/383576> (Accessed: 16 January 2019).
- Daggett, V. and Fersht, A. (2003) 'The present view of the mechanism of protein folding', *Nature Reviews Molecular Cell Biology*, pp. 497-502. doi: 10.1038/nrm1126.
- Dagher, P. C. (2004) 'Apoptosis in ischemic renal injury: Roles of GTP depletion and p53', *Kidney International*, 66(2), pp. 506-509. doi: 10.1111/j.1523-1755.2004.761_7.x.
- Dai, C. and Gu, W. (2010) 'P53 post-translational modification: Deregulated in tumorigenesis', *Trends in Molecular Medicine*, 16(11), pp. 528-536. doi:

10.1016/j.molmed.2010.09.002.

Dai, M.-S. *et al.* (2004) 'Ribosomal Protein L23 Activates p53 by Inhibiting MDM2 Function in Response to Ribosomal Perturbation but Not to Translation Inhibition', *Molecular and Cellular Biology*, 24(17), pp. 7654-7668. doi: 10.1128/MCB.24.17.7654-7668.2004.

Das, U. *et al.* (2007) 'Inhibition of protein aggregation: Supramolecular assemblies of Arginine hold the key', *PLoS ONE*. Edited by S. Rutherford. Public Library of Science, 2(11), p. e1176. doi: 10.1371/journal.pone.0001176.

DeHart, C. J. *et al.* (2014) 'Extensive Post-translational Modification of Active and Inactivated Forms of Endogenous p53', *Molecular & Cellular Proteomics*, 13(1), pp. 1-17. doi: 10.1074/mcp.M113.030254.

Dei Tos, A. P. *et al.* (2000) 'Coordinated expression and amplification of theMDM2,CDK4, andHMGI-C genes in atypical lipomatous tumours', *The Journal of Pathology*, 190(5), pp. 531-536. doi: 10.1002/(SICI)1096-9896(200004)190:5<531::AID-PATH579>3.0.CO;2-W.

DeLeo, A. B. *et al.* (1979) 'Detection of a transformation-related antigen in chemically induced sarcomas and other transformed cells of the mouse', *Proceedings of the National Academy of Sciences of the United States of America*, 76(5), pp. 2420-4. doi: 10.1073/pnas.76.5.2420.

Derouet, M. *et al.* (2004) 'Granulocyte macrophage colony-stimulating factor signaling and proteasome inhibition delay neutrophil apoptosis by increasing the stability of Mcl-1', *Journal of Biological Chemistry*. American Society for Biochemistry and Molecular Biology, 279(26), pp. 26915-26921. doi: 10.1074/jbc.M313875200.

Deshaies, R. J. and Joazeiro, C. A. P. (2009) 'RING Domain E3 Ubiquitin Ligases', *Annual Review of Biochemistry*. Annual Reviews, 78(1), pp. 399-434. doi: 10.1146/annurev.biochem.78.101807.093809.

DiGiammarino, E. L. *et al.* (2001) 'Solution structure of the p53 regulatory

domain of the p19Arf tumor suppressor protein', *Biochemistry*. American Chemical Society, 40(8), pp. 2379-2386. doi: 10.1021/bi0024005.

Dill, K. A. (1990) 'Dominant Forces in Protein Folding', *Biochemistry*. American Chemical Society, 29(31), pp. 7133-7155. doi: 10.1021/bi00483a001.

Dill, K. A. and MacCallum, J. L. (2012) 'The protein-folding problem, 50 years on', *Science*, pp. 1042-1046. doi: 10.1126/science.1219021.

Ding, Q. *et al.* (2013) 'Discovery of RG7388, a potent and selective p53-MDM2 inhibitor in clinical development', *Journal of Medicinal Chemistry*, 56(14), pp. 5979-5983. doi: 10.1021/jm400487c.

Dou, H. *et al.* (2012) 'BIRC7-E2 ubiquitin conjugate structure reveals the mechanism of ubiquitin transfer by a RING dimer', *Nature Structural and Molecular Biology*, 19(9), pp. 876-883. doi: 10.1038/nsmb.2379.

Dou, H. *et al.* (2013) 'Essentiality of a non-RING element in priming donor ubiquitin for catalysis by a monomeric E3', *Nature Structural and Molecular Biology*, 20(8), pp. 982-986. doi: 10.1038/nsmb.2621.

Drozdetskiy, A. *et al.* (2015) 'JPred4: A protein secondary structure prediction server', *Nucleic Acids Research*, 43(W1), pp. W389-W394. doi: 10.1093/nar/gkv332.

Dumaz, N. *et al.* (2001) 'Critical roles for the serine 20, but not the serine 15, phosphorylation site and for the polyproline domain in regulating p53 turnover', *The Biochemical journal*, 359(Pt 2), pp. 459-64. doi: 10.1042/0264-6021:3590459.

Dumaz, N., Milne, D. M. and Meek, D. W. (1999) 'Protein kinase CK1 is a p53-threonine 18 kinase which requires prior phosphorylation of serine 15', *FEBS Letters*, 463(3), pp. 312-316. doi: 10.1016/S0014-5793(99)01647-6.

Dye, B. T. and Schulman, B. A. (2007) 'Structural Mechanisms Underlying Posttranslational Modification by Ubiquitin-Like Proteins', *Annual Review of*

Biophysics and Biomolecular Structure. Annual Reviews, 36(1), pp. 131-150. doi: 10.1146/annurev.biophys.36.040306.132820.

Edwin, F., Valkya Sharma, Y. and Jagannadham, M. V. (2002) 'Stabilization of molten globule state of papain by urea', *Biochemical and Biophysical Research Communications*. Academic Press, 290(5), pp. 1441-1446. doi: 10.1006/bbrc.2002.6368.

Eletr, Z. M. *et al.* (2005) 'E2 conjugating enzymes must disengage from their E1 enzymes before E3-dependent ubiquitin and ubiquitin-like transfer', *Nature Structural and Molecular Biology*, 12(10), pp. 933-934. doi: 10.1038/nsmb984.

Eletr, Z. M. and Kuhlman, B. (2007) 'Sequence Determinants of E2-E6AP Binding Affinity and Specificity', *Journal of Molecular Biology*. Academic Press, 369(2), pp. 419-428. doi: 10.1016/j.jmb.2007.03.026.

Elia, A. E. H. *et al.* (2015) 'Quantitative Proteomic Atlas of Ubiquitination and Acetylation in the DNA Damage Response', *Molecular Cell*. Elsevier, 59(5), pp. 867-881. doi: 10.1016/j.molcel.2015.05.006.

Emmerich, C. H. *et al.* (2013) 'Activation of the canonical IKK complex by K63/M1-linked hybrid ubiquitin chains', *Proceedings of the National Academy of Sciences*. National Academy of Sciences, 110(38), pp. 15247-15252. doi: 10.1073/pnas.1314715110.

Emsley, P. and Cowtan, K. (2004) 'Coot: Model-building tools for molecular graphics', *Acta Crystallographica Section D: Biological Crystallography*, 60(12 I), pp. 2126-2132. doi: 10.1107/S0907444904019158.

Eymin, B. *et al.* (2001) 'Human ARF binds E2F1 and inhibits its transcriptional activity', *Oncogene*, 20(9), pp. 1033-1041. doi: 10.1038/sj.onc.1204220.

Eymin, B. *et al.* (2003) 'p14ARF induces G2 arrest and apoptosis independently of p53 leading to regression of tumours established in nude mice', *Oncogene*, 22(12), pp. 1822-1835. doi: 10.1038/sj.onc.1206303.

Eymin, B. *et al.* (2006) 'p14ARF Activates a Tip60-Dependent and p53-Independent ATM/ATR/CHK Pathway in Response to Genotoxic Stress', *Molecular and Cellular Biology*, 26(11), pp. 4339-4350. doi: 10.1128/MCB.02240-05.

Eymin, B. *et al.* (2006) 'p14ARF triggers G2 arrest through ERK-mediated Cdc25C phosphorylation, ubiquitination and proteasomal degradation', *Cell Cycle*. Taylor & Francis, 5(7), pp. 759-765. doi: 10.4161/cc.5.7.2625.

Fåhraeus, R. and Olivares-Illana, V. (2014) 'MDM2's social network', *Oncogene*, 33(35), pp. 4365-4376. doi: 10.1038/onc.2013.410.

Fang, S. *et al.* (2000) 'Mdm2 is a RING finger-dependent ubiquitin protein ligase for itself and p53', *Journal of Biological Chemistry*, 275(12), pp. 8945-8951. doi: 10.1074/jbc.275.12.8945.

Feigin and Svergun, D. I. (1989) *Structure Analysis by Small-Angle X-Ray and Neutron Scattering*, *Acta Polymerica*. doi: 10.1002/actp.1989.010400317.

Feki, A. and Irminger-Finger, I. (2004) 'Mutational spectrum of p53 mutations in primary breast and ovarian tumors', *Critical Reviews in Oncology/Hematology*, 52(2), pp. 103-116. doi: 10.1016/j.critrevonc.2004.07.002.

Feldman, R. M. R. *et al.* (1997) 'A complex of Cdc4p, Skp1p, and Cdc53p/cullin catalyzes ubiquitination of the phosphorylated CDK inhibitor Sic1p', *Cell*, 91(2), pp. 221-230. doi: 10.1016/S0092-8674(00)80404-3.

Feng, J. *et al.* (2004) 'Stabilization of Mdm2 via decreased ubiquitination is mediated by protein kinase B/Akt-dependent phosphorylation', *Journal of Biological Chemistry*. American Society for Biochemistry and Molecular Biology, 279(34), pp. 35510-35517. doi: 10.1074/jbc.M404936200.

Feng, L. *et al.* (2005) 'Functional Analysis of the Roles of Posttranslational Modifications at the p53 C Terminus in Regulating p53 Stability and Activity', *Molecular and Cellular Biology*, 25(13), pp. 5389-5395. doi: 10.1128/MCB.25.13.5389-5395.2005.

- Feng, Z. and Levine, A. J. (2010) 'The regulation of energy metabolism and the IGF-1/mTOR pathways by the p53 protein', *Trends in Cell Biology*. Elsevier Current Trends, 20(7), pp. 427-434. doi: 10.1016/j.tcb.2010.03.004.
- Franke, D. and Svergun, D. I. (2009) 'DAMMIF, a program for rapid ab-initio shape determination in small-angle scattering', *Journal of Applied Crystallography*. International Union of Crystallography, 42(2), pp. 342-346. doi: 10.1107/S0021889809000338.
- Freeman-Anderson, N. E. *et al.* (2009) 'Expression of the Arf tumor suppressor gene is controlled by Tgf 2 during development', *Development*, 136(12), pp. 2081-2089. doi: 10.1242/dev.033548.
- Freemont, P. S., Hanson, I. M. and Trowsdale, J. (1991) 'A novel gysteine-rich sequence motif', *Cell*, 64(3), pp. 483-484. doi: 10.1016/0092-8674(91)90229-R.
- French, M. E. *et al.* (2017) 'Mechanism of ubiquitin chain synthesis employed by a HECT domain ubiquitin ligase', *Journal of Biological Chemistry*, 292(25), pp. 10398-10413. doi: 10.1074/jbc.M117.789479.
- French, M. E., Kretzmann, B. R. and Hicke, L. (2009) 'Regulation of the RSP5 ubiquitin ligase by an intrinsic ubiquitin-binding site', *Journal of Biological Chemistry*. American Society for Biochemistry and Molecular Biology, 284(18), pp. 12071-12079. doi: 10.1074/jbc.M901106200.
- Gajjar, M. *et al.* (2012) 'The p53 mRNA-Mdm2 interaction controls mdm2 nuclear trafficking and is required for p53 activation following dna damage', *Cancer Cell*, 21(1), pp. 25-35. doi: 10.1016/j.ccr.2011.11.016.
- Gannon, H. S., Woda, B. A. and Jones, S. N. (2012) 'ATM Phosphorylation of Mdm2 Ser394 Regulates the Amplitude and Duration of the DNA Damage Response in Mice', *Cancer Cell*, 21(5), pp. 668-679. doi: 10.1016/j.ccr.2012.04.011.
- Gasteiger, E. *et al.* (2005) 'Protein Identification and Analysis Tools on the ExPASy Server', in *The Proteomics Protocols Handbook*. Totowa, NJ: Humana

Press, pp. 571-607. doi: 10.1385/1-59259-890-0:571.

Gatti, M. *et al.* (2015) 'RNF168 promotes noncanonical K27 ubiquitination to signal DNA damage', *Cell reports*. Elsevier, 10(2), pp. 226-38. doi: 10.1016/j.celrep.2014.12.021.

Gershenson, A. and Gierasch, L. M. (2011) 'Protein folding in the cell: Challenges and progress', *Current Opinion in Structural Biology*, pp. 32-41. doi: 10.1016/j.sbi.2010.11.001.

Geyer, R. K., Yu, Z. K. and Maki, C. G. (2000) 'The MDM2 RING-finger domain is required to promote p53 nuclear export', *Nature Cell Biology*. Nature Publishing Group, 2(9), pp. 569-573. doi: 10.1038/35023507.

Ghosh, M., Weghorst, K. and Berberich, S. J. (2005) 'MdmX inhibits ARF mediated Mdm2 sumoylation', *Cell Cycle*. Taylor & Francis, 4(4), pp. 604-608. doi: 10.4161/cc.4.4.1597.

Gilks, N. (2004) 'Stress Granule Assembly Is Mediated by Prion-like Aggregation of TIA-1', *Molecular Biology of the Cell*, 15(12), pp. 5383-5398. doi: 10.1091/mbc.E04-08-0715.

Goldberg, Z. *et al.* (2002) 'Tyrosine phosphorylation of Mdm2 by c-Abl: Implications for p53 regulation', *EMBO Journal*. European Molecular Biology Organization, 21(14), pp. 3715-3727. doi: 10.1093/emboj/cdf384.

Gorovits, B. M., Seale, J. W. and Horowitz, P. M. (1995) 'Residual Structure in Urea-Denatured Chaperonin GroEL', *Biochemistry*, 34(42), pp. 13928-13933. doi: 10.1021/bi00042a026.

Grice, G. L. *et al.* (2015) 'The proteasome distinguishes between heterotypic and homotypic lysine-11-Linked polyubiquitin chains', *Cell Reports*. Elsevier, 12(4), pp. 545-553. doi: 10.1016/j.celrep.2015.06.061.

Grisendi, S. *et al.* (2006) 'Nucleophosmin and cancer', *Nature Reviews Cancer*. Nature Publishing Group, 6(7), pp. 493-505. doi: 10.1038/nrc1885.

- Guan, Y. *et al.* (2015) 'An equation to estimate the difference between theoretically predicted and SDS PAGE-displayed molecular weights for an acidic peptide', *Scientific Reports*. Nature Publishing Group, 5(1), p. 13370. doi: 10.1038/srep13370.
- Gudkov, A. V. and Komarova, E. A. (2010) 'Pathologies associated with the p53 response', *Cold Spring Harbor perspectives in biology*, 2(7), pp. 1180-1207. doi: 10.1101/cshperspect.a001180.
- Gustafsson, B. *et al.* (2000) 'Cellular expression of MDM2 and p53 in childhood leukemias with poor prognosis', *Medical and Pediatric Oncology*, 34(2), pp. 117-124. doi: 10.1002/(SICI)1096-911X(200002)34:2<117::AID-MPO9>3.0.CO;2-8.
- Haldeman, M. T. *et al.* (1997) 'Structure and function of ubiquitin conjugating enzyme E2-25K: The tail is a core-dependent activity element', *Biochemistry*, 36(34), pp. 10526-10537. doi: 10.1021/bi970750u.
- Hamilton, K. S. *et al.* (2001) 'Structure of a conjugating enzyme-ubiquitin thiolester intermediate reveals a novel role for the ubiquitin tail', *Structure (London, England : 1993)*. Elsevier, 9(10), pp. 897-904. doi: 10.1016/S0969-2126(01)00657-8.
- Hao, B. *et al.* (2007) 'Structure of a Fbw7-Skp1-Cyclin E Complex: Multisite-Phosphorylated Substrate Recognition by SCF Ubiquitin Ligases', *Molecular Cell*, 26(1), pp. 131-143. doi: 10.1016/j.molcel.2007.02.022.
- Hartl, F. U., Bracher, A. and Hayer-Hartl, M. (2011) 'Molecular chaperones in protein folding and proteostasis', *Nature*. Nature Publishing Group, pp. 324-332. doi: 10.1038/nature10317.
- Hashizume, R. *et al.* (2001) 'The RING heterodimer BRCA1-BARD1 is a ubiquitin ligase inactivated by a breast cancer-derived mutation', *The Journal of biological chemistry*. American Society for Biochemistry and Molecular Biology, 276(18), pp. 14537-14540. doi: 10.1074/jbc.C000881200.
- He, Y. *et al.* (2014) 'The anaphase-promoting complex/cyclosome is an E3

ubiquitin ligase for Mdm2', *Cell Cycle*, 13(13), pp. 2101-2109. doi: 10.4161/cc.29106.

Hemmati, P. G. *et al.* (2002) 'Adenovirus-mediated overexpression of p14ARF induces p53 and Bax-independent apoptosis', *Oncogene*. Nature Publishing Group, 21(20), pp. 3149-3161. doi: 10.1038/sj/onc/1205458.

Hershko, A. *et al.* (1982) 'Immunochemical analysis of the turnover of ubiquitin-protein conjugates in intact cells. Relationship to the breakdown of abnormal proteins.', *Journal of Biological Chemistry*, 257(23), pp. 13964-13970. doi: 10.2307/203669.

Hershko, A. *et al.* (1983) 'Components of ubiquitin-protein ligase system. Resolution, affinity purification, and role in protein breakdown.', *Journal of Biological Chemistry*, 258(13), pp. 8206-8214. doi: papers2://publication/uuid/C82E58FF-33C7-42BF-BC20-CDD10219EC6E.

Highbarger, L. A., Gerlt, J. A. and Kenyon, G. L. (1996) 'Mechanism of the Reaction Catalyzed by Acetoacetate Decarboxylase. Importance of Lysine 116 in Determining the pK_a of Active-Site Lysine 115', *Biochemistry*. American Chemical Society, 35(1), pp. 41-46. doi: 10.1021/bi9518306.

Hochstrasser, M. (2009) 'Origin and function of ubiquitin-like proteins', *Nature*, 458(7237), pp. 422-429. doi: 10.1038/nature07958.

Hornbeck, P. V *et al.* (2012) 'PhosphoSitePlus: A comprehensive resource for investigating the structure and function of experimentally determined post-translational modifications in man and mouse', *Nucleic Acids Research*. Oxford University Press, 40(D1), pp. D261-70. doi: 10.1093/nar/gkr1122.

Hu, W., Feng, Z. and Levine, A. J. (2012) 'The Regulation of Multiple p53 Stress Responses is Mediated through MDM2', *Genes and Cancer*, 3(3-4), pp. 199-208. doi: 10.1177/1947601912454734.

Huang, D. T. *et al.* (2007) 'Basis for a ubiquitin-like protein thioester switch toggling E1-E2 affinity', *Nature*, 445(7126), pp. 394-398. doi:

10.1038/nature05490.

Huang, L. *et al.* (1999) 'Structure of an E6AP-UbcH7 complex: Insights into ubiquitination by the E2-E3 enzyme cascade', *Science*. American Association for the Advancement of Science, 286(5443), pp. 1321-1326. doi: 10.1126/science.286.5443.1321.

Huibregtse, J. M. *et al.* (1995) 'A family of proteins structurally and functionally related to the E6-AP ubiquitin-protein ligase', *Proceedings of the National Academy of Sciences*, 92(7), pp. 2563-2567. doi: 10.1073/pnas.92.7.2563.

Hyoung, T. K. *et al.* (2007) 'Certain pairs of ubiquitin-conjugating enzymes (E2s) and ubiquitin-protein ligases (E3s) synthesize nondegradable forked ubiquitin chains containing all possible isopeptide linkages', *Journal of Biological Chemistry*, 282(24), pp. 17375-17386. doi: 10.1074/jbc.M609659200.

Illuzzi, J. *et al.* (2009) 'DNA breakage and induction of DNA damage response proteins precede the appearance of visible mutant huntingtin aggregates', *Journal of Neuroscience Research*, 87(3), pp. 733-747. doi: 10.1002/jnr.21881.

Inoue, S. *et al.* (2013) 'Mule/Huwe1/Arf-BP1 suppresses Ras-driven tumorigenesis by preventing c-Myc/Miz1-mediated down-regulation of p21 and p15', *Genes and Development*, 27(10), pp. 1101-1114. doi: 10.1101/gad.214577.113.

Inuzuka, H. *et al.* (2010) 'Phosphorylation by Casein Kinase I Promotes the Turnover of the Mdm2 Oncoprotein via the SCFB-TRCP Ubiquitin Ligase', *Cancer Cell*. Cell Press, 18(2), pp. 147-159. doi: 10.1016/J.CCR.2010.06.015.

Invernizzi, G. *et al.* (2012) 'Protein aggregation: Mechanisms and functional consequences', *International Journal of Biochemistry and Cell Biology*. Pergamon, pp. 1541-1554. doi: 10.1016/j.biocel.2012.05.023.

Iqbal, N. S. *et al.* (2014) 'Isolation and characterization of mammalian cells expressing the Arf promoter during eye development', *BioTechniques*. NIH Public Access, 56(5), pp. 239-249. doi: 10.2144/000114166.

- Itahana, K. *et al.* (2007) 'Targeted Inactivation of Mdm2 RING Finger E3 Ubiquitin Ligase Activity in the Mouse Reveals Mechanistic Insights into p53 Regulation', *Cancer Cell*, 12(4), pp. 355-366. doi: 10.1016/j.ccr.2007.09.007.
- Jabbur, J. R. and Zhang, W. (2002) 'p53 antiproliferative function is enhanced by aspartate substitution at threonine 18 and serine 20', *Cancer Biology and Therapy*, 1(3), pp. 277-283. doi: 10.4161/cbt.81.
- Jackson, M. W. and Berberich, S. J. (2000) 'MdmX protects p53 from Mdm2-mediated degradation', *Molecular and cellular biology*, 20(3), pp. 1001-1007. doi: 10.1128/MCB.20.3.1001-1007.2000.
- Jackson, M. W., Lindström, M. S. and Berberich, S. J. (2001) 'MdmX Binding to ARF Affects Mdm2 Protein Stability and p53 Transactivation', *Journal of Biological Chemistry*, 276(27), pp. 25336-25341. doi: 10.1074/jbc.M010685200.
- Jahn, T. R. and Radford, S. E. (2008) 'Folding versus aggregation: Polypeptide conformations on competing pathways', *Archives of Biochemistry and Biophysics*. Academic Press, pp. 100-117. doi: 10.1016/j.abb.2007.05.015.
- Jenkins, L. M. M. *et al.* (2012) 'p53 N-terminal phosphorylation: A defining layer of complex regulation', *Carcinogenesis*, 33(8), pp. 1441-1449. doi: 10.1093/carcin/bgs145.
- Jin, L. *et al.* (2008) 'Mechanism of Ubiquitin-Chain Formation by the Human Anaphase-Promoting Complex', *Cell*, 133(4), pp. 653-665. doi: 10.1016/j.cell.2008.04.012.
- Jones, S. N. *et al.* (1995) 'Rescue of embryonic lethality in Mdm2-deficient mice by absence of p53', *Nature*, 378(6553), pp. 206-208. doi: 10.1038/378206a0.
- Kachala, M., Valentini, E. and Svergun, D. I. (2015) 'Application of SAXS for the Structural Characterization of IDPs', in. Springer, Cham, pp. 261-289. doi: 10.1007/978-3-319-20164-1_8.
- Kamadurai, H. B. *et al.* (2009) 'Insights into Ubiquitin Transfer Cascades from a

Structure of a Ubch5B~Ubiquitin-HECT NEDD4L Complex', *Molecular Cell*. Elsevier, 36(6), pp. 1095-1102. doi: 10.1016/j.molcel.2009.11.010.

Kamadurai, H. B. *et al.* (2013) 'Mechanism of ubiquitin ligation and lysine prioritization by a HECT E3', *eLife*. eLife Sciences Publications, Ltd, 2013(2), pp. 1-26. doi: 10.7554/eLife.00828.001.

Kamijo, T. *et al.* (1997) 'Tumor Suppression at the Mouse INK4a Locus Mediated by the Alternative Reading Frame Product p19 ARF', *Cell*, 91(5), pp. 649-659. doi: 10.1016/S0092-8674(00)80452-3.

Kamijo, T. *et al.* (1998) 'Functional and physical interactions of the ARF tumor suppressor with p53 and Mdm2', *Medical Sciences*, 95(14), pp. 8292-8297. doi: 10.1073/pnas.95.14.8292.

Kamijo, T. *et al.* (1999) 'Tumor spectrum in ARF-deficient mice', *Cancer Research*, 59(9), pp. 2217-2222. doi: 10.1158/0008-5472.can-11-1472.

Kar, G. *et al.* (2012) 'Human proteome-scale structural modeling of E2-E3 interactions exploiting interface motifs', *Journal of Proteome Research*. American Chemical Society, 11(2), pp. 1196-1207. doi: 10.1021/pr2009143.

Karplus, M. and Weaver, D. L. (1976) 'Protein-folding dynamics', *Nature*. Nature Publishing Group, 260(5550), pp. 404-406. doi: 10.1038/260404a0.

Kass, E. M. *et al.* (2009) 'Mdm2 and PCAF increase Chk2 ubiquitination and degradation independently of their intrinsic E3 ligase activities', *Cell Cycle*. Taylor & Francis, 8(3), pp. 430-437. doi: 10.4161/cc.8.3.7624.

Kentsis, A., Gordon, R. E. and Borden, K. L. B. (2002) 'Control of biochemical reactions through supramolecular RING domain self-assembly', *Proceedings of the National Academy of Sciences of the United States of America*, 99(24), pp. 15404-15409. doi: 10.1073/pnas.202608799.

Kikhney, A. G. and Svergun, D. I. (2015) 'A practical guide to small angle X-ray scattering (SAXS) of flexible and intrinsically disordered proteins', *FEBS Letters*.

No longer published by Elsevier, 589(19), pp. 2570-2577. doi:
10.1016/J.FEBSLET.2015.08.027.

Kim, H. C. *et al.* (2011) 'Structure and function of a HECT domain ubiquitin-binding site', *EMBO Reports*, 12(4), pp. 334-341. doi: 10.1038/embor.2011.23.

Kim, H. C. and Huibregtse, J. M. (2009) 'Polyubiquitination by HECT E3s and the Determinants of Chain Type Specificity', *Molecular and Cellular Biology*. American Society for Microbiology, 29(12), pp. 3307-3318. doi:
10.1128/MCB.00240-09.

Kirisako, T. *et al.* (2006) 'A ubiquitin ligase complex assembles linear polyubiquitin chains', *The EMBO Journal*, 25(20), pp. 4877-4887. doi:
10.1038/sj.emboj.7601360.

Kirkpatrick, D. S. *et al.* (2006) 'Quantitative analysis of in vitro ubiquitinated cyclin B1 reveals complex chain topology', *Nature Cell Biology*. Nature Publishing Group, 8(7), pp. 700-710. doi: 10.1038/ncb1436.

Kitagaki, J. *et al.* (2008) 'Targeting tumor cells expressing p53 with a water-soluble inhibitor of Hdm2', *Molecular Cancer Therapeutics*. American Association for Cancer Research, 7(8), pp. 2445-2454. doi: 10.1158/1535-7163.MCT-08-0063.

Komander, D. (2009) 'The emerging complexity of protein ubiquitination', *Biochemical Society transactions*. Portland Press Limited, 37(5), pp. 937-53. doi:
10.1042/BST0370937.

Komander, D. and Rape, M. (2012) 'The Ubiquitin Code', *Annual Review of Biochemistry*, 81(1), pp. 203-229. doi: 10.1146/annurev-biochem-060310-170328.

Korgaonkar, C. *et al.* (2005) 'Nucleophosmin (B23) Targets ARF to Nucleoli and Inhibits Its Function', *Molecular and Cellular Biology*. American Society for Microbiology, 25(4), pp. 1258-1271. doi: 10.1128/MCB.25.4.1258-1271.2005.

Kostic, M. *et al.* (2006) 'Solution Structure of the Hdm2 C2H2C4 RING, a Domain

Critical for Ubiquitination of p53', *Journal of Molecular Biology*, 363(2), pp. 433-450. doi: 10.1016/j.jmb.2006.08.027.

Kozin, M. B. and Svergun, D. I. (2001) 'Automated matching of high- and low-resolution structural models', *Journal of Applied Crystallography*. International Union of Crystallography, 34(1), pp. 33-41. doi: 10.1107/S0021889800014126.

Kozlov, G. *et al.* (2007) 'Structural basis for UBA-mediated dimerization of c-Cbl ubiquitin ligase', *Journal of Biological Chemistry*. American Society for Biochemistry and Molecular Biology, 282(37), pp. 27547-27555. doi: 10.1074/jbc.M703333200.

Kozopas, K. M. *et al.* (1993) 'MCL1, a gene expressed in programmed myeloid cell differentiation, has sequence similarity to BCL2', *Proceedings of the National Academy of Sciences of the United States of America*, 90(8), pp. 3516-20. doi: 10.1073/pnas.90.8.3516.

Krimpenfort, P. *et al.* (2001) 'Loss of p16Ink4a confers susceptibility to metastatic melanoma in mice', *Nature*. Nature Publishing Group, 413(6851), pp. 83-86. doi: 10.1038/35092584.

Krummel, K. A. *et al.* (2005) 'The C-terminal lysines fine-tune P53 stress responses in a mouse model but are not required for stability control or transactivation', *Proceedings of the National Academy of Sciences*, 102(29), pp. 10188-10193. doi: 10.1073/pnas.0503068102.

Kruse, J. P. and Gu, W. (2009) 'Modes of p53 Regulation', *Cell*, 137(4), pp. 609-622. doi: 10.1016/j.cell.2009.04.050.

Kulikov, R., Boehme, K. A. and Blattner, C. (2005) 'Glycogen Synthase Kinase 3-Dependent Phosphorylation of Mdm2 Regulates p53 Abundance', *Molecular and Cellular Biology*, 25(16), pp. 7170-7180. doi: 10.1128/MCB.25.16.7170-7180.2005.

Kulikov, R., Winter, M. and Blattner, C. (2006) 'Binding of p53 to the central domain of Mdm2 is regulated by phosphorylation', *Journal of Biological*

Chemistry, 281(39), pp. 28575-28583. doi: 10.1074/jbc.M513311200.

Kuo, M. L. *et al.* (2004) 'N-terminal polyubiquitination and degradation of the Arf tumor suppressor', *Genes and Development*. Cold Spring Harbor Laboratory Press, 18(15), pp. 1862-1874. doi: 10.1101/gad.1213904.

Kussie, P. H. *et al.* (1996) 'Structure of the MDM2 oncoprotein bound to the p53 tumor suppressor transactivation domain', *Science*. American Association for the Advancement of Science, 274(5289), pp. 948-953. doi: 10.1126/science.274.5289.948.

Lake, M. W. *et al.* (2001) 'Mechanism of ubiquitin activation revealed by the structure of a bacterial MoeB-MoaD complex', *Nature*, 414(6861), pp. 325-329. doi: 10.1038/35104586.

Landers, J. E., Cassel, S. L. and George, D. L. (1997) 'Translational enhancement of mdm2 oncogene expression in human tumor cells containing a stabilized wild-type p53 protein', *Cancer research*, 57(16), pp. 3562-3568. Available at: <http://www.ncbi.nlm.nih.gov/pubmed/9270029> (Accessed: 27 April 2018).

Lane, D. P. and Crawford, L. V (1979) 'T antigen is bound to a host protein in SV40-transformed cells', *Nature*. Nature Publishing Group, 278(5701), pp. 261-263. doi: 10.1038/278261a0.

Lea, W. A. and Simeonov, A. (2011) 'Fluorescence polarization assays in small molecule screening.', *Expert opinion on drug discovery*. NIH Public Access, 6(1), pp. 17-32. doi: 10.1517/17460441.2011.537322.

Levine, A. J. *et al.* (2011) 'The p53 family: Guardians of maternal reproduction', *Nature Reviews Molecular Cell Biology*. Nature Publishing Group, 12(4), pp. 259-265. doi: 10.1038/nrm3086.

Levinthal, C. (1969) 'How to fold graciously', *Mössbauer Spectroscopy in Biological Systems Proceedings*, 24(41), pp. 22-24. doi: citeulike-article-id:380320.

- Levkowitz, G. *et al.* (1999) 'Ubiquitin ligase activity and tyrosine phosphorylation underlie suppression of growth factor signaling by c-Cbl/Sli-1', *Molecular Cell*, 4(6), pp. 1029-1040. doi: 10.1016/S1097-2765(00)80231-2.
- Li, C., Chen, L. and Chen, J. (2002) 'DNA Damage Induces MDMX Nuclear Translocation by p53-Dependent and -Independent Mechanisms', *Molecular and Cellular Biology*. American Society for Microbiology (ASM), 22(21), pp. 7562-7571. doi: 10.1128/MCB.22.21.7562.
- Li, J. *et al.* (2012) 'The RIP1/RIP3 necrosome forms a functional amyloid signaling complex required for programmed necrosis', *Cell*, 150(2), pp. 339-350. doi: 10.1016/j.cell.2012.06.019.
- Li, M. *et al.* (2003) 'Mono- Versus Polyubiquitination: Differential Control of p53 Fate by Mdm2', *Science*, 302(5652), pp. 1972-1975. doi: 10.1126/science.1091362.
- Li, M. *et al.* (2004) 'A dynamic role of HAUSP in the p53-Mdm2 pathway', *Molecular Cell*. Cell Press, 13(6), pp. 879-886. doi: 10.1016/S1097-2765(04)00157-1.
- Lim, W. K., Rosgen, J. and Englander, S. W. (2009) 'Urea, but not guanidinium, destabilizes proteins by forming hydrogen bonds to the peptide group', *Proceedings of the National Academy of Sciences*. National Academy of Sciences, 106(8), pp. 2595-2600. doi: 10.1073/pnas.0812588106.
- Lin, H. K. *et al.* (2002) 'Phosphorylation-dependent ubiquitylation and degradation of androgen receptor by Akt require Mdm2 E3 ligase', *EMBO Journal*, 21(15), pp. 4037-4048. doi: 10.1093/emboj/cdf406.
- Linares, L. K. *et al.* (2003) 'HdmX stimulates Hdm2-mediated ubiquitination and degradation of p53', *Proceedings of the National Academy of Sciences*, 100(21), pp. 12009-12014. doi: 10.1073/pnas.2030930100.
- Linares, L. K. *et al.* (2007) 'Intrinsic ubiquitination activity of PCAF controls the stability of the oncoprotein Hdm2', *Nature Cell Biology*, 9(3), pp. 331-338. doi:

10.1038/ncb1545.

Linke, K. *et al.* (2008) 'Structure of the MDM2/MDMX RING domain heterodimer reveals dimerization is required for their ubiquitylation in trans', *Cell Death and Differentiation*. Nature Publishing Group, 15(5), pp. 841-848. doi:

10.1038/sj.cdd.4402309.

Linzer, D. I. H. and Levine, A. J. (1979) 'Characterization of a 54K Dalton cellular SV40 tumor antigen present in SV40-transformed cells and uninfected embryonal carcinoma cells', *Cell*, 17(1), pp. 43-52. doi: 10.1016/0092-8674(79)90293-9.

Llanos, S. *et al.* (2001) 'Stabilization of p53 by p14ARF without relocation of MDM2 to the nucleolus', *Nature Cell Biology*. Nature Publishing Group, 3(5), pp. 445-452. doi: 10.1038/35074506.

Lohrum, M. A. E. *et al.* (2000) 'Contribution of two independent MDM2-binding domains in p14(ARF) to p53 stabilization', *Current Biology*. Cell Press, 10(9), pp. 539-542. doi: 10.1016/S0960-9822(00)00472-3.

Lohrum, M. A. E. *et al.* (2003) 'Regulation of HDM2 activity by the ribosomal protein L11', *Cancer Cell*, 3(6), pp. 577-587. doi: 10.1016/S1535-6108(03)00134-X.

Lois, L. M. and Lima, C. D. (2005) 'Structures of the SUMO E1 provide mechanistic insights into SUMO activation and E2 recruitment to E1', *EMBO Journal*, 24(3), pp. 439-451. doi: 10.1038/sj.emboj.7600552.

Lopes, M. A. *et al.* (2001) 'Amplification and protein expression of chromosome 12q13-15 genes in osteosarcomas of the jaws', *Oral Oncology*, 37(7), pp. 566-571. doi: 10.1016/S1368-8375(00)00130-5.

Lopez-Pajares, V., Kim, M. M. and Yuan, Z. M. (2008) 'Phosphorylation of MDMX mediated by Akt leads to stabilization and induces 14-3-3 binding', *Journal of Biological Chemistry*, 283(20), pp. 13707-13713. doi: 10.1074/jbc.M710030200.

Love, I. M. and Grossman, S. R. (2012) 'It Takes 15 to Tango: Making Sense of the Many Ubiquitin Ligases of p53', *Genes and Cancer*, 3(3-4), pp. 249-263. doi: 10.1177/1947601912455198.

Lowe, S. W. *et al.* (1993) 'p53-dependent apoptosis modulates the cytotoxicity of anticancer agents', *Cell*. Cell Press, 74(6), pp. 957-967. doi: 10.1016/0092-8674(93)90719-7.

Lu, X. *et al.* (2007) 'The Wip1 Phosphatase Acts as a Gatekeeper in the p53-Mdm2 Autoregulatory Loop', *Cancer Cell*, 12(4), pp. 342-354. doi: 10.1016/j.ccr.2007.08.033.

Luchinat, E. *et al.* (2018) 'Identification of a novel nucleophosmin-interaction motif in the tumor suppressor p14arf', *FEBS Journal*, 285(5), pp. 832-847. doi: 10.1111/febs.14373.

Lukas, J. *et al.* (2001) 'Alternative and aberrant messenger RNA splicing of the mdm2 oncogene in invasive breast cancer', *Cancer research*, 61(7), pp. 3212-3219. Available at: <http://www.ncbi.nlm.nih.gov/pubmed/11306511> (Accessed: 7 May 2018).

Luna, R. M. D. O., Wagner, D. S. and Lozano, G. (1995) 'Rescue of early embryonic lethality in mdm2-deficient mice by deletion of p53', *Nature*, 378(6553), pp. 203-206. doi: 10.1038/378203a0.

Mace, P. D. *et al.* (2008) 'Structures of the cIAP2 RING domain reveal conformational changes associated with ubiquitin-conjugating enzyme (E2) recruitment', *Journal of Biological Chemistry*, 283(46), pp. 31633-31640. doi: 10.1074/jbc.M804753200.

MacLaine, N. J. and Hupp, T. R. (2011) 'How phosphorylation controls p53', *Cell Cycle*, 10(6), pp. 916-921. doi: 10.4161/cc.10.6.15076.

Maji, S. K. *et al.* (2009) 'Functional amyloids as natural storage of peptide hormones in pituitary secretory granules', *Science*, 325(5938), pp. 328-332. doi: 10.1126/science.1173155.

- Malbert-Colas, L. *et al.* (2014) 'HDMX Folds the Nascent p53 mRNA following Activation by the ATM Kinase', *Molecular Cell*, 54(3), pp. 500-511. doi: 10.1016/j.molcel.2014.02.035.
- Mallery, D. L., Vandenberg, C. J. and Hiom, K. (2002) 'Activation of the E3 ligase function of the BRCA1/BARD1 complex by polyubiquitin chains', *EMBO Journal*, 21(24), pp. 6755-6762. doi: 10.1093/emboj/cdf691.
- Marcel, V. *et al.* (2011) 'Biological functions of p53 isoforms through evolution: Lessons from animal and cellular models', *Cell Death and Differentiation*, 18(12), pp. 1815-1824. doi: 10.1038/cdd.2011.120.
- Marechal, V. *et al.* (1994) 'The ribosomal L5 protein is associated with mdm-2 and mdm-2-p53 complexes', *Molecular and cellular biology*, 14(11), pp. 7414-20. doi: 10.1128/MCB.14.11.7414.Updated.
- Mari, S. *et al.* (2014) 'Structural and functional framework for the autoinhibition of nedd4-family ubiquitin ligases', *Structure*, 22(11), pp. 1639-1649. doi: 10.1016/j.str.2014.09.006.
- Marine, J. C. and Jochemsen, A. G. (2005) 'Mdmx as an essential regulator of p53 activity', *Biochemical and Biophysical Research Communications*, 331(3), pp. 750-760. doi: 10.1016/j.bbrc.2005.03.151.
- Martins, C. P., Brown-Swigart, L. and Evan, G. I. (2006) 'Modeling the Therapeutic Efficacy of p53 Restoration in Tumors', *Cell*, 127(7), pp. 1323-1334. doi: 10.1016/j.cell.2006.12.007.
- Maspero, E. *et al.* (2011) 'Structure of the HECT:ubiquitin complex and its role in ubiquitin chain elongation', *EMBO Reports*. EMBO Press, 12(4), pp. 342-349. doi: 10.1038/embor.2011.21.
- Maspero, E. *et al.* (2013) 'Structure of a ubiquitin-loaded HECT ligase reveals the molecular basis for catalytic priming', *Nature Structural and Molecular Biology*. Nature Publishing Group, 20(6), pp. 696-701. doi: 10.1038/nsmb.2566.

- Matsusaka, H. *et al.* (2006) 'Targeted deletion of p53 prevents cardiac rupture after myocardial infarction in mice', *Cardiovascular Research*, 70(3), pp. 457-465. doi: 10.1016/j.cardiores.2006.02.001.
- Matthews, B. W. (1968) 'Solvent content of protein crystals', *Journal of Molecular Biology*, 33(2), pp. 491-497. doi: 10.1016/0022-2836(68)90205-2.
- Maya, R. *et al.* (2001) 'ATM-dependent phosphorylation of Mdm2 on serine 395: Role in p53 activation by DNA damage', *Genes and Development*, 15(9), pp. 1067-1077. doi: 10.1101/gad.886901.
- McCoy, A. J. *et al.* (2007) 'Phaser crystallographic software', *Journal of Applied Crystallography*, 40(4), pp. 658-674. doi: 10.1107/S0021889807021206.
- McGuffin, L. J., Bryson, K. and Jones, D. T. (2000) 'The PSIPRED protein structure prediction server', *Bioinformatics*. Oxford University Press, 16(4), pp. 404-405. doi: 10.1093/bioinformatics/16.4.404.
- McLaughlin, M. E. and Sidhu, S. S. (2013) 'Engineering and analysis of peptide-recognition domain specificities by phage display and deep sequencing', *Methods in Enzymology*. Academic Press, 523, pp. 327-349. doi: 10.1016/B978-0-12-394292-0.00015-1.
- Meek, D. W. (2015) 'Regulation of the p53 response and its relationship to cancer', *The Biochemical journal*, 469(3), pp. 325-46. doi: 10.1042/BJ20150517.
- Meek, D. W. and Anderson, C. W. (2009) 'Posttranslational modification of p53: cooperative integrators of function', *Cold Spring Harbor perspectives in biology*, 1(6), pp. 950-966. doi: 10.1101/cshperspect.a000950.
- Mendrysa, S. M. *et al.* (2006) 'Tumor suppression and normal aging in mice with constitutively high p53 activity', *Genes and Development*. Cold Spring Harbor Laboratory Press, 20(1), pp. 16-21. doi: 10.1101/gad.1378506.
- Menéndez, S. *et al.* (2003) 'Oligomerization of the human ARF tumor suppressor and its response to oxidative stress', *Journal of Biological Chemistry*. American

Society for Biochemistry and Molecular Biology, 278(21), pp. 18720-18729. doi: 10.1074/jbc.M211007200.

Midgley, C. A. *et al.* (2000) 'An N-terminal p14ARF peptide blocks Mdm2-dependent ubiquitination in vitro and can activate p53 in vivo', *Oncogene*. Nature Publishing Group, 19(19), pp. 2312-2323. doi: 10.1038/sj.onc.1203593.

Migliorini, D. *et al.* (2002) 'Hdmx recruitment into the nucleus by Hdm2 is essential for its ability to regulate p53 stability and transactivation', *Journal of Biological Chemistry*. American Society for Biochemistry and Molecular Biology, 277(9), pp. 7318-7323. doi: 10.1074/jbc.M108795200.

Mirza, A. *et al.* (2003) 'Global transcriptional program of p53 target genes during the process of apoptosis and cell cycle progression', *Oncogene*, 22(23), pp. 3645-3654. doi: 10.1038/sj.onc.1206477.

Mitrea, D. M. *et al.* (2016) 'Nucleophosmin integrates within the nucleolus via multi-modal interactions with proteins displaying R-rich linear motifs and rRNA', *eLife*. eLife Sciences Publications Limited, 5(e13571), pp. 1-33. doi: 10.7554/eLife.13571.001.

Mitrea, D. M. and Kriwacki, R. W. (2018) 'On the relationship status for Arf and NPM1 - it's complicated', *FEBS Journal*, 285(5), pp. 828-831. doi: 10.1111/febs.14407.

Miyazaki, Y. *et al.* (2016) 'A method to rapidly create protein aggregates in living cells', *Nature Communications*. Nature Publishing Group, 7, p. 11689. doi: 10.1038/ncomms11689.

Mizushima, T. *et al.* (2007) 'Structural basis for the selection of glycosylated substrates by SCF(Fbs1) ubiquitin ligase', *Proceedings of the National Academy of Sciences of the United States of America*. National Academy of Sciences, 104(14), pp. 5777-5781. doi: 10.1073/pnas.0610312104.

Momand, J. *et al.* (1992) 'The mdm-2 oncogene product forms a complex with the p53 protein and inhibits p53-mediated transactivation', *Cell*, 69(7), pp.

1237-1245. doi: 10.1016/0092-8674(92)90644-R.

Momand, J. *et al.* (1998) 'The MDM2 gene amplification database', *Nucleic acids research*, 26(15), pp. 3453-3459. Available at: <http://www.ncbi.nlm.nih.gov/pubmed/9671804> (Accessed: 7 May 2018).

Monsellier, E. *et al.* (2008) 'Aggregation propensity of the human proteome', *PLoS Computational Biology*. Edited by R. Nussinov. Public Library of Science, 4(10), p. e1000199. doi: 10.1371/journal.pcbi.1000199.

Morjana, N. A., McKeone, B. J. and Gilbert, H. F. (1993) 'Guanidine hydrochloride stabilization of a partially unfolded intermediate during the reversible denaturation of protein disulfide isomerase.', *Proceedings of the National Academy of Sciences*. National Academy of Sciences, 90(6), pp. 2107-2111. doi: 10.1073/pnas.90.6.2107.

Muyldermans, S. (2013) 'Nanobodies: Natural Single-Domain Antibodies', *Annual Review of Biochemistry*, 82(1), pp. 775-797. doi: 10.1146/annurev-biochem-063011-092449.

Myant, K. B. *et al.* (2017) 'HUWE1 is a critical colonic tumour suppressor gene that prevents MYC signalling, DNA damage accumulation and tumour initiation', *EMBO Molecular Medicine*. Wiley-Blackwell, 9(2), pp. 181-197. doi: 10.15252/emmm.201606684.

Nishikawa, H. *et al.* (2004) 'Mass Spectrometric and Mutational Analyses Reveal Lys-6-linked Polyubiquitin Chains Catalyzed by BRCA1-BARD1 Ubiquitin Ligase', *Journal of Biological Chemistry*, 279(6), pp. 3916-3924. doi: 10.1074/jbc.M308540200.

Nomura, K. *et al.* (2017) 'Structural analysis of MDM2 RING separates degradation from regulation of p53 transcription activity', *Nature Structural and Molecular Biology*, 24(7), pp. 578-587. doi: 10.1038/nsmb.3414.

Nuber, U. and Scheffner, M. (1999) 'Identification of determinants in E2 ubiquitin-conjugating enzymes required for hec E3 ubiquitin-protein ligase

interaction', *Journal of Biological Chemistry*. American Society for Biochemistry and Molecular Biology, 274(11), pp. 7576-7582. doi: 10.1074/jbc.274.11.7576.

O'Campo, J. *et al.* (2002) 'Aberrant p53, mdm2, and proliferation differ in glioblastomas from long-term compared with typical survivors', *Clinical Cancer Research*, 8(1), pp. 180-187. Available at: <http://www.ncbi.nlm.nih.gov/pubmed/11801556> (Accessed: 7 May 2018).

Ofir-Rosenfeld, Y. *et al.* (2008) 'Mdm2 Regulates p53 mRNA Translation through Inhibitory Interactions with Ribosomal Protein L26', *Molecular Cell*, 32(2), pp. 180-189. doi: 10.1016/j.molcel.2008.08.031.

Ogunjimi, A. A. *et al.* (2010) 'The ubiquitin binding region of the smurf HECT domain facilitates polyubiquitylation and binding of ubiquitylated substrates', *Journal of Biological Chemistry*. American Society for Biochemistry and Molecular Biology, 285(9), pp. 6308-6315. doi: 10.1074/jbc.M109.044537.

Okamoto, K. *et al.* (2002) 'Cyclin G recruits PP2A to dephosphorylate Mdm2', *Molecular Cell*, 9(4), pp. 761-771. doi: 10.1016/S1097-2765(02)00504-X.

Okamoto, K. *et al.* (2005) 'DNA Damage-Induced Phosphorylation of MdmX at Serine 367 Activates p53 by Targeting MdmX for Mdm2-Dependent Degradation', *Molecular and Cellular Biology*. American Society for Microbiology, 25(21), pp. 9608-9620. doi: 10.1128/MCB.25.21.9608-9620.2005.

Okuwaki, M. *et al.* (2001) 'Function of nucleophosmin/B23, a nucleolar acidic protein, as a histone chaperone', *FEBS Letters*, 506(3), pp. 272-276. doi: 10.1016/S0014-5793(01)02939-8.

Okuwaki, M., Tsujimoto, M. and Nagata, K. (2002) 'The RNA Binding Activity of a Ribosome Biogenesis Factor, Nucleophosmin/B23, Is Modulated by Phosphorylation with a Cell Cycle-dependent Kinase and by Association with Its Subtype', *Molecular Biology of the Cell*. American Society for Cell Biology, 13(6), pp. 2016-2030. doi: 10.1091/mbc.02-03-0036.

Oliner, J. D. *et al.* (1992) 'Amplification of a gene encoding a p53-associated

protein in human sarcomas', *Nature*, 358(6381), pp. 80-83. doi: 10.1038/358080a0.

Olsen, S. K. *et al.* (2010) 'Active site remodelling accompanies thioester bond formation in the SUMO E1', *Nature*, 463(7283), pp. 906-912. doi: 10.1038/nature08765.

Olsen, S. K. and Lima, C. D. (2013) 'Structure of a Ubiquitin E1-E2 Complex: Insights to E1-E2 Thioester Transfer', *Molecular Cell*, 49(5), pp. 884-896. doi: 10.1016/j.molcel.2013.01.013.

Ouelle, D. E. *et al.* (1995) 'Alternative reading frames of the INK4a tumor suppressor gene encode two unrelated proteins capable of inducing cell cycle arrest', *Cell*. Cell Press, 83(6), pp. 993-1000. doi: 10.1016/0092-8674(95)90214-7.

Ozenne, P. *et al.* (2010) 'The ARF tumor suppressor: Structure, functions and status in cancer', *International Journal of Cancer*, 127(10), pp. 2239-2247. doi: 10.1002/ijc.25511.

Palmero, I., Pantoja, C. and Serrano, M. (1998) 'p19(ARF) links the tumour suppressor p53 to Ras', *Nature*, 395(6698), pp. 125-126. doi: 10.1038/25870.

Pandya, R. K. *et al.* (2010) 'A structural element within the HUWE1 HECT domain modulates self-ubiquitination and substrate ubiquitination activities', *Journal of Biological Chemistry*. American Society for Biochemistry and Molecular Biology, 285(8), pp. 5664-5673. doi: 10.1074/jbc.M109.051805.

Pappu, R. V *et al.* (2008) 'A polymer physics perspective on driving forces and mechanisms for protein aggregation', *Archives of Biochemistry and Biophysics*. NIH Public Access, pp. 132-141. doi: 10.1016/j.abb.2007.08.033.

Pastore, A. and Temussi, P. A. (2012) 'The two faces of Janus: Functional interactions and protein aggregation', *Current Opinion in Structural Biology*, pp. 30-37. doi: 10.1016/j.sbi.2011.11.007.

Patrick, M. H. (2007) 'Crystallography made crystal clear: A guide for users of macromolecular models (3rd Ed.)', *Biochemistry and Molecular Biology Education*. Elsevier/Academic Press, 35(5), pp. 387-388. doi: 10.1002/bmb.89.

Pechmann, S. *et al.* (2009) 'Physicochemical principles that regulate the competition between functional and dysfunctional association of proteins', *Proceedings of the National Academy of Sciences*, 106(25), pp. 10159-10164. doi: 10.1073/pnas.0812414106.

Pereg, Y. *et al.* (2006) 'Differential Roles of ATM- and Chk2-Mediated Phosphorylations of Hdmx in Response to DNA Damage', *Molecular and Cellular Biology*. American Society for Microbiology, 26(18), pp. 6819-6831. doi: 10.1128/MCB.00562-06.

Perry, M. E. *et al.* (1993) 'The mdm-2 gene is induced in response to UV light in a p53-dependent manner', *Proceedings of the National Academy of Sciences of the United States of America*, 90(24), pp. 11623-7. doi: 10.1073/pnas.90.24.11623.

Perry, M. E. *et al.* (2000) 'p76(MDM2) inhibits the ability of p90(MDM2) to destabilize p53', *Journal of Biological Chemistry*. American Society for Biochemistry and Molecular Biology, 275(8), pp. 5733-5738. doi: 10.1074/jbc.275.8.5733.

Petroski, M. D. and Deshaies, R. J. (2005) 'Mechanism of lysine 48-linked ubiquitin-chain synthesis by the cullin-RING ubiquitin-ligase complex SCF-Cdc34', *Cell*, 123(6), pp. 1107-1120. doi: 10.1016/j.cell.2005.09.033.

Plechanovov, A. *et al.* (2012) 'Structure of a RING E3 ligase and ubiquitin-loaded E2 primed for catalysis', *Nature*, 489(7414), pp. 115-120. doi: 10.1038/nature11376.

Pomerantz, J. *et al.* (1998) 'The Ink4a tumor suppressor gene product, p19(Arf), interacts with MDM2 and neutralizes MDM2's inhibition of p53', *Cell*. Cell Press, 92(6), pp. 713-723. doi: 10.1016/S0092-8674(00)81400-2.

- Post, S. M. *et al.* (2010) 'A high-frequency regulatory polymorphism in the p53 pathway accelerates tumor development', *Cancer Cell*. Elsevier, 18(3), pp. 220-230. doi: 10.1016/j.ccr.2010.07.010.
- Poyurovsky, M. V *et al.* (2007) 'The Mdm2 RING domain C-terminus is required for supramolecular assembly and ubiquitin ligase activity', *EMBO Journal*, 26(1), pp. 90-101. doi: 10.1038/sj.emboj.7601465.
- Pruneda, J. N. *et al.* (2011) 'Ubiquitin in Motion: Structural studies of the E2-Ub conjugate', *Biochemistry*, 50(10), pp. 1624-1633. doi: 10.1021/bi101913m.
- Ptitsyn, O. B. (1987) 'Protein folding: Hypotheses and experiments', *Journal of Protein Chemistry*. Kluwer Academic Publishers, pp. 273-293. doi: 10.1007/BF00248050.
- Qi, C. F. *et al.* (2012) 'Characterization of ARF-BP1/HUWE1 interactions with CTCF, MYC, ARF and p53 in MYC-driven B cell neoplasms', *International Journal of Molecular Sciences*, 13(5), pp. 6204-6219. doi: 10.3390/ijms13056204.
- Quinn, J. G. *et al.* (2000) 'Development and Application of Surface Plasmon Resonance-Based Biosensors for the Detection of Cell-Ligand Interactions', *Analytical Biochemistry*, 281(2), pp. 135-143. doi: 10.1006/abio.2000.4564.
- Radfar, A. *et al.* (1998) 'p19(Arf) induces p53-dependent apoptosis during abelson virus-mediated pre-B cell transformation', *Proceedings of the National Academy of Sciences of the United States of America*. National Academy of Sciences, 95(22), pp. 13194-13199. doi: 10.1073/pnas.95.22.13194.
- Raman, B., Ramakrishna, T. and Rao, C. M. (1996) 'Refolding of denatured and denatured/reduced lysozyme at high concentrations', *Journal of Biological Chemistry*. American Society for Biochemistry and Molecular Biology, 271(29), pp. 17067-17072. doi: 10.1074/jbc.271.29.17067.
- Rambo, R. P. and Tainer, J. A. (2011) 'Characterizing flexible and intrinsically unstructured biological macromolecules by SAS using the Porod-Debye law', *Biopolymers*. John Wiley & Sons, Ltd, 95(8), pp. 559-571. doi:

10.1002/bip.21638.

Rayburn, E. *et al.* (2005) 'MDM2 and human malignancies: expression, clinical pathology, prognostic markers, and implications for chemotherapy', *Current cancer drug targets*, 5(1), pp. 27-41. doi: 10.2174/1568009053332636.

Receveur-Brechot, V. and Durand, D. (2012) 'How Random are Intrinsically Disordered Proteins? A Small Angle Scattering Perspective', *Current Protein & Peptide Science*, 13(1), pp. 55-75. doi: 10.2174/138920312799277901.

Reef, S. *et al.* (2006) 'A Short Mitochondrial Form of p19ARF Induces Autophagy and Caspase-Independent Cell Death', *Molecular Cell*, 22(4), pp. 463-475. doi: 10.1016/j.molcel.2006.04.014.

Reverter, D. and Lima, C. D. (2005) 'Insights into E3 ligase activity revealed by a SUMO-RanGAP1-Ubc9-Nup358 complex', *Nature*, 435(7042), pp. 687-692. doi: 10.1038/nature03588.

Richardson, P. G. *et al.* (2005) 'Bortezomib or High-Dose Dexamethasone for Relapsed Multiple Myeloma', *New England Journal of Medicine*, 352(24), pp. 2487-2498. doi: 10.1056/NEJMoa043445.

Ries, S. *et al.* (2000) 'Opposing effects of Ras on p53: transcriptional activation of mdm2 and induction of p19ARF', *Cell*, 103(2), pp. 321-30. Available at: <http://www.ncbi.nlm.nih.gov/pubmed/11057904> (Accessed: 30 April 2018).

Riling, C. *et al.* (2015) 'Itch WW Domains Inhibit Its E3 Ubiquitin Ligase Activity by Blocking E2-E3 Ligase Trans-thiolation.', *The Journal of biological chemistry*. American Society for Biochemistry and Molecular Biology, 290(39), pp. 23875-87. doi: 10.1074/jbc.M115.649269.

Rizos, H. *et al.* (2000) 'Two arginine rich domains in the p14ARF tumour suppressor mediate nucleolar localization', *Oncogene*. Nature Publishing Group, 19(26), pp. 2978-85. doi: 10.1038/sj.onc.1203629.

Rizos, H., Woodruff, S. and Kefford, R. F. (2005) 'p14ARF interacts with the

SUMO-conjugating enzyme Ubc9 and promotes the sumoylation of its binding partners', *Cell Cycle*, 4(4), pp. 597-603. doi: 10.4161/cc.4.4.1588.

Rodriguez, M. S. *et al.* (2000) 'Multiple C-terminal lysine residues target p53 for ubiquitin-proteasome-mediated degradation', *Molecular and cellular biology*, 20(22), pp. 8458-8467. doi: 10.1128/MCB.20.22.8458-8467.2000.

Rosano, G. L. and Ceccarelli, E. A. (2014) 'Recombinant protein expression in *Escherichia coli*: Advances and challenges', *Frontiers in Microbiology*, 5(APR), pp. 1-17. doi: 10.3389/fmicb.2014.00172.

Rotin, D. and Kumar, S. (2009) 'Physiological functions of the HECT family of ubiquitin ligases', *Nature Reviews Molecular Cell Biology*. Nature Publishing Group, 10(6), pp. 398-409. doi: 10.1038/nrm2690.

Rousseau, F., Serrano, L. and Schymkowitz, J. W. H. (2006) 'How evolutionary pressure against protein aggregation shaped chaperone specificity', *Journal of Molecular Biology*, 355(5), pp. 1037-1047. doi: 10.1016/j.jmb.2005.11.035.

Roxburgh, P. *et al.* (2012) 'Small molecules that bind the Mdm2 RING stabilize and activate p53', *Carcinogenesis*, 33(4), pp. 791-798. doi: 10.1093/carcin/bgs092.

Rubin, D. M. *et al.* (1998) 'Active site mutants in the six regulatory particle ATPases reveal multiple roles for ATP in the proteasome', *The EMBO Journal*. EMBO Press, 17(17), pp. 4909-4919. doi: 10.1093/emboj/17.17.4909.

Rupp, B. (2010) 'Biomolecular crystallography : principles, practice, and application to structural biology'. Garland Science, p. 809. Available at: https://books.google.co.uk/books/about/Biomolecular_Crystallography.html?id=BfmdGwAACAAJ (Accessed: 23 January 2019).

Ryu, K.-S. *et al.* (2008) 'Direct characterization of E2-dependent target specificity and processivity using an artificial p27-linker-E2 ubiquitination system.', *BMB reports*, 41(12), pp. 852-857. Available at: <http://www.ncbi.nlm.nih.gov/pubmed/19123975> (Accessed: 27 April 2018).

Saito, S. N. I. *et al.* (2002) 'ATM mediates phosphorylation at multiple p53 sites, including Ser46, in response to ionizing radiation', *Journal of Biological Chemistry*, 277(15), pp. 12491-12494. doi: 10.1074/jbc.C200093200.

Salvat, C. *et al.* (2004) 'The -4 Phenylalanine Is Required for Substrate Ubiquitination Catalyzed by HECT Ubiquitin Ligases', *Journal of Biological Chemistry*, 279(18), pp. 18935-18943. doi: 10.1074/jbc.M312201200.

Sander, B. *et al.* (2017) 'A conformational switch regulates the ubiquitin ligase HUWE1', *eLife*. eLife Sciences Publications Limited, 14(6), pp. 1-32. doi: 10.7554/eLife.21036.

Schäfer, A., Kuhn, M. and Schindelin, H. (2014) 'Structure of the ubiquitin-activating enzyme loaded with two ubiquitin molecules', *Acta Crystallographica Section D Biological Crystallography*, 70(5), pp. 1311-1320. doi: 10.1107/S1399004714002910.

Scherer, D. C. *et al.* (1995) 'Signal-induced degradation of I kappa B alpha requires site-specific ubiquitination', *Proceedings of the National Academy of Sciences*, 92(24), pp. 11259-11263. doi: 10.1073/pnas.92.24.11259.

Schwartz, A. L. and Ciechanover, A. (2009) 'Targeting Proteins for Destruction by the Ubiquitin System: Implications for Human Pathobiology', *Annual Review of Pharmacology and Toxicology*. Annual Reviews , 49(1), pp. 73-96. doi: 10.1146/annurev.pharmtox.051208.165340.

Schwarz, S. E., Rosa, J. L. and Scheffner, M. (1998) 'Characterization of human hect domain family members and their interaction with Ubch5 and Ubch7', *Journal of Biological Chemistry*. American Society for Biochemistry and Molecular Biology, 273(20), pp. 12148-12154. doi: 10.1074/jbc.273.20.12148.

Scrima, A. *et al.* (2008) 'Structural Basis of UV DNA-Damage Recognition by the DDB1-DDB2 Complex Supplemental Tables Table S1 : Data collection and refinement statistics for hsDDB1-drDDB2 complexes', *Cell*. Howard Hughes Medical Institute, 135(7), pp. 1213-23. doi: 10.1016/j.cell.2008.10.045.

Serrano, M. *et al.* (1996) 'Role of the INK4a locus in tumor suppression and cell mortality', *Cell*. Cell Press, 85(1), pp. 27-37. doi: 10.1016/S0092-8674(00)81079-X.

Sharpless, N. E. *et al.* (2001) 'Loss of p16Ink4a with retention of p19 predisposes mice to tumorigenesis', *Nature*. Nature Publishing Group, 413(6851), pp. 86-91. doi: 10.1038/35092592.

Sheng, Y. *et al.* (2012) 'A Human Ubiquitin Conjugating Enzyme (E2)-HECT E3 Ligase Structure-function Screen', *Molecular & Cellular Proteomics*, 11(8), pp. 329-341. doi: 10.1074/mcp.O111.013706.

Sherr, C. J. (2006) 'Divorcing ARF and p53: An unsettled case', *Nature Reviews Cancer*. Nature Publishing Group, 6(9), pp. 663-673. doi: 10.1038/nrc1954.

Sherr, C. J. (2012) 'Ink4-Arf locus in cancer and aging', *Wiley Interdisciplinary Reviews: Developmental Biology*, 1(5), pp. 731-741. doi: 10.1002/wdev.40.

Shimizu, H. *et al.* (2002) 'The conformationally flexible S9-S10 linker region in the core domain of p53 contains a novel MDM2 binding site whose mutation increases ubiquitination of p53 in vivo', *Journal of Biological Chemistry*, 277(32), pp. 28446-28458. doi: 10.1074/jbc.M202296200.

Shinozaki, T. *et al.* (2003) 'Functional role of Mdm2 phosphorylation by ATR in attenuation of p53 nuclear export', *Oncogene*, 22(55), pp. 8870-8880. doi: 10.1038/sj.onc.1207176.

Shvarts, A. *et al.* (1996) 'MDMX: a novel p53-binding protein with some functional properties of MDM2', *The EMBO journal*, 15(19), pp. 5349-5357. doi: 10.1002/J.1460-2075.1996.TB00919.X.

Shvarts, A. *et al.* (1997) 'Isolation and identification of the human homolog of a new p53-binding protein, Mdmx', *Genomics*, 43(1), pp. 34-42. doi: 10.1006/geno.1997.4775.

Sivakolundu, S. G. *et al.* (2008) 'Intrinsically Unstructured Domains of Arf and

Hdm2 Form Bimolecular Oligomeric Structures In Vitro and In Vivo', *Journal of Molecular Biology*. Academic Press, 384(1), pp. 240-254. doi: 10.1016/j.jmb.2008.09.019.

Stad, R. *et al.* (2000) 'Hdmx stabilizes Mdm2 and p53', *Journal of Biological Chemistry*, 275(36), pp. 28039-28044. doi: 10.1074/jbc.M003496200.

Stad, R. *et al.* (2001) 'Mdmx stabilizes p53 and Mdm2 via two distinct mechanisms', *EMBO Reports*. European Molecular Biology Organization, 2(11), pp. 1029-1034. doi: 10.1093/embo-reports/kve227.

De Stanchina, E. *et al.* (1998) 'E1A signaling to p53 involves the p19(ARF) tumor suppressor', *Genes and Development*, 12(15), pp. 2434-2442. doi: 10.1101/gad.12.15.2434.

Stark, C. (2006) 'BioGRID: a general repository for interaction datasets', *Nucleic Acids Research*. Oxford University Press, 34(90001), pp. D535-D539. doi: 10.1093/nar/gkj109.

Stefanou, D. G. *et al.* (1998) 'p53/MDM-2 immunohistochemical expression correlated with proliferative activity in different subtypes of human sarcomas: a ten-year follow-up study', *Anticancer Res*, 18(6B), pp. 4673-4681. Available at: <http://www.ncbi.nlm.nih.gov/pubmed/9891539> (Accessed: 7 May 2018).

Stewart, M. D. *et al.* (2016) 'E2 enzymes: More than just middle men', *Cell Research*, 26(4), pp. 423-440. doi: 10.1038/cr.2016.35.

Stommel, J. M. and Wahl, G. M. (2004) 'Accelerated MDM2 auto-degradation induced by DNA-damage kinases is required for p53 activation', *EMBO Journal*, 23(7), pp. 1547-1556. doi: 10.1038/sj.emboj.7600145.

Stott, F. J. *et al.* (1998) 'The alternative product from the human CDKN2A locus, p14(ARF), participates in a regulatory feedback loop with p53 and MDM2', *EMBO Journal*. EMBO Press, 17(17), pp. 5001-5014. doi: 10.1093/emboj/17.17.5001.

Streich, F. C. and Lima, C. D. (2016) 'Capturing a substrate in an activated RING

E3/E2-SUMO complex', *Nature*. Nature Publishing Group, 536(7616), pp. 304-308. doi: 10.1038/nature19071.

Sugasawa, K. *et al.* (2005) 'UV-induced ubiquitylation of XPC protein mediated by UV-DDB-ubiquitin ligase complex', *Cell*. Elsevier, 121(3), pp. 387-400. doi: 10.1016/j.cell.2005.02.035.

Sun, Y. *et al.* (2005) 'A role for the Tip60 histone acetyltransferase in the acetylation and activation of ATM', *Proceedings of the National Academy of Sciences of the United States of America*, 102(37), pp. 13182-13187. doi: 10.1073/pnas.0504211102.

Svergun, D. I. (1999) 'Restoring low resolution structure of biological macromolecules from solution scattering using simulated annealing', *Biophysical Journal*. Cell Press, 76(6), pp. 2879-2886. doi: 10.1016/S0006-3495(99)77443-6.

Swinehart, D. F. (1962) 'The Beer-Lambert Law', *Journal of Chemical Education*. Division of Chemical Education, 39(7), p. 333. doi: 10.1021/ed039p333.

Szebeni, A. and Olson, M. O. (1999) 'Nucleolar protein B23 has molecular chaperone activities', *Protein science : a publication of the Protein Society*, 8(4), pp. 905-12. doi: 10.1110/ps.8.4.905.

Tago, K., Chiocca, S. and Sherr, C. J. (2005) 'Sumoylation induced by the Arf tumor suppressor: a p53-independent function', *Proceedings of the National Academy of Sciences of the United States of America*. National Academy of Sciences, 102(21), pp. 7689-7694. doi: 10.1073/pnas.0502978102.

Tam, J. P. *et al.* (1991) 'Disulfide Bond Formation in Peptides by Dimethyl Sulfoxide. Scope and Applications', *Journal of the American Chemical Society*. American Chemical Society, 113(17), pp. 6657-6662. doi: 10.1021/ja00017a044.

Tang, J. *et al.* (2006) 'Critical role for Daxx in regulating Mdm2', *Nature Cell Biology*. Nature Publishing Group, 8(8), pp. 855-862. doi: 10.1038/ncb1442.

Tang, J. *et al.* (2013) 'Phosphorylation of Daxx by ATM Contributes to DNA

Damage-Induced p53 Activation', *PLoS ONE*, 8(2). doi: 10.1371/journal.pone.0055813.

Tavana, O., Chen, D. and Gu, W. (2014) 'Controlling ARF stability: New players added to the team', *Cell Cycle*, 13(4), pp. 497-498. doi: 10.4161/cc.27786.

Tian, X. *et al.* (2011) 'E2F1 inhibits MDM2 expression in a p53-dependent manner', *Cellular Signalling*, 23(1), pp. 193-200. doi: 10.1016/j.cellsig.2010.09.003.

Timasheff, S. N. (1998) *Control of protein stability and reactions by weakly interacting cosolvents: the simplicity of the complicated.*, *Advances in protein chemistry*. doi: 9615174.

Tokunaga, F. *et al.* (2009) 'Involvement of linear polyubiquitylation of NEMO in NF- κ B activation', *Nature Cell Biology*. Nature Publishing Group, 11(2), pp. 123-132. doi: 10.1038/ncb1821.

Truong, A. H. L. *et al.* (2005) 'Direct transcriptional regulation of MDM2 by Fli-1', *Oncogene*, 24(6), pp. 962-969. doi: 10.1038/sj.onc.1208323.

Turner, G. C., Du, F. and Varshavsky, A. (2000) 'Peptides accelerate their uptake by activating a ubiquitin-dependent proteolytic pathway', *Nature*, 405(6786), pp. 579-583. doi: 10.1038/35014629.

Uchida, T. *et al.* (2002) 'Clinical significance of p53, MDM2 and bcl-2 expression in transitional cell carcinoma of the bladder', *Oncology reports*, 9(2), pp. 253-259. Available at: <http://www.ncbi.nlm.nih.gov/pubmed/11836589> (Accessed: 7 May 2018).

Uldrijan, S., Pannekoek, W. J. and Vousden, K. H. (2007) 'An essential function of the extreme C-terminus of MDM2 can be provided by MDMX', *EMBO Journal*. European Molecular Biology Organization, 26(1), pp. 102-112. doi: 10.1038/sj.emboj.7601469.

Vassilev, L. T. *et al.* (2004) 'In Vivo Activation of the p53 Pathway by Small-

Molecule Antagonists of MDM2', *Science*. American Association for the Advancement of Science, 303(5659), pp. 844-848. doi: 10.1126/science.1092472.

Velimezi, G. *et al.* (2013) 'Functional interplay between the DNA-damage-response kinase ATM and ARF tumour suppressor protein in human cancer', *Nature Cell Biology*, 15(8), pp. 967-977. doi: 10.1038/ncb2795.

Ventura, A. *et al.* (2007) 'Restoration of p53 function leads to tumour regression in vivo', *Nature*, 445(7128), pp. 661-665. doi: 10.1038/nature05541.

Verdecia, M. A. *et al.* (2003) 'Conformational flexibility underlies ubiquitin ligation mediated by the WWP1 HECT domain E3 ligase', *Molecular Cell*, 11(1), pp. 249-259. doi: 10.1016/S1097-2765(02)00774-8.

Verdin, E. and Ott, M. (2015) '50 years of protein acetylation: from gene regulation to epigenetics, metabolism and beyond', *Nature Reviews Molecular Cell Biology*. Nature Publishing Group, 16(4), pp. 258-264. doi: 10.1038/nrm3931.

Vijay-kumar, S., Bugg, C. E. and Cook, W. J. (1987) 'Structure of ubiquitin refined at 1.8 Å resolution', *Journal of Molecular Biology*. Academic Press, 194(3), pp. 531-544. doi: 10.1016/0022-2836(87)90679-6.

Volkov, V. V. and Svergun, D. I. (2003) 'Uniqueness of ab initio shape determination in small-angle scattering', in *Journal of Applied Crystallography*, pp. 860-864. doi: 10.1107/S0021889803000268.

Vousden, K. H. and Prives, C. (2009) 'Blinded by the Light: The Growing Complexity of p53', *Cell*. Cell Press, 137(3), pp. 413-431. doi: 10.1016/j.cell.2009.04.037.

Vousden, K. H. and Ryan, K. M. (2009) 'P53 and metabolism', *Nature Reviews Cancer*. Nature Publishing Group, 9(10), pp. 691-700. doi: 10.1038/nrc2715.

Vu, B. *et al.* (2013) 'Discovery of RG7112: A small-molecule MDM2 inhibitor in clinical development', *ACS Medicinal Chemistry Letters*. American Chemical

Society, 4(5), pp. 466-469. doi: 10.1021/ml4000657.

Walden, H. *et al.* (2003) 'The Structure of the APPBP1-UBA3-NEDD8-ATP Complex Reveals the Basis for Selective Ubiquitin-like Protein Activation by an E1', *Molecular Cell*, 12(6), pp. 1427-1437. doi: 10.1016/S1097-2765(03)00452-0.

Wallace, M. *et al.* (2006) 'Dual-Site Regulation of MDM2 E3-Ubiquitin Ligase Activity', *Molecular Cell*, 23(2), pp. 251-263. doi: 10.1016/j.molcel.2006.05.029.

Wang, D. *et al.* (1994) 'The nucleic acid binding activity of nucleolar protein B23.1 resides in its carboxyl-terminal end', *Journal of Biological Chemistry*, 269(49), pp. 30994-30998. Available at: <http://www.jbc.org/content/269/49/30994.full.pdf> (Accessed: 22 April 2018).

Wang, H. *et al.* (2004) 'Role of histone H2A ubiquitination in Polycomb silencing', *Nature*, 431(7010), pp. 873-878. doi: 10.1038/nature02985.

Wang, M. and Pickart, C. M. (2005) 'Different HECT domain ubiquitin ligases employ distinct mechanisms of polyubiquitin chain synthesis', *EMBO Journal*, 24(24), pp. 4324-4333. doi: 10.1038/sj.emboj.7600895.

Wang, P. *et al.* (2006) 'Decreased Mdm2 expression inhibits tumor development induced by loss of ARF', *Oncogene*, 25(26), pp. 3708-3718. doi: 10.1038/sj.onc.1209411.

Wang, X. *et al.* (2001) 'MDM2 and MDMX can interact differently with ARF and members of the p53 family', *FEBS Letters*, 490(3), pp. 202-208. doi: 10.1016/S0014-5793(01)02124-X.

Waterman, H. (2002) 'A mutant EGF-receptor defective in ubiquitylation and endocytosis unveils a role for Grb2 in negative signaling', *EMBO Journal*, 21(3), pp. 303-313. doi: 10.1093/emboj/21.3.303.

Watson, I. R. *et al.* (2010) 'Chemotherapy induces NEDP1-mediated destabilization of MDM2', *Oncogene*, 29(2), pp. 297-304. doi: 10.1038/onc.2009.314.

- Weber, J. D. *et al.* (1999) 'Nucleolar Arf sequesters Mdm2 and activates p53', *Nature cell biology*, 1(1), pp. 20-6. doi: 10.1038/8991.
- Weber, J. D. *et al.* (2000) 'Cooperative Signals Governing ARF-Mdm2 Interaction and Nucleolar Localization of the Complex', *Molecular and Cellular Biology*, 20(7), pp. 2517-2528. doi: 10.1128/MCB.20.7.2517-2528.2000.Updated.
- Wenzel, D. M., Stoll, K. E. and Klevit, R. E. (2011) 'E2s: structurally economical and functionally replete', *Biochemical Journal*, 433(1), pp. 31-42. doi: 10.1042/BJ20100985.
- West, S. M., Guise, A. D. and Chaudhuri, J. B. (1997) 'A comparison of the denaturants urea and guanidine hydrochloride on protein refolding', *Food and Bioproducts Processing: Transactions of the Institution of Chemical Engineers, Part C*. Elsevier, 75(1), pp. 50-56. doi: 10.1205/096030897531360.
- Wetlaufer, D. B. (1973) 'Nucleation, Rapid Folding, and Globular Intrachain Regions in Proteins', *Proceedings of the National Academy of Sciences*, 70(3), pp. 697-701. doi: 10.1073/pnas.70.3.697.
- Wickliffe, K. E. *et al.* (2011) 'The mechanism of linkage-specific ubiquitin chain elongation by a single-subunit E2', *Cell*, 144(5), pp. 769-781. doi: 10.1016/j.cell.2011.01.035.
- Wiesner, S. *et al.* (2007) 'Autoinhibition of the HECT-Type Ubiquitin Ligase Smurf2 through Its C2 Domain', *Cell*. Cell Press, 130(4), pp. 651-662. doi: 10.1016/j.cell.2007.06.050.
- van Wijk, S. J. L. and Timmers, H. T. M. (2010) 'The family of ubiquitin-conjugating enzymes (E2s): deciding between life and death of proteins', *The FASEB Journal*, 24(4), pp. 981-993. doi: 10.1096/fj.09-136259.
- Wingfield, P. T. (1995) 'Use of Protein Folding Reagents', in *Current Protocols in Protein Science*. Hoboken, NJ, USA: John Wiley & Sons, Inc., p. A.3A.1-A.3A.4. doi: 10.1002/0471140864.psa03as00.

Winter, M. *et al.* (2004) 'Protein kinase CK1 δ phosphorylates key sites in the acidic domain of murine double-minute clone 2 protein (MDM2) that regulate p53 turnover', *Biochemistry*, 43(51), pp. 16356-16364. doi: 10.1021/bi0489255.

Wolynes, P. G., Onuchic, J. N. and Thirumalai, D. (1995) 'Navigating the folding routes', *Science*. American Association for the Advancement of Science, pp. 1619-1620. doi: 10.1126/science.7886447.

Wright, J. D., Mac, P. D. and Day, C. L. (2016) 'Secondary ubiquitin-RING docking enhances Arkadia and Ark2C E3 ligase activity', *Nature Structural and Molecular Biology*, 23(1), pp. 45-52. doi: 10.1038/nsmb.3142.

Wu, P. Y. *et al.* (2003) 'A conserved catalytic residue in the ubiquitin-conjugating enzyme family', *EMBO Journal*, 22(19), pp. 5241-5250. doi: 10.1093/emboj/cdg501.

Wu, X. *et al.* (1993) 'The p53-mdm-2 autoregulatory feedback loop', *Genes and Development*, 7(7A), pp. 1126-1132. doi: 10.1101/gad.7.7a.1126.

Xiao, Z. X. *et al.* (1995) 'Interaction between the retinoblastoma protein and the oncoprotein MDM2', *Nature*, 375(6533), pp. 694-8. doi: 10.1038/375694a0.

Xirodimas, D. *et al.* (2001) 'Different effect of p14ARF on the level of ubiquitinatd p53 and mdm2', *Oncogene*. Nature Publishing Group, 20(36), pp. 4972-4983. doi: 10.1038/sj.onc.1204656.

Xirodimas, D. P. *et al.* (2002) 'P14ARF promotes accumulation of SUMO-1 conjugated (H)Mdm2', *FEBS Letters*. Wiley-Blackwell, 528(1-3), pp. 207-211. doi: 10.1016/S0014-5793(02)03310-0.

Xu, C., Fan, C. D. and Wang, X. (2015) 'Regulation of Mdm2 protein stability and the p53 response by NEDD4-1 E3 ligase', *Oncogene*, 34(3), pp. 342-350. doi: 10.1038/onc.2013.557.

Xue, W. *et al.* (2007) 'Senescence and tumour clearance is triggered by p53 restoration in murine liver carcinomas', *Nature*, 445(7128), pp. 656-660. doi:

10.1038/nature05529.

Yang, T., Kozopas, K. M. and Craig, R. W. (1995) 'The intracellular distribution and pattern of expression of Mcl-1 overlap with, but are not identical to, those of Bcl-2', *Journal of Cell Biology*, 128(6), pp. 1173-1184. doi: 10.1083/jcb.128.6.1173.

Yang, Y. *et al.* (2000) 'Ubiquitin protein ligase activity of IAPs and their degradation in proteasomes in response to apoptotic stimuli', *Science*, 288(5467), pp. 874-877. doi: 10.1126/science.288.5467.874.

Yang, Y. *et al.* (2005) 'Small molecule inhibitors of HDM2 ubiquitin ligase activity stabilize and activate p53 in cells', *Cancer Cell*, 7(6), pp. 547-559. doi: 10.1016/j.ccr.2005.04.029.

Yao, W. *et al.* (2018) 'WW domain-mediated regulation and activation of E3 ubiquitin ligase Suppressor of Deltex.', *The Journal of biological chemistry*. American Society for Biochemistry and Molecular Biology, 293(43), pp. 16697-16708. doi: 10.1074/jbc.RA118.003781.

Yarbrough, W. G. *et al.* (2002) 'Human tumor suppressor ARF impedes S-phase progression independent of p53', *Cancer Research*. American Association for Cancer Research, 62(4), pp. 1171-1177. Available at: <http://www.ncbi.nlm.nih.gov/pubmed/11861400> (Accessed: 20 April 2018).

Yau, R. and Rape, M. (2016) 'The increasing complexity of the ubiquitin code', *Nature Cell Biology*, 18(6), pp. 579-586. doi: 10.1038/ncb3358.

Yu, G. W. *et al.* (2006) 'The central region of HDM2 provides a second binding site for p53', *Proceedings of the National Academy of Sciences of the United States of America*, 103(5), pp. 1227-32. doi: 10.1073/pnas.0510343103.

Yu, H. *et al.* (1996) 'Identification of a novel ubiquitin-conjugating enzyme involved in mitotic cyclin degradation', *Current Biology*, 6(4), pp. 455-466. doi: 10.1016/S0960-9822(02)00513-4.

- Yu, H. *et al.* (2017) 'Two strategies to engineer flexible loops for improved enzyme thermostability', *Scientific Reports*, 7(February), pp. 1-15. doi: 10.1038/srep41212.
- Yuan, W.-C. *et al.* (2014) 'K33-Linked Polyubiquitination of Coronin 7 by Cul3-KLHL20 Ubiquitin E3 Ligase Regulates Protein Trafficking', *Molecular cell*. Elsevier, 54(4), pp. 586-600. doi: 10.1016/j.molcel.2014.03.035.
- Yun, J. P. *et al.* (2003) 'Nucleophosmin/B23 Is a Proliferate Shuttle Protein Associated with Nuclear Matrix', *Journal of Cellular Biochemistry*, 90(6), pp. 1140-1148. doi: 10.1002/jcb.10706.
- Zardeneta, G. and Horowitz, P. M. (1994) 'Detergent, liposome, and micelle-assisted protein refolding', *Analytical Biochemistry*, pp. 1-6. doi: 10.1006/abio.1994.1537.
- Zauberman, A. *et al.* (1995) 'A functional p53-responsive intronic promoter is contained within the human mdm2 gene', *Nucleic Acids Research*. Oxford University Press, 23(14), pp. 2584-2592. doi: 10.1093/nar/23.14.2584.
- Zeng, X. *et al.* (1999) 'MDM2 suppresses p73 function without promoting p73 degradation', *Mol Cell Biol*, 19(5), pp. 3257-3266. doi: 10.1128/MCB.19.5.3257.
- Zhang, W. *et al.* (2016) 'System-Wide Modulation of HECT E3 Ligases with Selective Ubiquitin Variant Probes', *Molecular Cell*. Elsevier, 62(1), pp. 121-136. doi: 10.1016/j.molcel.2016.02.005.
- Zhang, Y. and Xiong, Y. (2001) 'A p53 Amino-Terminal Nuclear Export Signal Inhibited by DNA Damage-Induced Phosphorylation', *Science*, 292(5523), pp. 1910-1915. doi: 10.1126/science.1058637.
- Zhang, Y., Xiong, Y. and Yarbrough, W. G. (1998) 'ARF promotes MDM2 degradation and stabilizes p53: ARF-INK4a locus deletion impairs both the Rb and p53 tumor suppression pathways', *Cell*. Elsevier, 92(6), pp. 725-734. doi: 10.1016/S0092-8674(00)81401-4.

Zhao, X. *et al.* (2008) 'The HECT-domain ubiquitin ligase Huwe1 controls neural differentiation and proliferation by destabilizing the N-Myc oncoprotein', *Nature Cell Biology*, 10(6), pp. 643-653. doi: 10.1038/ncb1727.

Zheng, N. *et al.* (2000) 'Structure of a c-Cbl-UbcH7 Complex: RING Domain Function in Ubiquitin-Protein Ligases', *Cell*, 102(4), pp. 533-539. doi: 10.1016/S0092-8674(00)00057-X.

Zheng, N. and Shabek, N. (2017) 'Ubiquitin Ligases: Structure, Function, and Regulation', *Annual Review of Biochemistry*. Annual Reviews , 86(1), pp. 129-157. doi: 10.1146/annurev-biochem-060815-014922.

Zhong, Q. *et al.* (2005) 'Mule/ARF-BP1, a BH3-only E3 ubiquitin ligase, catalyzes the polyubiquitination of Mcl-1 and regulates apoptosis', *Cell*. Cell Press, 121(7), pp. 1085-1095. doi: 10.1016/j.cell.2005.06.009.

Zhou, B. P. *et al.* (2001) 'HER-2/neu induces p53 ubiquitination via Akt-mediated MDM2 phosphorylation', *Nature Cell Biology*, 3(11), pp. 973-982. doi: 10.1038/ncb1101-973.

Zhou, M. *et al.* (2000) 'Incidence and prognostic significance of MDM2 oncoprotein overexpression in relapsed childhood acute lymphoblastic leukemia', *Leukemia*, 14(1), pp. 61-67. doi: 10.1038/sj.leu.2401619.

Zhou, P. *et al.* (1997) 'Mcl-1, a Bcl-2 family member, delays the death of hematopoietic cells under a variety of apoptosis-inducing conditions.', *Blood*, 89(2), pp. 630-43. Available at: <http://www.ncbi.nlm.nih.gov/pubmed/9002967> (Accessed: 7 May 2018).

Zhu, K. *et al.* (2017) 'Allosteric auto-inhibition and activation of the Nedd4 family E3 ligase Itch', *EMBO reports*, 18(9), pp. 1618-1630. doi: 10.15252/embr.201744454.

Zietz, C. *et al.* (1998) 'MDM-2 oncoprotein overexpression, p53 gene mutation, and VEGF up-regulation in angiosarcomas', *American Journal of Pathology*, 153(5), pp. 1425-1433. doi: 10.1016/S0002-9440(10)65729-X.

Zindy, F. *et al.* (1998) 'Myc signaling via the ARF tumor suppressor regulates p53-dependent apoptosis and immortalization', *Genes and Development*. Cold Spring Harbor Laboratory Press, 12(15), pp. 2424-2433. doi: 10.1101/gad.12.15.2424.

Zou, Q. *et al.* (2014) 'USP15 stabilizes MDM2 to mediate cancer-cell survival and inhibit antitumor T cell responses', *Nature Immunology*, 15(6), pp. 562-570. doi: 10.1038/ni.2885.